

Drug Discoveries & Therapeutics

Volume 19, Number 5 October 2025



www.ddtjournal.com





ISSN: 1881-7831 Online ISSN: 1881-784X CODEN: DDTRBX Issues/Year: 6 Language: English Publisher: IACMHR Co., Ltd

Drug Discoveries & Therapeutics is one of a series of peer-reviewed journals of the International Research and Cooperation Association for Bio & Socio-Sciences Advancement (IRCA-BSSA) Group. It is published bimonthly by the International Advancement Center for Medicine & Health Research Co., Ltd. (IACMHR Co., Ltd.) and supported by the IRCA-BSSA.

Drug Discoveries & Therapeutics publishes contributions in all fields of pharmaceutical and therapeutic research such as medicinal chemistry, pharmacology, pharmaceutical analysis, pharmaceutics, pharmaceutical administration, and experimental and clinical studies of effects, mechanisms, or uses of various treatments. Studies in drug-related fields such as biology, biochemistry, physiology, microbiology, and immunology are also within the scope of this journal.

Drug Discoveries & Therapeutics publishes Original Articles, Brief Reports, Reviews, Policy Forum articles, Case Reports, Communications, Editorials, News, and Letters on all aspects of the field of pharmaceutical research. All contributions should seek to promote international collaboration in pharmaceutical science.

Editorial Board

International Field Chief Editors:

Nobuyoshi AKIMITSU The University of Tokyo, Tokyo, Japan

Fen-Er CHEN Fudan University, Shanghai, China

Hiroshi HAMAMOTO Yamagata University, Yamagata, Japan

Takashi KARAKO Japan Institute for Health Security, Tokyo, Japan

Hongzhou LU National Clinical Research Centre for Infectious Diseases, Shenzhen, Guangdong, China

Sven SCHRÖDER University Medical Center Hamburg Eppendorf (UKE), Hamburg, Germany

Kazuhisa SEKIMIZU Teikyo University, Tokyo, Japan

Corklin R. STEINHART CAN Community Health, FL, USA

Associate Editors:

Feihu CHEN Anhui Medical University, Hefei, Anhui, China

Jianjun GAO Qingdao University, Qingdao, Shandong, China

Chikara KAITO Okayama University, Okayama, Japan

Gagan KAUSHAL Jefferson College of Pharmacy, Philadelphia, PA, USA

Hironori KAWAKAMI Sanyo-Onoda City University, Yamaguchi, Japan

Xiao-Kang LI National Research Institute for Child Health and Development, Tokyo, Japan

Yasuhiko MATSUMOTO Meiji Pharmaceutical University, Tokyo, Japan

Atsushi MIYASHITA Teikyo University, Tokyo, Japan

Tomofumi SANTA The University of Tokyo, Tokyo, Japan

Tianqiang SONG Tianjin Medical University, Tianjin, China Sanjay K. SRIVASTAVA

Texas Tech University Health Sciences Center, Abilene, TX, USA

Hongbin SUN China Pharmaceutical University, Nanjing, Jiangsu, China

Fengshan WANG Shandong University, Jinan, Shandong, China.

Proofreaders:

Curtis BENTLEY Roswell, GA, USA Thomas R. LEBON Los Angeles, CA, USA

Editorial and Head Office:

Pearl City Koishikawa 603, 2-4-5 Kasuga, Bunkyo-ku, Tokyo 112-0003, Japan E-mail: office@ddtjournal.com

Drug Discoveries & Therapeutics

Editorial and Head Office

Pearl City Koishikawa 603, 2-4-5 Kasuga, Bunkyo-ku, Tokyo 112-0003, Japan

E-mail: office@ddtjournal.com URL: www.ddtjournal.com

Editorial Board Members

Alex ALMASAN (Cleveland, OH)

John K. BUOLAMWINI

(Memphis, TN) Jianping CAO (Shanghai) Shousong CAO (Buffalo, NY) Jang-Yang CHANG

(Tainan)

Zhe-Sheng CHEN (Queens, NY) Zilin CHEN (Wuhan, Hubei) Xiaolan CUI (Beijing) Saphala DHITAL

(Clemson, SC) Shaofeng DUAN (Lawrence, KS) Hao FANG (Ji'nan, Shandong) Marcus L. FORREST (Lawrence, KS)

Tomoko FUJIYUKI

(Tokvo)

Takeshi FUKUSHIMA (Funabashi, Chiba) Harald HAMACHER

(Tübingen, Baden-Württemberg)

Kenji HAMASE (Fukuoka, Fukuoka) Junqing HAN (Ji'nan, Shandong) Xiaojiang HAO (Kunming, Yunnan) Kiyoshi HASEGAWA

(Tokyo)

Waseem HASSAN (Rio de Janeiro) Langchong HE (Xi'an, Shaanxi) Rodney J. Y. HO (Seattle, WA) Hsing-Pang HSIEH (Zhunan, Miaoli) Yongzhou HU

(Hangzhou, Zhejiang)

Youcai HU (Beijing)

Yu HUANG (Hong Kong) Zhangjian HUANG (Nanjing Jiangsu)

Amrit B. KARMARKAR (Karad, Maharashra)

(Tokyo)

Ibrahim S. KHATTAB

Toshiaki KATADA

(Kuwait)

Shiroh KISHIOKA (Wakayama, Wakayama) Robert Kam-Ming KO (Hong Kong)

Nobuyuki KOBAYASHI (Nagasaki, Nagasaki) Toshiro KONISHI

(Tokyo) Peixiang LAN (Wuhan, Hubei) Chun-Guang LI (Melbourne) Minyong LI (Ji'nan, Shandong)

Xun LI

(Ji'nan, Shandong) Dongfei LIU (Nanjing, Jiangsu) Jian LIU (Hefei, Anhui) Jikai LIU (Wuhan, Hubei) Jing LIU

(Beijing) Xinyong LIU (Ji'nan, Shandong) Yuxiu LIU (Nanjing, Jiangsu)

Hongxiang LOU (Jinan, Shandong) Hai-Bin LUO (Haikou, Hainan) Xingyuan MA (Shanghai)

Ken-ichi MAFUNE (Tokyo) Sridhar MANI (Bronx, NY)

Tohru MIZUSHIMA (Tokyo)

Jasmin MONPARA (Philadelphia, PA)

Masahiro MURAKAMI

(Osaka)

Yoshinobu NAKANISHI (Kanazawa, Ishikawa) Munehiro NAKATA

(Hiratsuka) Siriporn OKONOGI (Chiang Mai) Weisan PAN

(Shenyang, Liaoning) Chan Hum PARK (Eumseong) Rakesh P. PATEL

(Mehsana, Guiarat) Shivanand P. PUTHLI (Mumbai, Maharashtra) Shafiqur RAHMAN (Brookings, SD)

Gary K. SCHWARTZ (New York, NY) Luqing SHANG (Tianjin) Yuemao SHEN

(Ji'nan, Shandong) Rong SHI (Shanghai)

Yoshitaka SHIMOTAI

(Yamagata)

Chandan M. THOMAS (Bradenton, FL) Michihisa TOHDA (Sugitani, Toyama) Li TONG (Xining, Qinghai) Murat TURKOGLU (Istanbul)

Hui WANG (Shanghai) Quanxing WANG (Shanghai) Stephen G. WARD

(Bath) Zhun WEI

(Qingdao, Shandong)

Tao XU

(Qingdao, Shandong)

Yuhong XU (Shanghai)

Yong XU

(Guangzhou, Guangdong)

Akiho YAGI (Sendai, Miyagi) Bing YAN (Ji'nan, Shandong) Chunyan YAN

(Guangzhou, Guangdong) Xiao-Long YANG (Chongqing) Yun YEN (Duarte, CA) Yongmei YIN (Tianjin)

(Tokvo) Yun YOU (Beijing) Rongmin YU

Yasuko YOKOTA

(Guangzhou, Guangdong)

Tao YU

(Qingdao, Shandong) Guangxi ZHAI (Ji'nan, Shandong) Liangren ZHANG

(Beijing) Lining ZHANG (Ji'nan, Shandong) Na ZHANG (Ji'nan, Shandong) Ruiwen ZHANG (Houston, TX) Xiu-Mei ZHANG (Ji'nan, Shandong) Xuebo ZHANG (Baltimore, MD) Yingjie ZHANG (Ji'nan, Shandong) Yongxiang ZHANG

(Beijing) Haibing ZHOU (Wuhan, Hubei) Jian-hua ZHU

(Guangzhou, Guangdong)

(As of June 2025)

Editorial

277-284 Changing epidemiology of respiratory pathogens since 2020: Shenzhen case study and global perspectives.

Chun Chen, Houming Liu, Jiaye Liu, Peifen Chen, Hongzhou Lu

Review

Indicators of a moist wound environment and care to maintain a moist environment for early healing: A scoping review.

Mao Kunimitsu, Karin Izumi, Yume Kawamizu, Kenshin Takezawa, Kanon Nishida, Hitomi Honda, Yuri Maeda, Rena Yamauchi, Risa Yoshida, Yukari Nakajima, Amika Yamada, Kanae Mukai, Makoto Oe

Food, medicine, and cosmetic homology: A comprehensive review of bioactive components, functions, and applications of *Torreya grandis*.

Xiaoyan Cui, Chuanyin Shi, Yan Sun

Original Article

Purification and characterization of a novel antioxidant protein from *Arca subcrenata*

Qing Yan, Hui Shi, Yue Gao, Chunlei Li, Lin Dong, Jianhua Zhu, Rongmin Yu

Development and reliability assessment of a liquid-phase measurement for skin taurine using skin blotting.

Katsunori Kato, Kazuhiro Ogai, Yoko Hasegawa, Chizuko Konya, Hiromi Sanada, Takeo Minematsu

325-336 TRPC6 expression is negatively correlated with breast cancer progression.

Yifei Ma, Guoning Li, Haoyang Yu, Baoke Wang, Zhihan Diao, Yuan Du, Hongbo Wang, Huiping Liu

Comparing gene-targeting efficiency of Agrobacterium tumefaciens-mediated transformation and electroporation in the pathogenic fungus Trichosporon asahii JCM2466.

Yasuhiko Matsumoto, Mei Nakayama, Yuta Shimizu, Sachi Koganesawa, Hiromi Kanai, Wakako Hayashi, Toma Matsuo, Tsuyoshi Yamada, Takashi Sugita

Brief Report

Solid phase extraction and high-performance liquid chromatographic determination of lazertinib in human plasma.

Yoshito Gando, Takeo Yasu

Tapeworm infection incidence in rural Japan points to a common environmental source of infection.

Dhammika Leshan Wannigama, Mohan Amarasiri, Phatthranit Phattharapornjaroen, Cameron Hurst, Yu Suzuki, Daisuke Akaneya, Mika Moriya, Taichi Adachi, Yoshikazu Okuma, Daisuke Ishizawa, Hitoshi Ishikawa, Kazuhiko Miyanaga, Longzhu Cui, Kazunori Moriya, Hirotake Mori, Naveen Kumar Devanga Ragupathi, Yoshitaka Shimotai, Daisuke Sano, Takashi Furukawa, Kazunari Sei, Talerngsak Kanjanabuch, Paul G. Higgins, Tetsuji Aoyagi, Anthony Kicic, Sam Trowsdale, Parichart Hongsing, Aisha Khatib, Kenji Shibuya, Shuichi Abe, Hiroshi Hamamoto

Correspondence

Paltusotine: The first selective nonpeptide agonist of somatostatin receptor 2 (SSTR2) for the treatment of acromegaly.

Yueyi Sun, Daoran Lu, Jianjun Gao

Editorial

DOI: 10.5582/ddt.2025.01108

Changing epidemiology of respiratory pathogens since 2020: Shenzhen case study and global perspectives

Chun Chen¹, Houming Liu², Jiaye Liu³, Peifen Chen^{1,*}, Hongzhou Lu^{4,*}

- ¹ Department of Respiratory Medicine, National Clinical Research Center for Infectious Disease, Shenzhen Third People's Hospital, Shenzhen, Guangdong, China;
- ² Department of Clinical Laboratory, National Clinical Research Center for Infectious Disease, Shenzhen Third People's Hospital, Shenzhen, Guangdong, China;
- ³ School of Public Health, Shenzhen University Medical School, Shenzhen, Guangdong, China;
- ⁴ Department of Infectious Diseases, National Clinical Research Center for Infectious Disease, Shenzhen Third People's Hospital, Shenzhen, Guangdong, China.

SUMMARY: The coronavirus disease 2019 (COVID-19) pandemic fundamentally disrupted global respiratory virus epidemiology through widespread non-pharmaceutical interventions. Analysis of a tertiary hospital in Shenzhen (2021-2024) reveals profound alterations in seasonal patterns. Influenza A exhibited multiple atypical peaks including summer circulation, while influenza B showed delayed resurgence with sustained winter activity. Respiratory syncytial virus demonstrated altered seasonality with substantial warm-season transmission replacing traditional winter patterns. World Health Organization (WHO) global surveillance confirmed parallel worldwide trends. Influenza activity collapsed dramatically in 2021 before resurging with irregular timing and unprecedented intensity through 2025. Respiratory syncytial virus exhibited off-season epidemics across multiple regions before gradually re-establishing modified seasonal patterns at elevated baseline levels. These epidemiological shifts resulted from immunity gaps created by reduced viral exposure, staggered lifting of pandemic restrictions across regions, and viral competition dynamics. Emerging technologies including AI-driven prediction models, expanded wastewater surveillance systems, and universal vaccine development offer promising approaches for managing future respiratory disease dynamics in this evolving post-pandemic landscape.

Keywords: respiratory viruses, epidemiological shift, seasonality

1. Introduction

The COVID-19 pandemic represents an unprecedented natural experiment in respiratory virus epidemiology. Widespread implementation of non-pharmaceutical interventions during 2020-2021 drastically suppressed seasonal respiratory viruses globally, creating historical circulation nadirs. However, subsequent relaxation of restrictions triggered atypical resurgences characterized by altered seasonality, irregular peak timing, and amplified disease burden. Understanding these epidemiological shifts holds critical implications for future surveillance strategies, vaccine development, and public health preparedness. This study analyzes local hospital surveillance data from Shenzhen (2021-2024) alongside global World Health Organization (WHO) monitoring systems to characterize post-pandemic respiratory virus dynamics, elucidate underlying mechanistic drivers, and identify emerging technologies for enhanced epidemic forecasting and control.

2. Local epidemiological patterns: Shenzhen hospital surveillance data (2021-2024)

A retrospective observational analysis was conducted on laboratory testing data from 101,151 patients with influenza-like illness (ILI) or severe acute respiratory infection (SARI) at Shenzhen Third People's Hospital (January 2021-December 2024). The study evaluated temporal detection patterns of seven respiratory viral pathogens: Influenza A virus (IAV) and influenza B virus (IBV), respiratory syncytial virus (RSV), adenovirus, rhinovirus (RV), and parainfluenza virus type I (PIV-I) and parainfluenza virus type III (PIV-III). The study primarily evaluated changes in the detection counts of six viral respiratory pathogens. Data from Shenzhen Third People's Hospital (2021-2024) reveal substantial year-to-year changes in respiratory virus activity (Figure 1). IAV was virtually undetected in 2021 but rebounded in subsequent years. Mid-2022 saw an atypical summer outbreak with elevated case counts peaking in June. IAV

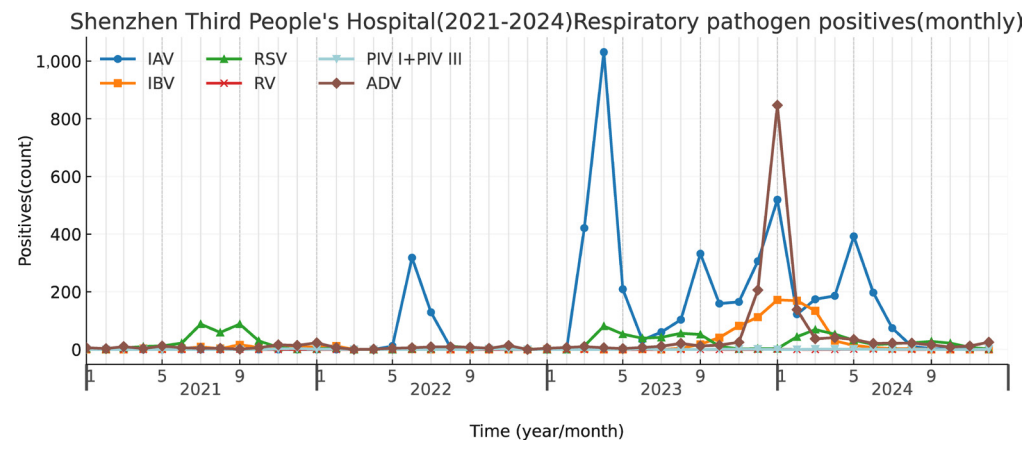


Figure 1. Monthly test-positivity rates for IAV, IBV, RSV, PIV I+III and ADV at Shenzhen Third People's Hospital, 2021-2024.

activity surged dramatically in 2023, with a spring peak in April recording 1,031 positive cases. Following this spring maximum, sustained autumn activity continued through November, culminating in a winter wave from December 2023 through February 2024 that peaked in January (519 cases). A subsequent spring to early summer increase occurred in 2024, reaching its highest point in May (392 cases), before declining rapidly by August and remaining at minimal levels throughout autumn (fewer than 15 cases monthly from August through December). Annual IAV case totals rose from near-zero in 2021 to higher levels in 2022, then surged in 2023 and remained elevated in 2024, demonstrating multiple seasonal peaks within individual years. IBV exhibited delayed resurgence. IBV remained at negligible levels through 2022. A substantial wave emerged in late 2023, with November 2023 recording increased cases. This wave peaked in January 2024 with 172 positive cases and persisted through February 2024 (169 cases), representing the first major IBV activity in the city since the pandemic onset. Following this sustained winter peak, IBV declined to very low levels by mid-2024 but remained at moderately higher baseline levels compared to the 2021–2022 period.

RSV exhibited altered seasonality throughout the observation period. In July 2021, RSV case counts surged to elevated summer levels (88 cases). RSV detections remained subdued throughout 2022. In 2023, activity continued to show atypical seasonal distribution, with April recording 81 positive cases and late summer showing additional increases. In 2024, RSV cases increased during spring, peaking in March (69 cases). These patterns indicate that RSV demonstrated altered seasonal characteristics in Shenzhen during 2021-2024, with substantial activity persisting in warmer months. Adenovirus (ADV) remained at low levels during 2021-2022 but experienced a concentrated outbreak from December 2023 through early 2024. This winter surge began in December 2023 (206 cases), peaked in January 2024 (847 cases), remained elevated in February 2024 (138 cases), and declined by March-April (37-41

cases). This outbreak represents a substantial increase in ADV circulation compared to earlier pandemic years, likely reflecting accumulated susceptibility during China's prolonged COVID-19 control measures through December 2022. RV, PIV-I, and PIV-III maintained relatively low case counts throughout the observation period without substantial surges comparable to other pathogens.

Overall findings demonstrate altered seasonal patterns from the pandemic period (2021–2022) to postpandemic years (2023–2024). IAV exhibited multiple peaks within individual years, with major spring 2023 activity, sustained autumn circulation, and winter 2023 increases. IBV showed delayed resurgence with a sustained winter 2023 peak. RSV peaked during summer and spring periods rather than winter. Multiple pathogens co-circulated at significant levels during 2023–2024. Although these data offer valuable insights into local respiratory virus dynamics, this analysis was conducted at a single tertiary care center and predominantly included patients seeking care for acute respiratory symptoms. As such, hospital-based case counts may not fully capture the broader patterns of community transmission.

3. Global surveillance evidence: WHO data analysis (2020-2025)

Globally, influenza activity experienced unprecedented disruption during the COVID-19 pandemic, followed by atypical recovery patterns that fundamentally altered traditional seasonal rhythms. Global influenza and respiratory syncytial virus surveillance data from January 2020 to August 2025 were obtained from the Global Influenza Surveillance and Response System (GISRS) (Figure 2). During January and February 2020, global influenza positivity rates exceeded 40%, with positive specimens exceeding 180,000 monthly. Following widespread non-pharmaceutical interventions, activity collapsed from March 2020 onward, declining to 18.6% positivity. Throughout 2021, influenza remained at

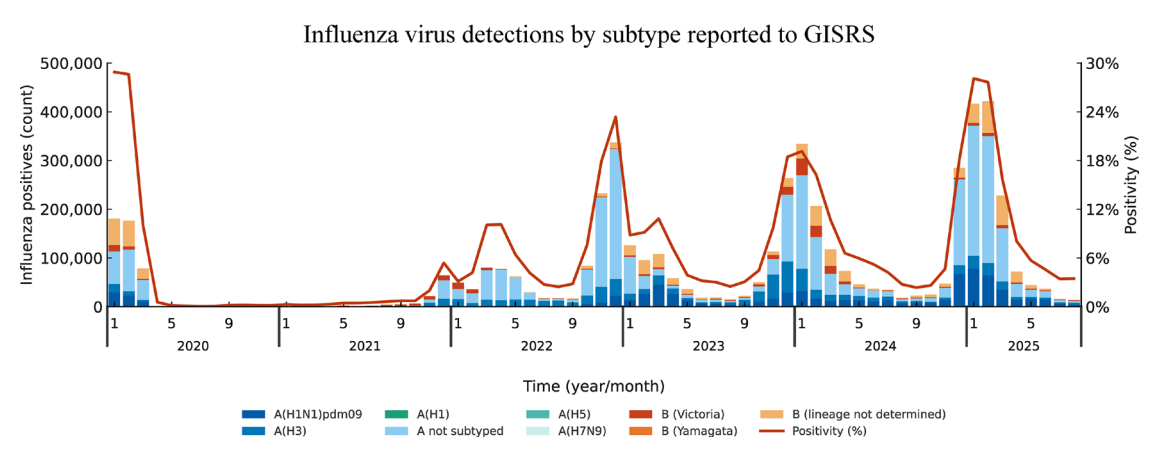


Figure 2. Influenza virus detections by subtype reported to GISRS, January 2020-August 2025.

historically low levels with an annual positivity rate of only 1.70% and total annual detections of 114,863 specimens. December 2021 exhibited a modest rebound with 64,776 cases, indicating initial stirring of circulation. March 2022 showed a secondary transitional peak before the true resurgence began in October 2022. November and December 2022 recorded sharp peaks with 232,910 and 337,079 positive specimens respectively, occurring one to two months earlier than traditional patterns. Activity declined through early 2023 but extended into April 2023, forming a secondary spring elevation. The 2023/24 season exhibited more conventional winter rhythms, peaking during December 2023 and January 2024 with 263,948 and 334,173 specimens respectively. However, the 2024/25 season demonstrated the highest recorded peaks in the entire surveillance period. December 2024 recorded 285,394 cases, followed by January and February 2025 reaching unprecedented levels with 417,206 and 421,509 positive specimens respectively. The five highest monthly case counts all occurred from December 2022 onward, demonstrating exceptional intensity of post-pandemic resurgence and ongoing instability in seasonal timing.

As pandemic restrictions were relaxed, atypical resurgences of these viruses were observed. Many regions saw off-season or earlier-than-usual outbreaks. In the United States and Europe, the influenza season of 2021–2022 was delayed and relatively mild, but the 2022–2023 season was early and intense, with influenza and RSV cases peaking roughly one to two months earlier than pre-pandemic norms (1). In some areas, multiple waves occurred within a single year. Australia and parts of East Asia noted significant influenza circulation during their summer months, a phenomenon virtually unheard of prior to COVID-19 (2). One study from India documented an unusual influenza surge in June through September 2022 instead of the usual winter peak. RSV peaked in autumn 2022 instead of spring (3). Similarly, Latin America reported altered timing of influenza. Chile saw early influenza outbreaks beginning in January 2022 ahead of the typical winter schedule. Brazil experienced unusual influenza activity in the offseason period of August through October 2022 (4,5). These observations underscore a shift in seasonality on a global scale.

Influenza type and subtype composition underwent significant reorganization. Influenza A maintained stable dominance, increasing from 65.4% in 2020 to 93.4 percent in 2022, then consistently representing 78% to 82% during 2023 through 2025. Influenza B remained suppressed at 6.6% in 2022 and generally below 22% subsequently. A critical progressive shift in influenza A subtype dominance occurred from 2021 through 2025, though interpretation is constrained by high proportions of A not subtyped specimens ranging from 63% to 76% annually. Among subtyped specimens, A(H3N2) clearly predominated during 2021 and 2022. A transitional phase emerged in 2023 when the relative proportions of A(H3N2) and A(H1N1)pdm09 converged closely, signaling an emerging shift in subtype dominance. This transition solidified in 2024 and strengthened further through 2025, with A(H1N1)pdm09 establishing clear dominance over A(H3N2) during this later period. Within influenza B detections, B/Yamagata effectively disappeared with 0% detection from 2022 onward, while B/Victoria persisted as the sole circulating lineage at reduced levels. These patterns demonstrate the complex interplay between pandemic control measures, immunity gaps, and viral competitive dynamics reshaping global influenza epidemiology.

The circulation hiatus created by pandemic measures left populations with varying levels of protective antibodies against H3N2, H1N1, and influenza B viruses. Viral strains encountering cohorts with reduced immunity gained competitive fitness advantages, resulting in strain-specific outbreak patterns (6). Such patterns were reported in 30 EU/EEA countries during the 2022/23 influenza season, where an atypical biphasic epidemic pattern emerged with co-circulation of A(H1N1)pdm09 (36%), A(H3N2) (64%), and B/Victoria lineage viruses, characterized by an initial influenza A-dominated peak followed by an influenza B-dominated

peak, while B/Yamagata lineage remained absent for the third consecutive season (7).

RSV has also shown globally altered behavior. WHO weekly RSV surveillance data aggregated globally (January 2020-August 2025) revealed that overall activity was markedly suppressed in 2020, followed by an off-season resurgence in 2021 peaking in November, indicating pronounced seasonal displacement (Figure 3). From 2022 through 2024, seasonality progressively reestablished with winter peaks occurring in December each year, and epidemic intensity exceeded the suppressed 2020 baseline. In 2025, activity peaked in January before declining to moderate-low levels through August, yet background transmission remained elevated compared to the 2020 baseline, consistent with re-balanced seasonality on a moderately elevated baseline. Numerous countries experienced out-of-season RSV epidemics in 2021 or 2022. For example, an off-season summer RSV wave occurred in Western Europe and the United States in mid-2021 when restrictions were briefly loosened. Post-2020, RSV seasons have often started earlier and been more intense compared to pre-pandemic years. Intensified circulation of RSV and associated hospital burden in the EU/EEA (8). Data from a study in Mexico indicated that RSV outbreaks post-pandemic began weeks earlier than usual and with higher case counts, consistent with the notion of an accumulating cohort of RSV-naive infants born during lockdown periods (9). By 2023–2024, there are signs that RSV seasonality is gradually realigning with its previous schedule in some regions, but the overall trend has been erratic timing and larger susceptible populations (10,11).

Other respiratory viruses experienced similar disruptions, including parainfluenza, seasonal coronaviruses, adenovirus, human metapneumovirus, and rhinovirus. Recovery patterns varied considerably across different pathogens. Non-COVID coronaviruses

and rhinoviruses were among the first to return to nearnormal circulation, frequently causing summer colds as early as 2021 (12). In contrast, certain viruses have not fully returned to their prior patterns. Reports suggest some seasonal viruses are still finding a new equilibrium. For example, one analysis noted that some respiratory pathogens "failed to return to pre-pandemic seasonality" even by 2023. Adenoviruses have been increasingly reported worldwide, including outbreaks of adenoviral respiratory illness in children after 2021, possibly due to lowered immunity and more frequent testing (13). Globally, respiratory virus epidemiology has undergone an uneven resetting process, with surge patterns shaped by regional variations in COVID-19 control measures and their subsequent relaxation.

4. Drivers of epidemiological shifts since 2020

Multiple factors underlie these epidemiological shifts. The foremost driver was the implementation of nonpharmacological interventions (NPIs) during the COVID-19 pandemic, which drastically reduced transmission opportunities for other respiratory viruses (14). Measures such as mask wearing, school and daycare closures, travel limitations, improved hand hygiene, and crowd avoidance broke the typical chains of infection for flu, RSV, and others. This resulted in historically low incidences in 2020-2021. A positive outcome was fewer respiratory infections during that period, but a side effect was the creation of an "immune debt" in the population (15). Because people were not exposed to these common viruses for one or two seasons, a larger susceptible pool accumulated. Once restrictions lifted, those viruses could spread more easily among immunologically naïve groups, leading to larger outbreaks than normal.

The staggered lifting of COVID-19 measures across different regions and times also contributed to out-of-

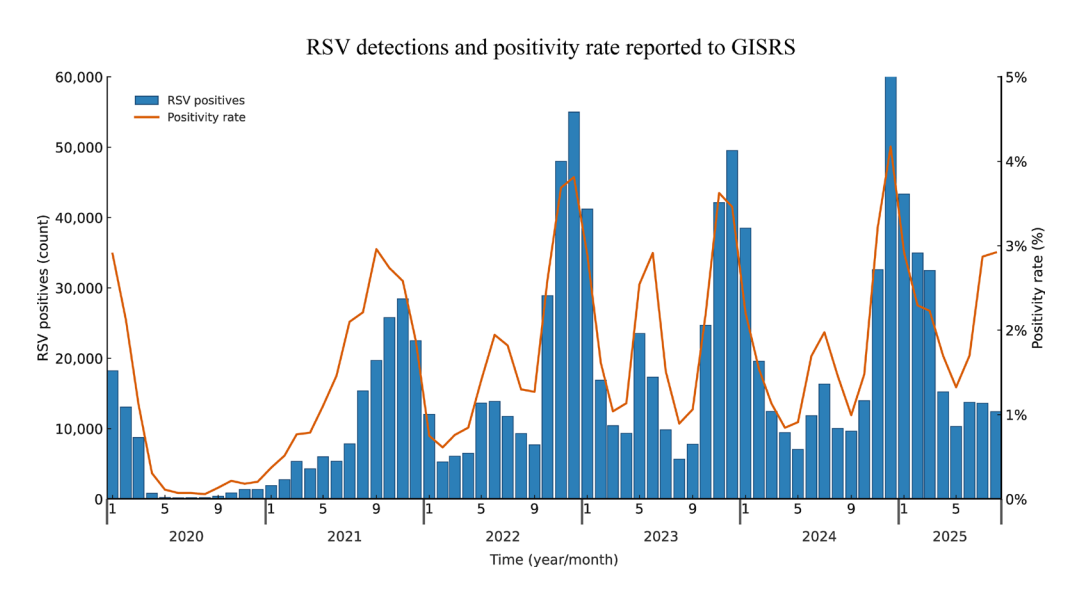


Figure 3. RSV detections and positivity rate reported to GISRS, January 2020-August 2025.

phase outbreaks. When one country or region relaxed interventions earlier than others, it often experienced an off-season resurgence of viruses. For example, Japan's early relaxation in mid-2021 coincided with a summer influenza outbreak there, and similarly, parts of China that eased measures in 2022 saw unseasonal flu waves. Each region's trajectory depended on when and how rapidly normal social mixing resumed, which explains why the timing of post-pandemic surges varied globally (16,17).

Viral interference and competition may have also played a role. During the pandemic, SARS-CoV-2 was the dominant circulating respiratory virus, and its high prevalence might have competitively suppressed other viruses to some extent (via viral interference mechanisms or simply by occupying ecological niches). As the prevalence of COVID-19 oscillated, other viruses found opportunities to resurge when COVID-19 waves subsided. There is some evidence that influenza and RSV did not significantly co-circulate with large COVID surges, but when COVID incidence dropped, flu and RSV filled the void (18). In late 2022, a "tripledemic" of COVID-19, influenza, and RSV was noted in some countries, suggesting that eventually co-circulation can occur, but the initial re-emergence dynamics were likely influenced by such interactions(19).

Changes in healthcare-seeking and testing during the pandemic also affected reported epidemiology. Routine surveillance was disrupted in many places, and people avoided hospitals except for severe illness. This led to under-detection of mild cases early in the pandemic. Later, increased testing (through multiplex PCR panels) meant that some viruses (like adenovirus or metapneumovirus) were detected more than before, which could partly contribute to higher case counts post-2020. However, the consensus is that true circulation changes (not just detection artifacts) occurred for major pathogens, given consistent signals from multiple locations.

In summary, the shifts since 2020 have been driven by a combination of behavioral, immunological, and virological factors. NPIs created a lull and subsequent rebound. Immunity gaps made populations more vulnerable when viruses returned. The synchronization of seasonal cycles was lost and is still readjusting. These drivers emphasize the interconnected nature of respiratory pathogen dynamics and how large-scale interventions can reset endemic disease patterns.

5. Emerging technologies for enhanced surveillance and prevention

AI-driven viral prediction technologies are fundamentally transforming influenza vaccine development paradigms. MIT's VaxSeer system, the Beth-1 model, and the University of Missouri's MAIVeSS framework represent three distinct yet complementary technical approaches.

VaxSeer's core advantage lies in using large protein language models to learn combinatorial mutation effects (20). Traditional methods analyze single amino acid mutations independently. VaxSeer captures synergistic interactions between multiple mutation sites. This approach better reflects the reality of viral evolution. In 10-year retrospective evaluations, vaccine strains selected by VaxSeer consistently showed superior genetic matching compared to WHO-recommended strains. More importantly, VaxSeer can predict dominant influenza strains months in advance. This provides valuable lead time for vaccine production. Beth-1 employs site-specific mutation fitness modeling (21). The model can calibrate mutation transition times and project fitness landscapes into the future. MAIVeSS compresses vaccine strain selection time from months to days (22). It also predicts yield potential of candidate viruses.

Wastewater surveillance has evolved from a COVID-19 emergency measure into a normalized population-level early warning system. The US CDC's National Wastewater Surveillance System (NWSS) now covers approximately 1,500 monitoring sites (23). The system monitors influenza A/B, RSV, SARS-CoV-2, and H5 avian influenza weekly. The core advantage of wastewater surveillance lies in providing viral concentration data within 24 hours. It captures viral shedding from asymptomatic individuals and those not seeking medical care. Most critically, it detects signals of increased viral activity before clinical cases appear. China conducted RSV wastewater surveillance in four regions: Yingkou, Xi'an, Nanchang, and Nanning. The research team first detected RSV RNA in fecal samples from 300 patients. This established patterns of viral excretion and concentration characteristics in feces. They then developed wastewater models based on these data. The research filled gaps in clinical surveillance. It provided local evidence for RSV vaccination strategy formulation (24). Additionally, China has conducted SARS-CoV-2 wastewater surveillance research. Coverage includes multiple cities such as Beijing, Shanghai, and Shenzhen (25). These studies established multi-level monitoring networks from community to city levels. This provided technical support for early warning and precise epidemic control.

Machine learning prediction models have achieved significant progress in outbreak forecasting. Rodriguez et al. developed feature-based time series classification methods (26). The study developed 32 prediction algorithms for identifying disease outbreak and non-outbreak situations. These algorithms predict by learning characteristic patterns from historical epidemic data. Accuracy rates exceed 90% on real-world datasets. A universal disease risk prediction system demonstrates powerful cross-disease prediction capabilities (27). The system integrates outbreak data from 43 diseases across 206 countries. The research team employed five different machine learning algorithms to build prediction models.

By integrating predictions from these algorithms, system accuracy reaches 80-90%. The system can predict risks across countries and diseases based on economic, cultural, social, and epidemiological factors.

Universal influenza vaccine development is a key breakthrough that will transform long-term prevention landscapes. WHO set clear standards in 2024 (28). Vaccines must work in all age groups, provide protection for at least 3 years against current circulating subtypes, and offer better protection than currently approved seasonal influenza vaccines. Current universal influenza vaccine research focuses primarily on immune targets in conserved viral regions. The EU-funded FLUniversal consortium is developing an intranasal universal influenza vaccine (29). The vaccine employs a primeboost strategy, using attenuated live vaccine strains combined with conserved antigen design to induce broadly protective immune responses. The vaccine is expected to enter clinical trials in 2025. Success of universal vaccines will fundamentally transform influenza prevention strategies. It will eliminate the need for annual vaccine strain updates. It will provide more reliable protection barriers for global influenza pandemic preparedness. This will not only reduce costs of vaccine research and production. It will also ensure more timely protection when novel influenza viruses emerge.

6. Strategic recommendations for global health security

WHO's expansion of GISRS into a comprehensive surveillance platform covering influenza, RSV, and SARS-CoV-2 marks a new era for global surveillance systems. However, significant gaps in surveillance capacity persist between different countries and regions. The international community needs to establish more equitable technology transfer mechanisms. Development of open-source platforms and tools can lower technical barriers and facilitate technology dissemination globally. Data sharing remains a main obstacle to global cooperation. More transparent data governance frameworks need establishment. Clearly defining data usage scope and benefit distribution.

Improving influenza vaccination coverage represents a critical yet underutilized public health intervention. Annual vaccination provides substantial protection, yet global uptake remains insufficient. China's influenza vaccination rate reached only 2.94% in the 2020-2021 flu season compared to 48.4% in the United States (30,31). This disparity reflects broader global inequities. High-income countries reach 40-50% coverage among priority populations. In contrast, only 34% of lowand lower-middle-income countries have policies supporting influenza vaccination, and these countries consume less than 5% of global vaccine supply (32). Seasonal influenza causes an estimated 290,000-650,000 respiratory deaths annually worldwide (33). Scaling up

vaccination programs could substantially reduce disease burden. It would simultaneously strengthen pandemic preparedness infrastructure.

Building a resilient global respiratory disease prevention and control system requires systems thinking. Multi-level surveillance networks form the foundation of resilient systems. Community-level surveillance can detect abnormal signals earliest. National-level surveillance provides a holistic perspective. Globallevel surveillance identifies cross-border transmission risks. Platform-based construction can improve system scalability. New pathogens and new surveillance technologies should be rapidly integrated into existing platforms. Rapid response capability determines system effectiveness. AI prediction technologies can help identify risks in advance. Wastewater surveillance provides early warning signals. But these technical advantages only matter when converted into actual public health actions. Adaptability is the most important characteristic of resilient systems. Systems must be able to continuously learn and improve. Interdisciplinary collaboration can bring innovative solutions. Only in this way can the world be truly prepared. Effectively addressing potential respiratory disease pandemic threats that may emerge in the future.

Funding: This work was supported by grants from the Shenzhen Clinical Research Center for Emerging Infectious Diseases (No. LCYSSQ20220823091203007), the Sanming Project of Medicine in Shenzhen (SZSM202311033), the Special Funds for Strategic Emerging Industry of Shenzhen (F-2022-Z99-502266) and the Shenzhen High-level Hospital Construction Fund.

Conflict of Interest: The authors have no conflicts of interest to disclose.

References

- Del Riccio M, Caini S, Bonaccorsi G, Lorini C, Paget J, van der Velden K, Meijer A, Haag M, McGovern I, Zanobini P. Global analysis of respiratory viral circulation and timing of epidemics in the pre-COVID-19 and COVID-19 pandemic eras, based on data from the Global Influenza Surveillance and Response System (GISRS). Int J Infect Dis. 2024; 144:107052.
- Lee SS, Viboud C, Petersen E. Understanding the rebound of influenza in the post COVID-19 pandemic period holds important clues for epidemiology and control. Int J Infect Dis. 2022; 122:1002-1004.
- Khan T, Das RS, Jaiswal A, Halder S, Majhi RM, Mahato A, Ghosh T, Satpathi P, Bhattacharya SD. Epidemiology and surveillance of influenza, RSV and SARS-CoV-2 in children admitted with severe acute respiratory infection in West bengal, India from 2022 to 2023. BMC Infect Dis. 2025; 25:1047.
- 4. Olivares Barraza MF, Fasce RA, Nogareda F, Marcenac P, Vergara Mallegas N, Bustos Alister P, Loayza S, Chard

- AN, Arriola CS, Couto P, García Calavaro C, Rodriguez A, Wentworth DE, Cuadrado C, Azziz-Baumgartner E. Influenza Incidence and Vaccine Effectiveness During the Southern Hemisphere Influenza Season Chile, 2022. MMWR Morb Mortal Wkly Rep. 2022; 71:1353-1358.
- Franco FC, Souza M, Fernandes SM, Dias AC, Passos YG, Fiaccadori FS. Influenza A, influenza B, and SARS-COV-2 circulation patterns in midwest Brazil during the 2022-2023 period. Braz J Microbiol. 2024; 55:3027-3030.
- 6. Fossum E, Rohringer A, Aune T, Rydland KM, Bragstad K, Hungnes O. Antigenic drift and immunity gap explain reduction in protective responses against influenza A(H1N1)pdm09 and A(H3N2) viruses during the COVID-19 pandemic: a cross-sectional study of human sera collected in 2019, 2021, 2022, and 2023. Virol J. 2024; 21:57.
- Broberg EK, Svartström O, Riess M, Kraus A, Vukovikj M, Melidou A; Members of the European Reference Laboratory Network for Human Influenza (ERLI-Net); Collaborators. Co-circulation of seasonal influenza A(H1N1)pdm09, A(H3N2) and B/Victoria lineage viruses with further genetic diversification, EU/EEA, 2022/23 influenza season. Euro Surveill. 2024; 29:2400020.
- 8. European Centre for Disease Prevention and Control. Intensified circulation of respiratory syncytial virus (RSV) and associated hospital burden in the EU/EEA.https://www.ecdc.europa.eu/en/publications-data/intensified-circulation-respiratory-syncytial-virus-rsv-and-associated-hospital. (accessed September 29, 2025)
- Leija-Martínez JJ, Cadena-Mota S, González-Ortiz AM, Muñoz-Escalante JC, Mata-Moreno G, Hernández-Sánchez PG, Vega-Morúa M, Noyola DE. Respiratory Syncytial Virus and Other Respiratory Viruses in Hospitalized Infants During the 2023-2024 Winter Season in Mexico. Viruses. 2024; 16:1917.
- Abu-Raya B, Viñeta Paramo M, Reicherz F, Lavoie PM. Why has the epidemiology of RSV changed during the COVID-19 pandemic? EClinicalMedicine. 2023; 61:102089.
- 11. Miyama T, Kakimoto K, Yamanaka Y, Nishida Y, Iritani N, Motomura K. Irregular seasonality of respiratory syncytial virus infection persists in 2023 in Osaka, Japan. IJID Reg. 2024; 13:100442.
- 12. Zhao C, Zhang T, Guo L, et al. Characterising the asynchronous resurgence of common respiratory viruses following the COVID-19 pandemic. Nat Commun. 2025; 16:1610.
- Wang C, Yang Y, Wu K, Wang C, Liu W, Zhu Y, Ye L, Li X, Zhou R, Zhu B, Tian X. An Outbreak of Human Adenovirus Infection Among Children Post COVID-19 Pandemic in Southern China. J Med Virol. 2024; 96:e70139.
- 14. Bin Saleh K, Badreldin HA, Alqahtani T, *et al.* Assessing the influence of COVID-19 on influenza prevalence: A multicenter time series study. J Infect Public Health. 2023; 16:1989-1993.
- Baker RE, Park SW, Yang W, Vecchi GA, Metcalf CJE, Grenfell BT. The impact of COVID-19 nonpharmaceutical interventions on the future dynamics of endemic infections. Proc Natl Acad Sci U S A. 2020; 117:30547-30553
- Hirotsu Y, Nagakubo Y, Maejima M, Shibusawa M, Hosaka K, Sueki H, Mochizuki H, Omata M. Changes in Viral Dynamics Following the Legal Relaxation of COVID-19 Mitigation Measures in Japan From Children

- to Adults: A Single Center Study, 2020-2023. Influenza Other Respir Viruses. 2024; 18:e13278.
- Zeng H, Cai M, Li S, Chen X, Xu X, Xie W, Xiong Y, Long X. Epidemiological characteristics of seasonal influenza under implementation of zero-COVID-19 strategy in China. J Infect Public Health. 2023; 16:1158-1166.
- Piret J, Boivin G. Viral Interference between Respiratory Viruses. Emerg Infect Dis. 2022; 28:273-281.
- Luo W, Liu Q, Zhou Y, Ran Y, Liu Z, Hou W, Pei S, Lai S. Spatiotemporal variations of "triple-demic" outbreaks of respiratory infections in the United States in the post-COVID-19 era. BMC Public Health. 2023; 23:2452.
- Shi W, Wohlwend J, Wu M, Barzilay R. Influenza vaccine strain selection with an AI-based evolutionary and antigenicity model. Nat Med. 2025. doi: 10.1038/s41591-025-03917-y.
- Lou J, Liang W, Cao L, et al. Predictive evolutionary modelling for influenza virus by site-based dynamics of mutations. Nat Commun. 2024; 15:2546.
- Gao C, Wen F, Guan M, Hatuwal B, Li L, Praena B, Tang CY, Zhang J, Luo F, Xie H, Webby R, Tao YJ, Wan XF. MAIVeSS: streamlined selection of antigenically matched, high-yield viruses for seasonal influenza vaccine production. Nat Commun. 2024; 15:1128.
- Chan EMG, Boehm AB. Respiratory Virus Season Surveillance in the United States Using Wastewater Metrics, 2023-2024. ACS ES T Water. 2025; 5:985-992.
- 24. Zhang Z, Li Q, He F, Wang Z, Zhu C, Tu J, Li H, Yi L, Deng Y, Fu S. Sewage surveillance revealed the seasonality and prevalence of respiratory syncytial virus and its implications for seasonal immunization strategy in low and middle-income regions of China. Water Res. 270:122828.
- Yang S, Dong Q, Li S, et al. Persistence of SARS-CoV-2 RNA in wastewater after the end of the COVID-19 epidemics. J Hazard Mater. 2022; 429:128358.
- Rodríguez A, Kamarthi H, Agarwal P, Ho J, Patel M, Sapre S, Prakash BA. Machine learning for data-centric epidemic forecasting. Nat Mach Intell. 2024; 6:1122-1131.
- 27. Zhang T, Rabhi F, Chen X, Paik HY, MacIntyre CR. A machine learning-based universal outbreak risk prediction tool. Comput Biol Med. 2024; 169:107876.
- Wang L, Xie Q, Yu P, Zhang J, He C, Huang W, Wang Y, Zhao C. Research Progress of Universal Influenza Vaccine. Vaccines (Basel). 2025; 13:863.
- Cnossen VM, Moreira PCL, Engelhardt OG, et al. Development of an intranasal, universal influenza vaccine in an EU-funded public-private partnership: the FLUniversal consortium. Front Immunol. 2025; 16:1568778.
- Liu XX, Song YF, Zhang ZN, et al. Analysis of estimated reported coverage of influenza vaccine in China in flu season 2014-2021. Chin J Viral Dis. 2023; 13:226-232. (in Chinese)
- 31. Centers for Disease Control and Prevention (CDC). Flu Vaccination Coverage, United States, 2020-2021 Influenza Season. https://www.cdc.gov/flu/fluvaxview/coverage-2021estimates.htm. (accessed October 17, 2025)
- 32. World Health Organization.WHO Seasonal Influenza Vaccine Global Market Study, January 2024. https://www.who.int/publications/m/item/who-seasonal-influenza-vaccine-global-market-study-january-2024. (accessed October 17, 2025)

33. Paget J, Spreeuwenberg P, Charu V, Taylor RJ, Iuliano AD, Bresee J, Simonsen L, Viboud C; Global Seasonal Influenza-associated Mortality Collaborator Network and GLaMOR Collaborating Teams. Global mortality associated with seasonal influenza epidemics: New burden estimates and predictors from the GLaMOR Project. J Glob Health. 2019; 9:020421.

Received October 2, 2025; Revised October 17, 2025; Accepted October 19, 2025.

*Address correspondence to:

Hongzhou Lu, Department of Infectious Diseases, National

Clinical Research Center for Infectious Diseases, Shenzhen Third People's Hospital, 29 Bulan Road, Shenzhen, Guangdong Province 518112, China.

E-mail: luhongzhou@fudan.edu.cn

Peifen Chen, Department of Respiratory Medicine, National Clinical Research Center for Infectious Disease, Shenzhen Third People's Hospital, 29 Bulan Road, Shenzhen, Guangdong Province 518112, China.

E-mail: drcpf@163.com

Released online in J-STAGE as advance publication October 23, 2025.

Review

DOI: 10.5582/ddt.2025.01083

Indicators of a moist wound environment and care to maintain a moist environment for early healing: A scoping review

Mao Kunimitsu^{1,2}, Karin Izumi³, Yume Kawamizu³, Kenshin Takezawa³, Kanon Nishida³, Hitomi Honda³, Yuri Maeda³, Rena Yamauchi³, Risa Yoshida³, Yukari Nakajima¹, Amika Yamada¹, Kanae Mukai¹, Makoto Oe^{1,*}

SUMMARY: Although maintaining a moist environment is important for wound healing, excess moisture can delay wound healing. Furthermore, recommended assessment methods for moist environments in the latest consensus guidelines are subjective. This scoping review aimed to map indicators to assess the moist environment in a wound and summarize the effectiveness of wound healing care in maintaining a moist environment, as assessed using these indicators. We searched four databases, the Medical Literature Analysis and Retrieval System On-Line, Cumulative Index to Nursing and Allied Health Literature, PubMed, and the Japan Medical Abstracts Society database, using a combination of chronic wound- and moisture-related terms. Independent researchers screening the articles based on the inclusion criteria and extracting relevant data afterward. After screening 2,727 articles, eight met the inclusion criteria: original articles/case studies, studies involving patients with chronic wounds, studies on care to maintain a moist wound environment, and studies assessing wound healing and moist wound environment. The articles included in this review demonstrated that dressings that absorb or hydrate exudates and care decisions based on the moisture content of the wound surface were effective care strategies for wound healing. Additional research is required to determine the best objective indicator for the assessment of a moist wound environment because despite the numerous existing indicators, only few reference values for healing have been reported.

Keywords: Chronic wounds, hard-to-heal wounds, maceration, exudate, wound healing

1. Introduction

A chronic wound fails to progress through the normal phases of healing in an orderly and timely manner (1). The condition has a high prevalence, estimated at 2.21 per 1000 individuals (2). In addition, chronic wounds exert significant effects on patients, including prolonged hospitalization (3), decreased quality of life (4), increased medical costs (4), and increased risk of death (5). Thus, preventing delayed wound healing is important in wound management.

In recent years, moist wound treatment has gained widespread acceptance as the gold standard for wound management. Moreover, a moist wound environment leads to faster and better healing. Specifically, it facilitates autolytic debridement, activates collagen synthesis, facilitates and promotes keratinocyte migration over the wound surface, and supports the presence and function of nutrients, growth factors, and other soluble

mediators in the wound microenvironment (6). However, excess moisture causes maceration (skin softening and breakdown due to prolonged moisture exposure) of the peri-wound skin (7). Maceration of the peri-wound skin has a significant effect on wound healing (8,9), and it can reduce the skin barrier function, leading to skin breakdown due to decreased susceptibility to physical injuries (10). Therefore, it is necessary to implement wound care that can maintain a moist environment suitable for wound healing, without insufficient or excess moisture.

The consensus document on wound exudate recommends assessing wound exudates based on gross findings on the wound surface and dressings and considering changes in care accordingly, such as using a more absorbent dressing or more frequent dressing changes (11). However, these assessment methods are generally quite subjective and vary in complexity and ease of use; consequently, no one approach is ideal (12).

¹ Faculty of Health Sciences, Institute of Medical, Pharmaceutical and Health Sciences, Kanazawa University, Ishikawa, Japan;

²Department of Gerontological Nursing/Wound Care Management, Graduate School of Medicine, The University of Tokyo, Tokyo, Japan;

³ School of Health Sciences, College of Medical, Pharmaceutical and Health Sciences, Kanazawa University, Ishikawa, Japan.

In addition, for inexperienced caregivers, making care choices based on the results of these assessments can be difficult.

The questions that guided this scoping review were: "Which indicators can be used to assess moist wound environments?" and "To what extent does the maintenance of a moist environment, as assessed using the evaluated indicators, lead to effective wound healing?" The objectives of this scoping review were to 1) map indicators for assessing the moist environment and 2) summarize the effectiveness of wound healing care in maintaining a moist environment, as assessed using these indicators.

2. Materials and Methods

2.1. Protocol and registration

This review protocol was not registered. This scoping review was performed according to the Preferred Reporting Items for Systematic Reviews and Meta-Analyses extension for Scoping Reviews (PRISMA-ScR) (13).

2.2. Eligibility criteria

The eligibility criteria for this review were as follows: 1) studies investigating patients with chronic wounds; 2) studies on care to maintain a moist wound environment; 3) studies assessing wound healing; and 4) studies assessing a moist wound environment. We included studies that included participants of all ages, regardless of the clinical setting and publication year. The study languages were limited to English and Japanese, and only original articles and case reports were included in the scoping review.

2.3. Information sources

The following bibliographic databases were searched for unlimited periods: Medical Literature Analysis and Retrieval System On-Line, Cumulative Index to Nursing and Allied Health Literature, and PubMed. In addition, we searched the Japan Medical Abstracts Society (JAMAS) database for articles in Japanese.

2.4. Search terms

The following search terms were used: (1. chronic wound, 2. hard-to-heal wound, 3. pressure injuries, 4. pressure injury, 5. leg ulcer, 6. diabetic foot ulcer, 7. ischemic ulcer, 8. ischemic preconditioning, 9. stasis dermatitis, 10. stasis ulcer) AND (1. moist environment, 2. moisture, 3. moist). The same combination of keywords in Japanese was used to search the JAMAS database.

2.5. Selection of sources of evidence

The search results were imported into Rayyan (Qatar Computing Research Institute, Doha, Qatar) and duplicates were eliminated (14). Article titles and abstracts were independently screened by three groups of researchers (KI, YK, KT, and RYa; KN, HH, YM, and RYo; and MK and AY). Articles that did not meet the eligibility criteria were excluded. Subsequently, the remaining full-text articles after the first screening were independently evaluated according to the inclusion criteria by three groups of researchers. Disagreements regarding the study selection were resolved through a discussion.

2.6. Data charting process

A data chart was developed to determine the data items to be extracted through a discussion. Eight authors were divided into pairs (KI and HH, YK and YM, KT and KN, and RYa and RYo), and data were extracted from the selected studies by the authors. Thereafter, the data were verified by 10 authors, including MK and YN. Discrepancies in the extracted data were resolved through discussions.

2.7. Data items

The following data were extracted: (a) study authors, year of publication, and country; (b) study design/participants; (c) wound type; (d) indicator of a moist environment; (e) evaluation methods of the indicators; (f) details of wound care; and (g) outcomes related to wound healing and a moist environment.

2.8. Synthesis of results

Data on study authors, year of publication, country, study design/participants and wound type were shown in Table 1. Studies were grouped according to the type of wound care. These data are presented in Tables 2 and 3.

3. Results

3.1. Selection of sources of evidence

The initial search yielded 2,727 studies, and after the removal of the duplicate studies, 2,265 studies remained. After subsequent title and abstract screening, 2,197 articles were excluded. Sixty studies were further excluded because they failed to meet the inclusion criteria for full-text screening. Thus, eight articles were included in the scoping review. Figure 1 presents the PRISMA-ScR flowchart used in this review.

3.2. Characteristics of sources of evidence

Table 1. Characteristics of the included studies	aded studies		
Study author/year/country	Study design	Participants	Wound type
Furuta et al., 1997, Japan (in Japanese) ¹⁹	Case report	N=4 A 75-year-old male, 58-year-old male, 61-year-old male, and 60-year-old female	Pressure injuries on the sacrum
Nagata <i>et al.</i> , 2000, Japan (in Japanese) ²⁰	Case report	N=2 A 50-year-old male and an 86-year-old female (Both with poor respiratory and nutritional conditions)	Pressure injuries, classified as stage IV (IAET classification), on the sacrum
Meuleneire et al., 2007, Germany ¹⁵	Prospective observational study	$N=74$ The mean age was 69.5 years (± 18); 45 women (61%) and 29 men (39%) participated.	Venous leg ulcers, arterial leg ulcers, mixed leg ulcers, pressure injuries, diabetic foot ulcers, tumors, acute traumatic wounds, burns, and others (e.g. split-thickness skin graft donor site)
Tachi <i>et al.</i> , 2008, Japan (in Japanese) ²²	Pre-post comparison study	N=50 The average age was 77.3 years (SD = 13.22); 29 women (58%) and 21 men (42%) participated.	Pressure injuries on the sacrum Venous leg ulcers, arterial leg ulcers, mixed leg ulcers, pressure injuries, and diabetic foot ulcers.
Ivins et al., 2018, Germany ¹⁶	Prospective observational study	N=15 The average age was 64.6 years (SD = 15.2); five women (33.3%) and 10 men (66.7%) participated.	Wound exudation was "heavy" in three (20%), "moderate-to-low" in 11 (73.3%), and "light" in one (6.7%) wound.
Koyanagi <i>et al.</i> , 2019, Japan ²¹	Prospective cohort study	N=16 The mean age of three groups ranged from 78 to 86 years; 50% or more of participants were male.	Pressure injuries (at a depth deeper than the dermis) diagnosed as being in a critical colonization state by a dermatologist or wound ostomy continence nurses. Critical colonization is a condition characterized by the absence of evident symptoms of infection and an intermediate state between colonization and overt infection.
Forder <i>et al.</i> , 2020, Poland ¹⁷	Pre-post comparison study	N = 53. There is no data on the characteristics of the participants.	Pressure injuries, diabetic foot ulcers, leg ulcers, surgical wounds, trauma wounds, and burns.
Zahel <i>et al.</i> , 2022, Germany ¹⁸	Prospective observational study	N=44 The average age was 66.9 years (SD = 15.94); 22 women (50%) and 22 men (50%) participated.	Venous leg ulcers, mixed leg ulcers, and diabetic foot ulcers
IAET, International Association for Enterostomal Therapy; SD, Standard deviation.	ostomal Therapy; SD, Standard dev	iation.	

Table 2. Car	Table 2. Care decision based on wound moisture content	und moisture content			
Study author	Objective indicators for a moist environment	Subjective indicators for a moist environment	Evaluation methods of the indicators	Wound care	Outcomes
Furuta et al. ¹⁹	Moisture content of the NA wound surface	NA	During wound care, the moisture content was measured by applying the Moisture Checker® (Scalar Corporation, Japan) to the wound surface.	During wound care, the moisture Based on the moisture content, a prescription was selected from content was measured by seven types of topical agents capable of absorbing or supplying applying the Moisture Checker® moisture. Film dressings (Bioclusive®, Smith & Nephew, UK) or (Scalar Corporation, Japan) to polyurethane foam dressings (Hydrocoll®, Paul Hartmann AG, the wound surface. Germany) were used and generally replaced once daily.	By maintaining the moisture content at about 70%, the wound area of Case 1 (category 3) went from 7.0 cm × 5.0 cm to 2.0 cm × 2.0 cm after 1 month of treatment; Case 2 (category 4) healed from 10.0 cm × 7.5 cm in 4 months; Case 3 (category 4) healed from 10.0 cm × 8.0 cm in 4 months; and Case 4 (category 4) improved from 12.0 cm × 6.7 cm to 6.0 cm × 7.5 cm in 4 months.
Nagata <i>et al</i> . ²⁰	Moisture content of the wound surface	The degree of exudate absorption by the gauze	The moisture content was measured immediately after removing a wound dressing by applying the Moisture Checker* (Scalar Corporation, Japan) to the wound surface.	Based on the amount of wound exudate, the moisture content of the topical agents, moisture absorption capacity of the base material of the topical agents, and moisture content of the wound surface, a prescription was selected from seven types of topical agents capable of absorbing or supplying moisture. After cleaning the wound with saline and disinfecting with iodine, Bescitin WA (Kobayashi Pharmaceutical Co., Ltd., Japan) was applied, followed by the application of ointment, gauze, and film dressing (Bioclusive®, Smith & Nephew, UK).	In Case 1, the wound area reduced from 8.0×6.0 cm to 3.5×2.5 cm after 5 months of treatment selected based on the degree of exudate. In Case 2, by maintaining the moisture content at $60-70\%$, the wound area decreased from 11.0×8.0 cm to 1.0×0.5 cm after 5 weeks of treatment.
NA, Not Appli.	NA, Not Applicable; UK, United Kingdom of Great Britain and Northern Ireland.	n of Great Britain and No	rthern Ireland.		

Z

Table 3. Application of dressings to manage wound exudates

	0	0			
Study author	Objective indicators for a moist environment	Subjective indicators for a moist environment	Evaluation methods of the indicators	Wound care	Outcomes
Meuleneire <i>et al.</i> ¹⁵	Maceration	Ϋ́Z	At each dressing change, the investigators evaluated the condition of the wound and perilesional skin. Overall, five dressing changes were documented, or until complete healing occurred.	Hydroactive-impregnated dressing (Hydrotul, Paul Hartmann AG, Germany) was used in accordance with the manufacture's recommendations. In the majority, there was a 2–3 day interval between the dressing changes.	The wound size decreased from 4.7cm (SD±4.3) × 3.2cm (SD±3.4) to 2.9cm (SD±4.1) × 2.1cm (SD±2.9). Twenty-two (29%) wounds were completely healed by the observation period. The percentage of perilesional skin without maceration increased from 43% (32 wounds) to 66% (49 wounds) at the final examination.
Tachi <i>et al.</i> .	Υ	Level of lateral leakage of wound exudate from the wound dressing	If there was no lateral leakage from the wound dressing, it was classified as a "marked effect." If there was minimal leakage, it was classified as "effective." If there was frequent leakage, it was classified as "ineffective." The researcher evaluated and recorded this every week.	After cleaning with sterile saline, Carboxymethylcellulose Sodium Silver (Aquacel® Ag, ConvaTec, USA) was applied and covered with gauze or a film dressing. The dressing was changed according to the amount of exudate (ranging from daily changes to a maximum of 7 days). Surgical debridement was performed as an adjunctive therapy when necessary. The treatment period was 8 weeks.	During the observation period, 14 cases (35.9%) healed. The average wound area contraction rate was 63.9%, with an average contraction area of 0.64 cm² per week. The level of lateral leakage of wound exudate from the wound dressing was rated as effective or marked effective in 44 of 49 cases (89.7%).
Ivins et al. ¹⁶	Maceration	Level of exudate absorption and wound hydration by dressing	The clinician conducted a visual assessment for maceration; a relative score was used to score maceration of 0 (no maceration), 1 (minimal maceration), 2 (moderate maceration), and 3 (excessive maceration and need to withdraw patient from study). In addition, they evaluated the effectiveness of the dressing, and presence of copious wound exudates was monitored at each dressing change.	After wound cleansing and sharp debridement if necrotic tissue was present, a gelling fiber dressing, which is made from sodium carboxymethyl cellulose and strengthening cellulose fibers (Biosorb, Acelity, UK) was applied in addition to standard of care. Wounds were treated until healing or for a maximum of 4 weeks.	During 4 weeks of treatment, granulation was completed in eight wounds (53.3%), 75% coverage in two wounds (13.3%), 50% coverage in three wounds (13.3%), and 25% coverage in two wounds (13.3%). No maceration was found in 10 (66.7%) wounds and minimal maceration in five (33.3%) wounds. Dressing's ability to absorb and retain wound exudates was rated "excellent" or "very good " in 80% of cases, "moderate" in 10%, and "poor" in 10%.

NA, Not Applicable; UK, United Kingdom of Great Britain and Northern Ireland; USA, the United States of America.

Table 3. Application of dressings to manage wound exudates (continued)

J J	10		(
Study author	Objective indicators for a moist environment	Subjective indicators for a moist environment	Evaluation methods of the indicators	Wound care	Outcomes
Koyanagi et al. ²¹	Change rate of exudate volume; change rate of the difference in the stratum corneum hydration between healthy skin and ulcersurrounding skin	NA	Exudate volume was measured by the ESTimation method, which estimates daily exudate volume (mL) using a regression equation utilizing several sub-scores of DESIGN-R®, which is a tool to score the severity of pressure ulcers. The stratum corneum hydration of the skin surrounding wounds was measured using a portable moisture meter (Mobile Moisture HP10-N®, Integral Co., Japan).	Group A, hydrating ointment with infection control or low exudate-absorption dressing material; Group B, high exudate-absorption dressing material; and Group C, hydrating ointment with exudate-absorption and infection control. Wounds were assessed at two time points: at baseline and after 1 week.	The total score of DESIGN-R was lower in Group C than in the other groups, indicating a lower effect on wound healing (Group A: -0.12 vs. Group B: -0.11 vs. Group C: -0.01). The median change rate of exudate volume was 0 in each group. Regarding the change rate of the difference in the stratum corneum hydration, the sum of the negative values in Group A was 0.52, and the sum of the values in Groups B and C were different (-0.97 and -0.87, respectively).
Forder et al. ¹⁷	Maceration	Level of moist environment maintenance via dressing	Y-Y	After evaluating the wound, silicone-form dressing was used based on the exudate level (ActivHeal® Silicone Foam [Advanced Medical Solutions Ltd., Cheshire, UK] was used for wounds with moderate to heavy exudate levels, and ActivHeal® Silicone Foam Lite [Advanced Medical Solutions Ltd.] was used for wounds with low exudate levels.) Wound healing was evaluated after 6 weeks.	The number of macerated cases decreased. More than 90% of users rated the maintenance of moist environment as "satisfied" or "very satisfied." [ActivHeal* Silicone Foam] The mean wound length, width, and depth were 4.2 cm, 2.6 cm, and 0.2 cm, respectively at baseline; at the end of the evaluation the values were 3.4 cm, 1.8 cm, and 0.2 cm, respectively. The number of macerated cases decreased. [ActivHeal* Silicone Foam Lite] The mean wound length, width, and depth were 3.4 cm, 1.9 cm, and 0.2 cm, respectively, at baseline; at the end of the evaluation the values were 2.7 cm, 1.4 cm, and 0.1 cm, respectively.
Zahel et al. ¹⁸	Maceration	Level of exudate absorption and wound hydration via dressing	Exudation and wound hydration were evaluated through interviews with participating physicians and care specialists.	Patients used bacterial cellulose hydrogel dressings (hydroactive BC wound dressing, Smith & Nephew, UK). There are no details regarding the application method.	There was a significant reduction in the mean wound size and depth over the study period of 28 days ($p < 0.006$). The case of healthy peri-wound skin was significantly increased. Users rated the exudate uptake as "good" to "satisfactory" and wound hydration as "good."

NA, Not Applicable; UK, United Kingdom of Great Britain and Northern Ireland; USA, the United States of America.

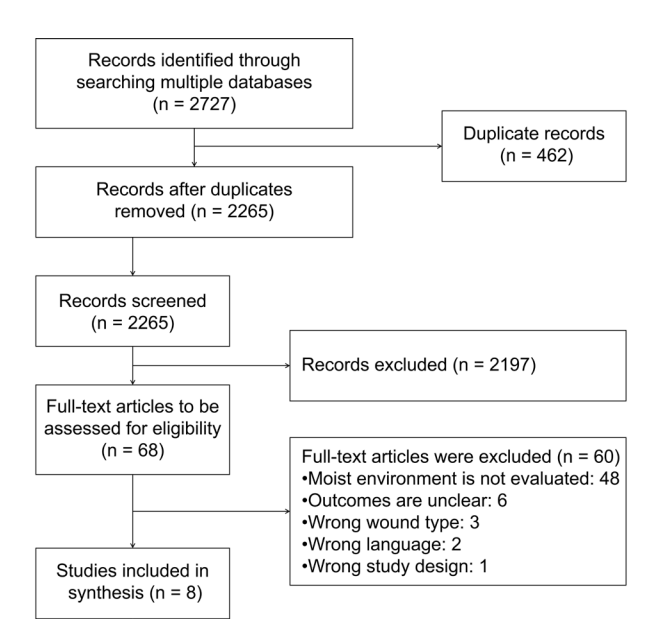


Figure 1. Flow chart of the present scoping review.

The characteristics of the included studies are summarized in Tables 1. Six of the studies were original articles and two were case studies. The included studies were published between 1997 and 2022, and they were conducted in Japan (four studies), Germany (three studies), and Poland (one study).

The number of participants in the studies was 2–74 (Table 1). Regarding wound types, seven studies focused on pressure injuries, four on diabetic foot ulcers, three on venous leg ulcers, and three on mixed leg ulcers. Some studies focused on more than one wound type (15-18).

3.3. Synthesis of results

3.3.1. Indicators of a moist environment

Four objective indicators were reported (Tables 2 and 3): the moisture content of the wound surface (19,20); number of maceration cases (15-18); change rate of exudate volume (21); and change rate of the difference in the stratum corneum hydration between healthy and ulcer-surrounding skin (21). In addition, five subjective indicators were reported: the degree of exudate absorption by the gauze (20); level of lateral leakage of wound exudate from the wound dressing (22); level of exudate absorption by dressing (16,18); level of moist environment maintained via dressing (17); and level of wound hydration via dressing (16,18). These indicators were evaluated by raters such as clinicians. Among these indicators, only the moisture content of the wound surface was mentioned as effective for wound healing, which was recommended to maintained at approximately 60-70% (19,20).

3.3.2. Care decision based on wound moisture content

Two studies evaluated the moisture content of the wound surface, and medications were selected to either supply or absorb moisture to regulate wound surface moisture (Table 2). Consequently, it was confirmed that maintaining a moisture content of approximately 70% led to reduced wound area (19,20).

3.3.3. Application of dressings to manage wound exudates

Six studies were conducted on dressings for the management of wound exudates (Table 3). The dressings investigated were a hydroactive triglyceride-based carboxymethylcellulose granules-containing dressing (15); sodium carboxymethylcellulose silver-containing dressing (22); gelling fiber dressing made from sodium carboxymethylcellulose and strengthening cellulose fibers (16); dressing made of polyurethane foam pad and hydrophobic soft silicone layer (17); and carbohydrate polymer bacterial cellulose dressing (18). The use of these dressings resulted in a reduction in wound size (15,17,18), improvement in wound area contraction rate (22), and granulation formation (16). In addition, a decrease in maceration cases associated with the use of these dressings was reported (15-18). Furthermore, users rated high the lateral leakage of wound exudates from the wound dressing (22), exudate absorption and wound hydration (16,18), and maintenance of a moist wound environment (17).

4. Discussion

4.1. Summary of evidence

This is the first scoping review summarizing the available evidence on indicators for assessing moist wound environments and its effectiveness on wound healing. We identified six original studies and two case studies published between 1997 and 2022. Nine objective and subjective indicators were used to evaluate the moist environment. In addition, two categories of care for maintaining a moist wound environment were reported: care decisions based on wound moisture content and the application of dressings to manage wound exudates, both of which were highly effective in wound healing.

4.2. Indicators of a moist wound environment

In the studies included in this review, the indicators of a moist wound environment included not only subjective assessments, which may vary among raters, but also objective assessments. In particular, the measurement of the moisture content of the wound surface allows easy real-time and non-invasive assessment by anyone who learns how to use the measurement device (19). Furthermore, the moisture content of the wound surface was the only indicator for which a reference value suitable

for healing was mentioned (19,20). Thus, it is likely to be highly useful for wound management. However, because a wide variety of indicators were reported in the literature, this review alone cannot determine the most effective indicator for moist environment assessment. Moreover, because most indicators lack reference values for healing, it is difficult to incorporate them into treatment decisions. Therefore, it is necessary to compare objective indicators to clarify the most useful indicators for maintaining a moist wound environment and investigate the reference values of these indicators.

4.3. Care to maintain a moist wound environment

Two studies investigated topical agents that supply or absorb moisture based on the measurement of the moisture content of the wound surface (19,20). These studies confirmed wound reduction and healing, indicating the appropriateness of the care decision. In addition, wearable devices have recently been developed to measure the moisture content of the wound surface and wound dressing (23,24). Based on these results, the moisture content of the wound surface will increasingly become a simple and effective indicator for assessing a moist wound environment. However, the number of individuals investigated in these studies was four in one study (19) and two in the other study (20). Thus, there is insufficient evidence to suggest that moisture content is the best indicator for assessing a moist wound environment. Therefore, measurement of moisture content and care protocols based on this assessment need to be established in studies with larger sample sizes.

Dressings have been investigated as the primary method of wound care for maintaining a moist environment and promoting early wound healing. In the studies included in this review, the use of dressings incorporating materials with exudate absorption and hydration functions, such as carboxycellulose (15,22), gelling fibers (16), polyurethane foam (17), and bacterial cellulose (18), prevented complications, such as maceration, and delayed healing owing to excess moisture in the wound environment. Thus, as recommended by a previous consensus document (11), the use of dressings with high absorbency and excellent moisture hydration are likely to be effective in maintaining a moist environment. However, the studies included in this review focused on comparisons with standard treatments; thus, the criteria for dressing selection were not clear. Therefore, studies that compare dressings that absorb and hydrate exudates to identify the dressing that is most effective in maintaining a moist environment are warranted.

4.4. Limitations of the included literature

Most studies included in this review were case reports, cohort studies, or pre-post comparison studies with small sample sizes, yielding relatively low levels of evidence. Therefore, randomized controlled trials with high levels of evidence are required to validate the identified indicators that can assess moist environments suitable for early wound healing. As such, no specific indicators or care methods can currently be recommended based on the existing literature.

Furthermore, the studies span a long time period, from 1997 to 2022; caution is therefore warranted regarding potential variations in results due to differences in study periods and advances in wound care technologies. Notably, studies reporting care selection based on indicators of a moist environment were limited to only a few early studies published in 1997 (19) and 2000 (20); as such, whether similar results would be obtained with current wound care products and assessment devices remains unclear. Therefore, further validation using modern products and technologies is warranted.

In addition, the included studies were geographically concentrated in Japan (n = 4), Germany (n = 3), and Poland (n = 1), with no reports from other regions in Africa, the Americas, or Oceania. Given the potential differences in race, culture, and medical practices across regions, caution is required when generalizing these findings, and further studies from diverse countries are desirable.

4.5. Limitations of the review

This scoping review had some limitations. The review focused on studies in English and Japanese languages, therefore, results from studies in other languages were excluded. Thus, there may be bias in the race, healthcare system, and cultural background of the target population. In addition, the eligibility criteria in this review included that the study assessed both wound healing and the moist wound environment. Accordingly, studies that examined dressings to manage exudates were excluded except they did not assess the moist environment.

5. Conclusion

This scoping review summarized the indicators for assessing the moist environment and the effectiveness of wound healing care in the maintenance of a moist environment. The articles included in this review showed that the application of dressings that absorb or hydrate exudates and care decisions based on the moisture content of the wound surface are effective in wound healing. However, there are a variety of indicators for assessing a moist environment, and further studies comparing the objective indicators are warranted.

Acknowledgements

We would like to thank Editage (https://www.editage.

com) for the language editing and review of this manuscript.

Funding: This study was supported by grants from JSPS KAKENHI (JP 24K20272).

Conflict of Interest: The authors have no conflicts of interest to disclose.

References

- Youn C, Archer NK, Miller LS. Research techniques made simple: Mouse bacterial skin infection models for immunity research. J Invest Dermatol. 2020; 140:1488-1497.e1.
- 2. Martinengo L, Olsson M, Bajpai R, Soljak M, Upton Z, Schmidtchen A, Car J, Järbrink K. Prevalence of chronic wounds in the general population: systematic review and meta-analysis of observational studies. Ann Epidemiol. 2019; 29:8-15.
- Nakagami G, Morita K, Matsui H, Yasunaga H, Fushimi K, Sadana H. Association between pressure injury status and hospital discharge to home: a retrospective observational cohort study using a national inpatient database. Ann Clin Epidemiol. 2020; 2:38-50.
- Demarré L, Van Lancker A, Van Hecke A, Verhaeghe S, Grypdonck M, Lemey J, Annemans L, Beeckman D. The cost of prevention and treatment of pressure ulcers: A systematic review. Int J Nurs Stud. 2015; 52:1754-1774.
- Bauer K, Rock K, Nazzal M, Jones O, Qu W. Pressure ulcers in the United States' inpatient population from 2008 to 2012: Results of a retrospective nationwide study. Ostomy Wound Manag. 2016; 62:30-38.
- Nuutila K, Eriksson E. Moist wound healing with commonly available dressings. Adv Wound Care. 2021; 10:685-698.
- Anderson K, Anderson LE, Glanze WD. Mosby's medical, nursing and allied health dictionary. St. Luiis: Mosby-Year Book Inc; 1998.
- Haryanto H, Arisandi D, Suriadi S, Imran I, Ogai K, Sanada H, Okuwa M, Sugama J. Relationship between maceration and wound healing on diabetic foot ulcers in Indonesia: a prospective study. Int Wound J. 2017; 14:516-522
- Tsuchiya S, Suriadi, Sanada H, Sugama J, Oe M. Relationship between items of DMIST and healing of diabetic foot ulcers. Int Wound J. 2023; 20:345-350.
- Cutting KF, White RJ. Maceration of the skin and wound bed 1: its nature and causes. J Wound Care. 2002; 11:275-278.
- Harding K, Carville K, Chadwick P, Moore Z, Nicodème M, Percival S, Romanelli M, Schultz G, Tariq G. Wound exudate: effective assessment and management. WUWHS consensus document. Wounds Int. 2019; 1-34.
- Iizaka S, Sanada H, Nakagami G, Koyanagi H, Konya C, Sugama J. Quantitative estimation of exudate volume for full-thickness pressure ulcers: the ESTimation method. J Wound Care. 2011; 20:453-463.

- Tricco AC, Lillie E, Zarin W, et al. PRISMA extension for scoping reviews (PRISMA-ScR): Checklist and explanation. Ann Intern Med. 2018; 169:467-473.
- Ouzzani M, Hammady H, Fedorowicz Z, Elmagarmid A. Rayyan-a web and mobile app for systematic reviews. Syst Rev. 2016; 5:1-10.
- Meuleneire F, Zoellner P, Swerev M, Holfeld O, Effing J, Bapt S, Tholon N, Felder E, Streit B, Kapp H, Smola H. A prospective observational study of the efficacy of a novel hydroactive impregnated dressing. J Wound Care. 2007; 16:177-182.
- Ivins N, Braumann C, Kirchhoff JB, Waldemar U, Jones NJ. Use of a gelling fibre dressing in complex surgical or chronic wounds: a case series. J Wound Care. 2018; 27:444-454.
- 17. Forder R, Burns R. Post-market clinical evaluation of the safety and performance of activheal® silicone foam and activheal® silicone foam lite dressings. Wounds UK. 2020; 16:68-76.
- Zahel P, Beekmann U, Eberlein T, Schmitz M, Werz O, Kralisch D. Bacterial cellulose — Adaptation of a natureidentical material to the needs of advanced chronic wound Care. Pharmaceuticals. 2022; 15:683.
- 19. Furuta K, Okuda S, Tetsumasa U. Conservative treatment based on measurement of moisture content of pressure ulcer surfaces. CHIRYO. 1997; 79:185-192. (in Japanese)
- Nagata M. Some observation on the choice of drugs for severe pressure ulcers. Japanese J Press Ulcers. 2000; 2:316-323. (in Japanese)
- 21. Koyanagi H, Kitamura A, Nakagami G, Sanada H, Sugama J. Prospective study on local wound management of pressure ulcers in a critical colonization state. J Wellness Health Care. 2019; 42:23-32.
- Tachi M, Hirabayashi S, Kajiyama W, Hisano C, Shimoda M, Naritomi Y, Tsujita J. Assessment of the clinical effect of sodium carboxymethylcellulose primary wound dressing containing silver on decubitus ulcers: A multicenter open trial. Japanese J Press Ulcers. 2008; 10:561-572. (in Japanese)
- McColl D, Cartlidge B, Connolly P. Real-time monitoring of moisture levels in wound dressings *in vitro*: An experimental study. Int J Surg. 2007;5:316-322.
- 24. Milne SD, Seoudi I, Hamad H Al, Talal TK, Anoop AA, Allahverdi N, Zakaria Z, Menzies R, Connolly P. A wearable wound moisture sensor as an indicator for wound dressing change: An observational study of wound moisture and status. Int Wound J. 2016; 13:1309-1314.

Received August 13, 2025; Revised October 7, 2025; Accepted October 12, 2025.

*Address correspondence to:

Makoto Oe, Faculty of Health Sciences, Institute of Medical, Pharmaceutical and Health Sciences, Kanazawa University, 5-11-80 Kodatsuno, Kanazawa, Ishikawa 920-0942, Japan. E-mail: moe-tky@umin.ac.jp

Released online in J-STAGE as advance publication October 16, 2025.

Review

DOI: 10.5582/ddt.2025.01092

Food, medicine, and cosmetic homology: A comprehensive review of bioactive components, functions, and applications of *Torreya grandis*

Xiaoyan Cui^{1,2}, Chuanyin Shi^{1,2,*}, Yan Sun^{2,3,*}

SUMMARY: *Torreya grandis* (*T. grandis*) is one of the evergreen tree species in China. The kernels of *T. grandis* have been used as traditional medicine and food for thousands of years in China. In recent years, it has also been developed as raw materials for cosmetics. *T. grandis* is rich in bioactive components, including unsaturated fatty acids, vitamins, protein, amino acids, trace elements, minerals, polyphenols, squalene, phytosterol, terpenes, *etc.* Therefore, *T. grandis* possesses a wide range of biological activities such as anti-oxidation, anti-inflammation, microbiota alteration, effects on blood pressure, blood glucose and lipids, neuroprotective effect, brightening, reducing uric acid (UA) level, ameliorating bone metabolism disorders, alleviating slow transit constipation, and antinociceptive activity. This review presents a comprehensive analysis of *T. grandis* on its active components and functions, and explores its existing and potential applications in food, medicine, and cosmetics.

Keywords: Anti-oxidation, anti-inflammation, unsaturated fatty acids, microbiota alteration

1. Introduction

Torreya grandis (T. grandis, Taxaceae) is an evergreen economic tree species in China. It is a tertiary relict plant and belongs to gymnosperms. With a cultivation history over 1,000 years (1), the kernels of T. grandis have been used as traditional medicine and food since ancient time. T. grandis is an important component of many classical prescriptions to expel intestinal parasites, prevent hair loss, and relieve cough (2). The first credible medical record of T. grandis appeared in the Classic of the Materia Medica during the Three Kingdoms era of China and dated back to the 3rd century AD (3). More than 400 years ago, the Compendium of Materia Medica listed T. grandis nuts as a prescription for repelling internal parasites, preventing hair loss, and relieving sudden hematemesis. For thousands of years, the components, biological activities and functions of T. grandis have been developed and applied (Figure 1).

T. grandis fruit includes a thick layer of soft peel (aril), seed coat, and kernel, each structure contains different bioactive components. T. grandis comprises abundant unsaturated fatty acids, tocopherol, amino acids, trace elements, minerals, polyphenol, squalene, phytosterol, terpenoid, etc. which accounts for its various beneficial

functions (4) (Figure 2). Modern pharmacological studies showed that *T. grandis* extracts or its main components have biological activities such as antioxidation, anti-inflammation, microbiota regulation, angiotensin-converting enzyme inhibitory (ACE-I) activity, tyrosinase inhibition, lowering blood glucose, regulating blood lipids, and protecting nerve activities (5-8). This review summarizes recent research progresses of bioactive components and biological functions of *T. grandis*, providing theoretical basis for *T. grandis* in the development of related food, medicine, and cosmetics.

2. Bioactive components of T. grandis

It takes 17 months for the seed of *T. grandis* to reach maturity and the oil content of *T. grandis* kernel varies enormously in different *T. grandis* landraces (11.15%-59.47%) (9,10). In *T. grandis*, biotin carboxylase (BC), acyl-ACP thioesterase A (FATA), diacylglycerol acyltransferase (PDAT), and TgLBD40 exert significant influence on its oil accumulation (9). The expression level of TgLBD40 and oil concentration both increase during the kernel development and reach the highest level in September (3,11). Hence, the optimal harvest time of *T. grandis* fruits is mid-September (11,12) while

¹ Shanghai University Mengchao Cancer Hospital, Shanghai, China;

² Shanghai Cell Therapy Group Co., Ltd., Shanghai, China;

³ School of Medicine, Shanghai University, Shanghai, China.

TIMELINE

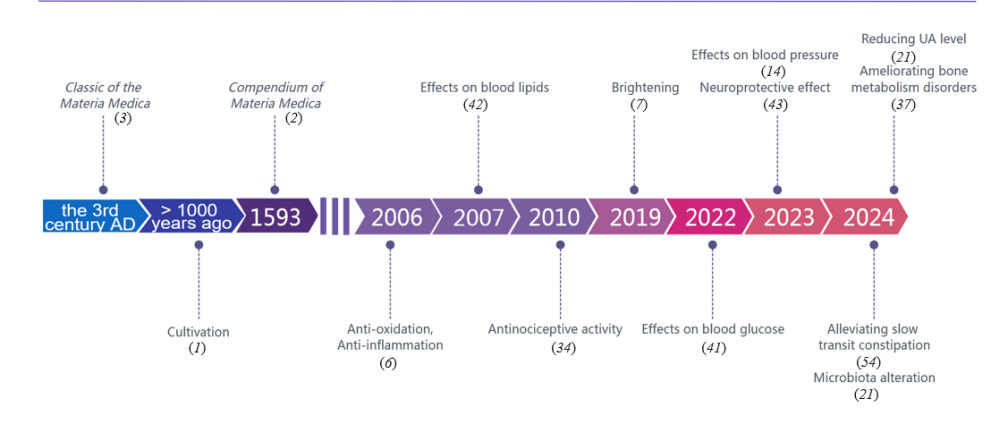


Figure 1. For thousands of years, the biological activities and functions of *T. grandis* have been developed and applied. Created with MedPeer (medpeer.cn)

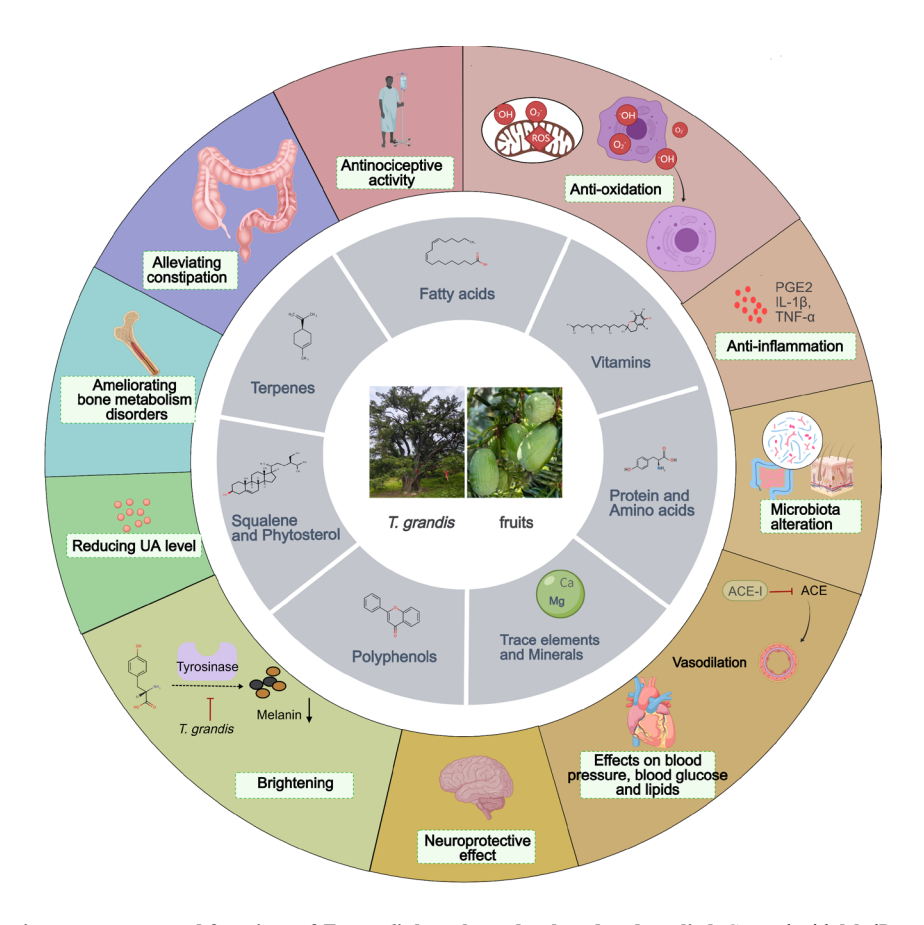


Figure 2. The bioactive components and functions of T. grandis have been developed and applied. Created with MedPeer (medpeer.cn)

the actual harvest time may still vary by weeks due to regional climate changes.

2.1. Fatty acids

T. grandis kernel is rich in unsaturated fatty acids, especially oleic acid, linoleic acid (11), and sciadonic acid (3). The total unsaturated fatty acid content is more than 80% in T. grandis kernel oil (3,13) among which linoleic acid is the highest (Table 1). The polyunsaturated

fatty acids are the main bioactive components as they have multiple medicinal properties, including antiinflammation and anti-atherosclerotic (*II*).

2.2. Vitamins

T. grandis contains several kinds of vitamins, including vitamin B_1 , vitamin B_2 , vitamin B_3 , nicotinic acid, folic acid, and tocopherols. Tocopherols account for the highest content and possess potent antioxidant effects

Table 1. Major fatty acids in T. grandis kernel oil

Fatty acids	T. grandis kernel oil (%)	References
Palmitic acid (C16:0)	3.23-10.44	11; 5 ; 13; 57; 58
Stearic acid (C18:0)	2.20-6.07	11; 5; 13; 57; 58
Oleic acid (C18:1)	25.50-34.85	11; 5; 13; 57; 10
Linoleic acid (C18:2)	25.94-46.80	11; 5; 13; 57; 10
Linolenic acid (C18:3)	0.45- 17.12	11; 5; 13; 56; 10; 58
Eicosanoic acid (C20:0)	0.00-0.18	11; 5; 13; 56
cis-11-eicosenoic acid (C20:1)	0.50-1.33	11; 5; 13; 56; 58
cis-11,14-eicosadienoic acid (C20:2)	2.08-4.40	11; 5; 13; 56; 58
cis-5,11,14-eicosatrienoic acid (C20:3)	8.35- 13.93	11; 3; 5; 13; 10
Unsaturated fatty acid (UFA)	87.28-90.84	11; 5; 13
Monounsaturated fatty acid (MUFA)	26.00-35.44	11; 13
Polyunsaturated fatty acid (PUFA)	49.16-61.50	11; 13; 58
Saturated fatty acid (SFA)	11.33-16.80	11; 5; 13; 58
Free fatty acids (FFA)	0.23±0.02 mg/g	11

which can scavenge reactive oxygen species and free radicals as well as inhibit membrane lipid peroxidation (11). Therefore, tocopherols have a protective effect on cells. The total tocopherol contents vary enormously in different T. grandis cultivars (0.28-167.31 mg/100 g) (Table 2) and β -tocopherol is the major type. In the tocopherol accumulation of T. grandis kernels, homogentisate phytyltransferase coding gene (TgVTE2b) and γ -tocopherol methyltransferase coding gene (TgVTE4) may be highly associated (12).

2.3. Protein and amino acids

Protein is one of the main nutritional components in *T. grandis* kernel. The protein content of *T. grandis* seeds varies from 10.34% to 25.30% depending on the cultivar (11,14). *T. grandis* kernel proteins consist of 20 kDa to 43 kDa peptides. Bioactive peptides possess antioxidant and ACE-I activities (15).

T. grandis kernel contains 16 amino acids, with a total amino acid content of 12.3 g/100 g(I). It contains eight of the nine essential amino acids for human body: leucine, valine, lysine, isoleucine, phenylalanine, threonine, histidine, methionine. The mass proportion of essential amino acids accounts for 38.6% of the total amino acids in T. grandis kernels which meets the standards for high-quality protein stipulated by FAO/WHO.

2.4. Trace elements and minerals

Trace elements and minerals are essential nutrients that sustain fundamental physiological homeostasis in the human body, and are critically involved in metabolism, normal growth, and development. *T. grandis* is abundant in both Mg and Ca with similar concentration in the nut: 1,045.88~1,846.82 mg/kg (Mg) and 948.21~1,459.74 mg/kg (Ca) (*16*). Besides, *T. grandis* also contains Fe, Co, Cu, Zn, Se.

2.5. Polyphenols

Table 2. Tocopherol composition and content in *T. grandis* kernel oil

Tocopherols	mg·100 g ⁻¹	References
α-tocopherol	0.04 -33.30	11;12; 13; 56
β-tocopherol	0.23-133.75	11;12; 13; 56
γ-tocopherol	0.00-0.26	11;12; 13; 56
δ-tocopherol	ND	11;12; 13; 56
Total tocopherol	0.28-167.31	11;12; 56

T. grandis is rich in polyphenols, including flavonoids, phenolic acids, etc. Flavonoids are a very important class of bioactive compounds with high antioxidant, antiinflammatory, and antibacterial activities in T. grandis kernels. Compounds in T. grandis kernels that highly correlated with antioxidant activity include hesperetin, naringenin, and quercetin (17). Hesperetin can inhibit oxidative stress, neuroinflammation, apoptotic cell death, and cognitive consolidation by regulating Tolllike receptor 4 (TLR4) / nuclear factor-kappa B (NFκB) signal pathway (18). Naringenin and quercetin possess anti-inflammatory and antiallergic activities in mice and have therapeutic potential for sepsis, fibrosis, and cancer caused by inflammation (19). The main components of flavonoids vary among different varieties of T. grandis, and the content and diversity of flavonoids were more ample in T. grandis 'Shishengfei' compared to T. grandis 'Xifei' (20). The unigenes encoding chalcone synthase (CHS), dihydroflavonol 4-reductase (DFR), and anthocyanidin synthase (ANS) serve as critical regulators of flavonoids biosynthesis (17). Phenolic acids in T. grandis kernels include gallic acid, shikimic acid, sinapinic acid (7), 4-hydroxybenzoic acid, carnosic acid, and caffeic acid (21) which all possess high antioxidant activities.

2.6. Squalene and phytosterol

Squalene and β -sitosterol are considered pharmacologically significant in antimicrobial, anti-inflammatory, anti-oxidative, anticancer, and

immunomodulating effects (22). Also, squalene is an important constituent of skin-care products, oxidation-resistant industrial lubricants, and numerous vaccines (23). Squalene is widely used in the cosmetic industry due to its moisturizing and antioxidant properties on the skin (24). Additionally, β -sitosterol is one of the most important phytosterols and is considered to reduce cholesterol level (24). The contents of squalene and β -sitosterol varies between cultivars (22) (Table 3).

2.7. Terpenes

The aroma components of the *T. grandis* differ with processing methods (fried, roasted, and raw) for nuts and shedding time of arils. The main aroma components are terpene, benzene, ether, ketone, aldehyde, esters, alkanes, and alcohol compounds (25-27). Terpenes have the highest portion (41.99%-86.7%) among the aroma substances of *T. grandis* kernel oil (25,27,28) and D-limonene is the highest terpene.

3. Biological functions

Since rich in components, various beneficial effects such as anti-oxidation, anti-inflammation, microbiota regulation, ACE-I activity, tyrosinase inhibitory activity have been discovered for *T. grandis*. Among the abundant contents, unsaturated fatty acids, flavonoids, phenolic acids, and terpenes account for the main functional components.

3.1. Anti-oxidation

Oxidation is essential for living organisms to generate energy which fuels biological processes. However, oxidative processes *in vivo* continuously generate free radicals and reactive oxygen species, and these excessive highly reactive species play an important role in aging, neurodegenerative diseases, and plentiful debilitating diseases, including diabetes, cirrhosis, and cancer (29).

The ethanol extracts from T. grandis seed have significant antioxidant effects. The 2,2-diphenyl-1picrylhydrazyl (DPPH) radical scavenging activity of the ethanol extract at a high concentration (2 mg/ mL) was close to that of vitamin C which has a half inhibitory concentration (IC₅₀) value of 0.43 ± 0.04 mg/ mL (21). The 2,2'-azino-bis(3-ethylbenzothiazoline-6sulfonic acid) (ABTS) radical scavenging ability of the ethanol extract increased rapidly as the concentration of the extract rised (0-6.25 mg dried material/mL), with IC₅₀ value of 0.70 mg dried material/mL (7). Moreover, both raw extraction and purified 2-hydroxy-2-(4-hydroxyphenylethyl) malonic acid from seed coat demonstrated potent ABTS, DPPH, and hydroxyl radical-scavenging activity (30). The free radical scavenging ability of T. grandis seeds is greater than that of *T. grandis* arils. An essential oil extraction from the *T.*

Table 3. Squalene and β-sitosterol in *T. grandis* kernel

Compounds	Content (mg /kg)	References
Squalene	13-72	13; 22
β-sitosterol	900-4,100	13; 22; 56

grandis cv. Merrillii arils can scavenge ABTS and DPPH radicals, with IC₅₀ values of 4.14 ± 0.06 mg/mL and 20.73 ± 1.56 mg/mL, respectively (31).

Treatment of human dermal fibroblasts with the seed extract at 50 and 250 µg/mL demonstrated significant protection against hydrogen peroxide-induced oxidative stress (6). Under the same concentrations, it also demonstrated significant suppression of lactate dehydrogenase (LDH) enzyme leakage from fibroblasts. This reveals the antioxidant protective effect of *T. grandis* seed on hydrogen peroxide-induced fibroblast injury.

Bivariate correlation analysis demonstrated that flavonoids exhibited the strongest correlation with DPPH radical scavenging activity (r = -0.805), significantly surpassing that of phenolics (r = -0.500). This suggests that flavonoids likely serve as the primary contributors to the radical scavenging capacity of T. grandis kernels (7). The bioactive peptides from T. grandis nut protein extract also exhibited antioxidant effect which is higher than its protein extract, especially in DPPH radicals scavenging (32).

Furthermore, the antioxidant capacity and total flavonoid content were significantly higher in *T. grandis* kernels from 100- and 1000-year-old trees compared to those from 10-year-old trees. Flavonoids were strongly correlated with enhanced antioxidant activity in older trees, and seven genes were identified as potentially involved in age-dependent flavonoid biosynthesis. Additionally, the differential accumulation of flavonoids with tree age may be regulated by abscisic acid and gibberellin (*33*).

3.2. Anti-inflammation

T. grandis has huge potential to suppress the inflammatory response (Figure 3). Topical administration of the ethanol extracts from T. grandis seed exhibited dose-dependent inhibition against either arachidonic acid (AA)- or 12-O-tetradecanoylphorbol-13-acetate (TPA)-induced ear-edema in mice (6). The butanol fraction of T. grandis leaves reduced edema by 63.8% and 72.1% at the dose of 100 mg/kg and 200 mg/kg respectively. In comparison, aspirin at 200 mg/kg reduced edema 45.2% against the acute inflammation in xylene-induced ear edema (34). Moreover, T. grandis aril also exhibited anti-inflammatory activity where its extracts (torregrandin A, torregrandin B, methyl 12-hydroxy-7-oxodehydroabietate, and torreyagrandate) can inhibit nitric oxide (NO) production with IC₅₀ values of 49.4,

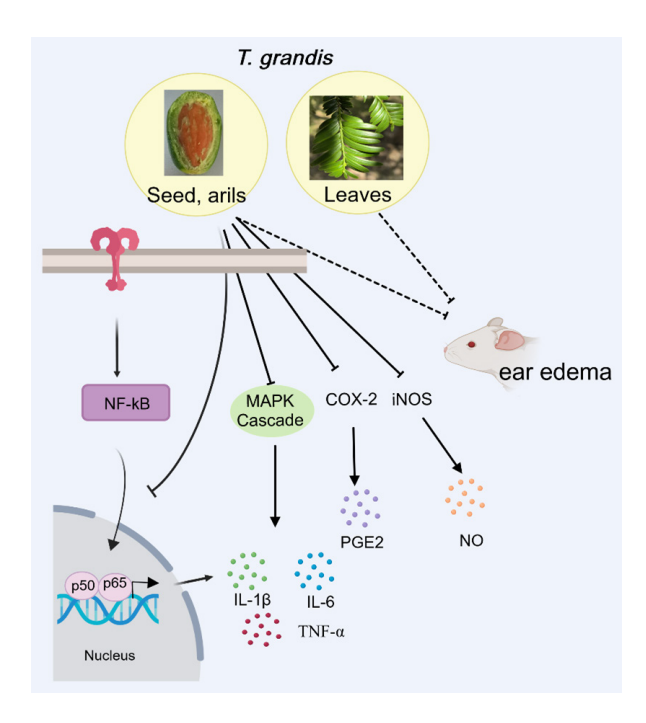


Figure 3. Anti-inflammatory property of *T. grandis.* Created with MedPeer (*medpeer.cn*)

41.9, 38.4, and 52.6 μ M respectively. This demonstrated the anti-neuroinflammatory activity for *T. grandis* in LPS-induced BV-2 cells (35).

The ethanol extracts from T. grandis seed can effectively reduce the expression of kidney prostaglandin E2 (PGE2) and decrease the expression of kidney interleukin-1β (IL-1β) and tumour necrosis factor α (TNF- α) in a mouse model of hyperuricemia (21). T. grandis kernel contains sciadonic acid (SCA) which can decrease the production of PGE2, NO, TNF-a, and interleukin-6 (IL-6) in macrophages. When incubated under different concentrations of SCA (0, 10, 25, 50 or 100 μM) followed by LPS-stimulation, macrophages exhibited significantly reduced the production of PGE2, NO, TNF-a, and IL-6 by 29%, 31%, 14%, and 34%, respectively, as compared to the control groups (36). Moreover, SCA can decrease the production of proinflammatory factor IL-1β and TNF-α in high-fat diet mice. Both low and high doses of SCA significantly reduced the relative expression of IL-1β, and the high dose additionally suppressed TNF-α expression in high-fat diet mice (37). The suppression of proinflammatory mediators partly attributed to reduced expression of inducible nitric oxide synthase (iNOS) and cyclooxygenase-2 (COX-2). The reduction of PGE2 synthesis by SCA was probably due to its suppression of COX-2 expression and reducing proportions of phospholipid arachidonic acid (AA) in cell membrane. In addition, SCA also inhibited the expression of total mitogen-activated protein kinases (MAPK) and phosphorylated MAPK, and the translocation of NF-κB p65 (36).

Furthermore, water-soluble polysaccharides in T.

grandis nuts possess strong anti-inflammatory activity (38). Heteropolysaccharide TGP-0a significantly lowered pro-inflammatory cytokines IL-1 β and IL-6. Moreover, TGP-0a decreased the level of inflammatory mediators (NO and reactive oxygen species (ROS)) by reducing the levels of iNOS and COX-2.

3.3. Microbiota alteration

Extracts from T. grandis seeds play a dual role in microbiota alteration by increasing microbial diversity and beneficial bacteria while suppressing those harmful ones. This dual role mainly comes from the direct functions by its rich bio-active contents or through regulations under various microenvironments, and yet many of the detailed mechanisms remain to be fully addressed. The α -diversity index (the Shannon index) for the microbiota of the ethanol extracts from T. grandis seed group was elevated compared to that of the model group and the positive drug group (21). The ethanol extracts of T. grandis seed modulated the gut microbiota composition, significantly enriching beneficial bacteria including Akkermansia muciniphila, Corynebacterium parvum, Enterorhabdus, Muribaculaceae, Marvinbryantia, and Blautia (21). On the other hand, the defensin 4 protein from T. grandis nuts significantly suppressed the proliferations of B. subtilis, E. coli DH5a, S. aureus, and P. aeruginosa, M. albican and S. cerevisiae (32).

On the suppression side, dehydroabietinol and dehydroabietic acid from the arils of T. grandis significantly inhibited methicillin-resistant Staphylococcus aureus (MRSA), with MIC values (the lowest concentration of the tested compounds which completely inhibited the growth of bacteria) of 100 μ M (35).

Furthermore, the abietane-type diterpenoids from the twigs and leaves of *T. grandis*, including torgranol E, 12-hydroxy-6,7-seco-abieta-8,11,13-triene-6,7-dial, 6,11,12-trihydroxyabieta-5,8,11,13-tetraen-3,7-dione, and 6α-hydroxysugiol, moderately inhibited *M. tb* H37v, demonstrating equivalent MIC values at 16 μg/mL (*39*). Moreover, both compounds (6,11,12-trihydroxyabieta-5,8,11,13-tetraen-3,7-dione and 6α-hydroxysugiol) demonstrated potent inhibition of the *S. aureus* ATCC 29213, exhibiting MIC of 16 and 4 μg/mL respectively (*39*). Dehydroabietinol, dehydroabietic acid, and abietane-type diterpenoids mainly exert their antibacterial effects through multiple mechanisms such as destroying microbial cell membranes and inhibiting key enzymes (*35*,*39*).

On the enriching part, SCA from the seeds of *T. grandis* can modulate the intestinal flora composition by selectively enriching beneficial bacteria (such as *Lactobacillus* and *Bifidobacterium*) and suppressing potentially detrimental bacteria (such as *Faecalibaculum*, *norank_f_Desulfovibrionaceae*, and *Romboutsia*). Such a dual role effect to the gut microbiota was suggested

to be associated with short-chain fatty acids (SCFAs) and other metabolites from *T. grandis* (40). Intervention with SCA significantly increased the acetic acid content and slightly elevated the levels of propionic acid and butyric acid. Acetic, propionic, and butyric acids belong to SCFAs, and they can regulate hormone secretion and beneficially alter the structural composition of the gut microbiota (40). Therefore, SCA can stimulate the growth and proliferation of acid-producing bacteria, regulate the SCFAs contents, and improve gut microbiota composition. However, the potential mechanisms of SCA on the acid-producing bacteria remain unclear.

3.4. Effects on blood pressure, blood glucose and lipids

Hypertension is an important contributing factor to cardiovascular disease. Inhibition or inactivation of angiotensin-converting enzyme is considered an effective way to alleviate hypertension. ACE-I oligopeptides and peptides were identified in *T. grandis* nuts, and the former has been reported in the treatment of several diseases including cardiovascular disease, type 2 diabetes, increased blood pressure, increased level of triglycerides in the blood, and obesity (*32*). Moreover, a new ACE-I peptide (VW-7) identified from *T. grandis* meal protein has an IC₅₀ value of 205.98 μM (*14*). These results indicate the blood pressure-lowering potential of *T. grandis* nuts.

T. grandis kernel extracts exhibit pronounced α-glucosidase inhibition effect in a dose-related manner. The 70% ethanol extract possesses the best α-glucosidase inhibition with the lowest IC₅₀ value of 0.60 mg DM/mL and yields better activity than acarbose (0.76 mg/mL), a clinical drug treating diabetes (7). This suggests the hypoglycemic potential of T. grandis kernel.

T. grandis leaves also exhibit blood glucose regulating activity. When treated with the n-butanol fraction of the 75% ethanol extract of T. grandis leaves (BFTL), serum biochemical indexes exhibited a significant reduction while superoxide dismutase and glutathione peroxidase levels exhibited a significant increase as compared to the type 2 diabetes mellitus (T2DM) group without treatment (41). The BFTL treatment also ameliorated oral glucose tolerance and the pathological changes of the liver, kidney, and pancreas. It significantly reduced cytochrome and caspase-3 expression in pancreatic and augmented the Bcl-2/Bax ratio (41).

Dyslipidemia, especially the elevation of total cholesterol, triglycerides and low-density lipoprotein cholesterol (LDL-C), is another important risk factor for cardiovascular disease. Plasma triacylglycerol level was markedly lower in the *T. grandis* kernel oil group (113 \pm 12 mg/dl) relative to both soybean (161 \pm 15 mg/dl) and corn oil (179 \pm 20 mg/dl) controls. The liver triacylglycerol level was also markedly lower in the *T. grandis* kernel oil group (15.4 \pm 1.8 mg/g) relative to both soybean (29.9 \pm 1.9 mg/g) and corn oil (30.7 \pm 2.0

mg/g) controls (42).

SCA from the seeds of *T. grandis* can alleviate the increase of total cholesterol (TC), triacylglycerol (TG), and LDL-C levels and decrease of high-density lipoprotein cholesterol (HDL-C) level under high-fat diet in a dose-dependent manner (*37*). Both SCA treatment groups effectively suppressed body weight gain relative to the model group. SCA regulate lipid metabolism by activating the expression of the PPARα/SREBP-1C/FAS protein pathway (*40*). SCA, especially high dose group, decreased SREBP-1c and increased PPARα, compared with the high-fat diet group.

3.5. Neuroprotective effect

T. grandis oil possesses a neuroprotective effect on a scopolamine (SCAOP)-induced C57BL/6J mouse model (43). The administration of SCAOP impaired short-term non-spatial recognition memory and working memory while T. grandis oil can effectively reverse the trend. The T. grandis oil can attenuate the substantial decline in acetylcholine (ACh) activity and increase in acetylcholinesterase (AChE) activity in the cortex of the SCAOP group, therefore protecting against cholinergic dysfunction.

Neuroinflammation underlies various central nervous system (CNS) conditions, and it is central to the pathology of neurodegenerative diseases, including Parkinson's disease (PD) and Alzheimer's disease (AD) (44). The T grandis oil can inhibit neuroinflammation and oxidative stress (43). The T grandis oil alleviated the upregulation of microglia in the cortical and hippocampal CA1 regions and the mRNA expressions of TNF- α , IL-1 β , IL-6, and iNOS in the cortex by SCAOP induction. Moreover, it alleviated the upregulation of malondialdehyde (MDA) and down-regulation of glutathione (GSH) and superoxide dismutase (SOD) by SCAOP induction.

The neuroprotective effects of the *T. grandis* oil are due to, in part, unsaturated fatty acids (UFAs) which can prevent the accumulation of lipoprotein-associated A β , alleviate neuroinflammation and oxidative stress (45). For example, oleic acid pretreatment strongly attenuated lipoteichoic acid (LTA)-induced IL-6 secretion in BV2 microglia (46). Prenatal oleic acid administration enhanced brain weight and the synthesis of postsynaptic density 95 in Down syndrome model mice (47). Oral α -linoleic acid administration suppressed neuroinflammation and TLR4 to ameliorate memory dysfunction (48). In addition, torregrandin A, torregrandin B, methyl 12-hydroxy-7-oxodehydroabietate, and torreyagrandate from *T. grandis* aril inhibited NO production, confirming their antineuroinflammatory activities (35).

T. grandis oil can also participate in the gut-brain axis regulation where its administration can effectively reverse the decrease of SCFA levels in SCOP mice. SCFAs are vital metabolites produced by gut microbiota and play a mediational role within the gut-brain axis

(43). SCFAs modulate CNS processes through direct and indirect patterns. In addition to crossing the bloodbrain barrier (BBB) via endothelial monocarboxylate transporters, SCFAs strengthen BBB integrity through the upregulation of tight junction proteins. Furthermore, within the CNS, SCFAs modulate neuroinflammation via two primary mechanisms: by regulating glial cell morphology and function, and by controlling the levels of neurotrophic factors. These actions collectively enhance neurogenesis, support serotonin biosynthesis, and promote neuronal homeostasis and function. On the other hand, the activation of specific receptors on enteroendocrine cells by SCFAs mediates indirect communication with the brain through systemic circulation or vagal pathways. This is achieved by stimulating the release of signaling molecules, such as the gut hormones glucagon-like peptide 1 (GLP1) and peptide YY (PYY), alongside the neurotransmitters γ-aminobutyric acid (GABA) and serotonin (5-HT) (49). This indicates the treatment of T. grandis oil could regulate gut microbiota and it might be associated with the functions of *T. grandis* oil on cognitive impairment induced by SCOP.

3.6. Brightening

Tyrosinase is a key rate-limiting enzyme that can catalyze enzymatic browning and melanin synthesis (31). Tyrosinase exhibits monophenolase and diphenolase activities, which catalyze the hydroxylation of L-tyrosine to L-dihydroxyphenylalanine (L-DOPA) and the oxidation of L-DOPA to dopaquinone, leading to nonenzymatic polymerization and then dark pigments (50,51). In humans, the overexpression of tyrosinase will cause melanin overproduction in the skin, which can trigger hyperpigmentation effects such as freckles, melasma, age spots, and melanoma (52). T. grandis seed and aril demonstrate an inhibitory eaffect on the oxidation of L-DOPA and L-tyrosine. T. grandis seed oil inhibited the oxidation of L-DOPA and L-tyrosine with IC₅₀ values of 237.42 \pm 2.23 µg/mL and 849.42 \pm 4.37 µg/mL, respectively (10). Ethanol extracts from T. grandis seed inhibited tyrosinase activity with IC₅₀ value of 6.60 \pm 0.15 mg DM/mL (7). The essential oil from T. grandis ev. Merrillii aril inhibited tyrosinase activity with IC₅₀ value of 11.04 ± 0.76 mg/mL (31,53).

Total phenolics and total flavonoids are involved in tyrosinase inhibition (54), and correlation coefficients between tyrosinase inhibition and these two substances were -0.867 and -0.809, respectively in *T. grandis* seed (7). D-limonene and α -pinene are the predominant constituents of the essential oil from the *T. grandis* ev. Merrillii aril and they might account for the inhibitory effect on tyrosinase of this essential oil (31).

3.7. Reducing uric acid (UA) level

The ethanol extracts from T. grandis seed exhibit

significant effects in reducing UA level and protecting the kidneys in hyperuricemia mice. The extract treatment decreased the serum UA level by 71.9%, exhibiting efficacy equivalent to that of xanthine. The mechanism of the extracts in reducing UA level is by inhibiting xanthine oxidase activity and promoting UA excretion (21).

3.8. Ameliorating bone metabolism disorders

SCA, the substance from *T. grandis* seeds, can regulate the bone formation-related OPG/RANKL/RANK signaling pathway through reducing inflammation and modulating the lipid metabolic state (*37*). SCA improves bone health by regulating the proportion of factors associated with bone resorption and formation and inhibiting fat vacuoles in bone (*37*).

3.9. Alleviating slow transit constipation

Slow transit constipation (STC) is mainly caused by weakened colonic motility and reduced intestinal peristalsis speed. *T. grandis* nuts have been used as a prescription for repelling internal parasites in traditional medicine. *T. grandis* kernel oil effectively mitigated constipation, rescued intestinal barrier damage, and ameliorated intestinal inflammation and intestinal flora *via* promoting the colonic expressions of Occludin/Claudin-1/zonula occludens-1 and 5-hydroxytryptamine 3R/4R (55).

3.10. Antinociceptive activity

T. grandis leaves exhibit antinociceptive activity. The extract and fractions of T. grandis leaves (100 and 200 mg/kg) significantly decreased acetic acid-induced writhing in mice. Especially, the writhing inhibition percentage of butanol fraction of T. grandis (200 mg/kg, 82.3%) was higher than that of the standard drug aspirin at the same dose (47.8%). Moreover, T. grandis extract and its fractions significantly inhibited the second phase of formalin-induced nociception and reduced the licking time in mice (34).

4. Applications

4.1. Food applications

The seed of *T. grandis* is rich in multiple types of nutrients including unsaturated fatty acids, vitamins, protein, essential amino acids, trace elements, and minerals. Unsaturated fatty acids, including oleic acid and linoleic acid, accounts for 87.28%-90.84% of all fatty acids in *T. grandis* kernel. It contains eight of the nine essential amino acids that cannot be synthesized by the human body. Moreover, *T. grandis* kernel contains anti-inflammatory or anti-oxidative bioactive

components, such as sciadonic acid, tocopherols, polyphenols, squalene, and β -sitosterol, terpenes. Owing to these nutrients and bioactive components, *T. grandis* kernel is a suitable source for diverse food products, including nut snacks and edible oil.

The essential oil of *T. grandis* aril is rich in volatile compounds, such as limonene (35.6%-37.1%), α -pinene (20.1%-24.1%), and δ -carene (3.3%-3.9%) which exhibits typical flavors (53). Therefore, the essential oil can be helpful for the flavoring of foods. In addition, the essential oil possesses various bioactive functions, such as anti-oxidation, tyrosinase inhibition, antibacterial and antiseptic effects (31) and it can be used for food preservation. The decay index of the treatment with the essential oil of *T. grandis* aril was significantly reduced. The decline rate of the ascorbic acid, an important indicator for evaluating the nutritional quality of loquat fruits, was relatively slow under the treatment with T. grandis essential oil. The activities of catalase and peroxidase, important indicators for the postharvest storage quality of fruits, reached the peak in fruits treated with essential oil on the 12th day of storage (31).

4.2. Medicine applications

With records dated back to the ancient times and the long application history of *T. grandis* kernel in Traditional Chinese Medicine to expel intestinal parasites, prevent hair loss, and relieve cough, *T. grandis* exhibited various other beneficial functions on human health. In summary, *T. grandis* possesses anti-oxidation, anti-inflammation, microbiota alteration, reducing blood pressure, reducing blood glucose, reducing blood lipids, neuroprotective effect, reducing UA level, ameliorating bone metabolism disorders, alleviating slow transit constipation, and antinociceptive activity. With these exhibited functional activities, more potential values are to be discovered in future medicine development.

4.3. Cosmetic applications

T. grandis extract and T. grandis seed extract are both listed in the cosmetic raw material catalog. The essential oil of T. grandis aril exhibits a characteristic aroma like galbanum and can be added to the cosmetics, soap, and daily used perfume to impart a desirable fragrance. The essential oil of T. grandis aril and kernel oil possess antioxidation, anti-inflammation, brightening, hair care, and regulation of skin microecology. The ethanol extract of T. grandis seed exhibits a protective effect on fibroblast oxidative injury induced by H_2O_2 (6). The pinene and D-limonene in the essential oil exhibit an inhibitory effect on tyrosinase (31). T. grandis seed oil inhibits the oxidation of L-DOPA and tyrosinase (10). The extracts of T. grandis are included in skin care products such as creams, serums, and masks to enhance the moisturization and repair functions.

5. Conclusion and future perspectives

The fruit of T. grandis and its extracts possess a wide range of bioactive components and functions. Therefore, T. grandis has extensive application potential in food, medicine, and cosmetics. Although new mechanisms associated with their components were discovered in recent years, more were yet to be explored. The challenges encountered in T. grandis include: (1) T. grandis is rich in bioactive components, which is the key factor influencing its biological activities. Hundreds of components of T. grandis have been reported so far, including those unique ones, but its bioactive constituents and their targets are not fully understood. (2) The landrace, maturation stage, and extraction process of T. grandis have certain influences on its active components and biological activities. Therefore, it is important to conduct a systematic comparison of the effective components of different landraces, tree ages, harvest time, and extraction processes. (3) To formulate the quality control standards of the T. grandis extract, it is necessary to clarify the composition and content of the most critical bioactive compounds. Through comprehensive and in-depth research of T. grandis, new processing method development, exploration on nontraditional components such as exosome or RNA, more ingredients and more mechanisms and functions are expected to be found. In addition, further development and wider utilization of T. grandis, such as T. grandis leave, aril, bark, etc. may be realized.

Funding: None.

Conflict of Interest: The authors have no conflicts of interest to disclose.

References

- 1. Zhu J, Chai Z, Wu C, Huang Y, Wu X. Comprehensive research on the quality of *Torreya grandis* and its oil in Zhejiang Province. J Chin Cereals Oils Assoc. 2019; 34:67-73.
- Li SZ. Fruit. In: Compendium of Materia Medica (Vol. 31). China, 1593; pp. 1080.
- Lou H, Zheng S, Chen W, Yu W, Jiang H, Farag MA, Xiao J, Wu J, Song L. Transcriptome-referenced association study provides insights into the regulation of oil and fatty acid biosynthesis in *Torreya grandis* kernel. J Adv Res. 2024; 62:1-14.
- Xiao M, Huang M, Huan W, Dong J, Xia J, Wu J, Wang D, Song L. Effects of *T. grandis* kernel oil on lipid metabolism and intestinal flora in C57BL/6J mice. Oxid Med Cell Longev. 2022; 4472751.
- Dong D, Wang H, Xu F, Xu C, Shao X, Li H. Supercritical carbon dioxide extraction, fatty acid composition, oxidative stability, and antioxidant effect of *Torreya* grandis seed oil. J Am Oil chem Soc. 2014; 91:817-825.
- Chen BQ, Cui XY, Zhao X, Zhang YH, Piao HS, Kim JH, Lee BC, Pyo HB, Yun YP. Antioxidative and acute antiinflammatory effects of *Torreya grandis*. Fitoterapia.

- 2006; 77:262-267.
- Zhu MF, Tu ZC, Zhang L, Liao H. Antioxidant, metabolic enzymes inhibitory ability of *Torreya grandis* kernels, and phytochemical profiling identified by HPLC-QTOF-MS/ MS. J Food Biochem. 2019; 43:e13043.
- Laghari AH, Kandhro AA, Memon AA. Chapter 4 Cold pressed *Torreya grandis* kernel oil. In: Cold pressed oils: Green technology, bioactive compounds, functionality, and applications (Ramadan MF eds.). Academic Press, 2020; pp. 31-38.
- 9. Ding M, Lou H, Chen W, Zhou Y, Zhang Z, Xiao M, Wang Z, Yang Y, Yang L, Zhang F, Wu J, Song L. Comparative transcriptome analysis of the genes involved in lipid biosynthesis pathway and regulation of oil body formation in *Torreya grandis* kernels. Ind Crops Prod. 2020; 145:112051.
- Cui HX, Duan FF, Jia SS, Cheng FR, Yuan K. Antioxidant and tyrosinase inhibitory activities of seed oils from *Torreya grandis* Fort. ex Lindl. Biomed Res Int. 2018; 2018:5314320.
- Wang Y, Yao X, Yang L, Fei X, Cao Y, Wang K, Guo S. Effects of harvest time on the yield, quality and active substance of *Torreya grandis* nut and its oil. J Oleo Sci. 2021; 70:175-184.
- 12. Lou H, Ding M, Wu J, Zhang F, Chen W, Yang Y, Suo J, Yu W, Xu C, Song L. Full-length transcriptome analysis of the genes involved in tocopherol biosynthesis in *Torreya grandis*. J Agric Food Chem. 2019; 67:1877-1888.
- 13. Ren C, Zhang Y, Tang F, Shen D, Mo R. Analysis of main chemical components in camellia oil, olive oil, walnut oil and *Torreya* seeds oil. J Food Saf Qual. 2015; 6:5011-5016.
- 14. Wu F, Luo X, Zhang Y, Wang P, Chang Y, He Z, Liu X. Purification, identification, and inhibitory mechanisms of a novel ACE inhibitory peptide from *Torreya grandis*. Nutrients. 2023; 15:2374.
- Zongo AW, Jin C, Hao G, Yu N, Zogona D, Nie X, Lu Y, Ye Q, Meng X. Functional compounds of *Torreya grandis* nuts and their processing byproducts: Extraction process, health benefits, and food applications - A comprehensive review. Food Res Int. 2024; 197(Pt 1):115232.
- 16. Ni L, Shi WY. Composition and free radical scavenging activity of kernel oil from *Torreya grandis*, *Carya cathayensis*, and *Myrica rubra*. Iran J Pharm Res. 2014; 13:221-226.
- 17. Zhang F, Ma Z, Qiao Y, Wang Z, Chen W, Zheng S, Yu C, Song L, Lou H, Wu J. Transcriptome sequencing and metabolomics analyses provide insights into the flavonoid biosynthesis in *Torreya grandis* kernels. Food Chem. 2022; 374:131558.
- Ikram M, Muhammad T, Rehman SU, Khan A, Jo MG, Ali T, Kim MO. Hesperetin confers neuroprotection by regulating Nrf2/TLR4/NF-κB signaling in an Aβ mouse model. Mol Neurobiol. 2019; 56:6293-6309.
- Escribano-Ferrer E, Queralt Regué J, Garcia-Sala X, Boix Montañés A, Lamuela-Raventos RM. *In vivo* antiinflammatory and antiallergic activity of pure naringenin, naringenin chalcone, and quercetin in mice. J Nat Prod. 2019; 82:177-182.
- Tao H, Zhu M, Chen M, Liu K, Zhang Z, Song L, Gao F. Diversity of flavonoids in five *Torreya grandis* cultivars: Integrating metabolome and transcriptome to elucidate potential applications for health and metabolic engineering. Food Res Int. 2024; 198:115374.
- 21. Yao J, Bai E, Duan Y, Huang Y. Ethanol extracts from *Torreya grandis* seed have potential to reduce

- hyperuricemia in mouse models by influencing purine metabolism. Foods. 2024; 13:840.
- Suo J, Tong K, Wu J, Ding M, Chen W, Yang Y, Lou H, Hu Y, Yu W, Song L. Comparative transcriptome analysis reveals key genes in the regulation of squalene and β-sitosterol biosynthesis in *Torreya grandis*. Ind Crop Prod. 2019; 131:182-193.
- Fox CB. Squalene emulsions for parenteral vaccine and drug delivery. Molecules. 2009; 14:3286-3312.
- 24. Hu Y, Suo J, Jiang G, Shen J, Cheng H, Lou H, Yu W, Wu J, Song L. The effect of ethylene on squalene and β-sitosterol biosynthesis and its key gene network analysis in *Torreya grandis* nuts during post-ripening process. Food Chem. 2022; 368:130819.
- Yang L, Zhao D, Hu Y, Suo J, Yu W, Wu J, Lou H, Song L. Comparative analysis of aroma components and oil quality of *Torreya grandis* 'Merrillii' nuts with different processing techniques. Zhejiang Nong Lin Da Xue Xue Bao. 2022; 39:22-31. (in Chinese)
- 26. Wei X, Hu Y, Zhu G, Yu W, Zhang Z, Wu J, Song L. Effects of different shedding time on aroma and nutrients of *Torreya grandis* 'Merrillii' seed kernel. Nanjing Lin Ye Da Xue Xue Bao. 2024; 48:51-60. (in Chinese)
- Hu Y, Zhang Z, Hua B, Tao L, Chen W, Gao Y, Suo J, Yu W, Wu J, Song L. The interaction of temperature and relative humidity affects the main aromatic components in postharvest *Torreya grandis* nuts. Food Chem. 2022; 368:130836.
- Zhang C, Fang X, Chen Z, Luo F, Zhong H, Du M. Effects
 of processing process on the composition of volatile
 substances in *Torreya* seed oil. China Oils Fats. 2024;
 49:22-28.
- Neagu E, Radu GL, Albu C, Paun G. Antioxidant activity, acetylcholinesterase and tyrosinase inhibitory potential of *Pulmonaria officinalis* and *Centarium umbellatum* extracts. Saudi J Biol Sci. 2018; 25:578-585.
- 30. Quan W, Xu Y, Xie Y, Peng F, Lin Y. *In vitro* antioxidant properties and phenolic profile of acid aqueous ethanol extracts from *Torreya grandis* seed coat. Molecules. 2022; 27:5560.
- Wang H, Zheng Y, Tang X, Zhang T. Formulation of a stable oil-in-water microemulsion of *Torreya grandis* cv. Merrillii aril essential oil and its application in loquat fruit preservation. Foods. 2023; 12:4005.
- 32. Durrani R, Meiyun Y, Yang B, Durand E, Delavault A, Bowen H, Weiwei H, Yiyang L, Lili S, Fei G. Identification of novel bioactive proteins and their produced oligopeptides from *Torreya grandis* nuts using proteomic based prediction. Food Chem. 2023; 405(Pt A):134843.
- 33. Yan J, Zeng H, Chen W, Zheng S, Luo J, Jiang H, Yang B, Farag M, Lou H, Song L, Wu J. Effects of tree age on flavonoids and antioxidant activity in *Torreya grandis* nuts *via* integrated metabolome and transcriptome analyses. Food Frontiers. 2023; 4:358-367.
- 34. Saeed MK, Deng Y, Dai R, Li W, Yu Y, Iqbal Z. Appraisal of antinociceptive and anti-inflammatory potential of extract and fractions from the leaves of *Torreya grandis* Fort Ex. Lindl. J Ethnopharmacol. 2010; 127:414-418.
- Gao Y, Yang J, Zhang Y, Gao L, Tian J, Han W, Gao J. Abietane-type diterpenoids from the arils of *Torreya grandis*. Molecules. 2024; 29:1905.
- 36. Chen SJ, Huang WC, Yang TT, Lu JH, Chuang LT. Incorporation of sciadonic acid into cellular phospholipids reduces pro-inflammatory mediators in murine

- macrophages through NF-κB and MAPK signaling pathways. Food Chem Toxicol. 2012; 50:3687-3695.
- 37. Yao S, Lu H, Zhou T, Jiang Q, Jiang C, Hu W, Li M, Tan CP, Feng Y, Du Q, Shen G, Xiang X, Chen L. Sciadonic acid attenuates high-fat diet-induced bone metabolism disorders in mice. Food Funct. 2024; 15:4490-4502.
- Yang L, Hu Y, Deng H, Li Y, Zhang R, Zhang Q, Yang L, Pang H, Liu F, Fu C. Water-soluble polysaccharides from *Torreya grandis* nuts: Structural characterization and anti-inflammatory activity. Int J Biol Macromol. 2025; 291:138935.
- 39. Cui JJ, Li WJ, Wang CL, Huang YQ, Lin W, Zhou B, Yue JM. Antimicrobial abietane-type diterpenoids from *Torreya grandis*. Phytochemistry. 2022; 201:113278.
- 40. Chen L, Jiang Q, Jiang C, Lu H, Hu W, Yu S, Li M, Tan CP, Feng Y, Xiang X, Shen G. Sciadonic acid attenuates high-fat diet-induced obesity in mice with alterations in the gut microbiota. Food Funct. 2023; 14:2870-2880.
- 41. Li XQ, Jia SS, Yuan K, Jin SH. Hypoglycemic effect of the n-butanol fraction of *Torreya grandis* leaves on type 2 diabetes mellitus in rats through the amelioration of oxidative stress and enhancement of β -cell function. Biomed Res Int. 2022; 2022:5648896.
- Endo Y, Osada Y, Kimura F, Shirakawa H, Fujimoto K. Effects of Japanese Torreya (*Torreya nucifera*) seed oil on the activities and mRNA expression of lipid metabolismrelated enzymes in rats. Biosci Biotechnol Biochem. 2007; 71:231-233.
- Ma J, Yuan T, Gao Y, Zeng X, Liu Z, Gao J. *Torreya grandis* oil attenuates cognitive impairment in scopolamine-induced mice. Food Funct. 2023; 14:10520-10534.
- 44. Thakur S, Dhapola R, Sarma P, Medhi B, Reddy DH. Neuroinflammation in Alzheimer's disease: current progress in molecular signaling and therapeutics. Inflammation. 2023; 46:1-17.
- Galloway S, Takechi R, Nesbit M, Pallebage-Gamarallage MM, Lam V, Mamo JCL. The differential effects of fatty acids on enterocytic abundance of amyloid-beta. Lipids Health Dis. 2019; 18:209.
- Howe AM, Burke S, O'Reilly ME, McGillicuddy FC, Costello DA. Palmitic acid and oleic acid differently modulate TLR2-mediated inflammatory responses in microglia and macrophages. Mol Neurobiol. 2022; 59:2348-2362.
- García-Cerro S, Rueda N, Vidal V, Puente A, Campa V, Lantigua S, Narcís O, Velasco A, Bartesaghi R, Martínez-Cué C. Prenatal administration of oleic acid or linolenic acid reduces neuromorphological and cognitive alterations in Ts65dn Down Syndrome mice. J Nutr. 2020; 150:1631-1643.
- Ali W, Ikram M, Park HY, Jo MG, Ullah R, Ahmad S, Abid NB, Kim MO. Oral administration of alpha linoleic

- acid rescues $A\beta$ -Induced glia-mediated neuroinflammation and cognitive dysfunction in C57BL/6N mice. Cells. 2020; 9:667.
- Silva YP, Bernardi A, Frozza RL. The role of shortchain fatty acids from gut microbiota in gut-brain communication. Front Endocrinol (Lausanne). 2020; 11:25.
- Ebanks JP, Wickett RR, Boissy RE. Mechanisms regulating skin pigmentation: the rise and fall of complexion coloration. Int J Mol Sci. 2009; 10:4066-4087.
- Ramsden CA, Riley PA. Tyrosinase: the four oxidation states of the active site and their relevance to enzymatic activation, oxidation and inactivation. Bioorg Med Chem. 2014; 22:2388-2395.
- Yamaguchi Y, Brenner M, Hearing VJ. The regulation of skin pigmentation. J Biol Chem. 2007; 282:27557-27561.
- 53. Feng T, Hu Z, Song S, Yao L, Sun M, Zhu X, Lu J. The antioxidant and tyrosinase inhibition properties of essential oil from the peel of Chinese *Torreya grandis* Fort. RSC Adv. 2019; 9:42360-42366.
- Zolghadri S, Bahrami A, Hassan Khan MT, Munoz-Munoz J, Garcia-Molina F, Garcia-Canovas F, Saboury AA. A comprehensive review on tyrosinase inhibitors. J Enzyme Inhib Med Chem. 2019; 34:279-309.
- 55. Wang X, Guo R, Yu Z, Zikela L, Li J, Li S, Han Q. *Torreya grandis* kernel oil alleviates loperamide-induced slow transit constipation *via* up-regulating the colonic expressions of Occludin/Claudin-1/ZO-1 and 5-HT3R/5-HT4R in BALB/c mice. Mol Nutr Food Res. 2024; 68:e2300615.
- Chen Z, Ni Z, Mo R., Zhong D, Tang F. Comprehensive evaluation on quality of oils from seven kinds of woody oilcrops. China Oils Fats. 2018; 43:80-85.
- Wu F, Han Q, Yu Y, Ni S. GC-MS analysis of fatty acids from *Torreya grandis* and *Camellia oleifera* seed. Chin Wild Plant Res. 2014; 33:36-39.
- Ni Q, Gao Q, Yu W, Liu X, Xu G, Zhang Y. Supercritical carbon dioxide extraction of oils from two *Torreya grandis* varieties seeds and their physicochemical and antioxidant properties. LWT Food Sci Technol. 2015; 60:1226-1234.

Received September 4, 2025; Revised October 14, 2025; Accepted October 18, 2025.

*Address correspondence to:

Chuanyin Shi and Yan Sun, Shanghai Cell Therapy Group Co., Ltd., Shanghai, China.

E-mail: shicy@shcell.com (C. Shi), suny@shcell.com (Y. Sun)

Released online in J-STAGE as advance publication October 25, 2025.

Original Article

DOI: 10.5582/ddt.2025.01053

Purification and characterization of a novel antioxidant protein from *Arca subcrenata* Lischke

Qing Yan^{1,2,§}, Hui Shi^{1,3,§}, Yue Gao¹, Chunlei Li¹, Lin Dong^{1,3}, Jianhua Zhu^{1,*}, Rongmin Yu^{4,5,*}

SUMMARY: A novel protein, G1H2GC2, was isolated from Arca subcrenata Lischke using homogenization and ammonium sulfate precipitation, and further purified by several column chromatography techniques including diethylaminoethanol (DEAE) Sepharose Fast Flow anion exchange, gel filtration chromatography (Sephadex G-25), Phenyl Sepharose CL-4B hydrophobic chromatography and reversed-phase high-performance liquid chromatography (RP-HPLC). The purity of G1H2GC2 was over 97% in RP-HPLC, and its high purity was further verified by the appearance of a single band on sodium dodecyl sulfate polyacrylamide gel electrophoresis (SDS-PAGE). The protein content of G1H2GC2 was found to be over 99% by Bradford assay. The molecular weight was determined as 25.6 kDa by electrospray ionization-mass spectrometry (ESI-MS/MS). The isoelectric point of G1H2GC2 was measured to be 7.71 by isoelectric focusing-polyacrylamide gel electrophoresis (IEF-PAGE). Matrix-assisted laser desorption ionization time-offlight mass spectrometry (MALDI-TOF MS/MS) was employed to detect and identify the protein by mass fingerprinting coupled with fragmentation patterns. No matched protein was found, confirming that G1H2GC2 was a novel protein. An attempt was made to detect the N-terminal amino acid sequence of G1H2GC2 by Edman degradation, but the sequence of G1H2GC2 was found to be blocked. The scavenging percentage of G1H2GC2 at 15 mg/mL against 2,2'-azino-bis (3-ethylbenzothiazoline-6-sulfonic acid) (ABTS⁺) was 52.84%. The median effective concentration (EC₅₀) value of G1H2GC2 against ABTS⁺⁺ was 17.67 mg/mL. The results showed that G1H2GC2 might be developed as a potential food additive agent.

Keywords: Arca subcrenata protein, purification and characterization, antioxidant activity

1. Introduction

Proteins are the molecular carriers of biological functions and occupy a pivotal position within living organisms. Nutritionally, they are sources of essential amino acids, are indispensable for growth and maintenance, and are a source of energy (1). Structurally, they are composed of a sequence of amino acids beginning with an N-terminal and ending with a C-terminal amino acid residue (2). Isolating proteins from plants and animals, followed by in-depth investigations into their structures and functions, holds significant scientific value for elucidating the essential roles these biomolecules play in human physiological processes. Bioactive proteins hold broad application prospects as drugs, healthcare products, and food ingredients. Natural proteins exhibit diverse biological activities, including antioxidant (3-5), antihypertensive (6-8), antidiabetes (9,10), antiobesity (11,12), immunomodulatory (13,14), and antitumor (15,16). Marine organisms are crucial resources for the discovery and development of marine biological resources. They inhabit extremely harsh, competitive, and aggressive environments, exhibiting significant differences from terrestrial organisms in many aspects. The unique amino acid sequences of their proteins may arise from adaptations to these specialized ecological niches (17,18). Recently, increasing investigations have focused on bioactive proteins from marine organisms. Numerous bioactive proteins have been isolated from various marine animals, including Spongia officinalis, Chrysaora quinquecirrha, Hippospongia communis, bryozoans, nudibranchs, and other marine species (19,20).

Several methods are used to obtain bioactive proteins and peptides, including isolation, fermentation, enzymatic hydrolysis and a combination of these (1). Isolation and purification are the most common techniques (2). By exploiting the variability in

¹Biotechnological Institute of Chinese Materia Medica, Jinan University, Guangzhou, Guangdong, China;

² Jincheng Center for Adverse Drug Reaction Monitoring, Administration for Market Regulation, Jincheng, Shanxi, China;

³ Department of Pharmacology, College of Pharmacy, Jinan University, Guangzhou, Guangdong, China;

⁴Department of Chinese Medicine, Guangzhou Huali Science and Technology Vocational College, Guangdong, China;

⁵ Department of Natural Chemistry, College of Pharmacy, Jinan University, Guangzhou, Guangdong, China.

molecular weights, charges and affinities of bioactive proteins, a series of advances in methodology and instrumentation has enabled the accurate separation of specific bioactive proteins and peptides (2). Among the main techniques used to extract proteins are solvent extraction, which is used to isolate proteins from biological sources, and ultrafiltration and nanofiltration, which separate mixtures of proteins by size (21,22). Chromatography has also become an indispensable tool for the purification of proteins. Advances in the understanding of protein structure/function relationships have also driven the generation of more sophisticated chromatographic techniques for protein separation (23), including size-exclusion chromatography and reversedphase high-performance liquid chromatography (RP-HPLC) (2). Given the special marine environment, various proteins and peptides with therapeutic application have been generated from marine organisms by the isolation and purification techniques above (1,24).

Arca subcrenata Lischke, a bivalve mollusk that lives in the muddy sediment of the shallow coastal waters of the north-western Pacific, belongs to the Arcidae family under phylum Mollusca, class Bivalvia (25). A traditional Chinese remedy, wa leng zi (also known as Concha Arcae), is made from A. subcrenata (26). Furthermore, the body of this species has been used for centuries to treat tumors, anemia, inflammation and dyspepsia in traditional Chinese medicine (26). Proteins derived from A. subcrenata have been reported to be highly bioactive, with significant pharmacological and medicinal value. Modern research demonstrates that A. subcrenata exhibits diverse biological activities, including antitumor, antibacterial, antioxidant, immunomodulatory, and antiinflammatory properties (27-33). A polypeptide fraction from A. subcrenata, P2, had antiproliferative capability against seven human tumor cell lines, especially HeLa, which was much more sensitive to P2 than the other tumor cell lines. Furthermore, a purified protein (H3), isolated from P2, exhibited significant antitumor and antioxidant activity (27). A polypeptide fraction from A. subcrenata (PAS) inhibit HT-29 cells proliferation via suppression of insulin-like growth factor 1 receptor (IGF-1R)/protein kinase B (Akt)/mammalian target of rapamycin (mTOR) signaling and adenosine triphosphate (ATP) production (28). And a novel protein (ASP-3) with unique antitumor activity from A. subcrenata Lischke (29,30).

Continuing this work, here we report a novel protein, G1H2GC2, isolated from *A. subcrenata* Lischke using a variety of purification techniques. The protein was shown to possess ABTS⁺⁺ radical-scavenging activity. The complete identification and characterization of G1H2GC2 will help the future investigation of its biological activity.

2. Materials and Methods

2.1. Materials

Samples of A. subcrenata Lischke were collected from Huangsha seafood market, Guangzhou, China. All samples were positively identified by Rongmin Yu (Jinan University, Guangzhou, China). The visceral mass was dissected from the samples, weighed and stored at -20 °C until used. Diethyl-aminoethanol (DEAE) Sepharose Fast Flow and Phenyl Sepharose CL-4B were purchased from GE Healthcare (Chicago, PO, USA). Sephadex G-25, Tris, sodium dodecyl sulfate (SDS), and Coomassie Brilliant Blue R-250 were purchased from Sigma Chemical Co. (St. Louis, MO, USA). Coomassie Brilliant Blue G-250 and bovine serum albumin were obtained from Sino-American Biotechnology Co., USA. Molecular weight markers were obtained from Shanghai Puyi Biotechnology Co., Ltd., China. Other commercially available chemicals and reagents were of analytical grade.

2.2. Extraction of crude protein

The crude protein of A. subcrenata Lischke was extracted by the ammonium sulfate precipitationcentrifugation method of Chen et al. (27). Briefly, the visceral mass of A. subcrenata Lischke was washed with 4°C tap water three times, followed by 4°C distilled water three times. It was then homogenized with triple volume of phosphate-buffered saline (PBS) (0.03 M, pH 8.0). After extraction with ultrasound at 4°C for 40 min, the homogenate was centrifuged at 10,000 rpm for 30 min at 4°C. The supernatant was precipitated with 70%-100% saturation of solid ammonium sulfate. The precipitate was obtained by centrifugation (10,000 × g for 30 min), then re-dissolved in 30 mM Tris-HCl buffer (pH 8.0) and dialyzed against distilled water for 48 h to remove ammonium sulfate. The dialyzed solution was then lyophilized for further use to obtain crude protein JNY-1.

2.3. Purification of protein

2.3.1. DEAE Sepharose Fast Flow chromatography

The crude protein (JNY-1) was dissolved in 0.03 M Tris-HCl buffer (pH 8.0) at a proportion of 1:10 (w/v), and loaded onto a DEAE Sepharose Fast Flow anion exchange column (2.5 cm × 40 cm), which was preequilibrated with the aforementioned Tris-HCl buffer. The column was stepwise eluted with 0, 0.1, 0.3 and 2 M NaCl prepared in the same buffer at a flow rate of 7 mL/min to obtain the fraction P2.

2.3.2. Sephadex G-25 exclusion chromatography

The fraction P2 was collected, dialyzed, freeze-dried and loaded onto a Sephadex G-25 column (1 cm × 80 cm)

that was pre-equilibrated with distilled water. A stepwise elution was carried out with distilled water at a flow rate of 1 mL/min to obtain the fraction G1.

2.3.3. Phenyl Sepharose CL-4B hydrophobic chromatography

G1 was freeze-dried, dissolved in 1.0 M $(NH_4)_2SO_4$ prepared with 30 mM phosphate buffer (pH 8.0) and loaded onto a Phenyl Sepharose CL-4B hydrophobic chromatography column (2.5 cm \times 40 cm), which had previously been equilibrated with the same buffer. Then the column was stepwise eluted with decreasing concentrations of 1.0, 0.5 and 0 M $(NH_4)_2SO_4$ mixed into the above buffer and finally eluted with distilled water at a flow rate of 1 mL/min to obtain the fraction G1H2.

2.3.4. Sephadex G-25 exclusion chromatography and HPLC

After being dialyzed and freeze-dried, G1H2 was purified again on a Sephadex G-25 column (1 cm × 80 cm) to obtain the fraction G1H2G, and G1H2G was separated twice on a Shimadzu series LC-20AB HPLC system (Shimadzu Co., Kyoto, Japan) fitted with a ZORBAX® 300SB-C8 column (Agilent Co., Palo Alto, CA, USA; $4.6 \text{ mm} \times 250 \text{ mm}$). The elution solvent was composed of water-trifluoroacetic acid (TFA) (solvent A; 100:0.1, v/v) and acetonitrile-TFA (solvent B; 100:0.1, v/v) (34). Firstly, gradient elution was performed from 10% to 16% of solvent B at 0-7.5 min, from 16% to 37% (7.5-10 min), from 37% to 50% (10-50 min), from 50% to 100% (50-55 min), and then held at 100% of solvent B (55-63 min). Secondly, the protein obtained from RP-HPLC was further separated by gradient elution from 10% to 10% at 0-10 min, from 10% to 35% (10-15 min), from 35% to 55% (15-40 min), from 55% to 100% (40-55 min), and then held at 100% of solvent B (55-60 min). Gradient elution was performed with a flow rate of 1 mL/min and column temperature of 25°C. The detection wavelength was set at 280 nm in all experiments.

2.4. Characterization of protein

2.4.1. Determination of protein and saccharide content

The protein content was estimated using the Bradford method. Bovine serum albumin (BSA) was used as a standard protein. The absorbance at 595 nm was used to determine the amount of protein in each sample. The saccharide content was measured by the phenol-sulfuric acid method with a 100 µg/mL glucose solution as standard. The absorbance at 490 nm was used to determine the amount of carbohydrate in each sample.

2.4.2. Sodium dodecyl sulfate polyacrylamide gel electrophoresis (SDS-PAGE)

The purity and molecular weight of the protein were determined by SDS-PAGE according to the method described by Laemmli, using an acrylamide concentration of 5% for the stacking gel and 16% for the separating gel. The separation was first manipulated with a voltage of 60 V for 0.5 h, and then 80 V for approximately 2.5 h. The gel was stained with Coomassie Brilliant Blue R-250 for 1 h and then destained using 40% methanol and 10% acetic acid for 2 h. The molecular weight of the purified protein was determined by comparison of its electrophoretic mobility with that of the molecular weight marker proteins, using a middle-molecular-weight calibration kit (Thermo Scientific, Waltham, MA, USA).

2.4.3. Isoelectric focusing-polyacrylamide gel electrophoresis (IEF-PAGE)

The isoelectric point of the protein sample was determined by immobilized pH gradient (IPG) IEF-PAGE. Ampholyte (40%, pH 3.5-10.0) was used to prepare isoelectric focusing gel with an acrylamide concentration of 5%. The experiment was carried out at 150 V for 0.5 h, then at 200 V for 2.5 h in an electrophoresis apparatus (Protean II, BioRAD, Hercules, CA, USA). The IEF-PAGE gel-unloaded samples were washed with double-distilled water, and sliced into pieces 0.5 cm in length from acidic terminus to basic terminus, then separately dipped into glass tubes containing 2.0 mL of 10 mM KCl for 30 min. The pH value of the liquid around each slice was measured. The gel-loaded sample was fixed with 10% trichloroacetic acid for 30 min, stained with Coomassie Brilliant Blue R-250 overnight, and then destained until faded from the background. Data were derived from the calibration curve of the isoelectric points with the length of gel as abscissa and pH value as ordinate (33).

2.4.4. Reversed-phase high-performance liquid chromatography (RP-HPLC)

The sample was prepared for RP-HPLC by dissolving the protein in distilled water, which was then filtered and loaded into a Shimadzu series LC-20AB HPLC system fitted with a ZORBAX $^{\$}$ 300SB-C8 column (Agilent Co., Palo Alto, CA, USA; 4.6 mm \times 250 mm). The mobile phase was composed of 0.1% TFA in water (solvent A) and 0.1% TFA in acetonitrile (solvent B). The column was eluted with a gradient of 10% to 100% solvent B for 30 min with a flow rate of 1 mL/min and a detection wavelength of 280 nm.

2.4.5. UV-wavelength scanning by photodiode array (PDA) detector

The protein was dissolved in distilled water to a concentration of 1.0 mg/mL and scanned by a PDA detector (Shimadzu Co., Kyoto, Japan). The scan range

was 190-700 nm, and distilled water was used as the blank control.

2.4.6. Molecular weight determination

To determine the precise molecular weight of the purified protein, the protein was dissolved in water of HPLC grade and loaded into an API type 4000 QTRAP mass spectrometer (Applied Biosystems, Foster City, CA, USA). The sample was passed at a flow rate of 20 μ L/min *via* the electrospray interface, which was operated in the positive electrospray ionization (ESI +ve) mode. The gas used for drying (35 psi) and ESI nebulization (45 psi) was high-purity nitrogen.

2.4.7. Identification of protein by MALDI-TOF-MS

The Coomassie Blue-stained protein spots were cut out from the gels and sent to GuangZhou FitGene Biological Technology Co. Ltd, Guangzhou, China, for trypsin in-gel digestion and matrix-assisted laser desorption ionization time-of-flight mass spectrometry (MALDI-TOF-MS) (Thermo Co., Waltham, MA, USA) analysis. Peptide mass fingerprints coupled with peptide fragmentation patterns were used to identify the protein in the non-redundant sequence database UniProt (Homo sapiens—animal database: Mascot Search Results: Protein View and Homo sapiens-Arcidae database: Mascot Search Results: Protein View) using the MASCOT search engine (http://www.matrixscience.com).

2.5. Assay of ABTS⁺⁺ radical-scavenging activity

ABTS⁺⁺ was generated by mixing an ABTS stock solution (7 mM) with potassium persulfate (2.45 mM). The mixture was left in the dark at room temperature for 12-16 h. The ABTS⁺⁺ radical cation solution was diluted in 5 mM PBS at pH 7.4 until an absorbance of 0.7 (± 0.02) at 734 nm was reached. 190 μL ABTS⁺⁺ solution was mixed with 10 μL samples of the protein at different concentrations (0.01, 2.50, 5.00, 10.00, 15.00, 20.00 and 25.00 mg/mL). Ascorbic acid (AA) was used as the positive control. Ten min later, the absorbances were measured at 734 nm against the corresponding blanks. The ABTS⁺⁺-scavenging activities of the samples were calculated using the following equation:

ABTS*+-scavenging activity (%) = $[(A0 - A1)/A0] \times 100$

where A0 is the absorbance (without sample) and A1 is the absorbance in the presence of the sample.

2.6. Statistical analysis

The experimental data are expressed as the mean \pm standard deviation obtained from triplicate experiments in all figures. Statistical analysis was performed using

GraphPad Prism 5.0 (GraphPad Software, San Diego, CA, USA).

3. Results

3.1. Extraction and purification of protein from *A. subcrenata* Lischke

The crude proteins were released from the muscle of *A. subcrenata* Lischke and fractionated by salting-out at increasing saturation levels of ammonium sulfate. The crude protein extracted at 70%-100% saturation of ammonium sulfate was named JNY-1.

JNY-1 was separated into four fractions (P1-P4) on the DEAE Sepharose Fast Flow column. P1-P4 were eluted with increasing concentrations of NaCl in 0.03 M Tris-HCl buffer (pH 8.0), i.e., 0, 0.1, 0.3, and 2 M NaCl (Figure 1A). Then, as depicted in Figure 1B, P2 was separated into three subfractions (G1, G2, and G3) by size exclusion chromatography with Sephadex G-25. After the SDS-PAGE analysis and determination of the protein content of G1-G3 (Table 1), G1, which had the highest protein content, was further purified with a Phenyl Sepharose CL-4B hydrophobic chromatography column. Through stepwise elution with decreasing concentrations of 1.0, 0.5 and 0 M (NH₄)₂SO₄ and distilled water, as shown in Figure 1C, four proteins with different hydrophobicity were isolated and named consecutively G1H1-G1H4. G1H2 was purified again on a Sephadex G-25 column to obtain the fraction G1H2G (Figure 1D), which contained two proteins, G1H2-1 and G1H2-2, that had identical electrophoretograms in SDS-PAGE (Figure 2E). The protein content of G1H2 was only 14.03%, while after purification on the Sephadex G-25 column, the protein content of G1H2G (combining G1H2-1 and G1H2-2) increased to 87.12% (Table 1). Then, G1H2G was separated twice by RP-HPLC to obtain the single protein G1H2GC2 (Figures 1E and 1F).

All the elution profiles were shown in Figure 1. Throughout the process of purification, every fraction obtained from every purification step was analyzed by SDS-PAGE to determine its molecular weight and purity, and the electrophoretograms from SDS-PAGE were shown in Figure 2. The protein and saccharide contents of the fractions were shown in Table 1.

3.2. Characterization of purified protein from *A. subcrenata* Lischke

As shown in Figure 2G, G1H2GC2 gave a single band in SDS-PAGE, indicating that it was electrophoretically homogeneous. Furthermore, the RP-HPLC elution profile (Figure 3A) showed a single sharp peak, from which the purity of G1H2GC2 was calculated to be over 97.2% by the normalized peak area method. Thus, both techniques demonstrated that G1H2GC2 had been purified to homogeneity. Furthermore, in IEF-PAGE, G1H2GC2 again showed a single band, and its isoelectric point was

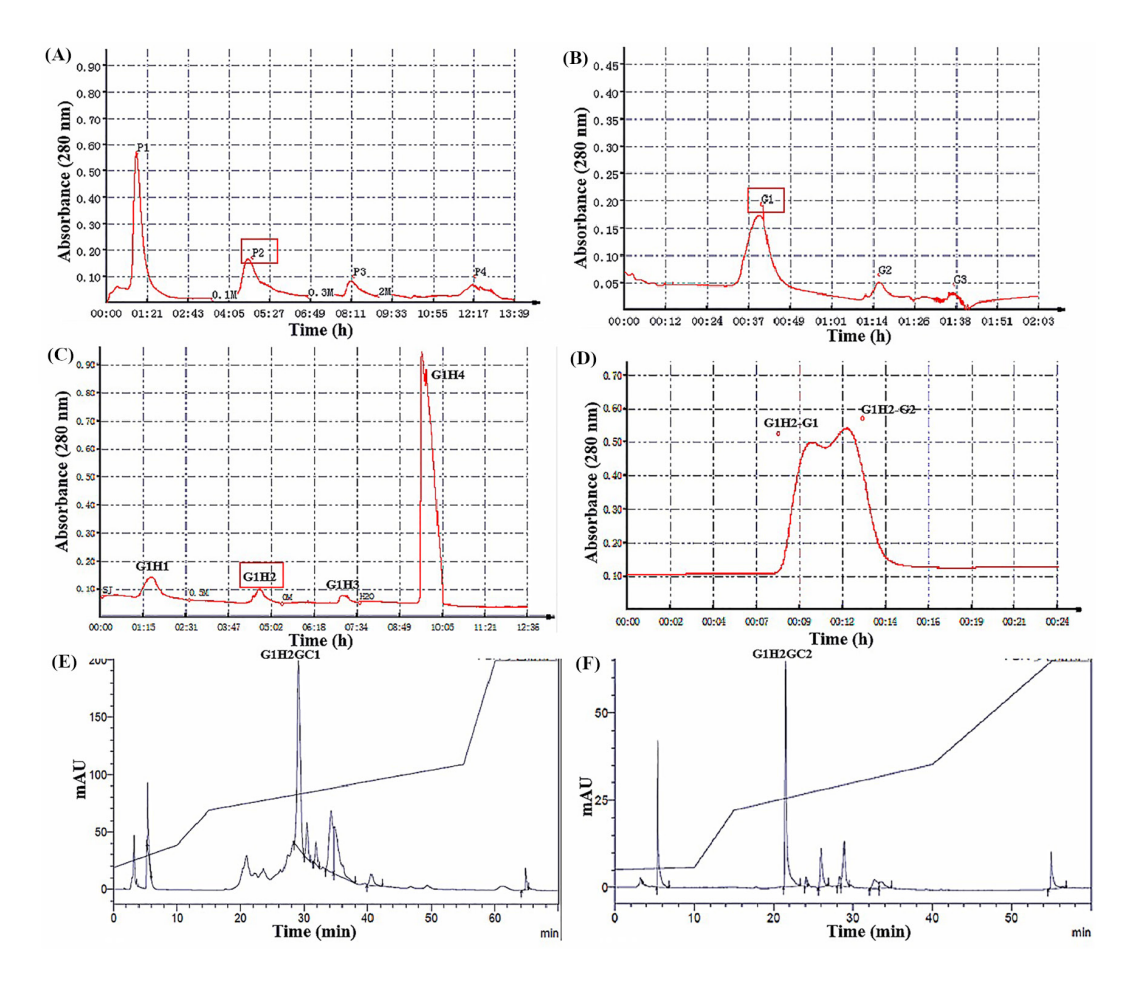


Figure 1. Purification of the proteins from *A. subcrenata* **Lischke. (A)** P2: separated from JNY-1 by anion exchange chromatography on a DEAE-Sepharose Fast Flow column. **(B)** G1: separated from P2 by size exclusion chromatography on Sephadex G-25. **(C)** G1H1-G1H4: separated from G1 on a Phenyl Sepharose CL-4B hydrophobic chromatography column. **(D)** G1H2G: (combining G1H2-1 and G1H2-2) enriched by Sephadex G-25. **(E)** G1H2GC1: separated from G1H2G by RP-HPLC. **(F)** G1H2GC2: separated from G1H2GC1 by RP-HPLC.

Table 1. Protein and saccharide content of different fractions

Sample	JNY-1	P2	G1	G2	G3	G1H2	G1H2G	G1H2GC2
Protein (%) Saccharide (%)	47.06	77.14	89.76	3.81	4.21	14.03	87.12	99.8
	49.88	21.06	9.81	4.96	3.57	3.84	4.06	n.d.

n.d. not detected.

found to be 7.71 (Figure 3B). The purified G1H2GC2 had an approximate molecular weight of 28 kDa as determined by comparison of the single band on the SDS-PAGE with the molecular weight markers (Figure 2G). According to a more precise analysis by ESI-MS/MS, the molecular mass of the protein was 25.6 kDa (Figure 3C). Additionally, in UV-wavelength scanning, the spectrum of G1H2GC2 contained an absorption peak at 278 nm (Figure 3D), which is a characteristic absorption of proteins.

3.3. Homology identification of protein from *A. subcrenata* Lischke

The protein G1H2GC2 with a molecular weight of 25.6 kDa was excised from the Coomassie-stained preparative

gel for mass spectrometric analysis by MALDI-TOF MS to obtain its peptide mass fingerprints. The resulting primary and secondary mass spectrograms of G1H2GC2 were shown in Figure 4. They were used for protein identification by matching them in the non-redundant sequence database UniProt (Homo sapiens-animal) using the MASCOT search engine, which combines de novo peptide sequencing with database identifications. G1H2GC2 was found to be a previously unknown protein: the closest existing match had a match score of only 17 and a sequence coverage of 5%, as shown in Figure 5. Amino acid sequence alignment showed that G1H2GC2 does not share the same amino acid sequence as the proteins ASP-3 and H3 derived from A. subcrenata Lischke (27,29). Therefore, G1H2GC2 is a novel protein from A. subcrenata Lischke.

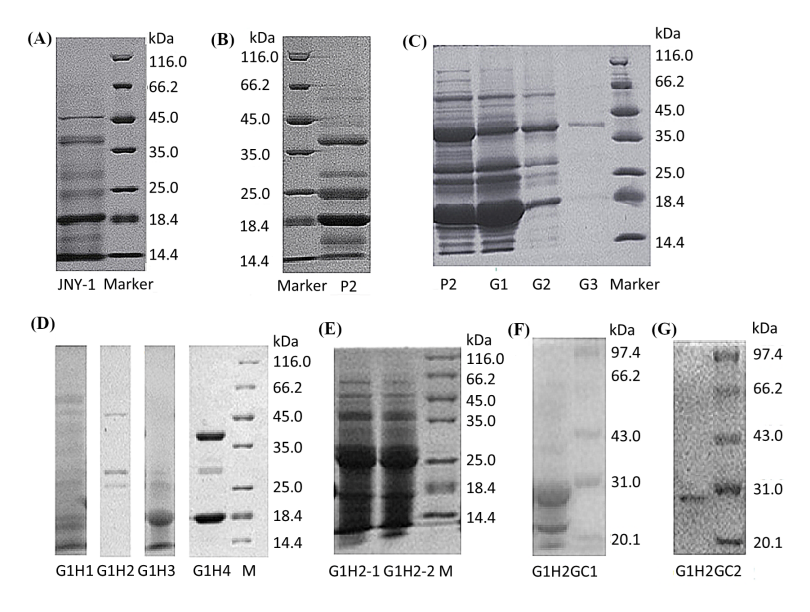


Figure 2. SDS-PAGE electrophoretic analysis of proteins obtained at each purification step. (A) JNY-1: the crude protein extracted from *A. subcrenata* Lischke. (B) P2: isolated from JNY-1 on a DEAE Sepharose Fast Flow column. (C) G1, G2 and G3: fractionated from P2 by Sephadex G-25. (D) G1H1-G1H4: fractionated from G1 by Phenyl Sepharose CL-4B hydrophobic chromatography. (E) G1H2-1 and G1H2-2: separated from G1H2 by Sephadex G-25. Both proteins were combined in one fraction, G1H2G, because of their identical electrophoretograms. (F) G1H2GC1: separated from G1H2G by RP-HPLC. (G) G1H2GC2: separated from G1H2GC1 by RP-HPLC.

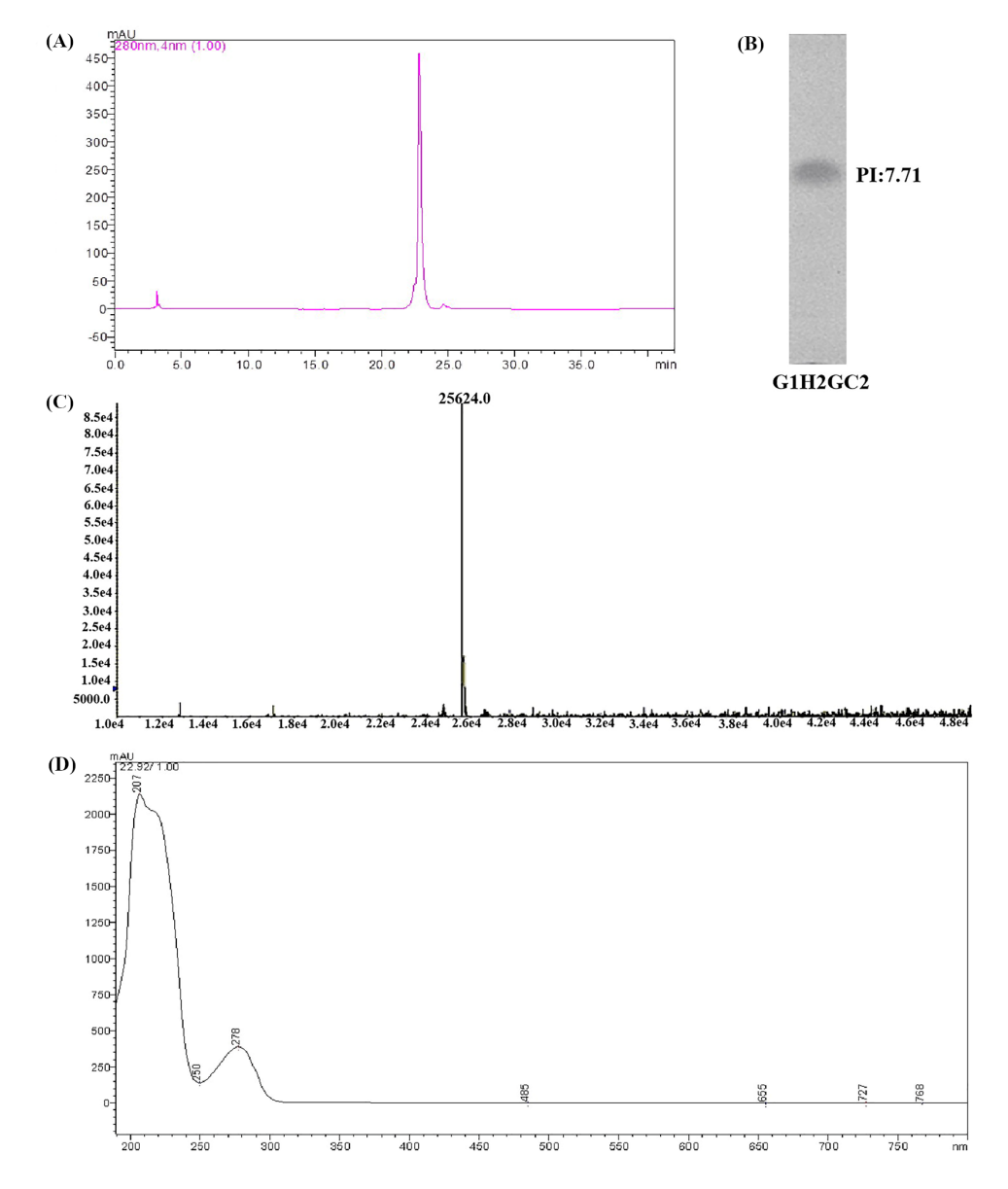


Figure 3. Purity, isoelectric point analysis and mass spectrum analysis of G1H2GC2. (A) Reversed-phase high-performance liquid chromatography (RP-HPLC) profile of G1H2GC2. (B) Isoelectric point determination of G1H2GC2 by IEF-PAGE. (C) Mass spectrum of G1H2GC2. (D) UV-wavelength scanning of G1H2GC2.

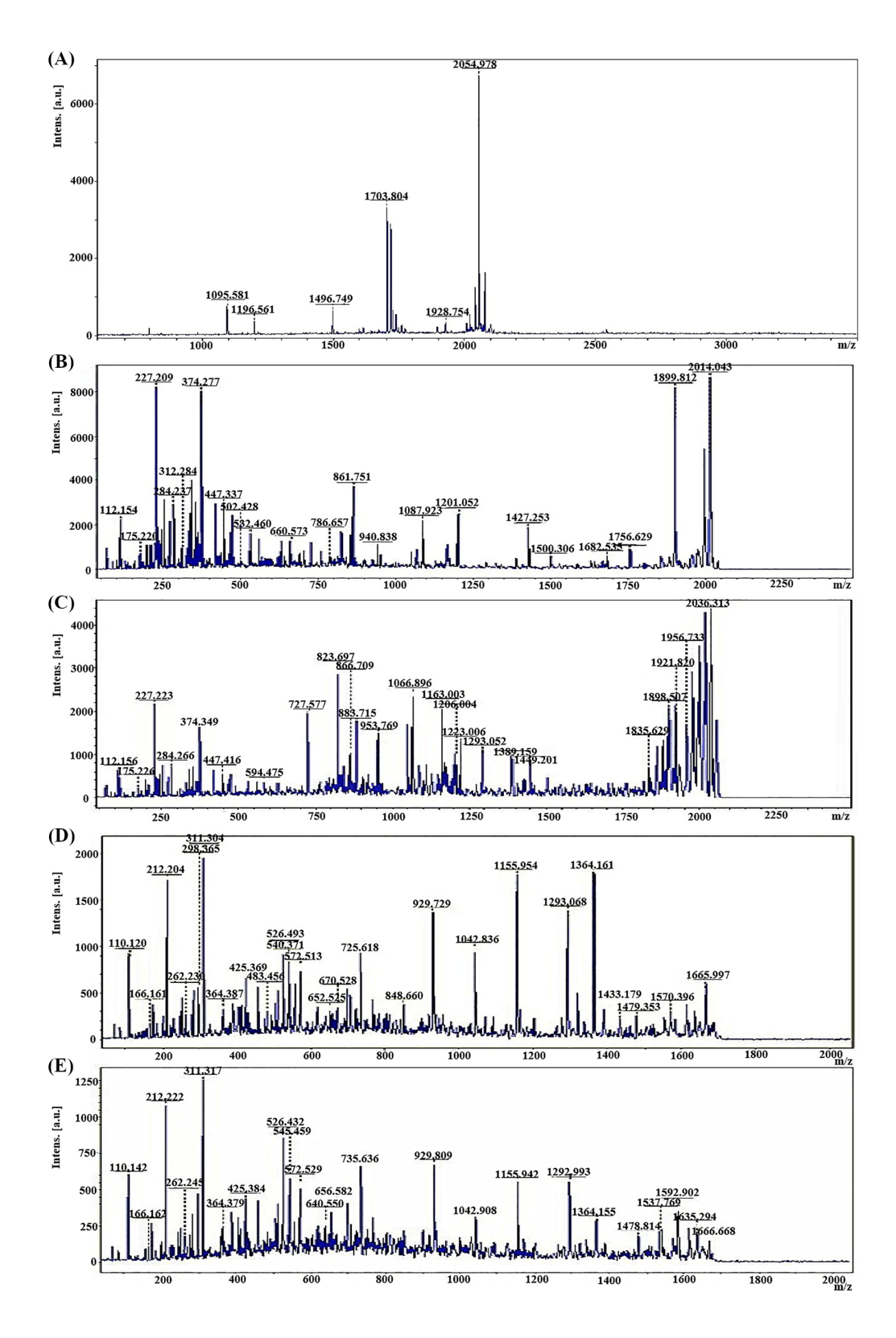


Figure 4. Mass spectrograms of G1H2GC2. (A) Primary mass spectrogram of G1H2GC2. (B-E) Secondary mass spectrogram of G1H2GC2.

3.4. ABTS*+ scavenging activity

The ABTS^{*+} assay is based on the generation of the blue/green radical cation species ABTS^{*+}, which can be reduced by antioxidants; the resulting decrease in absorbance can be monitored at 734 nm. The ability

of G1H2GC2 to scavenge ABTS* was measured to evaluate its antioxidant activities. As shown in Figure 6, G1H2GC2 was found to eliminate ABTS* in vitro in a dose-dependent manner, in which the radical-scavenging activity increased as the protein concentrations in the samples increased. The percentage scavenging activities



Figure 5. Protein identification of G1H2GC2: Text in red showed the parts of the sequence that could be matched.

of G1H2GC2 for ABTS⁺⁺ were 52.84% at a concentration of 15 mg/mL and 43.81% at a concentration of 10 mg/mL. The EC₅₀ value of G1H2GC2 against ABTS⁺⁺ was 17.67 mg/mL.

4. Discussion

Proteins, as a crucial material foundation for human survival, participate in all forms of life activities within biological organisms. Isolating proteins from animals and plants and conducting in-depth research on their structures and functions is of great significance for understanding the primary roles of proteins in human life activities. Most natural proteins are mixtures, and many important proteins exist in low concentrations in animals and plants. The separation of proteins without affecting their structure and function has always been a challenging aspect of protein research. There are numerous methods for protein extraction, including alkali solubilization, ultrasound extraction, organic solvent extraction, and enzymatic extraction. Research indicates that ultrasound-assisted extraction achieves a higher protein extraction rate (35-37). Therefore, we used ultrasound-assisted extraction to extract crude proteins from A. subcrenata Lischke.

There are numerous methods for protein separation and purification, including precipitation, chromatography,

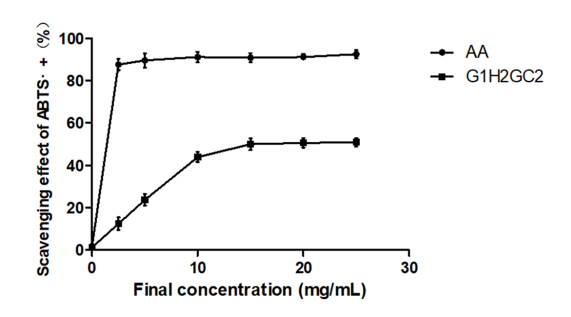


Figure 6. ABTS** scavenging activity of G1H2GC2.

and ultrafiltration (38). Different separation and purification methods operate on distinct principles, allowing the combination of multiple approaches for effective purification. To purify the protein G1H2GC2 from A. subcrenata Lischke, we employed a multi-step strategy. Initially, the target protein was precipitated using ammonium sulfate salting-out. Subsequently, guided by protein purity tracking, we applied a series of chromatographic techniques, including DEAE Sepharose Fast Flow anion exchange, gel filtration chromatography (Sephadex G-25), Phenyl Sepharose CL-4B hydrophobic chromatography and RP-HPLC. A protein from Yarrowia lipolytica was isolated and purified by ultrasonic assisted extraction, ammonium sulfate precipitation, anion exchange chromatography and gel filtration chromatography (39).

Many shellfish species have been identified as possessing potential pharmaceutical or food additive value. Bioactive proteins and their derivatives isolated from various shellfish have demonstrated multiple biological functions, including antioxidant, antitumor, antibacterial, and anti-inflammatory activities (40-42). A mucus protein derived from pearl oyster (Pinctada martensii) was shown to significantly accelerate wound healing and stimulate collagen regeneration in rats (43). Additionally, another water-soluble matrix protein isolated from pacific oysters (Crassostrea gigs) exhibits anti-osteoporosis activity (44). Consequently, shellfish represent a valuable natural resource with potential applications in the nutritional supplement and pharmaceutical industries. Therefore, it is essential to investigate the meat of A. subcrenata Lischke and reveal its latent functional components.

In this study, a novel protein, G1H2GC2, with molecular weight 25.6 kDa and isoelectric point 7.71, was purified from *A. subcrenata* Lischke by several column chromatography techniques including anion exchange, gel filtration chromatography, hydrophobic chromatography and RP-HPLC. In addition, the physicochemical and structural properties of G1H2GC2 were characterized by two electrophoresis techniques as well as Bradford assay, the phenol-sulfuric acid method, ESI-MS and MALDI-TOF MS. The antioxidant activity of G1H2GC2 was investigated by measuring its ABTS*+

scavenging ability. The results showed that G1H2GC2 might be developed as a potential food additive agent.

Funding: This research work was financially supported by the Guangdong Basic and Applied Basic Research Foundation (No. 2023A1515012077).

Conflict of Interest: The authors have no conflicts of interest to disclose.

References

- de Castro RJS, Sato HH. Biologically active peptides: Processes for their generation, purification and identification and applications as natural additives in the food and pharmaceutical industries. Food Res Int. 2015; 74:185-198.
- Saadi S, Saari N, Anwar F, Abdul Hamid A, Ghazali HM. Recent advances in food biopeptides: Production, biological functionalities and therapeutic applications. Biotechnol Adv. 2015; 33:80-116.
- 3. Guan L, Zhu L, Zhang X, Han Y, Wang K, Ji N, Yao X, Zhou Y, Li B, Chen Q, Fan J, Sha D, Lu S. Perilla seed oil and protein: Composition, health benefits, and potential applications in functional foods. Molecules. 2024; 29:5258.
- Zhou N, Zhong Y, Liu H. Characterization and relationship analysis of antioxidant and anti-inflammatory peptides in pomelo fruitlet albumin. Food Chem. 2024; 446:138798.
- Guo C, Ling N, Tian H, Wang Z, Gao M, Chen Y, Ji C. Comprehensive review of extraction, purification, structural characteristics, pharmacological activities, structure-activity relationship and application of seabuckthorn protein and peptides. Int J Biol Macromol. 2025; 294:139447.
- 6. Xie J, Chen S, Huan P, Wang S, Zhuang Y. A novel angiotensin I-converting enzyme inhibitory peptide from walnut (*Juglans sigillata*) protein hydrolysates and its evaluation in Ang II-induced HUVECs and hypertensive rats. Int J Biol Macromol. 2024; 266:131152.
- Li W, Chen W, Wu D, Zhang Z, Liu P, Li Z, Yang Y. Mechanistic insights into antihypertensive activity of mushroom-derived protein-peptides *via* metabolomic and proteomic approaches. Int J Biol Macromol. 2024; 283:137189.
- 8. de Carvalho Oliveira L, Martinez-Villaluenga C, Frias J, Elena Cartea M, Francisco M, Cristianini M, Peñas E. High pressure-assisted enzymatic hydrolysis potentiates the production of quinoa protein hydrolysates with antioxidant and ACE-inhibitory activities. Food Chem. 2024; 447:138887.
- Vadher KR, Sakure AA, Mankad PM, Rawat A, Bishnoi M, Kondepudi KK, Patel A, Sarkar P, Hati S. A comparative study on antidiabetic and anti-inflammatory activities of fermented whey and soy protein isolates and the release of biofunctional peptides: an *in vitro* and *in silico* studies. J Sci Food Agric. 2025; 105:3826-3842.
- Vinayashree S, Hemakumar C, Veeranna RP, Kumar R, Pavithra V, Mahendra VP, Vasu P. *In vitro* studies of pumpkin (*Cucurbita moschata* var. Kashi Harit) seed protein fraction(s) to evaluate anticancer and antidiabetic properties. Plant Foods Hum Nutr. 2024; 79:632-640.
- López-Yoldi M, Riezu-Boj JI, Abete I, Ibero-Baraibar I, Aranaz P, González-Salazar I, Izco JM, Recalde JI,

- González-Navarro CJ, Milagro FI, Zulet MA. Antiobesity effects of a collagen with low digestibility and high swelling capacity: A human randomized control trial. Nutrients. 2024; 16:3550.
- 12. Hirose Y, Kurimoto M, Yuda N, Tanaka M. Identification of whey protein-derived anti-obesity peptides through 3T3-L1 adipocyte differentiation assay. Food Sci Nutr. 2024; 12:9641-9650.
- 13. Zhang ZH, Liao TT, Deng CM, Li B, Okeke ES, Feng WW, Chen Y, Zhao T, Mao GH, Wu XY. Purification and characterization of Se-enriched Grifola frondosa glycoprotein, and evaluating its amelioration effect on As³⁺ -induced immune toxicity. J Sci Food Agric. 2022; 102:2526-2537.
- Lopes-Ferreira M, Sosa-Rosales I, Silva Junior PI, Conceicao K, Maleski ALA, Balan-Lima L, Disner GR, Lima C. Molecular characterization and functional analysis of the nattectin-like toxin from the venomous fish thalassophryne maculosa. Toxins (Basel). 2021; 14:2.
- Li Y, Zhou C, Wang G, Xin H, Xiao Y, Qin C. Identification and validation of the role of ZNF281 in 5-fluorouracil chemotherapy of gastric cancer. J Cancer Res Clin Oncol. 2024; 150:307.
- Wang H, Wang L, Luo X, Guan J, Zhang X, Zhang L, Xiang Y. Molecular characterization, expression and antitumor function analysis of yak IFITM2 gene. Int J Biol Macromol. 2022; 209:405-412.
- 17. Giuliani ME, Bigossi G, Lai G, Marcozzi S, Brunetti D, Malavolta M. Marine compounds and age-related diseases: The path from pre-clinical research to approved drugs for the treatment of cardiovascular diseases and diabetes. Mar Drugs. 2024; 22:210.
- Aneiros A, Garateix A. Bioactive peptides from marine sources: pharmacological properties and isolation procedures. J Chromatogr B Analyt Technol Biomed Life Sci. 2004; 803:41-53.
- 19. Newman DJ, Cragg GM. Marine natural products and related compounds in clinical and advanced preclinical trials. J Nat Prod. 2004; 67:1216-1238.
- Galasso C, Ruocco N, Mutalipassi M, Barra L, Costa V, Giommi C, Dinoi A, Genovese M, Pica D, Romano C, Greco S, Pennesi C. Marine polysaccharides, proteins, lipids, and silica for drug delivery systems: A review. Int J Biol Macromol. 2023; 253:127145.
- Picot L, Ravallec R, Fouchereau-Péron M, et al. Impact of ultrafiltration and nanofiltration of an industrial fish protein hydrolysate on its bioactive properties. J Sci Food Agric. 2010; 90:1819-1826.
- Quirós A, Chichón R, Recio I, Lópezfandiño R. The use of high hydrostatic pressure to promote the proteolysis and release of bioactive peptides from ovalbumin. Food Chem. 2007; 104:1734-1739.
- Kallberg K, Johansson HO, Bulow L. Multimodal chromatography: an efficient tool in downstream processing of proteins. Biotechnol J. 2012; 7:1485-1495.
- 24. Schwartsmann G, Brondani da Rocha A, Berlinck RG, Jimeno J. Marine organisms as a source of new anticancer agents. Lancet Oncol. 2001; 2:221-225.
- 25. Hu X, Song L, Huang L, Zheng Q, Yu R. Antitumor effect of a polypeptide fraction from *Arca subcrenata in vitro* and *in vivo*. Mar Drugs. 2012; 10:2782-2794.
- Zheng Y, Shi H, Li C, Dong L, Zhang M, Yu R, Song L, Zhu J. Identification and characterization of two proteins from Walengzi, the shell of *Arca inflata* and their antioxidant activity. Process Biochem. 2024; 142:24-37.

- Chen L, Song L, Li T, Zhu J, Xu J, Zheng Q, Yu R. A new antiproliferative and antioxidant peptide isolated from *Arca subcrenata*. Mar Drugs. 2013; 11:1800-1814.
- 28. Hu X, Zheng W, Luo Y, Ou X, Song L, Zhang S, He T, Guo Z, Zhu J, Shi H, Huang W, Yu R. *Arca subcrenata* polypeptides inhibit human colorectal cancer HT-29 cells growth *via* suppression of IGF-1R/Akt/mTOR signaling and ATP production. Nutr Cancer. 2020; 72:260-272.
- 29. Guo Z, Shi H, Li C, Luo Y, Bi S, Yu R, Wang H, Liu W, Zhu J, Huang W, Song L. Identification and characterization of a novel protein ASP-3 purified from *Arca subcrenata* and its antitumor mechanism. Mar Drugs. 2019; 17:528.
- Shi H, Panjikar S, Li C, Ou X, Zhou Y, Zhang K, Song L, Yu R, Sun L, Zhu J. Characterization of a novel recombinant calcium-binding protein from *Arca* subcrenata and its anti-hepatoma activities in vitro and in vivo. Int J Biol Macromol. 2023; 245:125513.
- Shi H, Hu X, Zheng H, Li C, Sun L, Guo Z, Huang W, Yu R, Song L, Zhu J. Two novel antioxidant peptides derived from *Arca subcrenata* against oxidative stress and extend lifespan in *Caenorhabditis elegans*. J Funct Foods. 2021; 81:104462.
- 32. Chen Y, Li C, Zhu J, Xie W, Hu X, Song L, Zi J, Yu R. Purification and characterization of an antibacterial and anti-inflammatory polypeptide from *Arca subcrenata*. Int J Biol Macromol. 2017; 96:177-184.
- 33. Song L, Li T, Yu R, Yan C, Ren S, Zhao Y. Antioxidant activities of hydrolysates of *Arca subcrenata* prepared with three proteases. Mar Drugs. 2008; 6:607-619.
- 34. Xu J, Chen Z, Song L, Chen L, Zhu J, Lv S, Yu R. A new *in vitro* anti-tumor polypeptide isolated from *Arca inflata*. Mar Drugs. 2013; 11:4773-4787.
- Rafique H, Peng P, Hu X, Saeed K, Khalid MZ, Khalid W, Morya S, Alsulami T, Mugabi R, Nayik GA. Ultrasoundassisted modification of oat protein isolates: Structural and functional enhancements. Ultrason Sonochem. 2025; 112:107204.
- Zou X, Zhao M, Fei J, Zheng M, Sun P, Ruan H, Yang K, Hao G. Extraction, purification, structural identification, and anti-senescent activity of novel pearl peptides on human dermal fibroblasts. Food Res Int. 2024; 198:115357.
- Zhao F, Zhai X, Liu X, Lian M, Liang G, Cui J, Dong H, Wang W. Effects of high-intensity ultrasound pretreatment on structure, properties, and enzymolysis of walnut protein isolate. Molecules. 2021; 27:208.
- Echave J, Fraga-Corral M, Garcia-Perez P, Popović-Djordjević J, H Avdović E, Radulović M, Xiao J, A Prieto

- M, Simal-Gandara J. Seaweed protein hydrolysates and bioactive peptides: Extraction, purification, and applications. Mar Drugs. 2021; 19:500.
- Li X, Ren JN, Fan G, Zhang LL, Pan SY. Isolation, purification, and mass spectrometry identification of the enzyme involved in citrus flavor (+)-valencene biotransformation to (+)-nootkatone by *Yarrowia lipolytica*. J Sci Food Agric. 2023; 103:4792-4802.
- 40. Karaulova EP, Yakush EV, Slutskaya TN, Shulgina LV. Proximate composition, antioxidant properties, and hepatoprotective activity of three species of shellfish of the pacific coast of Russia. Molecules. 2021; 26:3397.
- 41. Liu P, Li W, Peng Y, Han S, Liang Z, Cen Y, Li X, Wang P, Lv H, Zhang Q, Chen H, Lin J. Molecular cloning, expression, and functional analysis of a putative lectin from the pearl oyster (*Pinctada fucata*, Gould 1850). Fish Shellfish Immunol. 2023; 143:109215.
- 42. Kemp DC, Kwon JY. Fish and shellfish-derived anti-inflammatory protein products: Properties and mechanisms. Molecules. 2021; 26:3225.
- 43. Zeng T, Liu L, Mo D, Yang Q, Hu X, Lu C, Sun R, Zheng L, Zhou B, Xu S. Proteins extracted from pearl oyster (*Pinctada martensii*) with efficient accelerated wound healing *in vitro* through promoting cell proliferation, migration, and collagen formation. Heliyon. 2024; 10:e24239.
- 44. Feng X, Jiang S, Zhang F, Wang R, Zhang T, Zhao Y, Zeng M. Extraction and characterization of matrix protein from pacific oyster (*Crassostrea gigs*) shell and its anti-osteoporosis properties in vitro and in vivo. Food Funct. 2021; 12:9066-9076.

Received June 11, 2025; Revised August 12, 2025; Accepted October 6, 2025.

§These authors contributed equally to this work.

*Address correspondence to:

Rongmin Yu, Department of Chinese Medicine, Guangzhou Huali Science and Technology Vacational College, Guangdong, China. Department of Natural Chemistry, College of Pharmacy, Jinan University, Guangzhou, Guangdong, China.

E-mail: tyrm@jnu.edu.cn

Jianhua Zhu, Biotechnological Institute of Chinese Materia Medica, Jinan University, Guangzhou, Guangdong, China. E-mail: tzhujh@jnu.edu.cn

Released online in J-STAGE as advance publication October 21, 2025.

Original Article

DOI: 10.5582/ddt.2025.01089

Development and reliability assessment of a liquid-phase measurement for skin taurine using skin blotting

Katsunori Kato^{1,2,§}, Kazuhiro Ogai^{3,§}, Yoko Hasegawa³, Chizuko Konya⁴, Hiromi Sanada⁵, Takeo Minematsu^{4,*}

SUMMARY: Skin taurine is an indicator of dehydration and can be noninvasively collected through skin blotting. However, conventional taurine measurement using ninhydrin raises safety and specificity concerns, limiting its application in point-of-care testing. In this study, we propose a novel liquid-phase measurement of taurine collected *via* skin blotting. The aim of this study was to develop a method for liquid-phase measurement of skin taurine and to demonstrate its validity and reliability. This study consisted of (1) determining optimal recovery conditions, including the type and concentration of recovery solution and shaking method (mild, intense, or no shaking), (2) evaluating the specificity of taurine measurement, and (3) assessing the intra- and inter-rater reliability of the developed method for skin taurine measurement. Optimal recovery was achieved by intense shaking for 10 min with a 110 mM sodium chloride solution, and this method could measure taurine concentrations from 31.25 to 500 μ M (r = 0.9983, p < 0.001), confirming its validity. Linear regression analysis showed that the addition of amino acids or skin lysates had little effect on taurine measurement. The developed method demonstrated high intra-rater reliability (intraclass correlation coefficient [ICC] (1,1) = 0.896, p < 0.001 for examiner A; ICC (1,1) = 0.755, p < 0.001 for examiner B), but inter-rater reliability was not significant (ICC (2,1) = 0.187, p = 0.15). The liquid-phase measurement of skin taurine demonstrated high sensitivity, specificity, and intra-rater reliability. Further studies are needed to improve inter-rater reliability for applying this method as a point-of-care tool for dehydration assessment.

Keywords: older adults, dehydration, taurine, skin blotting, liquid-phase measurement, taurine dioxygenase

1. Introduction

Hypertonic dehydration is defined as a loss of total body water (1) and leads to several disorders, such as headache, nausea, heat stroke, and in severe cases, impaired consciousness or death (2). In older adults, dehydration contributes to frailty (3,4), sarcopenia (5,6), and reduced activities of daily living, which further decrease fluid intake and exacerbate dehydration. Moreover, age-related changes in fluid distribution (7), reduced muscle mass (4), diminished thirst (8,9), and impaired osmotic regulation (10,11) make older adults particularly susceptible to dehydration. As dehydration worsens, the risks of hospitalization and mortality increase (3,12), along with healthcare costs (12,13). Its high prevalence, ranging from 19-28% among community-dwelling older adults (6,14) to 20-38% in nursing homes (9,14,15), underscores the urgent need for

dehydration prevention in older adults.

Early identification of dehydration is important to prevent related disorders; however, older adults often show few or no symptoms (16,17). Regular monitoring using point-of-care testing could allow for early detection. Such testing should be noninvasive, quick, portable, safe for home use, and accurate. Several methods exist for identifying dehydration, with serum osmolality being the most reliable (values ≥ 300 mOsm/ kg indicate hypertonic dehydration) (1). However, blood tests are invasive, time-consuming, and require laboratory analysis (18), making them unsuitable for point-of-care monitoring. Noninvasive methods have been proposed, but each has limitations. Physical assessment of dehydration based on symptoms shows poor validity (19). Body weight is not a reliable indicator due to fluctuations from diet and bowel movements (20). Urinalysis or saliva tests are affected by medications

¹Department of Adult Nursing, Graduate School of Nursing, Ishikawa Prefectural Nursing University, Ishikawa, Japan;

² Kanazawa University Hospital, Ishikawa, Japan;

³ Department of Bio-engineering Nursing, Graduate School of Nursing, Ishikawa Prefectural Nursing University, Ishikawa, Japan;

⁴Department of Adult Nursing, Faculty of Nursing, Ishikawa Prefectural Nursing University, Ishikawa, Japan;

⁵ Ishikawa Prefectural Nursing University, Ishikawa, Japan.

(21) and diet (22). Bioimpedance analysis has limited accuracy (23). Echocardiographic evaluation of inferior vena cava diameter shows no clear correlation with dehydration (24). Therefore, no current method fully meets the criteria for practical point-of-care dehydration monitoring.

Recently, a novel, noninvasive, and highly accurate method for detecting dehydration has been proposed. This is based on the skin blotting technique, in which a specific membrane is applied to the skin to collect soluble molecules from interstitial fluid (25). Among the various molecules captured by the skin blotting technique, taurine has emerged as a promising biomarker for dehydration. Taurine plays a key role in regulating keratinocyte volume: under hypertonic conditions, it is taken up by cells to mitigate osmotic stress from excess electrolytes, whereas under hypotonic conditions, it is expelled to restore normal cell volume (26,27). This osmotic regulation explains the correlation between skin taurine levels and changes in osmolarity. Accordingly, Higashimura reported that skin blotting measurement of skin taurine using an anion-exchange membrane could detect current or impending hypertonic dehydration (serum osmolality > 291 mOsm/L) with 77.3% sensitivity, 81.8% specificity, and an area under the receiver operating characteristic curve of 0.789 (16). However, this method relies on ninhydrin staining (16), which requires lengthy staining and a plate reader, limiting speed and portability. Tsuchiya et al. improved this approach by using a ninhydrin spray to shorten the measurement time (28). Nevertheless, safety concerns remain because ninhydrin is a known skin irritant. Additionally, ninhydrin is nonspecific; it reacts with amino acids other than taurine, although with a different color tone. Thus, skin blotting for dehydration detection requires improvements in specificity, speed, and portability.

Therefore, in this study, we aimed to improve taurine measurement using skin blotting. First, to increase specificity and safety, we developed a method using the redox reaction of taurine dioxygenase (29), which is more specific for taurine and safer than the previous ninhydrin method. Next, to enable enzyme reaction, we designed a method to collect taurine from an anionexchange membrane in the liquid phase. This approach builds on Ogai et al. (30), in which a recovery solution is applied to a membrane to collect proteins as a liquid phase. Because skin taurine is captured by the anionexchange membrane, it is speculated that applying an ionic solution to the membrane can extract the trapped taurine into the liquid phase (31). The redox reaction of taurine dioxygenase offers high specificity and sensitivity (32), and the colorimetric measurement can be performed using a portable spectrophotometer.

Based on the above, the aim of this study was to develop a liquid-phase method for measuring skin taurine using skin blotting and to demonstrate the reliability of the method.

2. Materials and Methods

2.1. Study 1: Development of a liquid-phase measurement method of taurine *via* skin blotting

In Study 1, we first aimed to determine the optimal conditions for liquid-phase measurement of taurine blotted onto an anion-exchange membrane, focusing on the type and concentration of the recovery solution and the shaking method used during taurine collection. Once the optimal conditions for liquid-phase measurement of taurine were identified, we next assessed the validity of the method by evaluating the relationship between the amount of taurine applied and the measured results.

2.1.1. Preliminary experiments for determination of the recovery solution

To identify an appropriate recovery solution, we conducted a preliminary experiment in which several ionic solutions were tested based on previous studies (33,34), namely sodium chloride, sodium dihydrogen phosphate, and sodium sulfate solutions. Among the solutions tested, sodium chloride was the most suitable for taurine recovery. Sodium dihydrogen phosphate caused precipitation during taurine measurement using the Taurine Assay Kit (MET-5071; Cell Biolabs, Inc., San Diego, CA, USA), and sodium sulfate appeared to interfere with the measurement reaction (data not shown).

We then performed an experiment to estimate the optimal concentration of sodium chloride for liquid-phase taurine measurement. Sodium chloride solutions ranging from 1 M down to 31.25 mM were tested with mild shaking (see Section 2.5) to evaluate recovery rates. The 110 mM sodium chloride solution yielded the most stable measurements (data not shown) and was, therefore, selected as the starting condition for subsequent validation experiments.

2.1.2. Effect of sodium chloride on taurine measurement

Because sodium chloride solution is not the standard diluent for the Taurine Assay Kit, we evaluated its effect on taurine quantification. Taurine solutions at 500, 250, 125, 62.5, 31.25, 15.6, 7.8, and 0 μ M were prepared with and without 110 mM sodium chloride in the assay buffer. The control group used distilled water (DW) instead of the sodium chloride solution. Taurine concentrations in both groups were measured using the Taurine Assay Kit. Absorbance was measured in triplicate for each sample, and the experiment was repeated three times.

2.1.3. Determination of the optimal sodium chloride concentration for liquid-phase taurine measurement

To determine the optimal sodium chloride concentration for taurine recovery, 0, 55, 110, and 220 mM sodium chloride solutions were used to collect taurine from an anion-exchange membrane preabsorbed with taurine *via* mild shaking (see Section 2.5). Taurine concentrations were then measured using the Taurine Assay Kit. Absorbance was measured in triplicate, and the experiment was repeated three times.

2.1.4. Determination of optimal shaking and time for liquid-phase taurine collection

To determine the optimal conditions for liquid-phase taurine collection, shaking intensity and duration were evaluated. An anion-exchange membrane prepared with a 149.8 μM taurine solution was used as a sample. This concentration was chosen based on the taurine threshold used to assess impending dehydration (serum osmolality > 291 mOsm/L) in a previous study (*16*). The recovery solution used in all conditions was 110 mM sodium chloride. The following shaking intensities and durations were tested: mild shaking for 60 min; intense shaking for 60, 10, or 1 min; and no shaking for 60, 10, or 1 min (see Section 2.5). The amount of taurine recovered under each condition was quantified using the Taurine Assay Kit, and the recovery rate was calculated.

2.1.5. Validation of the liquid-phase measurement of taurine

After determining the optimal conditions, we assessed the validity and measurable range of the method. Taurine solutions at concentrations of 500, 250, 125, 62.5, 31.25, 15.6, 7.8, and 0 µM were applied to anion-exchange membranes to allow taurine adsorption. Liquid-phase taurine measurement was then performed using the Taurine Assay Kit. To enable portable, point-of-care testing of skin taurine, a portable spectrophotometer (GDX-SVISPL; Vernier Science Education, Beaverton, OR, USA) was used for quantification. The correlation coefficient between readouts from the microplate reader (MPR-A100; AS ONE Corp., Osaka, Japan) and the portable spectrophotometer was 0.999, indicating high interchangeability of the two devices (supplementary Figure S1, https://www.ddtjournal.com/action/ getSupplementalData.php?ID=275). Absorbance was measured in triplicate for each sample, and the experiment was repeated three times.

2.2. Study 2: Evaluation of the specificity of taurine measurement

In skin blotting, various substances from the skin surface and underlying tissues are collected, including amino acids and proteins (35-37). Because taurine is an amino acid analog, the specificity of the taurine measurement used in this study was evaluated. To assess this, either

amino acids or skin lysates (rich in skin-derived amino acids and proteins) were individually added as potential interfering substances to taurine solutions, and their effects on taurine measurement were examined. Taurine solutions were prepared at concentrations of 500, 250, 125, 62.5, 31.25, 15.6, 7.8, and 0 μM. To each, either 0, 0.1, or 1.0 μmol of an essential amino acid mixture (L4461; Promega Corp., Madison, WI, USA) or 0, 10, or 100 ng of human skin lysate (NB820-59254; Novus Biologicals, LLC, Centennial, CO, USA) was added. Taurine concentration in each sample was quantified using the Taurine Assay Kit. All samples were measured in triplicate, and the experiment was repeated three times.

2.3. Study 3: Reliability of liquid-phase taurine measurement of skin taurine

The intra- and inter-rater reliabilities of the developed method were assessed as follows. Two researchers (examiner A, with 2 years of experience in scientific research and primarily responsible for this study, and examiner B, with 17 years of research experience and only marginally involved in this study) first underwent training in skin taurine measurement. Twenty volunteers (mean \pm standard deviation [SD]: 43.2 ± 8.7 years; 4 males and 16 females) were recruited, and four regions in total (1R, 2R on the right arm; 1L, 2L on the left arm) were designated on both arms of each participant, as shown in Figure 1. For each volunteer, examiner A randomly chose one site from each arm (1R or 2R, and 1L or 2L), and examiner B measured the region not selected by examiner A.

The skin blotting unit was prepared based on Tsuchiya et al. (28) with slight modifications. Specifically, while the structure consisting of a nitrocellulose membrane stacked with an anion-exchange membrane remained the same as in the previous study (28), a 2% agarose gel was incorporated to prewet the membrane (Figure 2). The skin blotting unit was applied to the skin in the same manner as the previous study (28). Briefly, the measurement region was first wiped with a nonwoven paper towel prewetted with distilled water, and the skin blotting unit was then attached for 20 min. After 20 min, the unit was removed and stored at 4°C until measurement. The sample size of 20 volunteers was determined by power analysis, assuming an intraclass correlation coefficient (ICC) (2,1) of 0.85 with a confidence interval (CI) of 0.2.

Each examiner performed liquid-phase collection of taurine from the anion-exchange membrane under the optimal conditions (10 min of intense shaking) determined in Study 1 and measured the collected taurine using the Taurine Assay Kit. A positive control (an anion-exchange membrane adsorbed with 7.35 nmol of taurine) was included in each measurement.

This experiment was approved by the Ethics

Committee of Ishikawa Prefectural Nursing University (reference number: 2024-12).

2.4. Taurine adsorption to the anion-exchange membrane

For Study 1, anion-exchange membranes adsorbed with different concentrations of taurine were prepared. Based on a previous study (16), a 10×10 mm filter paper was placed on a 12×12 mm anion-exchange membrane (A202-CE; Tokuyama Corp., Tokyo, Japan), and $30 \,\mu\text{L}$ of the designated concentration of taurine solution (32708-02; Nacalai Tesque, Inc., Kyoto, Japan) was applied to the filter paper. A 7.6-g weight was placed on top to ensure close contact between the filter paper and the membrane, and the assembly was left for $10 \, \text{min}$ to allow taurine

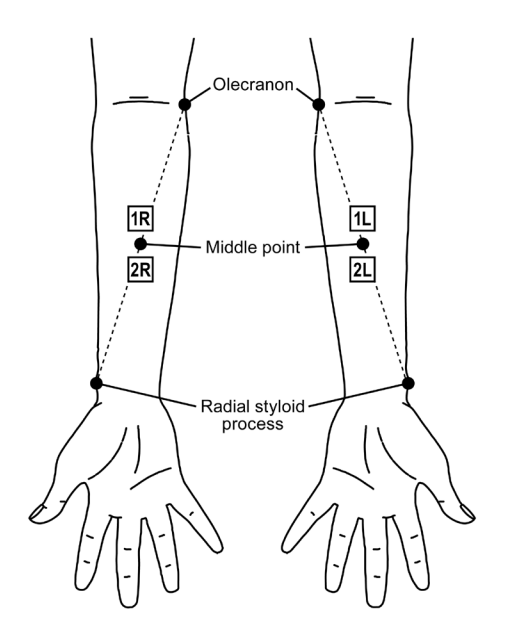


Figure 1. Position of skin blotting unit attachment. The middle point was determined as the midpoint between the olecranon and the radial styloid process of each arm.

adsorption. The anion-exchange membranes were then air-dried and used as samples in Study 1.

2.5. Shaking method for liquid-phase collection of taurine

To collect taurine from each anion-exchange membrane, the following shaking conditions were used: (1) Mild shaking, as in the previous study (30): Membranes were placed in a 24-well plate (#144530; Thermo Fisher Scientific Inc., Waltham, MA, USA) containing 500 µL of recovery solution and shaken on an orbital shaker (EM-36; Taitec Corp., Saitama, Japan) at 4.0 Hz = 240 revolutions per minute (rpm). (2) Intense shaking: The anion-exchange membrane and 125 µL of recovery solution were placed in a 1.5-mL microtube and set on a vortex mixer (Vortex-Genie 2; Scientific Industries, Inc., Bohemia, NY, USA) equipped with a tube support, with the tube lid facing down (Figure 3; the contact area of recovery solution and the membrane is 0.65 cm²). Tubes were mixed at intensity level 1 (7.0 Hz = 420 rpm). (3) No shaking: Prepared using the same method as for intense shaking, except that tubes were left stationary without any shaking.

2.6. Analysis

Data are presented as individual measurements or as means \pm SD. All statistical analyses were performed using Statistical Package for the Social Sciences (SPSS) software (version 29; IBM Corp., Armonk, NY, USA) and Microsoft Excel (version 2506; Microsoft Corp., Redmond, WA, USA). A *p*-value < 0.05 was considered statistically significant.

2.6.1. Study 1

Linear regression analysis was used to evaluate the relationship between taurine concentration and

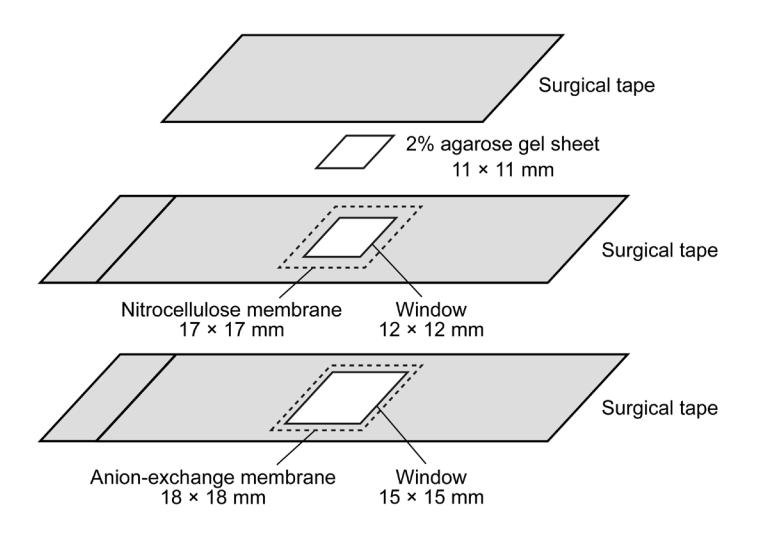


Figure 2. A skin blotting unit.

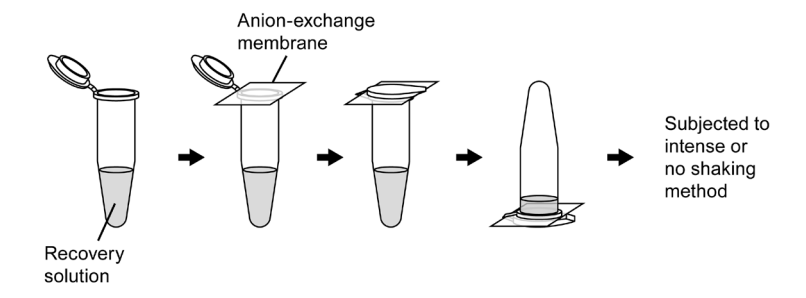


Figure 3. Modified method for liquid-phase collection of taurine.

background-adjusted absorbance, with the correlation coefficient (r) representing the strength of the linear association. The regression lines of the DW group and the 110 mM sodium chloride group were compared to determine whether the slope and intercept of the 110 mM sodium chloride group fell within the range of the mean \pm 0.5 SD of the slope and intercept of the DW group. The recovery rate was calculated as the ratio of the recovered taurine amount to the applied taurine amount.

2.6.2. Study 2

The percent coefficient of variation (%CV) was calculated as the SD divided by the mean, multiplied by 100. Two-way analysis of variance (ANOVA) with Tukey's *post hoc* adjustment was performed to evaluate the interaction between taurine concentration and potential contaminants (amino acids or skin extracts).

2.6.3. Study 3

ICC (1,1) and ICC (2,1) were calculated to evaluate intra- and inter-rater reliability, respectively. Additional reliability analyses were performed using Bland–Altman analysis: fixed error was evaluated with the 95% CI of differences, proportional error was assessed with regression analysis of the plots, and random error was evaluated using limits of agreement (LOA), standard error of measurement (SEM), minimum detectable change (MDC), and the ratio of MDC to the measured value (MDC%) (38).

3. Results

3.1. Study 1: Development of a liquid-phase measurement method of taurine *via* skin blotting

3.1.1. Effect of sodium chloride on taurine measurement

The effect of sodium chloride on taurine measurement is shown in Figure 4A. The linear regression equation for the DW group was $y = 4.68 \times 10^{-4}x + 0.0143$ (r = 0.991, p < 0.001), and for the sodium chloride group, it was $y = 4.42 \times 10^{-4}x + 0.0107$ (r = 0.980, p < 0.001).

The mean \pm 0.5 SD of the intercept in the DW group ranged from 0.0129 to 0.0157, and the mean intercept in the sodium chloride group (0.0108) fell below this range. Similarly, the mean \pm 0.5 SD of the slope in the DW group ranged from 4.44 \times 10⁻⁴ to 4.91 \times 10⁻⁴, and the mean slope in the sodium chloride group (4.42 \times 10⁻⁴) was also below the lower limit.

3.1.2. Liquid-phase collection of taurine at different sodium chloride concentrations

Figure 4B shows the recovery rates of taurine at different sodium chloride concentrations. The mean recovery rates (range) were 27.1% (14.4–41.3%) at 0 mM, 70.6% (56.4–79.5%) at 55 mM, 100.8% (97.7–106.4%) at 110 mM, and 124.6% (108.5–150.9%) at 220 mM.

3.1.3. Liquid-phase collection of taurine with different shaking methods and durations

Table 1 and Figure 4C present the results of the evaluation of shaking methods and durations on taurine recovery from the anion-exchange membrane. Mild shaking for 60 min yielded a mean recovery rate of 109.0 \pm 16.3% with a %CV of 15.0%, confirming high and stable taurine recovery close to 100%.

The intense shaking method yielded the following mean recovery rates \pm SD (%CV): $85.0 \pm 8.8\%$ (10.4%) at 1 min, $94.9 \pm 4.4\%$ (4.7%) at 10 min, and $92.7 \pm 5.2\%$ (5.6%) at 60 min. The no-shaking method yielded $27.5 \pm 3.1\%$ (11.2%) at 1 min, $58.6 \pm 22.5\%$ (38.3%) at 10 min, and $101.5 \pm 9.9\%$ (9.7%) at 60 min. Among the tested conditions, 10 min of intense shaking showed a recovery rate closest to 100% with the lowest %CV.

3.1.4. Measurable range and validation of the liquidphase measurement of taurine

The mean values (range) of background-adjusted absorbance at taurine concentrations of 7.8 μ M and 15.6 μ M were 0.0146 (0.0102–0.0188) and 0.0175 (0.0125–0.0233), respectively, both falling within the range observed at a taurine concentration of 0 μ M (0.0105–0.0173). Therefore, concentrations below or equal to

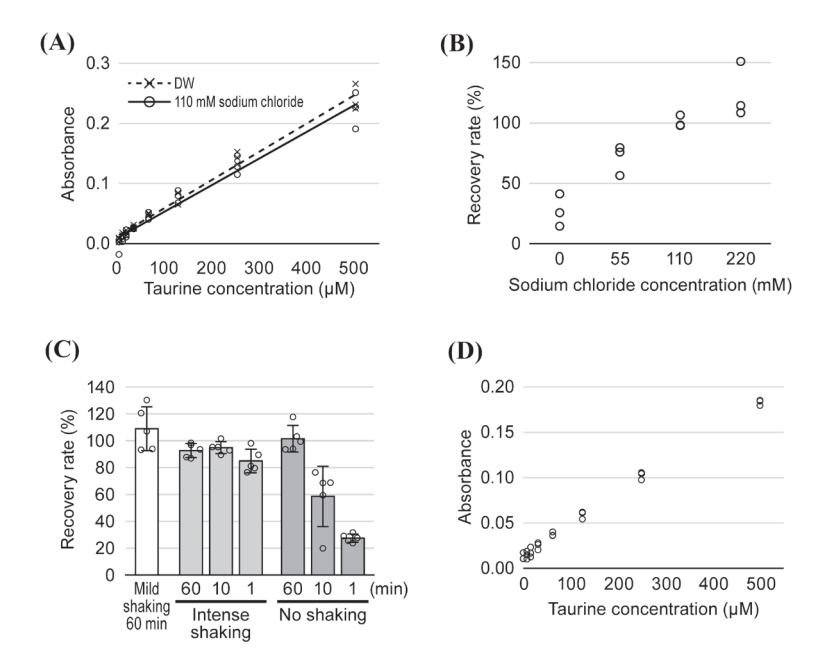


Figure 4. Evaluation of the liquid-phase measurement of taurine. (A) Effect of sodium chloride on taurine measurement. Absorbance values are background-adjusted. (B) Effect of sodium chloride concentration on taurine recovery in the liquid-phase measurement. Recovery rate is calculated as the ratio of taurine recovered to the amount applied to the anion-exchange membrane. (C) Effect of shaking method and time on taurine recovery. Data are expressed as mean \pm standard deviation. (D) Correlation between taurine concentration and measurement results obtained using the developed liquid-phase measurement method. Absorbance values are background-adjusted. DW: distilled water.

Table 1. Effect of shaking method and time on taurine recovery in liquid-phase collection

Shaking method	Time (min)	Recovery rate* (%)	%CV	
Mild Shaking [†]	60	109.0 ± 16.3	15.0	
Intense shaking	1	85.0 ± 8.8	10.4	
	10	94.9 ± 4.4	4.7	
	60	92.7 ± 5.2	5.6	
No shaking	1	27.5 ± 3.1	11.2	
-	10	58.6 ± 22.5	38.3	
	60	101.5 ± 9.9	9.7	

Mean \pm standard deviation; CV: coefficient of variation. *Ratio of taurine recovered to the amount of taurine applied to the anion-exchange membrane. †Used in a previous study (30).

15.6 μM were considered unreliable and excluded.

The relationship between taurine concentrations and measurement results is shown in Figure 4D. A significant correlation was observed for concentrations between 31.2 and 500 μ M, with the regression equation $y = 3.36 \times 10^{-4}x + 0.0165$ (r = 0.998, p < 0.001).

3.2. Study 2: Reaction specificity of taurine measurement

Figure 5A shows the results of adding amino acids to taurine solutions and their effect on taurine quantification. Two-way ANOVA revealed no significant interaction between taurine concentration and the amount of amino acids added (p = 0.91). However, both main effects were significant: taurine concentration (p < 0.001) and amino acid addition (p = 0.031). Multiple comparisons showed no significant differences in taurine

quantification between the 0- and 0.1- μ mol groups (p = 0.318) or between the 0.1- and 1.0- μ mol groups (p = 0.417). In contrast, a significant difference was observed between the 0- and 1.0- μ mol groups (p = 0.023).

Figure 5B shows the results of adding skin lysate to taurine solutions and its effect on absorbance. Two-way ANOVA indicated no significant interaction between taurine concentration and the amount of skin lysate added (p = 0.977). The main effect of taurine concentration was significant (p < 0.001), whereas the main effect of skin lysate amount was not significant (p = 0.061).

3.3. Study 3: Reliability of liquid-phase taurine measurement

The measured values for the positive control were 0.0597 for examiner A and 0.0587 for examiner B. Intra-rater reliability [ICC (1,1)] and its 95% CI were 0.896 (0.759–

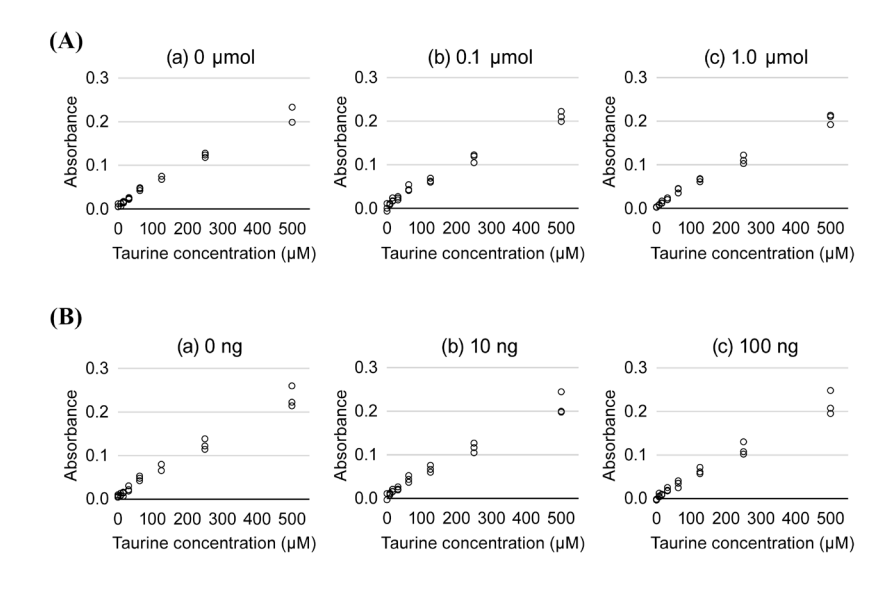


Figure 5. Specificity of taurine measurement. (A) Effect of amino acid addition on taurine measurement. Amounts added: (a) 0 μmol, (b) 0.1 μmol, (c) 1.0 μmol, (B) Effect of skin lysate addition on taurine measurement. Amounts added: (a) 0 ng, (b) 10 ng, (c) 100 ng. Absorbance values are background-adjusted.

0.957) for examiner A and 0.755 (0.485-0.894) for examiner B, both of which were statistically significant (p < 0.001 for both). Bland-Altman plots for each examiner are shown in Figure 6A. All measurements were within the LOA for examiner A, while one measurement for examiner B fell below the lower LOA. Measurement errors for each examiner, calculated from the Bland-Altman plots, are shown in Table 2. The 95% CI for the mean difference was 0.0005 to 0.0017 for examiner A and -0.0017 to -0.0004 for examiner B, with both ranges not including zero. Regression analysis of the Bland-Altman plot for proportional error showed no significant coefficients for examiner A (-0.11, p = 0.65) or examiner B (-0.02, p = 0.93). Random error analysis showed that the MDC%, representing the degree of random error relative to the measurement, was 26.9% for examiner A and 35.4% for examiner B.

Inter-rater reliability [ICC (2,1)] and its 95% CI between the two examiners was 0.187 (-0.160-0.536), which was not statistically significant (p = 0.15). The Bland–Altman plot for inter-rater reliability is shown in Figure 6B, and the measurement error between examiners is shown in Table 3. The mean difference in skin taurine between examiners A and B was 0.00524, and the LOA was -0.0114 to 0.0219. All measurements fell within the LOA, and the 95% CI for the mean difference in fixed error was -0.0066 to 0.0039, including zero. The regression coefficient for proportional error was not significant (0.32, p = 0.18). The random error indicator MDC% was 68.7%.

4. Discussion

In this study, we developed and evaluated a new method for measuring skin taurine *via* skin blotting,

employing liquid-phase collection of taurine from an anion-exchange membrane and redox reaction by taurine dioxygenase for faster, more specific, and safer quantification. The developed liquid-phase measurement method demonstrated higher specificity for taurine and greater measurement sensitivity than the conventional ninhydrin method. It also showed high intra-rater reliability, but inter-rater reliability was not significant, indicating the need to improve consistency between examiners. These results suggest that the developed method, once the remaining issues are addressed, has the potential to serve as a noninvasive point-of-care test for assessing skin taurine levels in clinical settings.

Preliminary experiments confirmed the feasibility of using sodium chloride solution for liquid-phase taurine collection. To evaluate its applicability, we examined the effect of sodium chloride on taurine quantification. Regression slopes and intercepts from the DW group were used as standards (mean \pm 0.5 SD) for comparison. The slope and intercept values for the sodium chloride group were slightly below the lower limits of the DW group, suggesting that 110 mM sodium chloride may mildly inhibit taurine quantification, possibly by reducing the substrate reactivity of taurine dioxygenase in the sodium chloride solution (39). Nevertheless, significantly high correlations between taurine concentration and measured values were observed in both groups, indicating that measurement accuracy is maintained using the sodium chloride-based liquid-phase collection method.

To determine the optimal sodium chloride concentration, taurine recovery was compared across different concentrations of sodium chloride. Recovery rates exceeded 100% under both the 110 mM and 220 mM conditions, with the 220 mM condition reaching

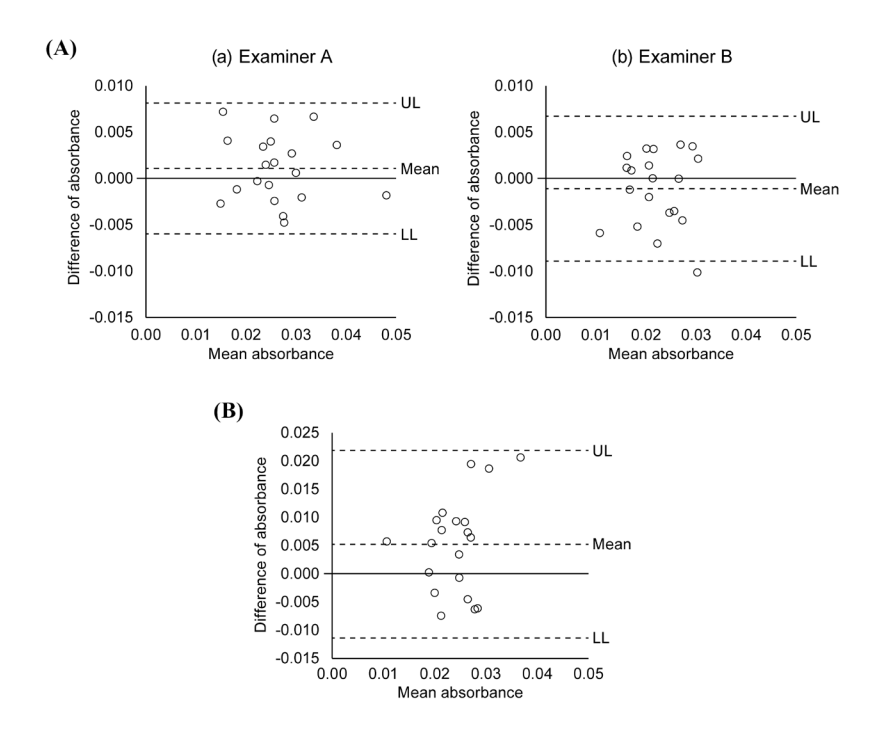


Figure 6. Bland-Altman plots of measurement errors. (A) Intra-rater error for each examiner. (B) Inter-rater error between the two examiners. UL: upper limit of agreement; LL: lower limit of agreement.

Table 2. Measurement error of each examiner in the Bland-Altman analysis

Examiner	104	Fixed error	Proportional error		Random error		
	LOA	95% CI	Regression coefficient	<i>p</i> -value	SEM	MDC	MDC%
A B	-0.0060 - 0.0081 -0.0089 - 0.0067	0.0005 - 0.0017 -0.00170.0004	-0.11 -0.02	0.65 0.93	0.0025 0.0028	0.0071 0.0078	26.9 35.4

LOA: limits of agreement; CI: confidence interval; SEM: standard error of measurement; MDC: minimal detectable change.

Table 3. Measurement error between the two examiners in the Bland-Altman analysis

LOA	Fixed error	Proportional error		Random error		
	95% CI	Regression coefficient	p-value	SEM	MDC	MDC%
-0.0114 - 0.0219	-0.0066 - 0.0039	0.32	0.18	0.0060	0.0166	68.7

LOA: limits of agreement; CI: confidence interval; SEM: standard error of measurement; MDC: minimal detectable change.

150.9%, considerably exceeding the theoretical maximum. This suggests that excessive sodium chloride may cause measurement instability (39). Therefore, 110 mM sodium chloride was selected as the optimal solution for stable taurine recovery.

Next, we evaluated the shaking methods and durations required for liquid-phase taurine collection from anion-exchange membranes using 110 mM sodium chloride. We considered nearly 100% recovery and low variability as essential conditions for effective collection, with desirable conditions including shorter shaking times and minimal use of equipment. Mild shaking for 60 min, as used in the previous study (30), served as a reference and achieved approximately 100%

recovery. The no-shaking method, the simplest collection approach, showed increasing recovery over time: 27.5% at 1 min, 58.6% at 10 min, and 101.5% at 60 min. In contrast, intense shaking achieved higher recovery in less time: 85.0% at 1 min and 94.5% at 10 min. To assess variability, we compared the %CV across conditions. The lowest %CV was 9.73% for the no-shaking method at 60 min and 4.67% for the intense shaking method at 10 min, indicating that 10 min intense shaking provided the best balance of recovery and reproducibility.

Using the optimized protocol (10-min intense shaking), we confirmed the validity and measurable range of liquid-phase taurine measurement. A strong, significant correlation was observed between taurine

concentration and measured values within the range of 31.25 to 500 μ M (r = 0.9983, p < 0.001). This range is lower than that reported in previous studies (51.4–6,400 μ M) (16,28), indicating improved sensitivity for detecting the dehydration threshold (149.8 μ M) estimated in earlier work (16).

Because skin blotting can collect various contaminants, such as amino acids other than taurine, skin proteins, sebum, and cells, we next evaluated the specificity of the liquid-phase taurine measurement. Adding a high concentration of the amino acid mixture (1.0 µmol) had a slight effect on quantification, but no significant effects were observed at the lower concentration (0.1 µmol) or with any of the skin lysate additions. Sylvestre et al. reported that the total amount of amino acids collected by iontophoresis from the stratum corneum ranged from 0.3 to 0.6 µmol/cm² (35). In the present study, taurine was measured from an anion-exchange membrane with a surface area of 0.65 cm², corresponding to an estimated amino acid contamination of 0.2-0.4 µmol. This value falls within the 0.1-1.0 µmol range of amino acids tested in this study. Because no statistically significant difference in taurine measurement was observed between the 0.1 µmol and 1.0 µmol groups, the influence of physiological amino acid contamination on skin taurine measurement appears negligible. Eichhorn et al. reported that taurine dioxygenase can react with several sulfonic acids other than taurine, but their reactivity is much lower than that of taurine (32). Moreover, these sulfonic acids are not naturally found in the human body (40). These findings further support the high specificity of the present method for measuring skin taurine.

Taurine is an amino acid analog, and ninhydrin, which has been used in previous studies, reacts with amino acids and proteins other than taurine to produce color, although the color is distinct from that of taurine (16). Therefore, taurine measurement by ninhydrin staining could be affected by skin contaminants. In contrast, the high specificity of the newly developed liquid-phase taurine measurement provides a significant advantage for more accurate quantification of skin taurine.

Intra-rater reliability [ICC (1,1)] was 0.896 for examiner A and 0.755 for examiner B, both of which meet the "good" criteria defined by Koo and Li (41), indicating high intra-rater reliability for both examiners. Bland–Altman plots showed significant fixed and random errors for both examiners, but these were considered within practical limits. In contrast, inter-rater reliability [ICC (2,1)] was not significant (p=0.15), indicating that inter-rater reliability could not be confirmed. This suggests that several factors may have contributed to the lower inter-rater reliability. Bland–Altman analysis revealed a large random error between examiners. The high degree of agreement between the positive control measurements performed by the two examiners suggests

that both could properly perform liquid-phase taurine collection and the subsequent measurement of taurine. This suggests that the random errors may arise from the procedure between the application and removal of the skin blotting unit.

In taurine measurement using skin blotting, the skin surface is wiped with a nonwoven cloth moistened with DW to remove contaminants before attaching the blotting unit (16,28). Differences between examiners in the amount of DW applied, the force used during wiping, or wiping speed may have contributed to higher random error. Indeed, previous studies report variation in the forces applied to the skin among skilled caregivers during bed baths (42), suggesting considerable variability in wiping parameters. Therefore, further standardization of techniques, along with prior education and training, is necessary for consistent results. Despite this, the higher intra-rater reliability indicates that the developed method can be considered reliable when performed by a single operator.

Currently, the entire process takes approximately 60 min (20 min for skin blotting, 10 min for liquid-phase collection, and 30 min for enzymatic reaction). While this study demonstrates the validity of the developed method, further work is needed to improve speed and confirm its clinical reliability.

A limitation of this study is that sampling sites on the inner sides of the forearms were assumed to be homogeneous, and reliability was evaluated based on this assumption. However, differences between sites may exist. To verify this, skin taurine concentration could be measured using invasive methods such as tissue biopsy or microdialysis, but these methods are not suitable because of their invasiveness. Future studies should clarify potential differences in skin taurine concentration depending on the sampling site.

5. Conclusion

In this study, we developed a novel method for measuring skin taurine using skin blotting by combining liquid-phase taurine collection with redox reaction by taurine dioxygenase. The developed method showed improved specificity and sensitivity, as well as high intra-rater reliability, although inter-rater reliability was not significant. By improving inter-rater reliability through measures such as operator training, this method has the potential to serve as a practical tool for skin taurine measurement and point-of-care dehydration testing, contributing to dehydration prevention and the maintenance of daily living activities and cognitive function in older adults.

Acknowledgements

The authors would like to thank Ms. Akiko Hayashi and Ms. Aya Ito for their technical assistance.

Funding: This study was supported in part by the Research Grant from Ishikawa Prefectural Nursing University.

Conflict of Interest: The prototype anion-exchange membrane used in this study was provided free of charge by Tokuyama Corp. (Tokyo, Japan). Kazuhiro Ogai and Yoko Hasegawa are affiliated with the Department of Bio-engineering Nursing, which received funding from Saraya Co., Ltd. (Osaka, Japan). The funder had no involvement in any stage of this research.

References

- Thomas DR, Cote TR, Lawhorne L, Levenson SA, Rubenstein LZ, Smith DA, Stefanacci RG, Tangalos EG, Morley JE, Dehydration C. Understanding clinical dehydration and its treatment. J Am Med Dir Assoc. 2008; 9:292-301.
- 2. Edmonds CJ, Foglia E, Booth P, Fu CHY, Gardner M. Dehydration in older people: A systematic review of the effects of dehydration on health outcomes, healthcare costs and cognitive performance. Arch Gerontol Geriatr. 2021; 95:104380.
- 3. Stookey JD, Purser JL, Pieper CF, Cohen HJ. Plasma hypertonicity: another marker of frailty? J Am Geriatr Soc. 2004; 52:1313-1320.
- Lorenzo I, Serra-Prat M, Yébenes JC. The Role of Water Homeostasis in Muscle Function and Frailty: A Review. Nutrients. 2019; 11:1857.
- Yoo JI, Choi H, Song SY, Park KS, Lee DH, Ha YC. Relationship between water intake and skeletal muscle mass in elderly Koreans: A nationwide population-based study. Nutrition. 2018; 53:38-42.
- Stookey JD. High prevalence of plasma hypertonicity among community-dwelling older adults: results from NHANES III. J Am Diet Assoc. 2005; 105:1231-1239.
- Ritz P. Chronic cellular dehydration in the aged patient. J Gerontol A Biol Sci Med Sci. 2001; 56:M349-352.
- Kenney WL, Chiu P. Influence of age on thirst and fluid intake. Med Sci Sports Exerc. 2001; 33:1524-1532.
- 9. Phillips PA, Johnston CI, Gray L. Disturbed fluid and electrolyte homoeostasis following dehydration in elderly people. Age Ageing. 1993; 22:S26-33.
- 10. Sato M, Kanikowska D, Sugenoya J, Inukai Y, Shimizu Y, Nishimura N, Iwase S. Effects of aging on thermoregulatory responses and hormonal changes in humans during the four seasons in Japan. Int J Biometeorol. 2011; 55:229-234.
- McLean KA, O'Neill PA, Davies I, Morris J. Influence of age on plasma osmolality: a community study. Age Ageing. 1992; 21:56-60.
- Paulis SJC, Everink IHJ, Halfens RJG, Lohrmann C, Schols JMGA. Prevalence and Risk Factors of Dehydration Among Nursing Home Residents: A Systematic Review. J Am Med Dir Assoc. 2018; 19:646-657.
- Hooper L, Bunn DK, Downing A, Jimoh FO, Groves J, Free C, Cowap V, Potter JF, Hunter PR, Shepstone L. Which Frail Older People Are Dehydrated? The UK DRIE Study. J Gerontol A Biol Sci Med Sci. 2016; 71:1341-1347.
- Parkinson E, Hooper L, Fynn J, Wilsher SH, Oladosu T, Poland F, Roberts S, Van Hout E, Bunn D. Low-intake dehydration prevalence in non-hospitalised older adults:

- Systematic review and meta-analysis. Clin Nutr. 2023; 42:1510-1520.
- 15. Marra MV, Simmons SF, Shotwell MS, Hudson A, Hollingsworth EK, Long E, Kuertz B, Silver HJ. Elevated Serum Osmolality and Total Water Deficit Indicate Impaired Hydration Status in Residents of Long-Term Care Facilities Regardless of Low or High Body Mass Index. J Acad Nutr Diet. 2016; 116:828-836.e2.
- 16. Higashimura S. Development of the measurement of taurine concentration by the skin blotting: A non-Invasive identifying method for chronic dehydration of vulnerable older people in home care setting. [dissertation]. Tokyo, Japan: The University of Tokyo; 2020.
- Higashimura S, Tamai N, Nakagami G, Tobe H, Sanada H. A pilot epidemiological study on chronic dehydration of older adults in home care setting. J Nurs Sci Eng. 2022; 9:123-135.
- Leibovitz A, Baumoehl Y, Lubart E, Yaina A, Platinovitz N, Segal R. Dehydration among long-term care elderly patients with oropharyngeal dysphagia. Gerontology. 2007; 53:179-183.
- Fortes MB, Owen JA, Raymond-Barker P, Bishop C, Elghenzai S, Oliver SJ, Walsh NP. Is This Elderly Patient Dehydrated? Diagnostic Accuracy of Hydration Assessment Using Physical Signs, Urine, and Saliva Markers. J Am Med Dir Assoc. 2015; 16:221-228.
- Vivanti A, Yu L, Palmer M, Dakin L, Sun J, Campbell K. Short-term body weight fluctuations in older wellhydrated hospitalised patients. J Hum Nutr Diet. 2013; 26:429-435.
- Johnson P, Hahn RG. Signs of Dehydration in Nursing Home Residents. J Am Med Dir Assoc. 2018; 19:1124-1128.
- 22. Ely BR, Cheuvront SN, Kenefick RW, Sawka MN. Limitations of salivary osmolality as a marker of hydration status. Med Sci Sports Exerc. 2011; 43:1080-1084.
- Kafri MW, Myint PK, Doherty D, Wilson AH, Potter JF, Hooper L. The diagnostic accuracy of multi-frequency bioelectrical impedance analysis in diagnosing dehydration after stroke. Med Sci Monit. 2013; 19:548-570.
- Nagae M, Umegaki H, Onishi J, Huang CH, Yamada Y, Watanabe K, Komiya H, Kuzuya M. Chronic Dehydration in Nursing Home Residents. Nutrients. 2020; 12:3562.
- Minematsu T, Horii M, Oe M, Sugama J, Mugita Y, Huang L, Nakagami G, Sanada H. Skin blotting: a noninvasive technique for evaluating physiological skin status. Adv Skin Wound Care. 2014; 27:272-279.
- Janeke G, Siefken W, Carstensen S, Springmann G, Bleck O, Steinhart H, Hoger P, Wittern KP, Wenck H, Stab F, Sauermann G, Schreiner V, Doering T. Role of taurine accumulation in keratinocyte hydration. J Invest Dermatol. 2003; 121:354-361.
- Kwon HM, Handler JS. Cell volume regulated transporters of compatible osmolytes. Curr Opin Cell Biol. 1995; 7:465-471.
- Tsuchiya H, Abe M, Tomida S, Higashimura S, Haba D, Minematsu T, Sanada H, Nakagami G. Development and evaluation of a rapid skin taurine measurement device using skin blotting for the early detection of dehydration. Jpn J Nurs Sci. 2025; 22:e70007.
- Matsuda M, Asano Y. A simple assay of taurine concentrations in food and biological samples using taurine dioxygenase. Anal Biochem. 2012; 427:121-123.
- 30. Ogai K, Hasegawa Y, Kato K, Takizawa R, Nuka N, Imakata Y, Onishi Y, Matsumoto C, Matsumoto M, Dai M,

- Konya C, Minematsu T. Validation of liquid-phase method of skin blot samples. J Nurs Sci Eng. 2024; 12:10-16.
- Alexandratos SD. Ion-exchange resins: a retrospective from industrial and engineering chemistry research. Ind Eng Chem Res. 2009; 48:388-398.
- Eichhorn E, van der Ploeg JR, Kertesz MA, Leisinger T. Characterization of α-ketoglutarate-dependent taurine dioxygenase from Escherichia coli. J Biol Chem. 1997; 272:23031-23036.
- Luo T, Abdu S, Wessling M. Selectivity of ion exchange membranes: A review. J Membr Sci. 2018; 555:429-454.
- 34. Pismenskaya N, Laktionov E, Nikonenko V, El Attar A, Auclair B, Pourcelly G. Dependence of composition of anion-exchange membranes and their electrical conductivity on concentration of sodium salts of carbonic and phosphoric acids. J Membr Sci. 2001; 181:185-197.
- Sylvestre JP, Bouissou CC, Guy RH, Delgado-Charro MB. Extraction and quantification of amino acids in human stratum corneum *in vivo*. Br J Dermatol. 2010; 163:458-465
- Clausen ML, Slotved HC, Krogfelt KA, Agner T. Tape Stripping Technique for Stratum Corneum Protein Analysis. Sci Rep. 2016; 6:19918.
- 37. Hughes AJ, Tawfik SS, Baruah KP, O'Toole EA, O'Shaughnessy RFL. Tape strips in dermatology research. Br J Dermatol. 2021; 185:26-35.
- Mohammad MT, Whitney SL, Marchetti GF, Sparto PJ, Ward BK, Furman JM. The reliability and response

- stability of dynamic testing of the vestibulo-ocular reflex in patients with vestibular disease. J Vestib Res. 2011; 21:277-288.
- Combes D, Ye WN, Zwick A, Monsan P. Effect of salts on enzyme stability. Ann N Y Acad Sci. 1988; 542:7-10.
- Wishart DS, Guo A, Oler E, et al. HMDB 5.0: the Human Metabolome Database for 2022. Nucleic Acids Res. 2022; 50:D622-D631.
- 41. Koo TK, Li MY. A Guideline of Selecting and Reporting Intraclass Correlation Coefficients for Reliability Research. J Chiropr Med. 2016; 15:155-163.
- 42. Ishii K, Nakada H, Kobayashi H. Wiping pressure of clinical nurses using pressure measurement film Comparison of cotton towel and disposable towel on normal skin. J Nurs Sci Eng. 2022; 10:37-43. (in Japanese)

Received August 22, 2025; Revised October 14, 2025; Accepted October 19, 2025.

These authors contributed equally to this work.

*Address correspondence to:

Takeo Minematsu, Department of Adult Nursing, Faculty of Nursing, Ishikawa Prefectural Nursing University, Gakuendai 1-1, Kahoku City, Ishikawa 929-1210, Japan.

E-mail: takeom@ishikawa-nu.ac.jp

Released online in J-STAGE as advance publication October 25, 2025.

Original Article

DOI: 10.5582/ddt.2025.01082

TRPC6 expression is negatively correlated with breast cancer progression

Yifei Ma^{1,§}, Guoning Li^{2,§}, Haoyang Yu¹, Baoke Wang¹, Zhihan Diao¹, Yuan Du¹, Hongbo Wang^{1,*}, Huiping Liu^{1,*}

SUMMARY: The transient receptor potential channel 6 (TRPC6), a Ca²⁺-permeable, non-selective cation channel, is a potential drug target widely expressed in most human tissues. However, the role of TRPC6 in breast cancer remains largely unknown. We comprehensively investigated the relationships between TRPC6 and breast cancer using online databases, including TIMER, cBioPortal, UALCAN, the Kaplan-Meier plotter, the Human Protein Atlas, STRING, and the LinkedOmics, to evaluate the prognostic value of TRPC6. We also tentatively explored the effects of TRPC6 modulation on proliferation and metastasis potential in several breast cancer cell lines by MTT assay, colony formation assay, flow cytometry, and scratch wound healing assay. The TCGA data showed lower TRPC6 gene expression in breast tumours versus normal breast tissues. The Human Protein Atlas revealed that the TRPC6 protein was generally expressed at low levels in both normal and breast carcinoma tissue. The Kaplan-Meier plotter showed that the low TRPC6 level is correlated with worse relapse-free survival probability in breast cancer. Moreover, the TRPC6 gene was linked to immune infiltration in breast cancer, and this relationship affected the prognosis of breast cancer. In contrast to published researches, we found that TRPC6 expression was negatively correlated with breast cancer cell proliferation and metastasis abilities, suggesting TRPC6 as a promising prognostic biomarker for breast cancer, where low expression of TRPC6 was related to worse prognoses. This research raises the necessity of rethinking the mechanism perspective and targetability of TRPC6 in breast cancer, which warrants further investigation.

Keywords: transient receptor potential channel, biomarker, metastasis

1. Introduction

The transient receptor potential canonical (TRPC) channels are nonselective cation channels belonging to the TRP family expressed in various tissues. The TRPC subfamily comprises seven transmembrane proteins (TRPC1-7). TRPC6 is a crucial membrane protein composed of multiple subunits that assemble to form a functional channel pore, which allows Ca²⁺ and Na⁺ ions to enter the cells between the fifth and sixth transmembrane domains. Among all TRPCs, TRPC6 deficiency or increased activity has been associated with many diseases (1). Aberrant overexpression of TRPC6 has been documented across multiple tumour types compared to normal tissues, including different types of cancers such as glioma (2), salivary gland tumours (3), renal cancer (4), prostate cancer (5), ovarian cancer (6), cervical cancer (7), and breast cancer (8).

Breast cancer is the most commonly diagnosed cancer and the leading cause of cancer-related deaths in women, accounting for one-quarter of all new female cancer cases diagnosed worldwide (9,10). Progress in clinical management strategies and earlier detection through increased awareness and use of mammography has improved survival for breast cancer patients, with 5-year relative survival rates of 89% (11). However, for metastatic breast cancer, the 5-year relative survival rate remains low at 27% (12). There is an urgent need for novel prognostic biomarkers and a deeper understanding of molecular mechanisms to drive innovations in more effective treatment options, especially for those more aggressive and metastatic breast cancer cases. Early studies have shown that TRPC6 mRNA and protein levels are elevated in breast carcinoma specimens compared to normal breast tissue, with functional channels present in MCF-7 and primary cultures (8,13). TRPC6 is the predominant amongst

¹ School of Pharmacy, Yantai University, Yantai, Shandong, China;

² Shandong Luye Pharmaceutical Co., Ltd., Yantai, Shandong, China.

all TRPCs in the samples of human breast ductal adenocarcinomas and breast cancer cell lines, such as MCF-7 and MDA-MB-231 (13). The specific activator of TRPC6, hyperforin, significantly reduced the growth and viability of the breast cancer cell lines but did not affect the non-cancerous breast cell line. Silencing of TRPC6 in MDA-MB-231 cells resulted in a significant reduction in cell growth but not viability (13). More recent research confirms that TRPC6 is overexpressed in ER-positive and triple-negative breast cancer cell lines (14).

While the relevance of TRPC6 in breast cancer have been proposed in several studies, its histological detection in breast tumour tissues, as well as its role in breast cancer progression, lacks systematic study. Studying TRPC6 in breast cancer could lead to new therapeutic options. The main focus of this study is to systematically explore the role of TRPC6 as a prognostic biomarker in breast cancer and the correlation of TRPC6 expression with breast cancer progression.

2. Materials and Methods

2.1. Gene expression databases, survival analysis

TIMER (https://cistrome.shinyapps.io/timer/) was used for analyzing TRPC6 gene expression across all TCGA tumours and the correlations between TRPC6 expression and abundance of multiple immune infiltrate cells as well as tumour purity in BRCA. "Survival" module of TIMER was applied to analyse the clinical relevance of different tumour immune subsets.

The cBioPortal for Cancer Genomics (http://cbioportal.org) was used for exploring, visualizing, and analysing the genetic alterations or changes in gene expression of TRPC6 in the TCGA breast cancer cases. The cancer study "Breast Invasive Carcinoma (TCGA, PanCancer Atlas, 1084 total samples)" was selected for genetic alterations or changes in gene expression analysis (mutations, structural variants, putative copynumber alterations, mRNA expression, and protein/phosphoprotein level) in breast cancer. In addition, clinical patient data in UALCAN (http://ualcan.path.uab.edu/analysis.html) was used to classify primary tumour samples and generate box plots for each gene expression level in each subgroup.

The Kaplan-Meier plotter (KM plotter, http://kmplot.com/analysis/) was applied to analyse the prognostic value of TRPC6 in breast cancer patients using the chip data. The parameter settings include "split patients by median", "only JetSet best probe set", and "follow up threshold = 120 months". The web tool TNMplot.com in KM plotter was applied for the comparison of TRPC6 gene expression in normal, tumour and metastatic tissues, and in selected tissues at different stages.

2.2. TRPC6 expression analysis from Human Protein Atlas

Direct comparisons of TRPC6 protein expression between normal and breast cancer tissues were based on the immunohistochemical analysis data from the Human Protein Atlas (HPA, https://www.proteinatlas.org).

2.3. Cell culture and cell transfection

Human breast cancer cell lines (MCF-7, MDA-MB-231, and MDA-MB-468) were purchased from the Chinese Academy of Sciences (Shanghai, China) and cultured in DMEM supplemented with 10% FBS (Procell, Wuhan, China) at 37°C in a humid atmosphere with 5% CO₂-95% air, routinely confirmed negative for mycoplasma and bacteria contamination.

The human TRPC6 expression plasmid (pcDNA3.1-hTRPC6-YFP) (15) was obtained from Addgene (Addgene plasmid # 21084, Massachusetts, USA). Plasmid transfections were carried out with jetPRIME transfection reagent (Polyplus, Illkirch, France). The TRPC6 knock-down transfection was carried out at 25 nM final concentration of siRNA with siRNA-Mate transfection reagent (Genepharma, Shanghai, China). The TRPC6 overexpression (vector vs hTRPC6 group) and knock-down (ncRNA vs siTRPC6 group) efficiency were verified by qPCR.

2.4. Cell proliferation by MTT and colony formation assay

For MTT assay, cells were collected and seeded in 96well plates $(3 \times 10^3/100 \mu L/well)$. After adherence, the cells were transfected for TRPC6 overexpression/ knock-down or treated with different concentrations of hyperforin (HY-116330A, MCE, Shanghai, China). Cells were then incubated for 48 h. MTT reagent (Solarbio, Beijing, China) was added after treatment (5 mg/mL in PBS, 10 μL/well), and then the cells were incubated at 37°C for 2 h. The medium was removed after centrifugation. DMSO was added (150 µL/well) to dissolve the formazan by shaking on an orbital shaker for 5 minutes. Light absorbance of the solution was measured at 570 nm on the SpectraMax iD3 plate reader (Molecular Devices, San Jose, CA). Cell viability was calculated as a percentage of the mean of the respective control group (vector/ncRNA or vehicle group).

For the colony formation assay, 500 cells were plated into 6-well plates and continuously cultured for ~ 7 days. After fixation with 4% paraformaldehyde for 15 min, staining with 0.2% crystal violet for 10 min, and washing, visible colonies were imaged and counted.

2.5. Scratch wound healing assay

Cells (2×10^5 cells/well) were grown in 24-well plates

overnight and then serum-starved for 24 h. Then, the cells were scratched using 200 µL pipette tips, immediately rinsed twice with PBS, and subsequently cultured in serum-free medium. Photos were taken under a microscope at 0 h, 12 h, 24 h, and 48 h after the scratches were made. The wound area was measured using Fiji/ImageJ.

2.6. Transwell invasion assay

Cells from each group were serum-starved for 24 h. Then, the cells were harvested and suspended in serum-free DMEM with 0.1% BSA. The cells were loaded into the upper chambers (1 × 10⁵ cells in 0.1 mL/insert) embedded with Matrigel and incubated for ~48 h. After incubation, the cells inside the inserts were gently removed using wet cotton swabs; the filter membrane was washed with PBS, fixed with 70% ethanol, and stained with 0.2% crystal violet. The number of invading cells was counted manually under a light microscope.

2.7. Flow cytometry analysis of cell apoptosis

Cells seeded in 6-well plates (2 × 10⁵ per well) were transfected with plasmid or siRNA for TRPC6 overexpression or knockdown. For cell apoptosis analysis, cells were harvested and washed with cold PBS 48 h after transfection. Then cell surface of phosphatidylserine in apoptotic cells was quantitatively estimated by using Annexin-V/FITC and PI apoptosis detection kit (E-CK-A211, Elabscience, Wuhan, China). Stained cells were subsequently analysed using a FACScan flow cytometer (Becton-Dickinson, New Jersey, USA) for cell apoptosis.

2.8. Interaction networks and enrichment analysis

STRING (https://string-db.org/), containing massive amounts of data on protein–protein interactions, was applied to construct TRPC6 interaction network. LinkedOmics (http://linke domics.org) includes 32 TCGA cancer-associated multi-dimensional datasets. The LinkFinder module in LinkedOmics was used to research differentially expressed genes associated with TRPC6 levels in the TCGA BRCA cohort (n = 1093). The results were analyzed using Pearson's correlation coefficient. All results are graphically represented in a volcano, heat map. We signed and sorted the LinkFinder results and used GSEA to analyze GO terminology (biological process) and KEGG pathway.

2.9. Statistical analysis

All experimental data were expressed as the mean \pm standard error of the mean (SEM) of at least three independent assays unless otherwise specified. The data were analysed using Prism 9 (GraphPad Software

Version 9.0.0, USA). Student's *t*-test was applied for comparing two-group experiments. ANOVA analysis, followed by Tukey's multiple comparisons test, was used when comparing more than two groups. The significance level was considered as below 0.05 in all experiments.

3. Results

3.1. TRPC6 expression in breast cancer patients

To understand the basic expression information of TRPC6 in breast cancer, TIMER was applied to identify TRPC6 gene expression at the transcriptional level across all TCGA tumours compared with the respective normal tissues. In breast carcinoma (BRCA) patients, the TRPC6 gene level in tumour tissues is significantly lower compared with the normal breast tissues (Figure 1A, p < 0.001). The lower TRPC6 in breast cancer tissues was further validated by ULCAN and KM plotter analysis (Figures 1B and 1C). In ULCAN analysis, there was no significant difference among the individual cancer stages (Figure 1E) or different nodal metastasis (Figure 1F), but in TNMplot analysis, TRPC6 expression level in stages II, III and IV was significantly lower than stage I (Figure 1D). Moreover, the subtype analysis in ULCAN showed that TRPC6 expression in more aggressive HER2 and triple negative subtypes was notably lower than that in the luminal subtype tumour (Figure 1G). The data suggest that TRPC6 downregulation may be correlated with more aggressive subtypes and higher metastatic potential, and TRPC6 might act as a tumour suppressor gene in breast cancer.

3.2. Genetic alteration in *TRPC6* gene and prognostic value of TRPC6 in BRCA patients and TRPC6 protein expression analysis in breast cancer tissues

The cBioPortal platform was applied to determine the genetic alterations or gene expression changes of the TRPC6 gene, which indicates that 4% (45 out of 1084, Figure 2A) of the sequenced BRCA cases/ patients have genetic alterations or changes in gene expression in the TRPC6 gene. We further investigated the prognostic value of TRPC6 in breast cancer patients using the Kaplan-Meier plotter. As shown in Figure 2B, although there is no significant difference in the overall survival (OS, p > 0.05), high TRPC6 gene expression is correlated with better relapse-free survival (RFS, HR = 0.8 (0.72 - 0.88), p = 21.5e - 0.5, follow-up time = 120months) (Figure 2C). The median RFS for breast cancer patients with high TRPC6 expression was 59 months, and 42 months for patients with low TRPC6 expression. These findings suggested that the changes of the TRPC6 gene could have an important clinical impact, although without statistical significance in a subset of breast cancer patients.

We next explored the TRPC6 protein expression in

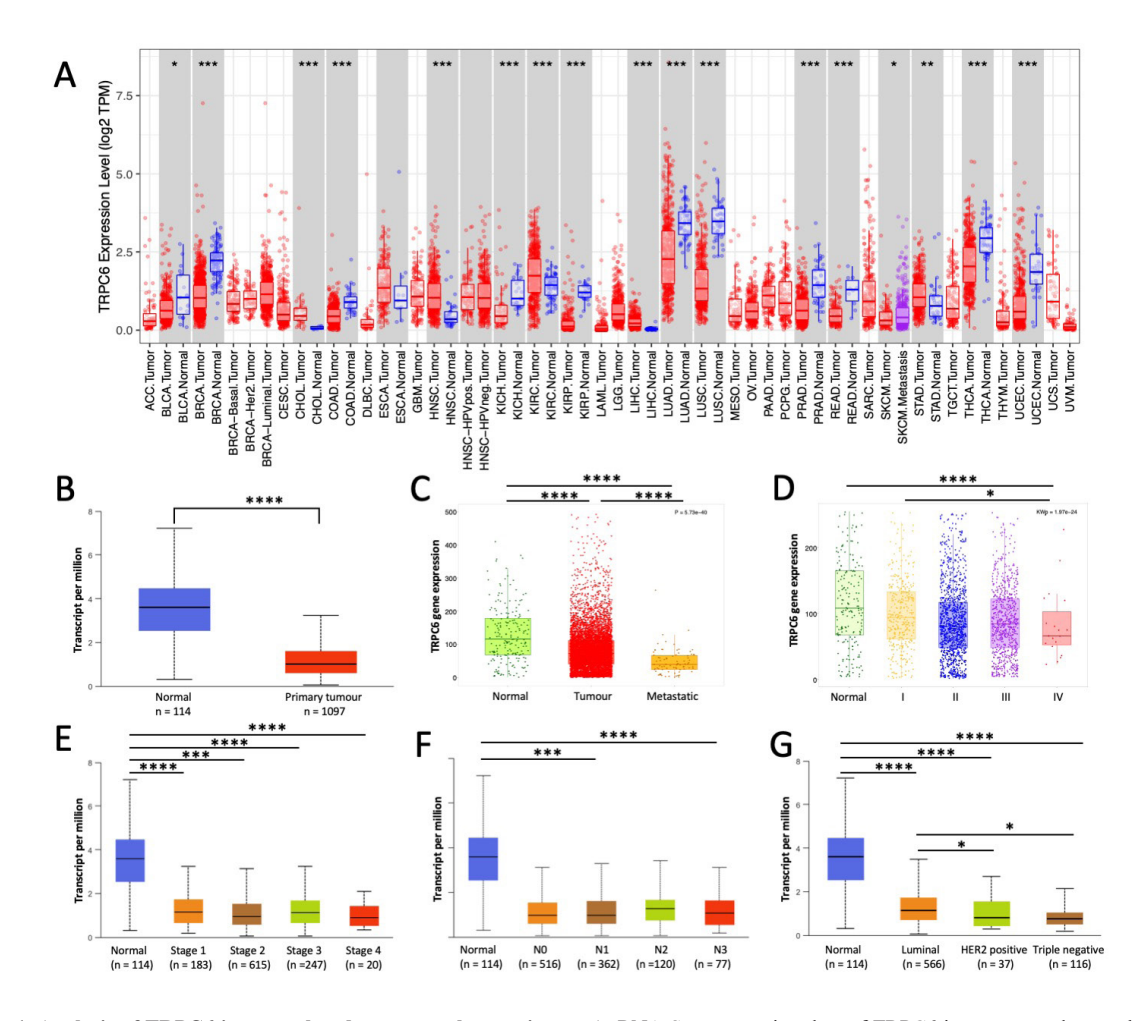


Figure 1. Analysis of TRPC6 in normal and cancerous breast tissues. A. RNA-Seq expression data of TRPC6 in tumour and normal tissues from each cancer type obtained from TIMER. Distributions of gene expression levels are displayed using box plots, with statistical significance of differential expression evaluated using the Wilcoxon test. B. Validation of TRPC6 downregulation in breast primary tumours from the UALCAN cohort analysis. C. Comparison of TRPC6 expression in normal, tumour, and metastatic tissues in TNMplot using gene chip based data. D. Comparison of TRPC6 expression in normal and BRCA tumours of different stages by the stage comparison tool in TNMplot using gene array data. E-G. Differential expression of TRPC6 among breast cancer patients with different molecular subtypes, individual cancer stages, and nodal metastasis status from the UALCAN analysis. ****p < 0.0001; **p < 0.001; **p < 0.01; **p < 0.05.

breast tumour tissues according to IHC staining from the HPA database, and the results are shown in Figures 2D and 2E. We noticed that the TRPC6 protein was generally lowly expressed in both normal breast tissues and breast carcinoma tissues. TRPC6 protein expression was detected in both normal and cancerous breast tissues, but not enhanced in either tissue type. In normal breast tissues, TRPC6 is present in glandular cells and myoepithelial cells, not in adipocytes (Figure 2D). In breast cancer tissues, TRPC6 is not detected in 7 out of 11 tissues (63.6%), low-stained in 2 out of 11 tissues (18.2%), and medium-stained in 2 out of 11 tissues (18.2%), respectively (Figure 2E).

3.3. Correlation of the *TRPC6* gene with immune infiltration in BRCA patients

The correlation of the *TRPC6* gene with immune infiltration in the breast tumour microenvironment was then analysed using TIMER. As shown in Figure 3, there

is a positive relationship between TRPC6 expression level and infiltration level of CD8⁺ T cells, CD4⁺ T cells, macrophage cells, neutrophil cells, and dendritic cells (r > 0.1, p < 0.01) (Figure 3A). These results indicate that the TRPC6 gene is involved in the immune infiltration of breast cancer. Boxplots comparing immune cell levels across copy number states of TRPC6 in Figure 3B showed that TRPC6 deletion correlates with lower immune cell levels, which suggests that the decreased copy number of TRPC6 in tumour tissues suppresses immune infiltration. The prognostic value of immune cell infiltration in BRCA was also analysed. Only B cell abundance was significantly related to better cumulative survival in BRCA patients, especially in the HER2 subtype (Figure 3C). These data suggest that TRPC6 might play a role in recruiting or supporting immune cells within the tumour microenvironment.

3.4. Effects of TRPC6 expression regulation on cell proliferation and cell migration

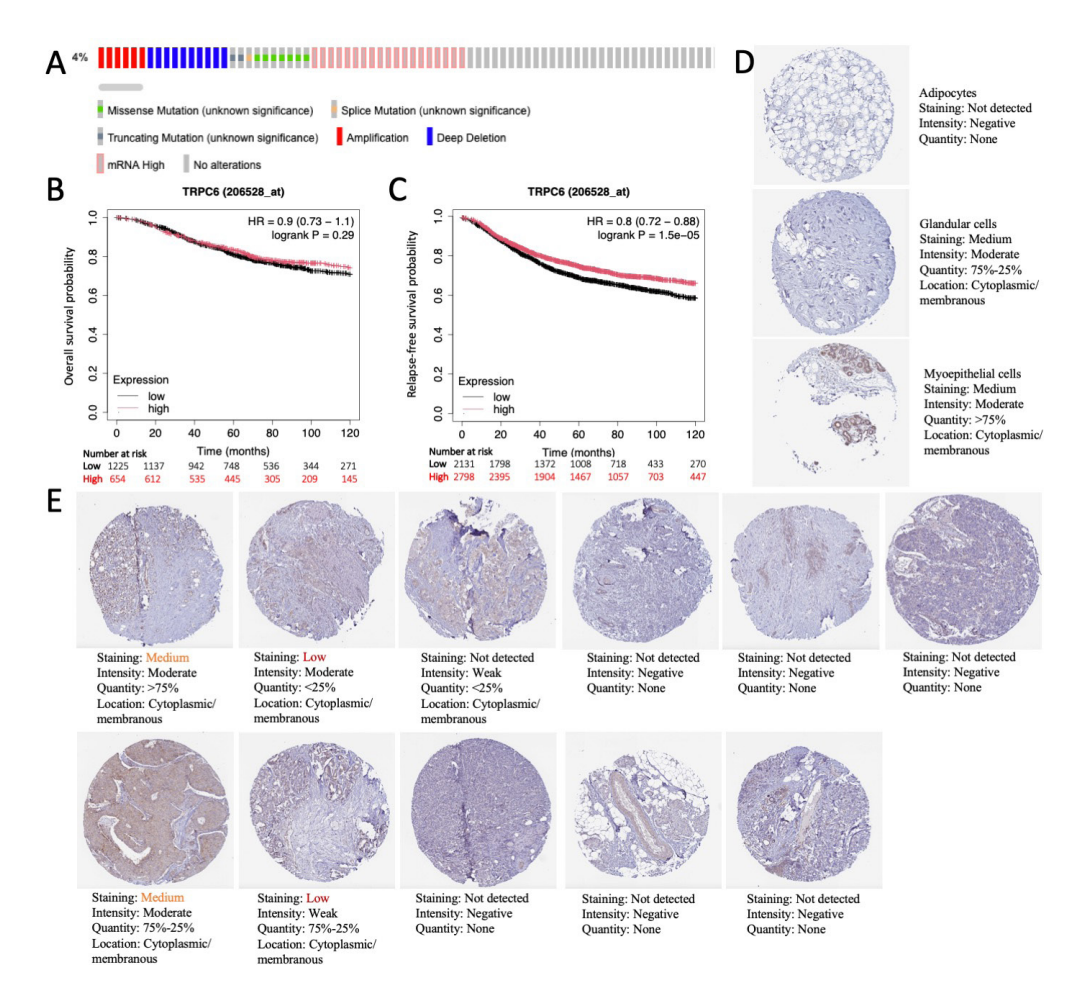


Figure 2. Genetic alteration in *TRPC6* gene, prognostic value of TRPC6 in BRCA patients, and TRPC6 protein expression analysis in breast cancer tissues. A. Genetic alterations and gene expression changes of TRPC6 in breast cancer. **B&C**. The effects of TRPC6 expression level on overall survival (B) and relapse-free survival (C) of breast cancer patients. Auto select best cut-off. Follow-up time = 120 months. **D&E**. TRPC6 protein expression in normal (D) and cancerous (E) breast tissues. TRPC6 protein is lowly expressed in both cancerous and normal breast tissues (HPA data, antibody: HPA045098), but not enhanced in either tissue type.

Since TRPC6 was lower in breast tumour tissues than normal breast tissues, we verified the molecular effects of TRPC6 expression on different breast cancer cell lines, including MCF-7, MDA-MB-231, and MDA-MB-468. Surprisingly, compared to previously published researches, we observed opposite effects of TRPC6 overexpression on breast cancer cell proliferation and migration abilities in breast cancer cells.

As shown in Figures 4A and 4B, TRPC6 overexpression correlated with delayed cell proliferation ability in all cell lines. On the other hand, TRPC6 knockdown by siRNA transfection significantly increased the cell proliferation abilities of all three cell lines above, as evidenced by MTT and colony formation assays (Figures 4A and 4B). We also tested the effects of hyperforin, a natural compound known as a TRPC6 agonist, on the proliferation of these three cell lines. We found that hyperforin could significantly inhibit the proliferation of MCF-7, MDA-MB-231, and MDA-MB-468 cell lines, with IC50 of 3.76 μ M, 14.47 μ M, and 9.96 μ M, respectively. Furthermore, we observed that changes in TRPC6 expression did not induce significant

cell apoptosis in the MDA-MB-231 and MDA-MB-468 cell lines, as detected by flow cytometry (Figure 4C), suggesting that TRPC6 affects only cell proliferation, but not cell viability.

We then explored the effects of TRPC6 expression regulation on cell migration and invasion ability using scratch wound healing assays and transwell invasion assays in the more metastatic triple-negative MDA-MB-231 and MDA-MB-468 cell lines. Again, we observed that TRPC6 expression was negatively correlated with cell migration ability (Figure 5A) and invasion ability (Figure 5B) of the aggressive TNBC cell lines MDA-MB-231 and MDA-MB-468 cells (Figure 5), which is contrary to previous reports. The observations of TRPC6 level being negatively related to cell proliferation and metastasis abilities raise the necessity of rethinking the mechanism perspective and targetability of TRPC6 in breast cancer.

3.5. Signalling pathway interaction networks analysis

The biological effects of a gene are shaped by the

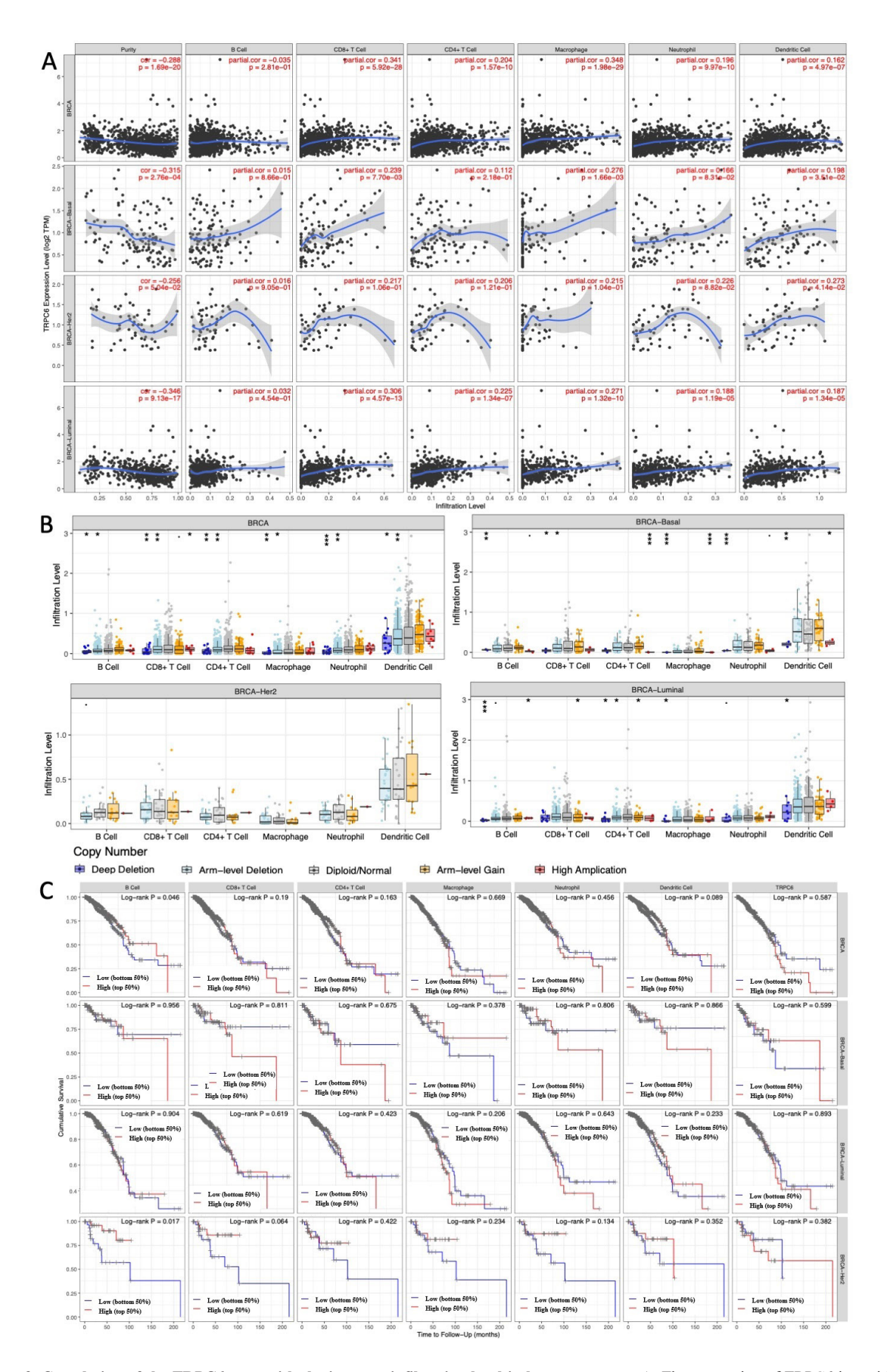


Figure 3. Correlation of the TRPC6 gene with the immune infiltration level in breast tumours. A. The expression of TRPC6 is positively associated with the infiltration abundance of CD8⁺ T cells, CD4⁺ T cells, macrophages, neutrophils, and dendritic cells. **B.** The comparison of tumour infiltration levels among tumours with different somatic copy number alterations for the TRPC6 gene in BRCA patients. Box plots are presented to show the distributions of each immune subset at each copy number status in BRCA patients (Deep Deletion, Shallow Deletion, Diploid, Gain, Amplification). **C.** The clinical relevance of different tumour immune subsets.

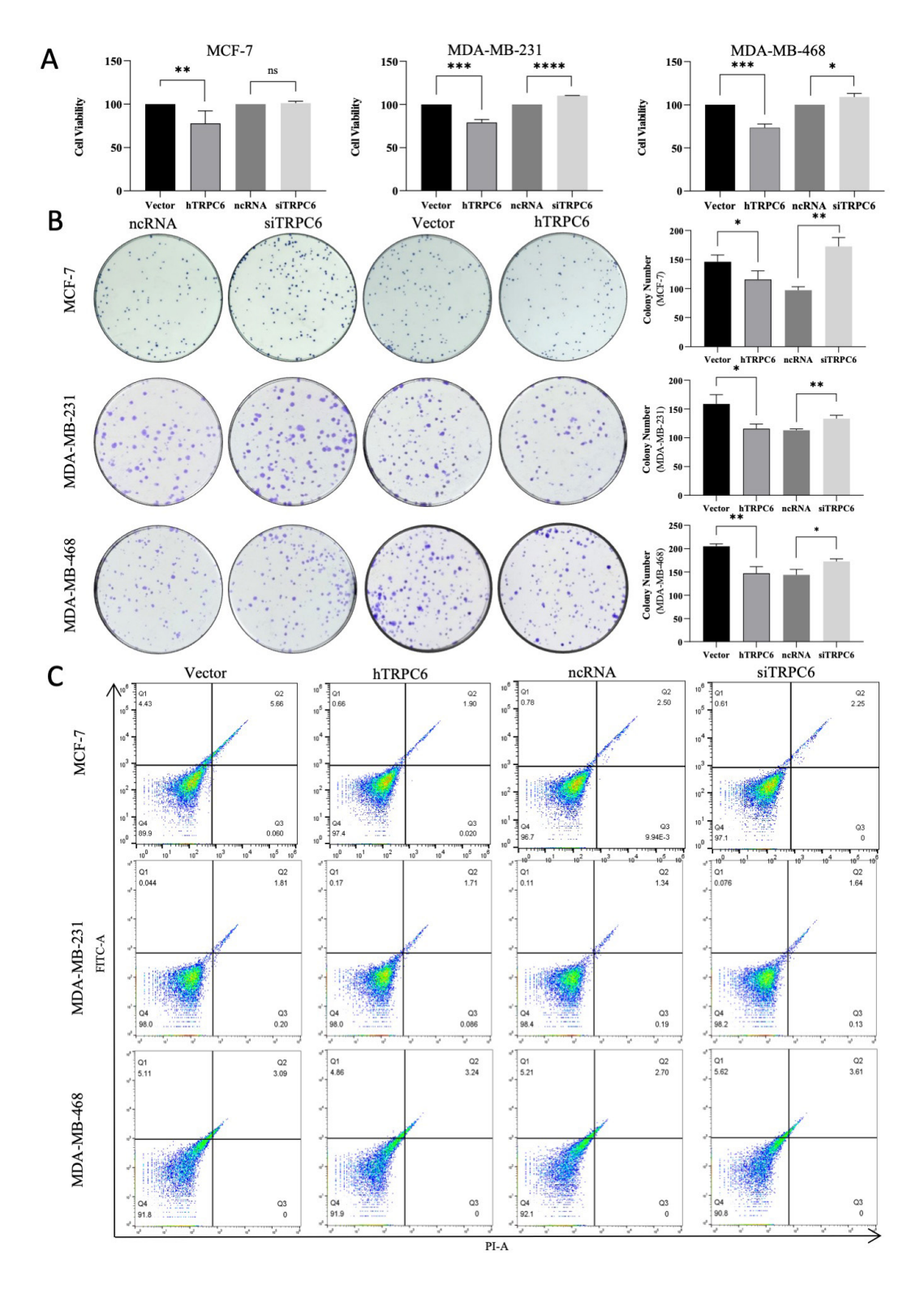


Figure 4. Effects of TRPC6 expression on the proliferation of breast cancer cell lines *in vitro*. MTT assay (**A**) and colony formation assay (**B**) assessing effects of TRPC6 expression modulation on breast cancer proliferation. **C.** Effects of TRPC6 expression on cell apoptosis detected by flow cytometry apoptosis assay. Vector, cells transfected with empty vector plasmid; hTRPC6, cells transfected with pcDNA3.1-hTRPC6-YFP plasmid for TRPC6 overexpression; ncRNA, cells transfected with scrambled RNA; siTRPC6, cells transfected with TRPC6-targeted siRNA for TRPC6 knock-down.

proteins or genes it interacts with. Understanding the interaction network for the *TRPC6* gene is crucial in biology and cancer research. Figure 6A shows the PPI (protein-protein interaction) network mapped by STRING, with the top 20 proteins highly functionally

associated with or interacting with TRPC6. The Function module of LinkedOmics was further used to analyze mRNA sequencing data from 1,093 patients with BRCA in TCGA. As shown in the volcano chart (Figure 6B) and heat map (Figures 6C and 6D), 50 gene sets were

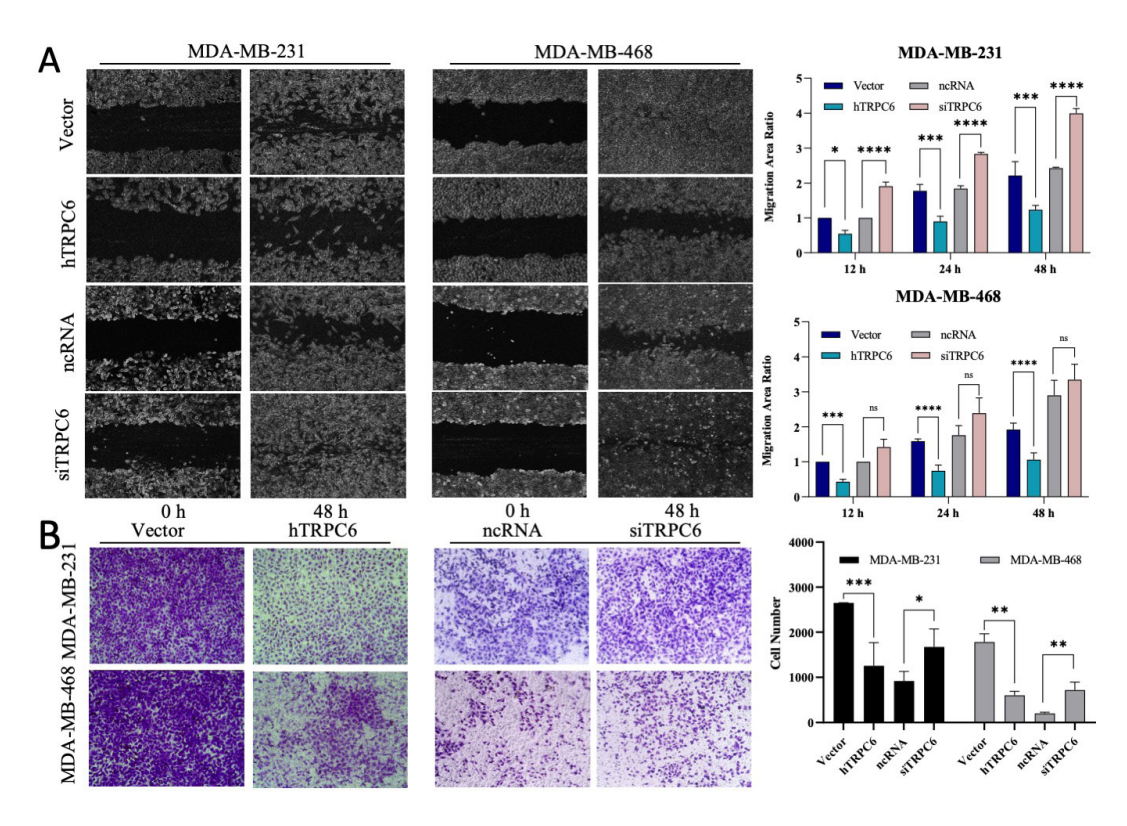


Figure 5. Effects of TRPC6 expression on migration and invasion abilities of breast cancer cell lines in vitro. A. Representative picture of scratch wound healing assay taken at 0 h and 48 h. The bar chart showed the cell migration ratio of different groups at 12 h, 24 h, and 48 h. Migration area ratio = (scratch area at 0 h of each group – scratch area at 12/24/48 h of each group)/(scratch area at 0 h of control group – scratch area at 12/24/48 h of each group)/(scratch area at 0 h of control group – scratch area at 12/24/48 h of each group)/(scratch area at 0 h of control group – scratch area at 12/24/48 h of each group)/(scratch area at 0 h of control group – scratch area at 12/24/48 h of each group)/(scratch area at 0 h of control group – scratch area at 12/24/48 h of each group)/(scratch area at 0 h of control group – scratch area at 12/24/48 h of each group)/(scratch area at 0 h of control group – scratch area at 12/24/48 h of each group)/(scratch area at 0 h of control group – scratch area at 12/24/48 h of each group)/(scratch area at 0/4 h of control group – scratch area at 12/24/48 h of each group)/(scratch area at 0/4 h of control group – scratch area at 12/24/48 h of each group)/(scratch area at 0/4 h, and 48/4 h. Migration area ratio = (scratch area at 0/4 h, and 48/4 h. Migration area ratio = (scratch area at 0/4 h, and 48/4 h. Migration area ratio = (scratch area at 0/4 h, and 48/4 h. Migration area ratio = (scratch area at 0/4 h, and 48/4 h. Migration area ratio = (scratch area at 0/4 h, and 48/4 h. Migration area ratio = (scratch area at 0/4 h, and 48/4 h. Migration area ratio = (scratch area at 0/4 h, and 48/4 h. Migration area ratio = (scratch area at 0/4 h, and 48/4 h. Migration area ratio = (scratch area at 0/4 h, and 48/4 h. Migration area ratio = (scratch area at 0/4 h, and 48/4 h. Migration area ratio = (scratch area at 0/4 h, and 48/4 h. Migration area ratio = (scratch area at 0/4 h, and 48/4 h. Migration area

substantially positively or negatively correlated with TRPC6. The results suggest that the TRPC6 expression level has a substantial effect on the transcriptome in breast cancer cells. TRPC6 expression showed a strong positive association with expression of CDH6 (Pearson correlation coefficient = 0.6782, p = 4.104e-148), GPR116 (Pearson correlation coefficient = 0.6772, p = 1.456e-147), and ELTD1 (Pearson correlation coefficient = 0.6453, p = 9.155e-130) (Figures 6E-6G). GO terms identified in gene set enrichment analysis (GSEA) revealed that differentially expressed genes correlated with TRPC6 were mainly involved in casculogenesis (Figure 6H). KEGG pathway analysis showed enrichment of ECM-receptor interaction, which regulates cancer-related signalling pathways (Figure 6I).

4. Discussion

Numerous studies have reported the involvement of TRP channels in cancer (16). However, limited studies have thoroughly analysed the expression pattern of TRPC6 or its possible role in the development of breast cancer. No previous studies have systematically investigated the TRPC6 expression in breast cancer according to the published sequencing datasets with a large sample size.

We comprehensively explore the potential role of TRPC6 in breast cancer from multiple aspects in this study, based on bioinformatic analysis and preliminary experimental data from our laboratory.

Previous researches have reported the overexpression of TRPC6 in breast cancer tissues compared to normal or adjacent tissues (8,13,17). However, our exploration presented herein shows a different observation of TRPC6 expression pattern in breast tissues. The ULCAN and TNMplot analyses based on multiple clinicopathological features in breast cancer samples in TCGA, GEO, GTex, TCGA, and TARGET databases consistently indicated lower expression of the TRPC6 gene in breast cancer tumour tissues than in normal controls. Sub-group analyses using TNMplot showed that TRPC6 expression level in stage I tumours was significantly higher than in stages II-IV (Figure 1D). The subtype analysis in ULCAN showed that TRPC6 expression in luminal subtype tumours was notably higher than the more aggressive HER2 and triple negative subtypes, which is also contrary to a previous study showing that TRPC6 is expressed substantially more in TNBC than in non-TNBC (ER⁺) tumour specimens (18). Moreover, high TRPC6 gene expression is correlated with better RFS (Figure 2C). We thus speculate that the lower TRPC6

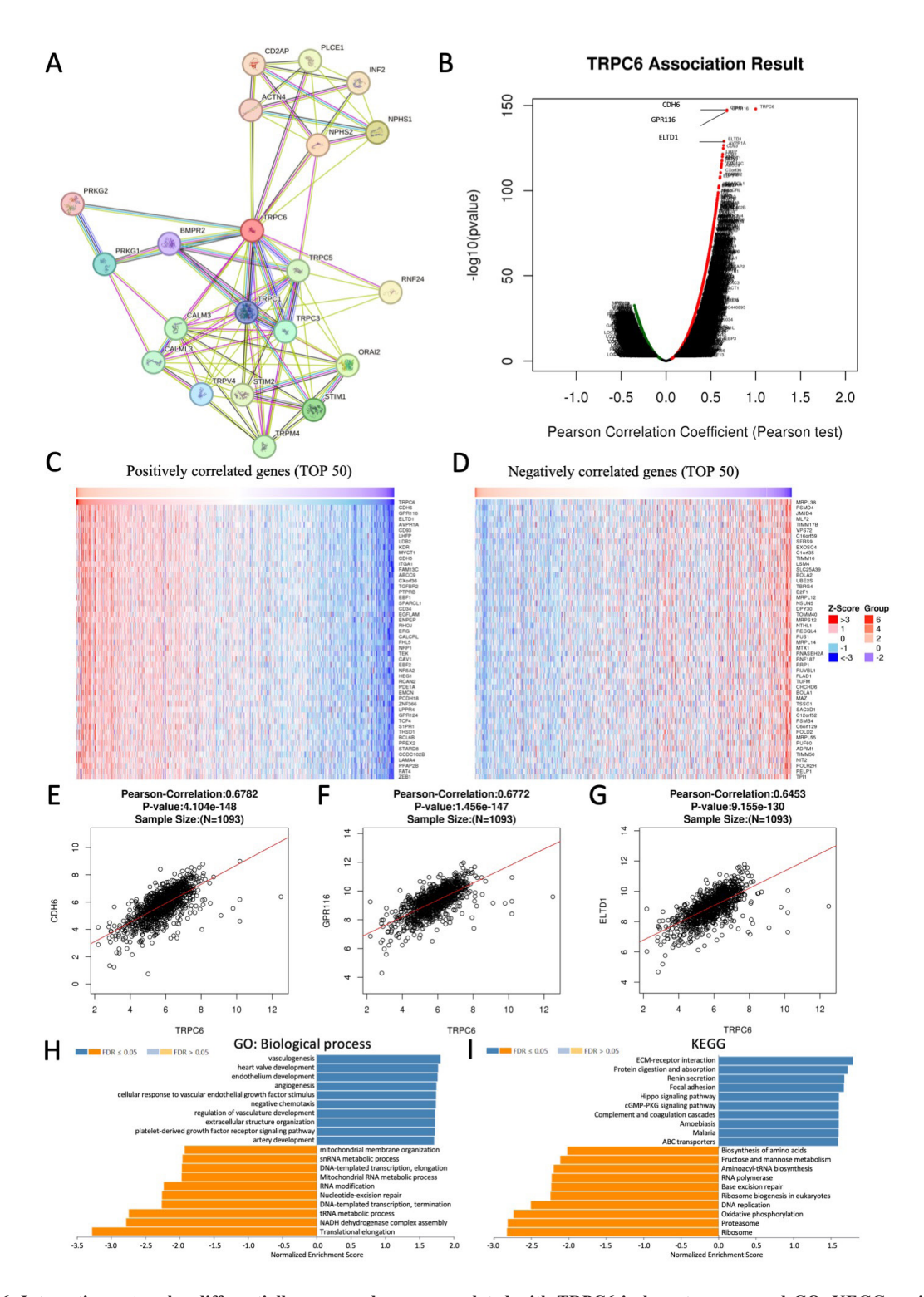


Figure 6. Interaction networks, differentially expressed genes correlated with TRPC6 in breast cancer, and GO, KEGG enrichment analysis. A. PPI network of TRPC6. B. Pearson correlation coefficients of relationships between TRPC6 and differentially expressed genes in BRCA. C&D. Heat maps showing genes positively and negatively correlated with TRPC6 in breast cancer (TOP 50). Red indicates positively correlated genes and green indicates negatively correlated genes. E–G. Scatter plot showing Pearson correlation coefficients for the relationship between TRPC6 expression and CDH6 (E), GPR116 (F), and ELTD1 (G). H&I. Significantly enriched GO annotations (H) and KEGG pathways (I) of TRPC6 in the BRCA cohort.

expression in BRCA tissues may be correlated with higher metastatic potential and more aggressive subtypes, and TRPC6 might be a novel prognostic marker of invasive and metastatic breast cancer.

Even so, gene expression may not always be in

accordance with the protein level. The Human Protein Atlas database was further applied for TRPC6 protein expression. We noticed that TRPC6 protein expression was detected in both normal and cancerous breast tissues, but not enhanced in either tissue type (Figures

2D and 2E). There were only 11 breast tumours and 3 normal breast tissues in the HPA database for TRPC6 protein analysis. The TRPC6 protein analysis with a larger sample size is warranted with reliable antibodies, not only for quantification but also for its localisation.

The tumour microenvironment consists of all noncancerous host cells and non-cellular components of the tumour. One of the most challenging questions is how the immune system affects cancer development and progression. Analysing immune infiltration within human tumours has become one of the most pivotal aspects of cancer research and precision oncology. Immune infiltrate characterisation using TIMER helped identify informative and reliable characteristics representative of the local immune tumour microenvironment related to TRPC6 expression, which could serve as independent predictors of cancer survival and guide the management of breast cancer patients. In this study, we noticed a positive relationship between TRPC6 expression level and infiltration level of CD8⁺ T cells, CD4⁺ T cells, macrophage cells, neutrophil cells, and dendritic cells, and TRPC6 deletion correlates with lower immune cell levels (Figures 3A and 3B). These data suggest that TRPC6 might play a role in recruiting or supporting immune cells within the tumour microenvironment. Loss of TRPC6 may promote tumour progression in BRCA by suppressing immune infiltration. Therefore, TRPC6 may play an important role in immune cell infiltration and may serve as a biomarker for guiding immunotherapy and prognosis in patients with breast cancer.

Multiple studies have revealed that TRPC6 downregulation or inhibition by small molecules may contribute to cancer inhibition (1,13,19,20). In the field of breast cancer research, silencing TRPC6 significantly reduced the growth but not the viability of the MDA-MB-231 cells (13). A recent research study showed that TRPC6 knockdown impaired cell proliferation, migration and invasion in both MCF7 and MDA-MB-231 cell lines (14). Nanoparticles carrying TRPC6targeting siRNA also showed inhibition effects on the growth and survival of breast cancer MCF-7 cells in vitro and 4T1 cells in the mouse model in vivo (21). TRPC6 could contribute to TNBC chemotherapy resistance, dependent on TRPC6-mediated Myc suppression (18). While most studies suggest that TRPC6 promotes cancer progression by enhancing proliferation, migration, invasion, chemoresistance, and shaping an immunosuppressive microenvironment, in this study, we surprisingly observed that TRPC6 expression was negatively correlated with proliferation and metastasis abilities, which were contradictory observations of the expression and role of TRPC6 in breast cancer compared to previously published researches. Our observations highlight the necessity of rethinking and evaluating the functional mechanism and targetability of TRPC6 in breast cancer. The contradictory observations may be due to different experimental environments and setups. The disadvantage of our preliminary data is that we did not test whether the TRPC6 is functional or not.

On the other hand, the role of TRPC6 in cancer can be context- and activation-level dependent. TRPC6 may also have tumour-suppressive roles under certain conditions. This is not an isolated case where TRP channels serve as a tumour-suppressive factor. A recent study demonstrates that TRPA1 (transient receptor potential ankyrin 1) suppressed colorectal carcinogenesis through its immunomodulatory functions within the colitis-cancer transformation axis (22). TRPC6 may still serve as a therapeutic target for inducing cancer cell death under certain conditions. TRPC6-targeted compounds may have a future role as therapeutic agents for a subset of breast cancer patients. Hyperforin, a compound from Hypericum perforatum (St John's wort), is a well-known TRPC6 agonist/activator (23). Hyperforin has been shown to inhibit proliferation, induce apoptosis, and reduce invasiveness across various cancer cell lines (e.g., glioblastoma, breast, colorectal, and melanoma). We confirmed that hyperforin could significantly inhibit the proliferation of MCF-7 (IC₅₀ = $3.76 \mu M$), MDA-MB-231 $(IC_{50} = 14.47 \mu M)$, and MDA-MB-468 $(IC_{50} = 9.96 \mu M)$ cells.

One of the key mechanisms of hyperforin-induced cancer inhibition can be attributed to calcium overload, triggering endoplasmic reticulum stress, disrupting mitochondrial membrane potential, and initiating intrinsic and extrinsic apoptotic pathways (24,25). The exact role of TRPC6 in breast cancer progression warrants further investigation. Therefore, the conflicting results regarding the role of TRPC6 in modulating breast cancer cell growth can be partially explained by differences in the status of TRPC6 activation. This does not contradict the role of TRPC6 as an oncogenic factor in many settings where its overexpression and moderate activity promote cancer cell growth, but it highlights its biphasic role in modulating cancer cell growth.

Under physiological or moderately elevated activity, TRPC6 promotes cancer cell growth and survival; while at hyperactivation conditions, TRPC6 can lead to intracellular calcium overload and trigger apoptotic pathways to induce cancer cell death. On the other hand, certain breast cancer cells may have dysregulated or deficient calcium influx pathways, making them less reliant on TRP channels or altering their ability to utilise calcium for signalling. For example, we previously found that the classical oxytocin receptor-mediated G_q pathway is compromised in the MDA-MB-231 cells (26). Understanding the interaction network of TRPC6 in breast cancer can reveal potential therapeutic targets and biomarkers for disease progression and treatment response. However, the exact role or TRPC6 in modulating cancer cell growth and strategies of targeting TRPC6 using small molecules for breast cancer management warrant further study both in vitro and in vivo.

5. Conclusion

In conclusion, this study demonstrates the potential role and function of TRPC6 in breast cancer from multidimensional aspects. TRPC6 is generally lowly expressed in both normal and breast carcinoma tissue, the elevated expression of TRPC6 may be a biomarker of a good prognosis for breast cancer patients. The limitation of the current study is that we did not test whether the TRPC6 is functional or not in the breast cancer cell lines, and the currently known TRPC6-targeted compounds were not tested in these cell lines for cancer inhibition or signalling pathway exploration. Further study of TRPC6 in breast cancer is warranted to provide new mechanistic insights and opportunities for more treatment options for breast cancer management.

Funding: Funding supported the study is listed as follows: H. L. is supported by Shandong Provincial Natural Science Foundation (ZR2023QH237) and National Natural Science Foundation of China (82404702). H. W. is supported by Taishan Scholar Project (tsqn202211112), National Natural Science Foundation of China (82273969, 82073888), and Shandong Provincial Natural Science Foundation (ZR2021LSW011). Y. M. is supported by Graduate Innovation Foundation of Yantai University (GGIFYTU2538).

Conflict of Interest: The authors have no conflicts of interest to disclose.

References

- Saqib U, Munjuluri S, Sarkar S, Biswas S, Mukherjee O, Satsangi H, Baig MS, Obukhov AG, Hajela K. Transient Receptor Potential Canonical 6 (TRPC6) Channel in the Pathogenesis of Diseases: A Jack of Many Trades. Inflammation. 2023; 46:1144-1160.
- 2. Ding X, He Z, Zhou K, Cheng J, Yao H, Lu D, Cai R, Jin Y, Dong B, Xu Y, Wang Y. Essential role of TRPC6 channels in G2/M phase transition and development of human glioma. J Natl Cancer Inst. 2010; 102:1052-1068.
- 3. Carl C, Wagner M, Linxweiler M, Schick B, Tschernig T. Immunohistochemical expression of the cation channel TRPC6 in the submandibular and lacrimal gland and in salivary gland tumors. Pathol Res Pract. 2024; 261:155483.
- Song J, Wang Y, Li X, Shen Y, Yin M, Guo Y, Diao L, Liu Y, Yue D. Critical role of TRPC6 channels in the development of human renal cell carcinoma. Mol Biol Rep. 2013; 40:5115-5122.
- Yue D, Wang Y, Xiao JY, Wang P, Ren CS. Expression of TRPC6 in benign and malignant human prostate tissues. Asian J Androl. 2009; 11:541-547.
- 6. Zeng B, Yuan C, Yang X, Atkin SL, Xu SZ. TRPC channels and their splice variants are essential for promoting human ovarian cancer cell proliferation and tumorigenesis. Curr Cancer Drug Targets. 2013; 13:103-116.
- 7. Wan Q, Zheng A, Liu X, Chen Y, Han L. Expression of

- transient receptor potential channel 6 in cervical cancer. Onco Targets Ther. 2012; 5:171-176.
- Guilbert A, Dhennin-Duthille I, Hiani YE, Haren N, Khorsi H, Sevestre H, Ahidouch A, Ouadid-Ahidouch H. Expression of TRPC6 channels in human epithelial breast cancer cells. BMC Cancer. 2008; 8:125.
- Bray F, Ferlay J, Soerjomataram I, Siegel RL, Torre LA, Jemal A. Global cancer statistics 2018: GLOBOCAN estimates of incidence and mortality worldwide for 36 cancers in 185 countries. CA Cancer J Clin. 2018; 68:394-424.
- Sung H, Ferlay J, Siegel RL, Laversanne M, Soerjomataram I, Jemal A, Bray F. Global cancer statistics 2020: GLOBOCAN estimates of incidence and mortality worldwide for 36 cancers in 185 countries. CA Cancer J Clin. 2021; 71:209-249.
- Miller KD, Siegel RL, Lin CC, Mariotto AB, Kramer JL, Rowland JH, Stein KD, Alteri R, Jemal A. Cancer treatment and survivorship statistics, 2016. CA Cancer J Clin. 2016; 66:271-289.
- 12. Siegel RL, Miller KD, Jemal A. Cancer statistics, 2020. CA Cancer J Clin. 2020; 70:7-30.
- 13. Aydar E, Yeo S, Djamgoz M, Palmer C. Abnormal expression, localization and interaction of canonical transient receptor potential ion channels in human breast cancer cell lines and tissues: a potential target for breast cancer diagnosis and therapy. Cancer Cell Int. 2009; 9:23.
- 14. Jardin I, Diez-Bello R, Lopez JJ, Redondo PC, Salido GM, Smani T, Rosado JA. TRPC6 Channels Are Required for Proliferation, Migration and Invasion of Breast Cancer Cell Lines by Modulation of Orai1 and Orai3 Surface Exposure. Cancers (Basel). 2018; 10:331.
- Kwon Y, Hofmann T, Montell C. Integration of phosphoinositide- and calmodulin-mediated regulation of TRPC6. Mol Cell. 2007; 25:491-503.
- Koivisto AP, Belvisi MG, Gaudet R, Szallasi A. Advances in TRP channel drug discovery: from target validation to clinical studies. Nat Rev Drug Discov. 2022; 21:41-59.
- 17. Dhennin-Duthille I, Gautier M, Faouzi M, Guilbert A, Brevet M, Vaudry D, Ahidouch A, Sevestre H, Ouadid-Ahidouch H. High expression of transient receptor potential channels in human breast cancer epithelial cells and tissues: correlation with pathological parameters. Cell Physiol Biochem. 2011; 28:813-822.
- Mukhopadhyay D, Goel HL, Xiong C, Goel S, Kumar A, Li R, Zhu LJ, Clark JL, Brehm MA, Mercurio AM. The calcium channel TRPC6 promotes chemotherapyinduced persistence by regulating integrin α6 mRNA splicing. Cell Rep. 2023; 42:113347.
- Cai R, Ding X, Zhou K, Shi Y, Ge R, Ren G, Jin Y, Wang Y. Blockade of TRPC6 channels induced G2/M phase arrest and suppressed growth in human gastric cancer cells. Int J Cancer. 2009; 125:2281-2287.
- Wei Y, Li M, Hu Y, Lu J, Wang L, Yin Q, Hong X, Tian J, Wang H. PCC0208057 as a small molecule inhibitor of TRPC6 in the treatment of prostate cancer. Front Pharmacol. 2024; 15:1352373.
- Uddin MB, Holl MMB, Chowdhury EH. Delivery of siRNAs Against Selective Ion Channels and Transporter Genes Using Hyaluronic Acid-coupled Carbonate Apatite Nanoparticles Synergistically Inhibits Growth and Survival of Breast Cancer Cells. Int J Nanomedicine. 2024; 19:7709-7727.
- 22. Dou F, Hu S, Lu D, Gao J. Trpa1 knockout favors colon

- tumorigenesis in dextran sulfate sodium (DSS)-induced colitis mice. Drug Discov Ther. 2025; 19:200-207.
- Leuner K, Kazanski V, Müller M, Essin K, Henke B, Gollasch M, Harteneck C, Müller WE. Hyperforin--a key constituent of St. John's wort specifically activates TRPC6 channels. FASEB J. 2007; 21:4101-4111.
- 24. Chiang IT, Chen WT, Tseng CW, Chen YC, Kuo YC, Chen BJ, Weng MC, Lin HJ, Wang WS. Hyperforin Inhibits Cell Growth by Inducing Intrinsic and Extrinsic Apoptotic Pathways in Hepatocellular Carcinoma Cells. Anticancer Res. 2017; 37:161-167.
- 25. Uslusoy F, Nazıroğlu M, Çiğ B. Inhibition of the TRPM2 and TRPV1 Channels through Hypericum perforatum in Sciatic Nerve Injury-induced Rats Demonstrates their Key Role in Apoptosis and Mitochondrial Oxidative Stress of Sciatic Nerve and Dorsal Root Ganglion. Front Physiol. 2017; 8:335.

 Liu H, Muttenthaler M. High Oxytocin Receptor Expression Linked to Increased Cell Migration and Reduced Survival in Patients with Triple-Negative Breast Cancer. Biomedicines. 2022; 10:1595.

Received August 12, 2025; Revised September 24, 2025; Accepted October 7, 2025.

Hongbo Wang and Huiping Liu, School of Pharmacy, Yantai University, Yantai, Shandong, 264005, China.

E-mail: hongbowang@ytu.edu.cn (H.W.); huipingliu@ytu.edu.cn (H.L.)

Released online in J-STAGE as advance publication October 16, 2025.

[§]These authors contributed equally to this work.

^{*}Address correspondence to:

Original Article

DOI: 10.5582/ddt.2025.01084

Comparing gene-targeting efficiency of *Agrobacterium* tumefaciens-mediated transformation and electroporation in the pathogenic fungus *Trichosporon asahii* JCM2466

Yasuhiko Matsumoto^{1,*}, Mei Nakayama¹, Yuta Shimizu¹, Sachi Koganesawa¹, Hiromi Kanai¹, Wakako Hayashi¹, Toma Matsuo¹, Tsuyoshi Yamada^{2,3}, Takashi Sugita¹

SUMMARY: Trichosporon asahii is a pathogenic fungus that causes severe deep-seated fungal infections in neutropenic patients. Ku70, a key component of the non-homologous end-joining (NHEJ) pathway involved in the repair of DNA double-strand breaks, influences gene-targeting efficiency in T. asahii MPU129 strain using electroporation, a gene transfer method. Although phenotypic traits such as morphology and biofilm formation vary among T. asahii strains, the impact of different gene transfer methods on gene-targeting efficiency remains poorly characterized. In this study, we compared the gene-targeting efficiency of Agrobacterium tumefaciens-mediated transformation (ATMT) and electroporation. In T. asahii JCM2466 (CBS2479), a strain with high hyphal-forming ability, the ku70 gene-deficient mutant exhibited a higher gene-targeting efficiency via ATMT than the wild-type strain when generating a cnb1 gene-deficient mutant. The cnb1 gene encodes the β-subunit of calcineurin. In contrast, in the ku70 gene-deficient background of T. asahii JCM2466, cnb1-deficient mutants could not be generated by electroporation. The gene-targeting efficiencies of ATMT and electroporation in the ku70 gene-deficient mutant of T. asahii JCM2466 were 18% and 0%, respectively. The cnb1 gene-deficient mutants exhibited sensitivity to high temperature and several stress-inducing compounds. These results suggest that ATMT is a suitable gene transfer method for generating gene-deficient mutants in the ku70-deficient T. asahii JCM2466 background. Therefore, the choice of gene transfer method should be carefully tailored to the genetic background and phenotypic characteristics of each T. asahii strain.

Keywords: Trichosporon asahii, gene transfer method, ku70 gene, gene-deficient mutant

1. Introduction

Trichosporon asahii, a basidiomycete yeast, is widely distributed in a variety of environments including soil and plants (1,2). Moreover, T. asahii is part of the normal microflora of the human skin, digestive tract, and respiratory system (3-6). In immunocompromised individuals, including neutropenic patients, T. asahii causes severe deep-seated fungal infections (7-9). The mortality rate of deep-seated mycosis caused by T. asahii is approximately 80% (10,11). T. asahii is resistant to echinocandin antifungals, and infectious diseases caused by T. asahii often occur in patients treated with micafungin (12,13). Moreover, T. asahii strains resistant to antifungals such as amphotericin B and fluconazole have been isolated from patients (14,15). Therefore, gaining insight into the infection mechanisms and

drug-resistant systems of *T. asahii* is crucial. *T. asahii* JCM2466 (type strain CBS2479, Riken BioResource Research Center) is widely used in research (*16,17*). The genome information of *T. asahii* JCM2466 (CBS2479) has been published (*18*). In *T. asahii* MPU129, a clinical isolate that exhibits high virulence in a silkworm infection model, several genetic approaches, including a gene-knockdown method, were developed (*19*).

Repair mechanisms for DNA double-strand breaks affect gene-targeting efficiency by introducing homologous DNA fragments. Homologous recombination (HR) and non-homologous end joining (NHEJ) repair are double-strand break repair mechanisms (20). HR is required to introduce mutations into a gene-targeting system using homologous DNA fragments (20,21), whereas NHEJ repair mediates the insertion of introduced homologous DNA fragments

¹Department of Microbiology, Meiji Pharmaceutical University, Tokyo, Japan;

² Teikyo University Institute of Medical Mycology, Tokyo, Japan;

³ Asia International Institute of Infectious Disease Control, Teikyo University, Tokyo, Japan.

into genome sites that differ from the target region (20). Therefore, NHEJ repair leads to a decrease in the genetargeting efficiency by HR (20,22). Ku70 and Ku80 heterodimers play essential roles in NHEJ repair (23). In several fungi, the lack of these proteins leads to increased gene-targeting efficiency for generating gene-deficient mutants (22,24,25). In *T. asahii* MPU129, the *ku70* gene is involved in the gene-targeting efficiency (19). Therefore, the *ku70* gene-deficient mutant of *T. asahii* JCM2466 may be a useful parental strain for generating gene-deficient mutants by HR.

Agrobacterium tumefaciens-mediated gene transformation (ATMT) is an advantageous method for gene recombination in several fungi (26,27) and a more efficient method than electroporation for obtaining gene-deficient mutants (28,29). In 2020, ATMT was used to generate a transgenic T. asahii JCM2466 strain expressing enhanced green fluorescent protein (eGFP) (30). On the other hand, a transgenic T. asahii JCM2466 wild-type strain expressing eGFP was not generated by electroporation. In the ku70 gene-deficient mutant of T. asahii MPU129, electroporation was used as a gene transfer method to generate the gene-deficient mutants (19,31,32) . However, efficiency to generate genedeficient mutants in the ku70 gene-deficient mutant T. asahii JCM2466 regarding gene transfer methods was not yet compared.

Calcineurin is a calcium-calmodulin-activated phosphatase consisting of a heterodimer with the catalytic and regulatory subunits Cna1 and Cnb1 (33). The calcineurin complex with calmodulin controls the expression of several genes by dephosphorylating the transcriptional regulator Crz1 (34,35). The cnb1 gene-deficient T. asahii MPU129 mutants exhibited sensitivities to high temperature, cell membrane stress, cell wall stress, and endoplasmic reticulum (ER) stress (19). Moreover, the cnb1 gene was used to evaluate gene-targeting efficacy in T. asahii (36).

In the present study, we found that ATMT was more efficient method to generate the *cnb1* gene-deficient mutants than electroporation in the *ku70* gene-deficient mutant of *T. asahii* JCM2466. In the *ku70* gene-deficient mutant of *T. asahii* JCM2466, the *cnb1* gene-deficient mutant was not obtained by electroporation. Our findings suggest that ATMT is an efficient method for generating gene-deficient mutants of *T. asahii* JCM2466. Therefore, we assumed that gene transfer method should be selected appropriately in generating *T. asahii* gene-deficient mutants for each strain.

2. Materials and Methods

2.1. Reagents

Cefotaxime, sodium dodecyl sulfate (SDS), and dithiothreitol (DTT), were purchased from Wako Pure Chemical Industries (Osaka, Japan). Nourseothricin and G418 were purchased from Jena Bioscience (Dortmund, Germany) and Enzo Life Science, Inc. (Farmingdale, NY, USA), respectively.

2.2. Culture of T. asahii

The *T. asahii* JCM2466 strain used in this study is a standard type strain available from the Riken BioResource Research Center (*https://web.brc.riken.jp/ja/*). Table 1 provides information on the strains used in this study. The *T. asahii* JCM2466 *ku70* gene-deficient mutant was grown on Sabouraud dextrose agar (SDA) containing G418 (50 μg/mL) and incubated at 27°C for 2 days. The *T. asahii* JCM2466 *cnb1* gene-deficient mutant was grown on SDA containing nourseothricin (100 μg/mL) and incubated at 27°C for 2 days.

2.3. Construction of gene-deficient *T. asahii* mutants

The plasmid for gene-deficient T. asahii strains was constructed according to a previous report (19). To generate the ku70 gene-deficient mutant and the cnb1 gene-deficient mutant, pAg1-5'-UTRku70-nptII-3'-UTRku70 and pAg1-5'-UTRcnb1-NAT1-3'-UTRcnb1 were used, respectively (19). The pAg1-5'-UTRku70nptII-3'-UTRku70 plasmid was introduced into T. asahii JCM2466 using the previously described ATMT method (30). Gene transfer using electroporation was performed according to a previous report (36). The 5'-UTR (cnb1) -NAT1-3'-UTR (cnb1) fragments were amplified by PCR with the primers shown in Table 2. The *T. asahii* competent cells (40 µL) with the DNA fragments (100 ng) were added to a 0.2-cm gap cuvette (Bio-Rad Laboratories, Inc.) and electroporated (Time constant protocol: 1,800 V, 5 ms) using a Gene Pulser Xcell (Bio-Rad Laboratories, Inc.). The cells were suspended by yeast peptone dextrose containing 0.6 M sorbitol and incubated at 27°C for 3 h. After incubation, the cells were applied to SDA containing nourseothricin (300 μg/ mL) and incubated at 27°C for 3 days.

2.4. Genotyping PCR

Table 1. T. asahii strains used in this study

T. asahii strains	Relevant genotype	Background	Reference
JCM2466 (Wild-type) $\Delta ku70$ (Parent strain) $\Delta cnb1$	ku70::nptII ku70::nptII, cnb1::NAT1	JCM2466 JCM2466 Δ <i>ku70</i>	Riken BioResource Research Center This study This study

Table 2. Primers used in this study

Primers	Nucleic acid sequence		
[Genotyping]			
Primers-1 for ku70 genotyping			
F ku70 gene locus	TCGAGGTCGCGACTTTGTTATTGCCAGGTCCTGA		
R ku70 gene locus	AGAGCTGCGATCGTGGGCTGATCCGTCC		
Primers-2 for <i>ku70</i> genotyping			
F ku70 gene ORF	TTTCAGCAACTCCGTCAGATCAGCGCCGAAGACA		
R ku70 gene ORF	ATCTGCGAAAGAGCGGCCGGGCC		
Primers-1 for <i>cnb1</i> genotyping			
F cnb1 gene locus	GGAGTGAAGAAGGCAGAGAGCAACAACAGCGGT		
R cnb1 gene locus	CCGTGATCGCATGGGGCGTGCACAAAGTG		
Primers-2 for <i>cnb1</i> genotyping			
F cnb1 gene ORF	CGGCTCGGGTACGGTAGACTTCCAGGAGTTTGTCG		
R cnb1 gene ORF	AACAGGTCCTCGAGCGTCATCTGCTTGACGATGT		
Primers-3 for <i>cnb1</i> genotyping			
F <i>cnb1</i> gene outside	GGACGGCGAGCAGGCGCTCTACATGAGC		
R cnb1 gene outside	CTGAGTCCCATCGGCCCTTGCCTTCAAGCTACC		
[Amplification of <i>cnb1</i> cassette for electroporation]			
F cnb1-cassette	CCGTGATCTGCTGCACGTTCGGGTCCG		
R cnb1-cassette	CTGTTCACCTCTGGCTACGACCCCCTCCTC		

Genotyping PCR was performed according to a previous report (19,36). To generate the ku70 genedeficient mutant, the transformants were grown on SDA containing G418 (300 µg/mL). To generate the cnb1 gene-deficient mutant, the transformants were grown on SDA containing nourseothricin (300 µg/mL). Colony PCR for ku70 genotyping and cnb1 genotyping was performed using primers (Table 2). The mutation in the genome of the transformants was confirmed using the extracted genome by PCR using the primers shown in Table 2.

2.5. Temperature sensitivity test

A temperature sensitivity test was performed according to the previous report (31). The *T. asahii* strains were grown on SDA and incubated at 27°C for 2 days. *T. asahii* cells were suspended in a physiologic saline solution (0.9% w/v NaCl) and filtered through a 40-μm cell strainer (Corning Inc., Corning, NY, USA). Absorbance of the *T. asahii* cell suspension at 630 nm was adjusted to 1. A series of 10-fold dilutions of the fungal suspension was prepared using saline. Cell suspensions (5 μL each) were spotted on the SDA. The agar plates were incubated at 27°C, 37°C, or 40°C for 24 h, and photographs were obtained.

For growth on liquid medium, Sabouraud liquid medium (1% hipolypepton, 4% dextrose) was used in this study. Suspensions of the *T. asahii* parent strain (Parent) and three *cnb1* gene-deficient mutants ($\Delta cnb1$ #1, #2, and #3) were prepared with Sabouraud medium and adjusted to 0.005 absorbance at 630 nm (A_{630}). The *T. asahii* cells were incubated at 27°C, 37°C, or 40°C for 4

days. A₆₃₀ value was measured using a microplate reader (iMarkTM microplate reader; Bio-Rad Laboratories Inc., Hercules, CA, USA).

2.6. Drug sensitivity test

A drug sensitivity test was performed according to the previous report (3I). The T. asahii strains were grown on SDA and incubated at 27°C for 2 days. T. asahii cells were suspended in physiologic saline solution (0.9% w/v NaCl) and filtered through a 40- μ m cell strainer (Corning Inc.). The A_{630} value of the T. asahii cell suspension was adjusted to 1. A series of 10-fold dilutions of the fungal suspension were prepared using saline. Cell suspensions (5μ L each) were spotted on the SDA containing SDS (0.01%), Congo red ($300 \mu g/m$ L), tunicamycin ($1 \mu g/m$ L), or DTT (12 mM). Each agar plate was incubated at 37°C for 24 h, and photographs were obtained.

3. Results

3.1. Generating the ku70 gene-deficient mutant in T. asahii JCM2466 by ATMT

A. tumefaciens harboring the targeting plasmid, pAg1-5'-UTRku70-nptII-3'-UTRku70, was used to generate a ku70 gene-deficient mutant of T. asahii JCM2466 (Figure 1A). Because pAg1-5'-UTRku70-nptII-3'-UTRku70 contains the nptII gene that leads to resistance against the aminoglycoside G418, the ku70 gene-deficient T. asahii mutant shows G418 resistance by recombination (Figure 1A). Through ATMT, the 192nd colony was selected by colony PCR as a candidate ku70 gene-deficient mutant

(Figure 1B). The transformant grew on SDA containing G418 (Figure 1C). DNA fragments of the predicted size were amplified by PCR with the genome as a template (Figures 1D and 1E). The results suggest that the *ku70* gene-deficient mutant in *T. asahii* JCM2466 was generated by ATMT.

3.2. *ku70* gene deficiency on the growth of *T. asahii* JCM2466

We investigated the effect of ku70 deficiency in T. asahii

JCM2466 on the growth. The ku70 gene-deficient mutant was similar growth to the wild-type at either 27°C, 37°C, or 40°C (Figure 2). These results suggest that the growth of T. asahii JCM2466 did not alter by ku70 gene deficiency.

3.3. Gene-targeting efficiency in a ku70 gene-deficient T. asahii mutant for gene transfer methods such as ATMT and electroporation

There are phenotypic differences between T. asahii

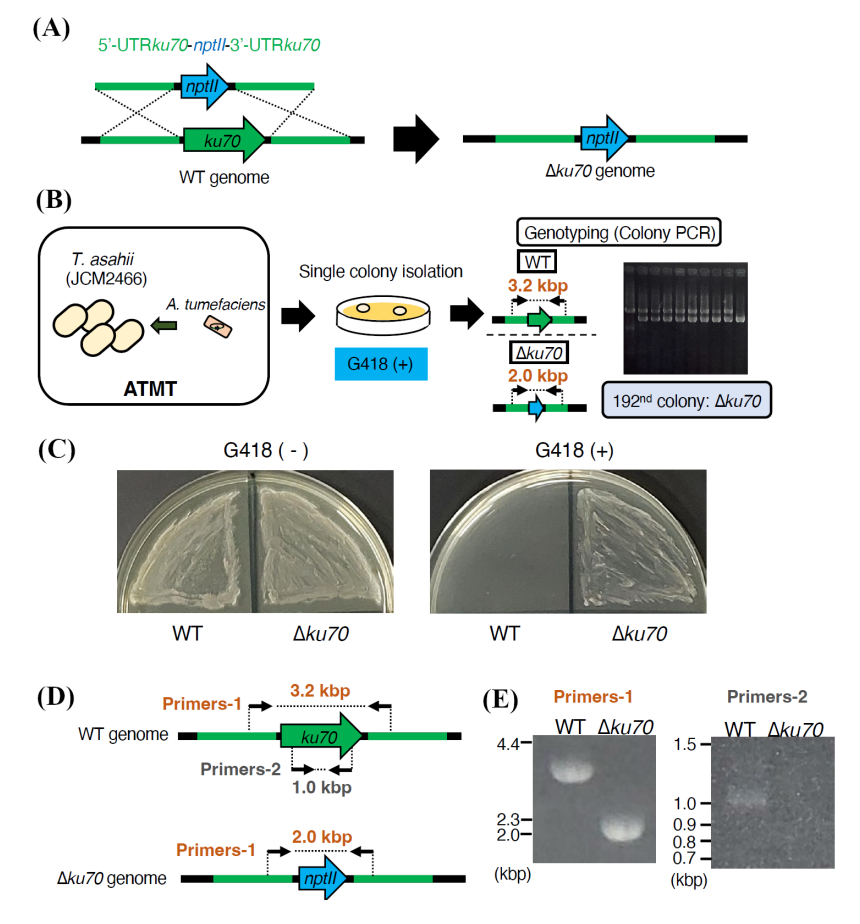


Figure 1. Establishment of the ku70 gene-deficient mutant of T. asahii JCM2466. (A) Illustration of replacement of the ku70 gene in T. asahii JCM2466 by recombination. The predicted genome structure of the ku70 gene-deficient mutant is shown. (B) Experimental scheme for obtaining candidate ku70 gene-deficient mutants of T. asahii JCM2466 by the ATMT system. (C) The wild-type (WT) and ku70 gene-deficient ($\Delta ku70$) candidate strains were spread on SDA with or without G418 (50 μ g/ml) and incubated at 27°C for 2 days. (D) Location of the primers for confirming the genome structure of the ku70 gene-deficient candidate by PCR. (E) Confirmation of the ku70 gene-deficiency of the ku70 gene-deficient candidate by PCR using extracted genome DNA.

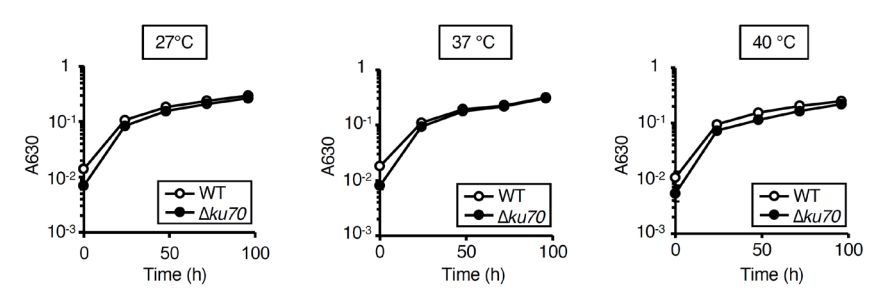


Figure 2. Growth of the ku70 gene-deficient mutant in T. asahii JCM2466. The wild-type (WT) and ku70 gene-deficient mutant ($\Delta ku70$) strains were inoculated in Sabouraud liquid medium and incubated at 27°C, 37°C, or 40°C. Absorbance of the culture at 630 nm was monitored.

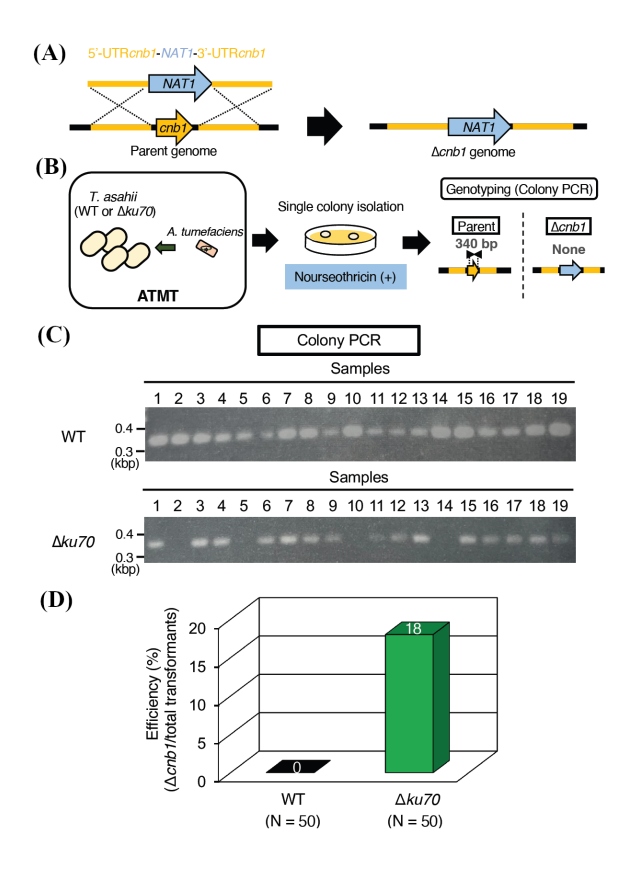


Figure 3. Increase in the ratio to obtain the gene-deficient mutant of T. asahii JCM2466 by ku70 gene deficiency. (A) Illustration of replacement of the cnb1 gene in T. asahii JCM2466 by recombination. The predicted genome structure of the cnb1 gene-deficient mutant is shown. (B) Experimental scheme for obtaining candidate cnb1 gene-deficient T. asahii JCM2466 mutants by the ATMT system. (C) Colony PCR was performed on colonies obtained from the wild-type (WT) or the ku70 gene-deficient mutant ($\Delta ku70$) grown on SDA containing nourseothricin (300 μ g/mL). (D) Efficacy of homologous replacement in the cnb1 gene region. Efficiency (%) was calculated as the ratio of cnb1 gene-deficient mutants ($\Delta cnb1$) per total transformants.

JCM2466 and MPU129. JCM2466 exhibits stronger hyphal formation ability compared with MPU129 (37). We examined the usefulness of ATMT for gene targeting in a JCM2466 ku70 gene-deficient mutant. The genetargeting efficiency was determined by calculating the ratio of the strain lacking the *cnb1* gene, which encodes the β-subunit of calcineurin (36). The cnb1 gene was deleted by ATMT using pAg1-5'-UTRcnb1-NAT1-3'-UTRcnb1 plasmid (Figure 3A). The cnb1 gene deficiency of nourseothricin-resistant strains was confirmed by colony PCR (Figures 3B and 3C). Of the 50 nourseothricin-resistant colonies obtained from the ku70 gene-deficient mutant by ATMT, 9 were deficient for the cnb1 gene (Figure 3D). On the other hand, none of the 50 nourseothricin-resistant colonies obtained from the wild-type by ATMT was deficient for the cnb1 gene (Figure 3D). In the *T. asahii* MPU129 strain, ku70 gene deficiency increased the gene-targeting efficiency by electroporation (19). Next, we examined the usefulness of electroporation for gene targeting in a JCM2466 ku70 gene-deficient mutant. Nourseothricin-resistant colonies

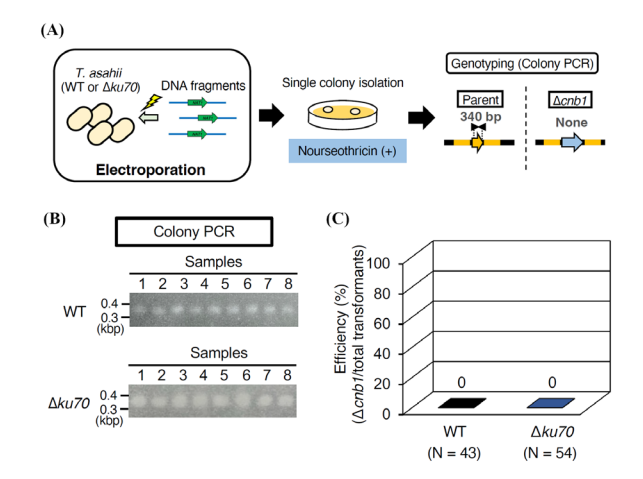


Figure 4. The ratio to obtain *cnb1* gene-deficient *T. asahii* mutant by electroporation. (A) Experimental scheme for obtaining candidate *cnb1* gene-deficient *T. asahii* JCM2466 mutants by the electroporation. (B) Colony PCR was performed on colonies obtained from the wild-type (WT) or the ku70 gene-deficient mutant ($\Delta ku70$) grown on SDA containing nourseothricin (300 µg/mL). (C) Efficacy of homologous replacement in the *cnb1* gene region. Efficiency (%) was calculated as the ratio of *cnb1* gene-deficient mutants ($\Delta cnb1$) per total transformants.

were obtained from the *T. asahii* JCM2466 and the JCM2466 *ku70* gene-deficient mutant (Figure 4). In all nourseothricin-resistant colonies, the inner region of *cnb1* gene was amplified by colony PCR (Figure 4). These results suggest that ATMT is efficient for gene targeting in a JCM2466 *ku70* gene-deficient mutant compared to electroporation.

3.4. Phenotypes of the *cnb1* gene-deficient mutants in *T. asahii* JCM2466

We examined whether cnb1 gene deficiency affects the stress resistance of T. asahii JCM2466. In this experiment, the ku70 gene-deficient T. asahii JCM2466 mutant was used as the parent strain. Moreover, three clones ($\triangle cnb1$ -#1, #2, and #3), which were selected at random from the candidates of cnb1 gene-deficient mutants obtained from the T. asahii JCM2466 ku70 genedeficient mutant by ATMT, were confirmed to have null mutation of the *cnb1* gene by PCR with the primers-1, 2, and 3, and nourseothricin susceptibility assay (Figure 5). Growth of the *cnb1* gene-deficient mutants at 40°C was slower than that of the parent strain (Figure 6). SDS and Congo red damage the cell membrane and cell wall, respectively (19). Growth was delayed in the cnb1 gene-deficient mutants treated with SDS and Congo red (Figure 7). DTT and tunicamycin induce ER stress (19). Growth of the cnb1 gene-deficient mutants was delayed by treatment with DTT and tunicamycin (Figure 7). These results suggest that cellular responses to high temperature, cell membrane damage, cell wall damage, and ER stress, were altered by cnb1 gene deficiency in the *T. asahii* JCM2466 ku70 gene-deficient mutant.

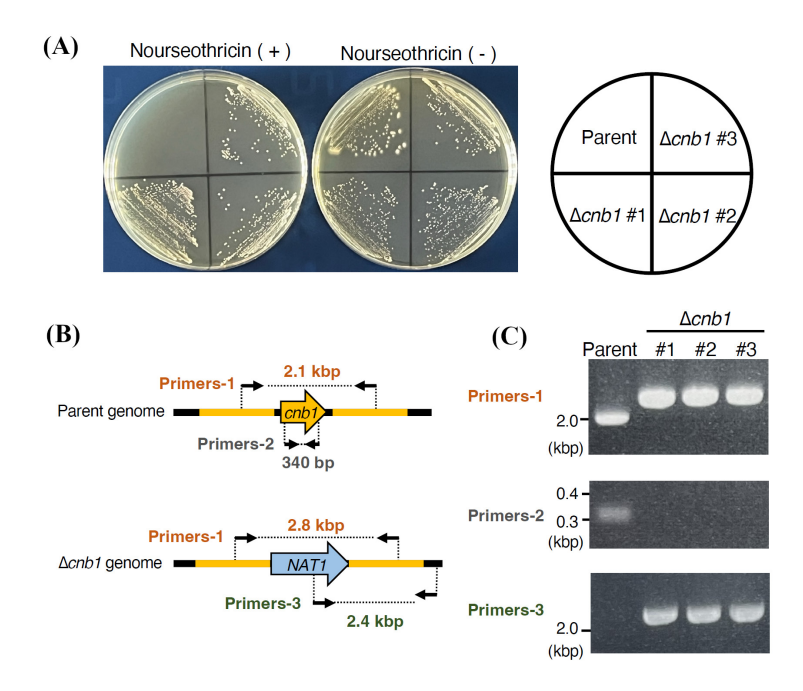


Figure 5. Confirmation of *cnb1* gene-deficient mutants in *T. asahii* JCM2466. (A) The ku70 gene-deficient mutant was used as the parent strain in this experiment. The *T. asahii* parent strain (Parent) and 3 *cnb1* gene-deficient candidates ($\Delta cnb1$ #1, #2, and #3) were spread on SDA with or without nourseothricin (300 µg/mL) and incubated at 27°C for 2 days. (B) Location of the primers for confirming the genome structure of the *cnb1* gene-deficient candidates by PCR. (C) Confirmation of the *cnb1* gene-deficient candidates by PCR using extracted genome DNA.

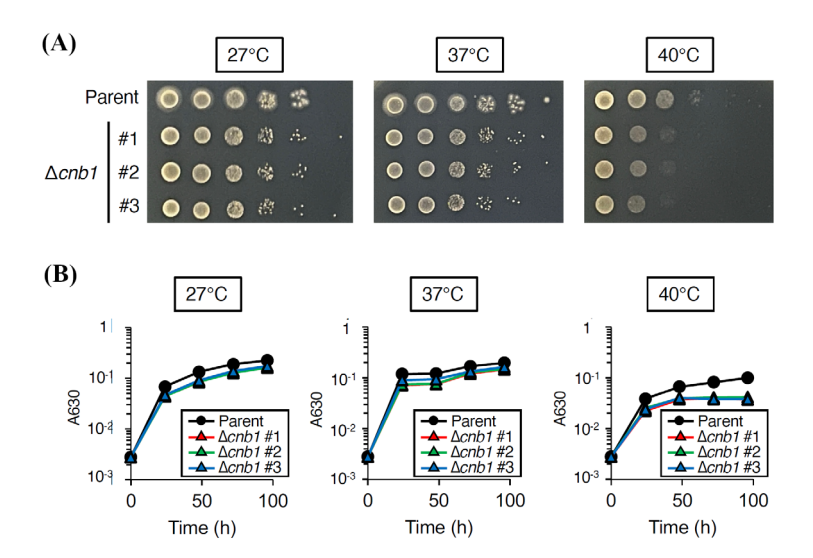


Figure 6. Temperature sensitivity of the *cnb1* gene-deficient mutants in *T. asahii* JCM2466. (A) The *ku70* gene-deficient mutant was used as the parent strain in this experiment. The *T. asahii* parent strain (Parent) and 3 *cnb1* gene-deficient mutants (Δ*cnb1* #1, #2, and #3) were grown on SDA and incubated at 27°C for 2 days. *T. asahii* cells were suspended in a physiologic saline solution and filtered through a 40-μm cell strainer. A series of 10-fold dilutions of the fungal suspension were prepared using saline. Cell suspensions (5 μL each) were spotted on the SDA. Agar plates were incubated at 27°C, 37°C, or 40°C for 24 h. (B) The *T. asahii* parent strain (Parent) and 3 *cnb1* gene-deficient mutants (Δ*cnb1* #1, #2, and #3) were inoculated in Sabouraud liquid medium and incubated at 27°C, 37°C, or 40°C. The absorbance of the culture at 630 nm was monitored.

	SDA	SDS (0.01%)	Congo red (300 µg/mL)	Tunicamycin (1 µg/mL)	Dithiothreitol (12 mM)
Par	ent 🔵 🔘 🕬 🕸	●●	• • • • •		• • • • •
	#1 🔵 🔘 🚳 🏶		•		• • •
∆cnb1	#2 • • • * *	(4)	•	• •	0 0
	#3 • • • * *			• •	0 0 4

Figure 7. Sensitivities of *cnb1* gene-deficient *T. asahii* JCM2466 mutants to stress inducers. The ku70 gene-deficient mutant was used as the parent strain in this experiment. The *T. asahii* parent strain (Parent) and 3 *cnb1* gene-deficient mutants ($\Delta cnb1$ #1, #2, and #3) were grown on SDA and incubated at 27°C for 2 days. *T. asahii* cells were suspended in a physiologic saline solution and filtered through a 40- μ m cell strainer. A series of 10-fold dilutions of the fungal suspension were prepared using saline. Cell suspensions (5 μ L each) were spotted on SDA containing SDS (0.01%), Congo red (300 μ g/mL), tunicamycin (1 μ g/mL), or DTT (12 mM). Each agar plate was incubated at 37°C for 24 h.

Table 3. Efficiency of homologous replacement in cnb1 gene region by electroporation

Strain	Total transformants	Homologous replacement $(\Delta cnbI)$	Efficiency (%) (Δ <i>cnb1</i> /total transformants)
JCM2466 wild type	51	0	0%
JCM2466 Δ <i>ku</i> 70	86	0	0%
MPU129 wild type ^a	120	0	0%
MPU129 Δ <i>ku70</i> ^a	21	4	19%

^aData are cited from Matsumoto et al. (19).

4. Discussion

In this study, we obtained a *ku70* gene-deficient mutant of *T. asahii* JCM2466 by ATMT. The *ku70* gene-deficient *T. asahii* JCM2466 mutant generated *cnb1* gene-deficient mutants at a high frequency in ATMT, but not in electroporation. These results suggest that ATMT is an appropriate gene transfer method for generating the gene-deficient mutants in the *ku70* gene-deficient *T. asahii* JCM2466 mutant.

The ku70 gene-deficient T. asahii JCM2466 mutant serves as a valuable parental strain for genetic studies. Deletion of the ku70 gene did not affect the growth of T. asahii JCM2466. Moreover, ku70 gene deficiency increased gene-targeting efficiency in ATMT. The frequency of obtaining cnb1 gene-deficient mutants from the ku70 gene-deficient T. asahii JCM2466 mutant by ATMT was 18%. In contrast, cnb1 gene-deficient mutants could not be obtained from the ku70 genedeficient T. asahii JCM2466 mutant by electroporation. These finding suggest that the combination of the ku70gene-deficient T. asahii JCM2466 mutant and ATMT is required for efficient gene targeting. In the T. asahii MPU129, however, electroporation proved effective for generating the cnb1 gene-deficient mutants from the ku70 gene-deficient mutant (Table 3) (19). Therefore, the choice of an appropriate gene transfer method should be tailored to each *T. asahii* strain. The underlying reasons for these strain-dependent differences will be addressed in future studies.

In *Neurospora crassa*, a filamentous fungus belonging to Ascomycota, deletion of the *ku70* or *ku80* genes increases the generating efficiency of genedeficient mutants to 90-100% (22). In *Aspergillus fumigatus*, a filamentous fungus also belonging to Ascomycota, deletion of the *ku80* gene increases the efficiency of obtaining a gene-deficient strain from 3% to 80% (38). On the other hand, in *C. neoformans*, which belongs to the same Basidiomycota as *T. asahii*, deletion of the *ku80* gene increased the efficiency of obtaining gene-deficient mutants, but only by 5-6% (29). Therefore, HR tends to be less efficient in Basidiomycota than in Ascomycota under the condition of dysfunction of NHEJ repair.

The genome information for *T. asahii* JCM2466 (CBS2479) is published and the correct primers can be ordered; therefore, we assumed that an efficient gene-

targeting system in *T. asahii* JCM2466 was established in this study. On the other hand, it is not clear at this time whether targeting efficiencies comparable to that of the *cnb1* locus can be obtained for many other gene loci. Further gene-targeting experiments should be performed in the future. *T. asahii* JCM2466 exhibited a higher hyphal formation ability than MPU129 (*37*). Hyphae possess a larger surface area per cell than yeast. *T. asahii* JCM2466 may offer a greater surface area accessible to *Agrobacterium tumefacies* than MPU129, potentially leading to higher gene transfer efficiency *via* the ATMT system.

Phenotypic analyses of gene-deficient mutants of *T. asahii* JCM2466 can be performed using the genetargeting method. The *cnb1* gene-deficient mutants exhibited phenotypes such as sensitivities to high temperature, cell membrane stress, cell wall stress, and ER stress inducers. These phenotypic characteristics were also recognized in the same type of mutants which had been generated from *T. asahii* MPU129 (19,31). These findings suggest that the *cnb1* gene is responsible for the stress responses of both *T. asahii* JCM2466 and MPU129. Therefore, the combined use of the *ku70* genedeficient *T. asahii* JCM2466 mutant and ATMT is useful for phenotypic analyses of gene-deficient mutants.

In conclusion, we established an efficient genetargeting system for standard type strain JCM2466 of *T. asahii* using the *ku70* gene-deficient mutant with ATMT. In electroporation, the gene targeting efficiencies of the *ku70* gene-deficient *T. asahii* JCM2466 mutant and the *ku70* gene-deficient *T. asahii* MPU129 mutant were 0% and 19%, respectively (Table 3). These findings suggest that optimization of the gene transfer method may be necessary to establish an efficient gene-targeting system for each *T. asahii* strain.

Acknowledgements

We thank Renta Endo, Momoka Yagi, and Haruka Ogino (Meiji Pharmaceutical University) for technical assistance in rearing the silkworms. We also thank SciTechEdit International LLC (Highlands Ranch, CO, USA) for editorial support.

Funding: This study was supported by JSPS KAKENHI grant number JP23K06141 (Scientific Research (C) to Y.M.) and in part by the Research Program on Emerging

and Re-emerging Infectious Diseases of the Japan Agency for Medical Research and Development, AMED (Grant number JP24fk0108679h0402 to T.S.).

Conflict of Interest: The authors have no conflicts of interest to disclose.

References

- 1. Sugita T, Nishikawa A, Ichikawa T, Ikeda R, Shinoda T. Isolation of *Trichosporon asahii* from environmental materials. Med Mycol. 2000; 38:27-30.
- Sugita T, Ichikawa T, Matsukura M, Sueda M, Takashima M, Ikeda R, Nishikawa A, Shinoda T. Genetic diversity and biochemical characteristics of *Trichosporon asahii* isolated from clinical specimens, houses of patients with summer-type-hypersensitivity pneumonitis, and environmental materials. J Clin Microbiol. 2001; 39:2405-2411.
- 3. Colombo AL, Padovan ACB, Chaves GM. Current knowledge of *Trichosporon* spp. and Trichosporonosis. Clin Microbiol Rev. 2011; 24:682-700.
- 4. Zhang E, Sugita T, Tsuboi R, Yamazaki T, Makimura K. The opportunistic yeast pathogen *Trichosporon asahii* colonizes the skin of healthy individuals: analysis of 380 healthy individuals by age and gender using a nested polymerase chain reaction assay. Microbiol Immunol. 2011; 55:483-488.
- Gouba N, Raoult D, Drancourt M. Eukaryote culturomics of the gut reveals new species. PLoS ONE. 2014; 9:e106994.
- Cho O, Matsukura M, Sugita T. Molecular evidence that the opportunistic fungal pathogen *Trichosporon asahii* is part of the normal fungal microbiota of the human gut based on rRNA genotyping. Int J Infect Dis. 2015; 39:87-88.
- Walsh TJ, Melcher GP, Lee JW, Pizzo PA. Infections due to *Trichosporon* species: new concepts in mycology, pathogenesis, diagnosis and treatment. Curr Top Med Mycol. 1993; 5:79-113.
- 8. Júnior JN de A, Hennequin C. Invasive *Trichosporon* Infection: a Systematic Review on a Re-emerging Fungal Pathogen. Front Microbiol. 2016; 7:1629.
- 9. Duarte-Oliveira C, Rodrigues F, Gonçalves SM, Goldman GH, Carvalho A, Cunha C. The Cell Biology of the *Trichosporon*-Host Interaction. Front Cell Infect Microbiol. 2017; 7:118.
- Krcmery V, Mateicka F, Kunová A, Spánik S, Gyarfás J, Sycová Z, Trupl J. Hematogenous trichosporonosis in cancer patients: report of 12 cases including 5 during prophylaxis with itraconazol. Support Care Cancer. 1999; 7:39-43.
- 11. Girmenia C, Pagano L, Martino B, D'Antonio D, Fanci R, Specchia G, Melillo L, Buelli M, Pizzarelli G, Venditti M, Martino P; GIMEMA Infection Program. Invasive infections caused by *Trichosporon* species and *Geotrichum capitatum* in patients with hematological malignancies: a retrospective multicenter study from Italy and review of the literature. J Clin Microbiol. 2005; 43:1818-1828.
- 12. Kimura M, Araoka H, Yamamoto H, *et al.* Micafungin Breakthrough Fungemia in Patients with Hematological Disorders. Antimicrob Agents Chemother. 2018; 62:324.
- 13. Kimura M, Asano-Mori Y, Sakoh T, et al. Factors associated with breakthrough fungemia caused by

- Candida, Trichosporon, or Fusarium species when the breakthrough fungemia developed in patients with hematological disorders. Antimicrob Agents Chemother. 2022; 66:e0208121.
- Toriumi Y, Sugita T, Nakajima M, Matsushima T, Shinoda T. Antifungal pharmacodynamic characteristics of amphotericin B against *Trichosporon asahii*, using timekill methodology. Microbiol Immunol. 2002; 46:89-93.
- Iturrieta-González IA, Padovan ACB, Bizerra FC, Hahn RC, Colombo AL. Multiple species of *Trichosporon* produce biofilms highly resistant to triazoles and amphotericin B. PLoS ONE. 2014; 9:e109553.
- Kurakado S, Miyashita T, Chiba R, Sato C, Matsumoto Y, Sugita T. Role of arthroconidia in biofilm formation by *Trichosporon asahii*. Mycoses. 2020; 185:377-347.
- Aoki K, Yamamoto K, Ohkuma M, Sugita T, Tanaka N, Takashima M. Hyphal Growth in *Trichosporon asahii* Is Accelerated by the Addition of Magnesium. Microbiol Spectr. 2023; 11:e04242-22.
- Yang RY, Li HT, Zhu H, Zhou GP, Wang M, Wang L. Draft Genome Sequence of CBS 2479, the Standard Type Strain of *Trichosporon asahii*. Eukaryot Cell. 2012; 11:1415-1416.
- Matsumoto Y, Nagamachi T, Yoshikawa A, Yamazaki H, Yamasaki Y, Yamada T, Sugita T. Development of an efficient gene-targeting system for elucidating infection mechanisms of the fungal pathogen *Trichosporon asahii*. Sci Rep. 2021; 11:18270.
- Ding Y, Wang KF, Wang WJ, Ma YR, Shi TQ, Huang H, Ji XJ. Increasing the homologous recombination efficiency of eukaryotic microorganisms for enhanced genome engineering. Appl Microbiol Biotechnol. 2019; 103:4313-4324.
- Gusa A, Jinks-Robertson S. Mitotic Recombination and Adaptive Genomic Changes in Human Pathogenic Fungi. Genes (Basel). 2019; 10:901.
- 22. Ninomiya Y, Suzuki K, Ishii C, Inoue H. Highly efficient gene replacements in *Neurospora* strains deficient for nonhomologous end-joining. Proc Natl Acad Sci USA. 2004; 101:12248-12253.
- Fell VL, Schild-Poulter C. The Ku heterodimer: function in DNA repair and beyond. Mutat Res Rev Mutat Res. 2015; 763:15-29.
- Yamada T, Makimura K, Hisajima T, Ishihara Y, Umeda Y, Abe S. Enhanced gene replacements in Ku80 disruption mutants of the dermatophyte, *Trichophyton* mentagrophytes. FEMS Microbiol Lett. 2009; 298:208-217.
- 25. Carvalho NDSP, Arentshorst M, Kwon MJ, Meyer V, Ram AFJ. Expanding the *ku70* toolbox for filamentous fungi: establishment of complementation vectors and recipient strains for advanced gene analyses. Appl Microbiol Biotechnol. 2010; 87:1463-1473.
- Yamada T, Makimura K, Satoh K, Umeda Y, Ishihara Y, Abe S. Agrobacterium tumefaciens-mediated transformation of the dermatophyte, Trichophyton mentagrophytes: an efficient tool for gene transfer. Med Mycol. 2009; 47:485-494.
- Idnurm A, Bailey AM, Cairns TC, Elliott CE, Foster GD, Ianiri G, Jeon J. A silver bullet in a golden age of functional genomics: the impact of *Agrobacterium*-mediated transformation of fungi. Fungal Biol Biotechnol. 2017: 4:6
- 28. Chang YC, Kwon-Chung KJ. Complementation of a capsule-deficient mutation of *Cryptococcus neoformans*

- restores its virulence. Mol Cell Biol. 1994; 14:4912-4919.
- Lin X, Chacko N, Wang L, Pavuluri Y. Generation of stable mutants and targeted gene deletion strains in *Cryptococcus neoformans* through electroporation. Med Mycol. 2015; 53:225-234.
- Matsumoto Y, Yamazaki H, Yamasaki Y, Tateyama Y, Yamada T, Sugita T. A novel silkworm infection model with fluorescence imaging using transgenic *Trichosporon* asahii expressing eGFP. Sci Rep. 2020; 10:10991.
- Matsumoto Y, Yoshikawa A, Nagamachi T, Sugiyama Y, Yamada T, Sugita T. A critical role of calcineurin in stress responses, hyphal formation, and virulence of the pathogenic fungus *Trichosporon asahii*. Sci Rep. 2022; 12:16126.
- Matsumoto Y, Sugiyama Y, Nagamachi T, Yoshikawa A, Sugita T. Hog1-mediated stress tolerance in the pathogenic fungus *Trichosporon asahii*. Sci Rep. 2023; 13:13539.
- Hemenway CS, Heitman J. Calcineurin. Structure, function, and inhibition. Cell Biochem Biophys. 1999; 30:115-151.
- Kozubowski L, Lee SC, Heitman J. Signalling pathways in the pathogenesis of *Cryptococcus*. Cell Microbiol. 2009; 11:370-380.
- Yadav V, Heitman J. Calcineurin: The Achilles' heel of fungal pathogens. PLOS Pathog. 2023; 19:e1011445.

- Matsumoto Y, Nagamachi T, Yoshikawa A, Yamada T, Sugita T. A joint PCR-based gene-targeting method using electroporation in the pathogenic fungus *Trichosporon* asahii. AMB Express. 2022; 12:91.
- Kurakado S, Miyashita T, Chiba R, Sato C, Matsumoto Y, Sugita T. Role of arthroconidia in biofilm formation by *Trichosporon asahii*. Mycoses. 2021; 64:42-47.
- 38. Ferreira ME da S, Kress MRVZ, Savoldi M, Goldman MHS, Härtl A, Heinekamp T, Brakhage AA, Goldman GH. The akuB(KU80) mutant deficient for nonhomologous end joining is a powerful tool for analyzing pathogenicity in Aspergillus fumigatus. Eukaryotic Cell. 2006; 5:207-211.

Received August 13, 2025; Revised October 6, 2025; Accepted October 12, 2025.

*Address correspondence to:

Yasuhiko Matsumoto, Department of Microbiology, Meiji Pharmaceutical University, 2-522-1, Noshio, Kiyose, Tokyo 204-8588, Japan.

E-mail: ymatsumoto@my-pharm.ac.jp

Released online in J-STAGE as advance publication October 17, 2025.

Brief Report

DOI: 10.5582/ddt.2025.01077

Solid phase extraction and high-performance liquid chromatographic determination of lazertinib in human plasma

Yoshito Gando, Takeo Yasu*

Department of Medicinal Therapy Research, Education and Research Unit for Comprehensive Clinical Pharmacy, Meiji Pharmaceutical University, Tokyo, Japan.

SUMMARY: Lazertinib is a novel third-generation tyrosine kinase inhibitor (TKI) developed for the treatment of epidermal growth factor receptor (EGFR) mutant non-small cell lung cancer (NSCLC). Reports on previous EGFR-TKIs have detailed significant associations between blood drug concentration and efficacy. In addition, significantly elevated blood concentrations of lazertinib have been observed in Asians compared to Caucasians, suggesting the influence of interethnic variability. In this study, we developed and validated a method to determine lazertinib concentrations in human plasma for therapeutic drug monitoring (TDM). Lazertinib and its internal standard, sotorasib, were extracted by solid-phase extraction using an Oasis hydrophilic lipophilic balance cartridge. Chromatographic separation was performed on a reversed-phase column with 0.5% KH₂PO₄ (pH4.5) and acetonitrile (52:48, v/v) as the mobile phases in an isocratic elution mode with a flow rate of 1.0 mL/min. The detection wavelength was 296 nm. The calibration curves were linear in the range of 25–2,000 ng/mL, with a coefficient of determination (r²) of 0.9997. The accuracy and precision of all validation experiments were within the criteria set by the Food and Drug Administration guidelines. This study represents the first development and validation of a method for quantifying lazertinib in human plasma. This study is expected to facilitate the widespread use of TDM in studies on lazertinib.

Keywords: lazertinib, high-performance liquid chromatography-ultraviolet, tyrosine kinase inhibitor, human plasma, therapeutic drug monitoring

1. Introduction

Lazertinib is a third-generation epidermal growth factor receptor-tyrosine kinase inhibitor (EGFR-TKI) that is used in combination with amivantamab to treat EGFR-mutated advanced non-small cell lung cancer (NSCLC) (1). The National Comprehensive Cancer Network (NCCN) guidelines recommend osimertinib as a first-line therapy for EGFR-mutated NSCLC (2). Recently, combination therapy with lazertinib and amivantamab has been shown to significantly prolong progression-free survival (PFS) compared to osimertinib therapy (1). Therefore, an increasing number of patients are expected to receive lazertinib instead of osimertinib.

Typical adverse events (all grades) associated with lazertinib are rash or acne (33%) and diarrhea (21%), with the dose being reduced or treatment discontinued at the approved dose (240 mg/d) in 17% and 4% of patients, respectively (3). Erlotinib and gefitinib, EGFR-TKIs similar to lazertinib, also show adverse reactions. There is a significant association between blood erlotinib concentration (4), various grades of skin rash, and diarrhea. Meanwhile, plasma gefitinib

trough concentrations ≥ 200 ng/mL are significantly associated with prolonged overall survival (5). Therefore, therapeutic drug monitoring (TDM) of trough concentrations has been recommended for these drugs (6).

However, the relationship among blood lazertinib concentration, clinical efficacy, and safety has not been clarified. The approved dose of lazertinib is 240 mg/d worldwide (7-9), even though the maximum plasma concentration (C_{max}) and area under the curve (AUC) are significantly higher in Asians than in Caucasians owing to interethnic variation (10). Therefore, TDM may be necessary for implementing effective and safe lazertinib therapy. In clinical trials, plasma lazertinib concentrations have been measured using liquid chromatographymass spectrometry (LC-MS); however, detailed LC-MS conditions have not been described (10).

To the best of our knowledge, there have been no reports on methods for quantifying lazertinib concentrations in human plasma. In addition, LC-MS is susceptible to ion suppression and may misinterpret samples containing multiple drugs with the same mass (11). Furthermore, LC-MS is expensive and has limited

application in general hospitals. Hence, we developed a method to determine the concentration of lazertinib in human plasma using high-performance liquid chromatography-ultraviolet (HPLC-UV), in accordance with the Food and Drug Administration (FDA) analytical validation guidelines (12).

2. Materials and Methods

Reagents and chemicals

Lazertinib and sotorasib (internal standard, IS) were obtained from MedChemExpress (Monmouth Junction, NJ, USA) and Toronto Research Chemicals, Inc. (Toronto, ON, Canada), respectively. Sotorasib is a Kirsten rat sarcoma viral oncogene (KRAS) inhibitor used to treat KRAS mutation-positive NSCLC that is not clinically concomitant with lazertinib (13). Acetaminophen, amlodipine, cimetidine, clarithromycin, droperidol, esomeprazole, fluconazole, furosemide, gabapentin, isavuconazole, lacosamide, loperamide, metformin, minocycline, nifedipine, omeprazole, posaconazole, and pregabalin were obtained from Tokyo Chemical Industry Co. (Tokyo, Japan). Arotinolol and tedizolid were obtained from Toronto Research Chemicals, Inc. (Toronto, ON, Canada) and ChemScene (Monmouth Junction, NJ, USA), respectively. HPLCgrade acetonitrile, methanol, distilled water (Kanto Chemical, Co., Inc., Tokyo, Japan), KH₂PO₄ (Fujifilm Wako, Osaka, Japan) were used in the HPLC mobile phase. Oasis hydrophilic-lipophilic balance (HLB) extraction cartridges were purchased from Waters Corp. (Milford, MA, USA). Human plasma (pooled) and ethylenediaminetetraacetic acid (EDTA)-2Na were purchased from Cosmo Bio Co., Ltd. (Tokyo, Japan).

2.2. Equipment and chromatographic conditions

The HPLC system consisted of pumps (PU-4180), a UV detector (UV-4075), and an autosampler (AS-4550; all from Jasco, Tokyo, Japan). The mobile phase consisted of 0.5% potassium dihydrogen phosphate (KH₂PO₄, pH 4.5) and acetonitrile (52:48, v/v). The flow rate was 1.0 mL/min and detected at 296 nm using Capcell Pak C18 MG II reversed phase (250 × 4.6 mm i.d., 5 μm) column (Osaka Soda, Tokyo, Japan). A rotary evaporator (CVE-2200) was purchased from Tokyo Rikakikai (Tokyo, Japan).

2.3. Preparation of stock solutions and working solutions

Stock solutions of lazertinib and the IS were prepared in methanol at a concentration of 1 mg/mL. The lazertinib stock solution was diluted further with methanol to obtain working solutions with concentrations of 0.5, 1, 2, 5, 20 and 40 μ g/mL. The IS was diluted with methanol to obtain a working solution of 12.5 μ g/mL.

2.4. Preparation of samples

A 10 µL lazertinib working solution was vortexed with 200 μL plasma for 60 s. Lazertinib-spiked plasma (210 μL), 10 μL of IS and 780 μL of HPLC-grade distilled water were added and vortexed for 30 s. This mixture was applied to an Oasis HLB extraction cartridge that had been activated previously with 1,000 µL methanol and then 1,000 µL distilled water. Following application of the sample, the cartridge was washed with 1,000 μL of distilled water and then 1,000 µL of 60% methanol in distilled water and was eluted with 1,000 µL of 100% acetonitrile. The eluates were dried by vortex-vacuum evaporation at 80°C using a rotary evaporator. The dried residues were reconstituted in 100 µL methanol, and vortexed for 60 s. After mixing well, the samples were sonicated for 60 s and 50 µL aliquots were injected into the HPLC system.

2.5. Selectivity and specificity assessments

Selectivity was evaluated using blank plasma samples from seven healthy volunteers without the addition of lazertinib or IS solution. Minocycline is often administered prophylactically to treat skin disorders, an adverse event of lazertinib, in clinical trials (1). Therefore, we tested the interference by 20 drugs (Table 1) that patients may receive concomitantly with lazertinib. Interference was defined as a retention time within a range of \pm 1 min of the lazertinib and IS retention times.

2.6. Calibration curves and quantitation

Accuracy and linearity were evaluated by analyzing a set of standards ranging from 25 to 2,000 ng/mL. Intraand inter-day precision and accuracy were determined by replicate analyses of five sets of samples spiked with six concentrations of lazertinib (25, 50, 100, 250, 1000, and 2,000 ng/mL) within the same day or on five consecutive days. The precision of the method for each concentration was determined by comparing the coefficient of variation (CV), obtained by calculating the standard deviation (SD) as a percentage of the calculated mean concentration. The limit of quantification (LOQ) was determined as the lowest nonzero concentration in the calibration curves. Methods were validated according to the Bioanalytical Method Validation Guidelines published by the FDA (12).

2.7. Stability studies

The stability of lazertinib was assessed using three different concentrations (25, 250, and 2000 ng/mL) in the evaluations of benchtop, short-term, long-term, freeze-thaw, and post-preparative stability. The bench-top stability samples were kept for 6 h at room temperature (22°C), short-term stability samples were stored at 4°C

for 24 h, long-term stability samples were stored for 4 weeks at -80°C, freeze-thaw samples underwent three cycles of freezing at -80°C or below in a freezer with thawing at room temperature, and post-preparative sample stability was analyzed after 24 h of storage in an autosampler at room temperature.

2.8. Recovery

Extraction recoveries from plasma were determined by comparing the peak height ratios of extracted plasma samples spiked with known amounts of lazertinib according to the above procedure with those of non-extracted quality control samples. Control samples were prepared by mixing solutions containing the same amount of compound that was added to the blank plasma samples; however, this compound was obtained by direct evaporation until dry, rather than by extraction. It was then reconstituted in methanol.

3. Results and Discussion

Table 1. Medications listed for the specificity evaluation

Medication	Retention times
Acetaminophen	< 3 min or none
Amlodipine	3.6 min
Arotinolol	< 3 min or none
Cimetidine	< 3 min or none
Clarithromycin	< 3 min or none
Droperidol	< 3 min or none
Esomeprazole	4.2 min
Fluconazole	< 3 min or none
Furosemide	3.4 min
Gabapentin	< 3 min or none
Isavuconazole	< 3 min or none
Lacosamide	< 3 min or none
Loperamide	< 3 min or none
Metformin	< 3 min or none
Minocycline	< 3 min or none
Nifedipine	11.0 min
Omeprazole	4.2 min
Posaconazole	< 3 min or none
Pregabalin	< 3 min or none
Tedizolid	3.6 min

We developed an HPLC-UV method for the determination of lazertinib concentrations in human plasma that meets the sensitivity and accuracy requirements for performing TDM according to the FDA's analytical validation guidelines. This assay can measure one sample in 8 min and is suitable for performing TDM in a clinical setting. In our method, linear calibration curves for lazertinib were obtained over a range of 25-2,000 ng/mL. In clinical trials, the geometric mean trough plasma concentration of lazertinib was reported to range from 195.0 to 211.4 ng/ mL and was similar in cycles 2 to 13 (14). Additionally, lazertinib has a two-step dose reduction protocol for adverse events, allowing dose adjustments of 160 and 80 mg/d (8). The trough concentrations of lazertinib at 160 and 80 mg/d are approximately 110 and 60 ng/mL, respectively (3). Therefore, the quantitative range of this assay system is appropriate even after the lazertinib dose is reduced and can be applied to TDM in daily clinical practice.

The six-point lazertinib standard calibration curve was expressed as y = 0.0053x + 0.0229 (r² = 0.9997). Table 2 shows the intra- and inter-day CVs and accuracies, with all CVs lying below 8.24%. The intra- and inter-day accuracies ranged from -7.23% to -3.85% and -3.88% to 2.86%, respectively. Solid phase extraction with an Oasis HLB cartridge resulted in a high recovery of > 91.28% (Table 2). The results of stability testing (Table 3) demonstrated quantifiable results for each concentration (25, 250, and 2,000 ng/ mL) under various clinical conditions. Figure 1 shows the chromatograms of blank human plasma samples, 25 ng/mL (LOQ), and 250 ng/mL lazertinib. The retention times of the lazertinib and IS were 7.0 and 4.9 min, respectively. The chromatograms were free of interfering peaks from the biological matrix, and no interfering peaks representing endogenous compounds were observed near the retention times of lazertinib or

In addition, 20 drugs that could be used concomitantly in patients with NSCLC were tested for interference. Eighteen drugs showed no interference. The retention time of esomeprazole and omeprazole

Table 2. Intra- and inter-day precision and accuracy results of lazertinib in human plasma using the proposed high-performance liquid chromatography method (n=5)

Added lazertinib	Intra	a-day $(n=5)$		Inte	r-day (n=5)		
concentration (ng/mL)	Detected (ng/mL) mean ± SD	CV (%)	Accuracy (%)	Detected (ng/mL) mean ± SD	CV (%)	Accuracy (%)	Recovery (%)
25	23.85 ± 1.25	5.24	-4.59	24.03 ± 1.92	7.99	-3.88	98.85
50	48.08 ± 2.80	5.83	-3.85	49.31 ± 2.91	5.90	-1.38	95.44
100	95.38 ± 7.65	8.02	-4.62	102.86 ± 6.33	6.15	2.86	91.28
250	231.92 ± 12.43	5.36	-7.23	256.21 ± 20.78	8.11	2.48	96.61
1000	958.70 ± 56.39	5.88	-4.13	987.24 ± 81.36	8.24	-1.28	99.60
2000	1898.82 ± 91.86	4.84	-5.06	2028.62 ± 166.34	8.20	1.43	98.63

CV, coefficient of variation; SD, standard deviation.

Table 3. Stability analysis

	Ratio of plasma concentration to the spiked value (%)				
Stability test conditions -	25 ng/mL (mean \pm SD)	250 ng/mL (mean \pm SD)	$2,000 \text{ ng/mL}$ (mean \pm SD)		
Benchtop storage (24°C, 6 h)	93.98 ± 3.34	105.06 ± 8.49	100.94 ± 3.72		
Short-term storage (4°C, 24 h)	102.02 ± 7.35	100.75 ± 4.46	100.70 ± 3.05		
Long-term storage (-60°C, 4 weeks)	102.25 ± 9.08	92.44 ± 5.63	97.92 ± 1.61		
Freeze–thaw, three cycles (-60°C to room temperature)	97.43 ± 6.98	94.63 ± 2.87	107.49 ± 9.68		
Post-preparative (24°C, 24 h)	101.05 ± 3.64	100.13 ± 7.63	92.92 ± 2.83		

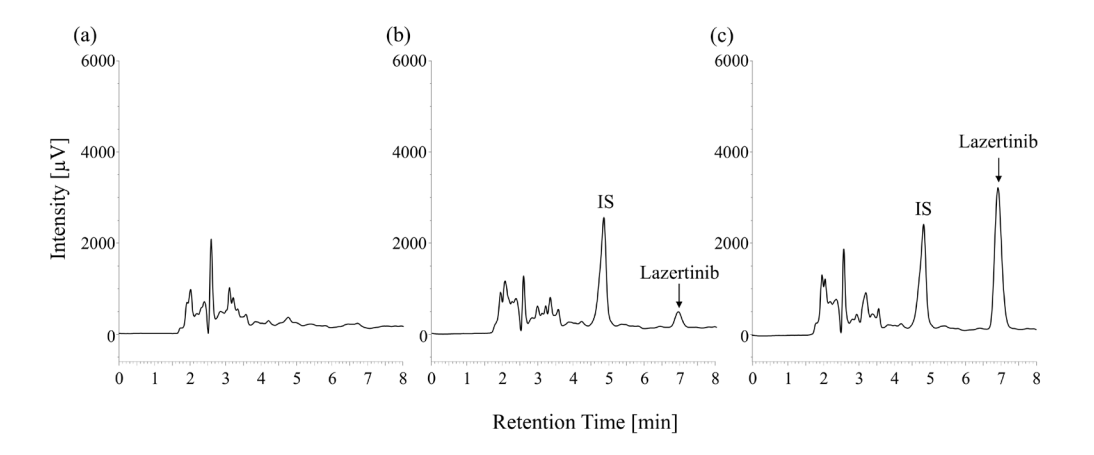


Figure 1. Chromatograms of (a) a blank plasma sample, (b) plasma sample containing lazertinib at 25 ng/mL, and (c) plasma sample containing lazertinib at 250 ng/mL.

was 4.2 min, indicating that they interfered with the IS. The C_{max} values for esomeprazole and omeprazole (both 20 mg/d) were 445 ng/mL and 430 ng/mL (15,16), respectively, with a half-life of ≤ 1 h (17). Assuming a C_{max} of 500 ng/mL for esomeprazole and omeprazole, these drugs were spiked into plasma and analyzed after pretreatment using the present method. The peak heights of both drugs were 1.2- to 1.9-fold higher than that of the IS, indicating that accurately quantifying lazertinib may be difficult when blood samples are collected at C_{max}. In contrast, when the plasma concentration of esomeprazole and omeprazole was set to 125 ng/mL at 3 h post-administration (assuming at least two half-lives had elapsed), their peak heights were 0.32- to 0.35-fold lower than the IS peak height, confirming that lazertinib quantification was not affected. These findings suggest that accurate quantification of lazertinib is feasible when trough blood sampling is performed at least 3 h after administering esomeprazole or omeprazole. Therefore, when performing TDM of lazertinib by trough blood collection, we expect that esomeprazole and omeprazole will be below the detection limit and thus will not affect the quantitation of lazertinib in plasma when taken concurrently with lazertinib. Gefitinib and erlotinib show decreased absorption when co-administered with acid-reducing agents (18); however, lazertinib has no effect on absorption when co-administered with such agents and is not

problematic from a pharmacokinetic perspective (19). Lazertinib should be administered orally with apixaban at a dose of 2.5 mg twice daily for the first 4 months of therapy (7). The trough concentration of apixaban at these doses was 21.0 ng/mL (20). We did not examine the interference with apixaban in this study. However, the low trough concentration of apixaban was difficult to quantify using HPLC-UV and was not expected to affect the quantification of lazertinib using this assay.

This study has several limitations. First, plasma lazertinib concentrations could not be determined in patients treated with lazertinib, as it has only been available on the market for a short period in Japan. Second, patients with NSCLC are often elderly and concomitantly take multiple medications to manage comorbidities and adverse events. Therefore, we could not evaluate the specificity of this method with respect to concomitant medications and their metabolites in patients receiving symptomatic therapy or medications for comorbidities. In the future, specificity should be confirmed using clinical specimens from patients receiving lazertinib.

In conclusion, we developed a novel method for determining lazertinib concentration in human plasma using HPLC-UV. Future studies should determine plasma samples from patients receiving lazertinib treatment and investigate the relationship between plasma concentrations, efficacy, and adverse events.

Acknowledgements

Yoshito Gando is supported by Nagai Memorial Research Scholarship from the Pharmaceutical Society of Japan.

Funding: None.

Conflict of Interest: The authors have no conflicts of interest to disclose.

References

- Cho BC, Lu S, Felip E, et al. Amivantamab plus Lazertinib in Previously Untreated EGFR-Mutated Advanced NSCLC. N Engl J Med. 2024; 391:1486-1498.
- NCCN Guidelines Non-Small Cell Lung Cancer Version 7.2025 https://www.nccn.org/professionals/physician_gls/ pdf/nscl.pdf (accessed July 25, 2025).
- Ahn MJ, Han JY, Lee KH, et al. Lazertinib in patients with EGFR mutation-positive advanced non-smallcell lung cancer: results from the dose escalation and dose expansion parts of a first-in-human, open-label, multicentre, phase 1-2 study. Lancet Oncol. 2019; 20:1681-1690.
- Fiala O, Hosek P, Pesek M, Finek J, Racek J, Stehlik P, Sorejs O, Minarik M, Benesova L, Celer A, Nemcova I, Kucera R, Topolcan O. Serum Concentration of Erlotinib and its Correlation with Outcome and Toxicity in Patients with Advanced-stage NSCLC. Anticancer Res. 2017; 37:6469-6476.
- Zhao YY, Li S, Zhang Y, Zhao HY, Zhao HY, Liao H, Guo Y, Shi YX, Jiang W, Xue C, Zhang L. The relationship between drug exposure and clinical outcomes of nonsmall cell lung cancer patients treated with gefitinib. Med Oncol. 2011; 28:697-702.
- Mueller-Schoell A, Groenland SL, Scherf-Clavel O, van Dyk M, Huisinga W, Michelet R, Jaehde U, Steeghs N, Huitema ADR, Kloft C. Therapeutic drug monitoring of oral targeted antineoplastic drugs. Eur J Clin Pharmacol. 2021; 77:441-464.
- 7. Japanese Ministry of Health, Labour and Welfare, Pharmaceuticals and Medical Devices Agency (PMDA), package insert. https://www.pmda.go.jp/PmdaSearch/iyakuDetail/ResultDataSetPDF/800155_4291091F1027_1 01 (accessed July 25, 2025).
- US Food and Drug Administration (FDA). LAZCLUZE (lazertinib) tablets, for oral use. Prescribing information. https://www.accessdata.fda.gov/drugsatfda_docs/label/2024/219008s000lbl.pdf (accessed July 25, 2025).
- European Medicines Agency (EMA). Lazcluze: Product information. https://www.ema.europa.eu/en/documents/ product-information/lazcluze-epar-product-information_ en.pdf (accessed July 25, 2025).
- 10. Huh KY, Lim Y, Yoon DY, Hwang JG, Sim S, Kang J, Wang J, Kim M, Jang SB, Shreeve SM, Mehta J, Haddish-Berhane N, Oh J, Lee S, Yu KS. Effects of food and race on the pharmacokinetics of lazertinib in healthy subjects

- and patients with EGFR mutation-positive advanced non-small cell lung cancer. Lung Cancer. 2023; 175:112-120.
- Sauvage FL, Gaulier JM, Lachâtre G, Marquet P. Pitfalls and prevention strategies for liquid chromatographytandem mass spectrometry in the selected reactionmonitoring mode for drug analysis. Clin Chem. 2008; 54:1519-1527.
- US DHHS, FDA, CDER, CVM; Guidance for industry: Bioanalytical method validation. US Department of Health and Human Services, Food and Drug Administration, Center for Drug Evaluation and Research and Center for Veterinary Medicine, Rockville, MD, (2018).
- de Langen AJ, Johnson ML, Mazieres J, et al. Sotorasib versus docetaxel for previously treated non-small-cell lung cancer with KRAS^{G12C} mutation: a randomised, openlabel, phase 3 trial. Lancet. 2023; 401:733-746.
- Lee KH, Cho BC, Ahn MJ, et al. Lazertinib versus Gefitinib as First-Line Treatment for EGFR-mutated Locally Advanced or Metastatic NSCLC: LASER301 Korean Subset. Cancer Res Treat. 2024; 56:48-60.
- 15. Choi HG, Jeon JY, Kwak SS, Kim H, Jin C, Im YJ, Kim EY, Wang HM, Kim Y, Lee SY, Kim MG. Pharmacokinetic comparison study of a combination containing 500 mg of Naproxen and 20 mg of Esomeprazole: a randomized, single-dose, 2-way crossover, open-label study in healthy Korean men. Clin Ther. 2015; 37:83-93.
- 16. Hassan-Alin M, Andersson T, Niazi M, Röhss K. A pharmacokinetic study comparing single and repeated oral doses of 20 mg and 40 mg omeprazole and its two optical isomers, S-omeprazole (esomeprazole) and R-omeprazole, in healthy subjects. Eur J Clin Pharmacol. 2005; 60:779-784.
- 17. Budha NR, Frymoyer A, Smelick GS, Jin JY, Yago MR, Dresser MJ, Holden SN, Benet LZ, Ware JA. Drug absorption interactions between oral targeted anticancer agents and PPIs: is pH-dependent solubility the Achilles heel of targeted therapy? Clin Pharmacol Ther. 2012; 92:203-213.
- 18. Kim B, Lee J, Jang H, Lee N, Mehta J, Jang SB. Effects of Acid-Reducing Agents on the Pharmacokinetics of Lazertinib in Patients with EGFR Mutation-Positive Advanced Non-Small-Cell Lung Cancer. Adv Ther. 2022; 39:4757-4771.
- Byon W, Garonzik S, Boyd RA, Frost CE. Apixaban: A Clinical Pharmacokinetic and Pharmacodynamic Review. Clin Pharmacokinet. 2019; 58:1265-1279.

Received July 25, 2025; Revised October 9, 2025; Accepted October 13, 2025.

*Address correspondence to:

Takeo Yasu, Department of Medicinal Therapy Research, Education and Research Unit for Comprehensive Clinical Pharmacy, Meiji Pharmaceutical University, 2-522-1, Noshio, Kiyose, Tokyo 204-8588, Japan.

E-mail: yasutakeo-tky@umin.ac.jp

Released online in J-STAGE as advance publication October 17, 2025.

Brief Report

DOI: 10.5582/ddt.2025.01070

Tapeworm infection incidence in rural Japan points to a common environmental source of infection

Dhammika Leshan Wannigama^{1-7,§,*}, Mohan Amarasiri^{2,8,§}, Phatthranit Phattharapornjaroen^{2,9,10}, Cameron Hurst^{2,11,12}, Yu Suzuki¹³, Daisuke Akaneya¹³, Mika Moriya¹³, Taichi Adachi¹³, Yoshikazu Okuma¹⁴, Daisuke Ishizawa¹⁴, Hitoshi Ishikawa^{2,3}, Kazuhiko Miyanaga¹⁵, Longzhu Cui¹⁵, Kazunori Moriya^{1,2}, Hirotake Mori¹⁶, Naveen Kumar Devanga Ragupathi^{6,17}, Yoshitaka Shimotai⁴, Daisuke Sano^{8,18}, Takashi Furukawa¹⁹, Kazunari Sei¹⁹, Talerngsak Kanjanabuch²⁰⁻²³, Paul G. Higgins²⁴⁻²⁶, Tetsuji Aoyagi²⁷, Anthony Kicic²⁸⁻³¹, Sam Trowsdale³², Parichart Hongsing^{2,4}, Aisha Khatib³³, Kenji Shibuya³⁴, Shuichi Abe^{1,2,*}, Hiroshi Hamamoto^{4,*}

¹ Department of Infectious Diseases and Infection Control, Yamagata Prefectural Central Hospital, Yamagata, Japan;

² Pathogen Hunter's Research Collaborative Team, Department of Infectious Diseases and Infection Control, Yamagata Prefectural Central Hospital, Yamagata, Japan;

³ Yamagata Prefectural University of Health Sciences, Yamagata, Japan;

⁴Department of Infectious Diseases, Faculty of Medicine, Yamagata University, Yamagata, Japan;

⁵ School of Medicine, Faculty of Health and Medical Sciences, The University of Western Australia, Nedlands, Western Australia, Australia;

⁶Biofilms and Antimicrobial Resistance Consortium of ODA receiving countries, The University of Sheffield, Sheffield, United Kingdom;

⁷The Lygodium Ceylon Health and Environmental Policy Research Center, Colombo, Sri Lanka;

⁸ Department of Civil and Environmental Engineering, Graduate School of Engineering, Tohoku University, Sendai, Miyagi, Japan;

⁹ Faculty of Health Science Technology, Chulabhorn Royal Academy, Bangkok, Thailand;

¹⁰ HRH Princess Chulabhorn Disaster and Emergency Medicine Center, Chulabhorn Royal Academy, Bangkok, Thailand;

¹¹ Center of Excellence in Applied Epidemiology, Thammasat University, Rangsit, Thailand;

¹² Department of Clinical Epidemiology, Faculty of Medicine, Thammasat University, Rangsit, Thailand;

¹³ Department of Clinical Laboratory, Yamagata Prefectural Central Hospital, Yamagata, Japan;

¹⁴ Department of Pharmacy, Yamagata Prefectural Central Hospital, Yamagata, Japan;

¹⁵Division of Bacteriology, School of Medicine, Jichi Medical University, Tochigi, Japan;

¹⁶ Department of General Medicine, Juntendo University Faculty of Medicine, Tokyo, Japan;

¹⁷ Division of Microbial Interactions, Department of Research and Development, Bioberrys Healthcare and Research Centre, Vellore, India;

¹⁸ Department of Frontier Sciences for Advanced Environment, Graduate School of Environmental Studies, Tohoku University, Sendai, Miyagi, Japan;

¹⁹ Laboratory of Environmental Hygiene, Department of Health Science, School of Allied Health Sciences, Kitasato University, Sagamihara-Minami, Kanagawa, Japan;

²⁰ Division of Nephrology, Department of Medicine, Faculty of Medicine, Chulalongkorn University, Bangkok, Thailand;

²¹ Center of Excellence in Kidney Metabolic Disorders, Faculty of Medicine, Chulalongkorn University, Bangkok, Thailand;

²² Dialysis Policy and Practice Program (DiP3), School of Global Health, Faculty of Medicine, Chulalongkorn University, Bangkok, Thailand;

²³ Peritoneal Dialysis Excellence Center, King Chulalongkorn Memorial Hospital, Bangkok, Thailand;

²⁴ Institute for Medical Microbiology, Immunology and Hygiene, Faculty of Medicine and University Hospital Cologne, University of Cologne, Cologne, Germany;

²⁵ German Centre for Infection Research, Partner site Bonn-Cologne, Cologne, Germany;

²⁶Center for Molecular Medicine Cologne, University of Cologne, Faculty of Medicine and University Hospital Cologne, Cologne, Germany;

²⁷ Department of Infectious Diseases, Internal Medicine, Tohoku University Graduate School of Medicine, Miyagi, Japan;

²⁸ Wal-Yan Respiratory Research Centre, Telethon Kids Institute, University of Western Australia, Nedlands, Western Australia;

²⁹ Centre for Cell Therapy and Regenerative Medicine, Medical School, The University of Western Australia, Nedlands, Western Australia;

³⁰ Department of Respiratory and Sleep Medicine, Perth Children's Hospital, Nedlands, Western Australia, Australia;

³¹ School of Population Health, Curtin University, Bentley, Western Australia, Australia;

³² School of Environment, University of Auckland, Auckland, New Zealand;

³³ Department of Family & Community Medicine, University of Toronto, Toronto, ON, Canada;

³⁴ Tokyo Foundation for Policy Research, Tokyo, Japan.

SUMMARY: Dibothriocephalus nihonkaiensis is a zoonotic tapeworm transmitted to humans through consumption of raw or undercooked fish or wild meat. Between 2022 and 2023, Yamagata Prefecture reported an increase in cases compared with 2017–2021, when none were observed. We conducted a clinical and environmental investigation to clarify infection sources. Four confirmed and one suspected patient were identified, all presenting with gastrointestinal symptoms. Exposures were linked to raw cherry salmon (Oncorhynchus masou) in three cases and undercooked bear meat in one case. Praziquantel treatment (10–20 mg/kg) was effective, with eight worms (76–210 cm) recovered. Environmental surveillance detected D. nihonkaiensis in 33.3% of bear feces (20/60) and 21.8% of wild fish samples (17/78). Phylogenetic analysis showed close genetic relatedness among human, bear, and fish isolates, indicating a shared transmission cycle. These findings confirm zoonotic transmission of D. nihonkaiensis in Yamagata and highlight the need for food safety awareness and environmental monitoring.

Keywords: Tapeworm infection, rural Japan, Dibothriocephalus nihonkaiensis, environmental source of infection

1. Introduction

Tapeworms, belonging to the class Cestoda, are complex parasitic flatworms with a life cycle involving intermediary hosts, frequently found in aquatic ecosystems (1,2). The consumption of raw or undercooked fish has long been recognized as a potential source of tapeworm infections, owing to the transmission of larval stages such as *Dibothriocephalus* spp. to humans (1,2). Japan's rich culinary heritage has long celebrated the art of sushi and sashimi, where the consumption of raw fish is a revered tradition (1). However, epidemiological data reveals a significant risk of tapeworm infections, and the primary source of *Dibothriocephalus* spp. infections in Japan are linked to the consumption of raw salmonids, particularly cherry salmon and immature chum salmon (1,2).

From the summer of 2022 to the spring of 2023, Yamagata Prefecture Central Hospital showed an increase in tapeworm cases compared to 2017-2021, when there were no reported cases. All cases are suspected to be associated with consuming raw or undercooked wild fish or bear meat. As part of an infection control strategy, an infection source tracking study was done, the results of which are described in this paper.

2. Methods

2.1. Environmental sample collection

Based on patients' epidemiological data, we conducted an environmental surveillance study in Yamagata Prefecture by collecting fecal samples from black bears living in wild forests and raw meat from wild fish in Yamagata rivers. In collaboration with hikers and recreational fishermen, a total of 60 bear fecal samples and 78 raw meat samples from wild fish were collected. Specimens were collected in 50-mL conical sampling tubes before immediate storage at -20°C. Samples were transferred to -80°C within one day of collection, where they were stored for up to 1 month.

2.2. Human sample collection

An adult worm of *D. nihonkaiensis* was isolated from an infected patient, and proglottids were recovered from the stool after treatment with praziquantel followed by a purge with MgSO₄ solution.

2.3. DNA extraction

A single proglottid was finely chopped and put in the tissue lysis buffer of the DNA extraction kit. Total genomic DNA was extracted using a DNeasy tissue Kit, Qiagen (Germany) according to the manufacturer's instructions. Protocols for bear fecal and wild fish sample processing and extraction were adapted from previously published procedures (1,2). Between 10-20 mg of sample (fecal sample/chopped proglottid) was added to a 2-mL screw cap tube with a rubber O-ring (Corning, USA). Next, 1,200 µL of PowerProtect DNA/ RNA (Qiagen, Germany) and 0.5 g silica zirconia beads (BioSpec, Singapore) were added, and the samples were homogenized using a BioSpec bead beater (BioSpec, Singapore). Between 100-200 µL of supernatant was filtered through a Centricon® Plus-70 centrifugal ultrafilters (100 kDa cut off; Merck Millipore, USA) via centrifugation at 1,500×g for 15 minutes at 4°C, with a resulting concentrate ranging between 2.11-4.13 g. To quantify DNA concentration, 1 mL of well-mixed Centricon® (Merck Millipore, USA) concentrates were added directly to a commercial kit optimized for isolation of total DNA from environmental samples according to the manufacturer's protocol (DNeasy tissue Kit, Qiagen, Germany) (3). Two replicate DNA extractions and analyses were performed for each sample. Isolated DNA pellets were dissolved in 50 µL of deoxyribonuclease-free water, and total DNA was measured by spectrophotometry (NanoDrop, Thermo Fisher Scientific) as previously described (3).

2.4. Molecular identification by real-time qPCR

D. nihonkaiensis cytochrome c oxidase subunit 1 (cox1) genes DNA was quantified by one-step qPCR using the primers previously described (Sequence $(5'\rightarrow 3')$ forward CTTTGTTGTCTGGCCTTCCT, and reverse ATGATAAGGGAYAGGRGCYCA) (2). The specificity of these primer/probe sets had been confirmed by others (2). Samples were analyzed using the Bio-Rad iTaq Universal SYBR Green One-Step Kit (Bio-Rad, USA) in 20-μL reactions run at 50°C for 10 min and 95°C for 1 min, followed by 40 cycles of 95°C for 10s and 60°C for 30 s per the manufacturer's recommendations. D. nihonkaiensis DNA concentrations were determined using a standard curve as previously described and presented as parasite DNA copies. For the generation of the standard curve, six 10-fold serially diluted positive control DNAs of *cox1* gene (concentration range, 5.0 $\times 10^{5}$ –5.0 $\times 10^{0}$ copies/2.5 μ L) were included in each qPCR run to obtain a standard curve. The primer set generated a standard curve with an efficiency of 97.8% and R^2 of 0.971. Threshold cycle (Ct) values above 40 were considered negative for cox1 gene.

2.5. Sequence and phylogenetic analyses

Sequences of a partial fragment of the cox1 gene were used for genetic analysis because of the numerous available sequences from the definitive and fish intermediate host species, and because of its usefulness for genetic differentiation of D. nihonkaiensis (2). A portion of the cox1 gene (approximately 710 bp) was amplified using the primer set: forward (5'-TTG ATC GTAAAT TTG GTT C-3'); reverse (5' -AAA GAA CCT ATT GAA CAA AG-3') (2). PCR amplification was performed in a volume of 25 µL using TaKaRa EX Taq Hot Start Version containing 10 PCR buffer, 20 mM MgCl₂, 2.5 mM of each dNTP, 5 units/μL of Takara Ex Taq HS DNA polymerase (TaKaRa Shuzo Co. Ltd., Shiga, Japan), 0.5 μM of each primer, and 2.5 μL of DNA sample. After denaturation at 94°C for 5 min, amplification was carried out by 35 cycles consisting of denaturation at 94°C for 30 s, annealing at 52°C for 30 s, and elongation at 72°C for 1 min, followed by a final extension step at 72°C for 7 min. Reactions were performed in a thermocycler (GeneAmp PCR System 9700 or 2720; Applied Biosystems, USA). Aliquots of the PCR products were separated by electrophoresis on a 3% agarose gel and were visualized under UV light after staining with ethidium bromide. The PCR products were purified using either the QIAquick Gel Extraction Kit or the QIAquick PCR Puri cation Kit (Qiagen Inc., Germany), and DNA sequencing was performed on an automated sequencer (ABI3130; Applied Biosystems, USA) using a BigDye Terminator v3.1 Cycle Sequencing kit with the primer sets used in the PCR. Sequence chromatograms from each strand were inspected using Sequencher DNA Sequence Analysis Software Version 4.1 (Gene Codes Corp., USA). Sequence alignment

was done using MEGA-11 Software. Best DNA models for maximum likelihood estimation were identified and phylogenetic trees were constructed (Hasegawa-Kishino-Yano Model with uniform rates among sites) with 1000 bootstrap replications (4,5). A discrete Gamma distribution was used to model evolutionary rate differences among sites (5 categories (+G, parameter = 0.1000)).

2.6. Data visualization

Data were analyzed and plotted using the ggplot 23.3.5, packages of R program version 4.1.0(6).

3. Results and Discussion

Between 2022 and 2023, four cases of D. nihonkaiensis infection were identified, along with one suspected case, affecting individuals aged 13 to 54 (Table 1). All patients reported intermittent gastrointestinal symptoms such as stomach pain, constipation, gas, nausea, or loose stools (Table 1). The infections were linked to the consumption of raw or undercooked wild fish (Cherry salmon, Oncorhynchus masou) in three cases, with one case also involving undercooked bear meat. The patients who consumed undercooked bear meat had no history of consuming raw or undercooked cherry salmon (O. masou) in the past five years. The patient, an avid wildlife hunter, reported occasionally cleaning bear carcasses in the wild after hunts. It is therefore plausible that exposure during the handling of bear meat and gastrointestinal contents contributed to contamination with tapeworm eggs. Microscopic examination confirmed the presence of tapeworm eggs (ova) in three cases, and PCR testing identified D. nihonkaiensis in all four. The suspected case had a history of sharing food with a domesticated cat (the cat has a previous history of Tapeworm infection, according to the patient). However, the suspected case refused to provide a faecal sample and declined any treatment. None of the patients had any underlying diseases or medical conditions.

Treatment with praziquantel, administered at doses of 10–20 mg/kg as a single dose, was effective in all treated cases. Following treatment, three patients excreted tapeworms measuring between 76 cm and 210 cm in length, with a total of eight worms excreted. The fourth patient did not provide any excreted worms for examination. Follow-up at three months showed no complications and negative faecal tests for eggs in all patients.

Environmental surveillance revealed that *D. nihonkaiensis* positive samples were spread across the region, with bear feces and Cherry salmon (*O. masou*) fish samples testing positive for *D. nihonkaiensis* in multiple areas of the prefecture (Figure 1a). Overall, 33.3% of bear faecal samples and 21.8% of wild fish meat samples (Cherry salmon, *O. masou*) tested positive

Fable 1. Demographics and clinical details of *D. nihonkaiensis* cases between Winter 2022 and Spring 2023

Human sample	Age	Sex	Microscopic Tapeworm/ identification for eggs proglottids in feces		PCR identification	Initial symptoms	Exposure history	Treatment	3-month follow-up
H3902980 13		Male	Postive	∞	D. nihonkaiensis	Intermittent stomach ache or stomach pain, upset stomach, nausea, weight loss.	Intermittent stomach ache or Eating raw fish (Cherry salmon, Praziquantel 20mg/kg Fecal negative for stomach pain, upset stomach, Oncorhynchus masou) one year ago single dose eggs/no complication nausea, weight loss.	Praziquantel 20mg/kg single dose	Fecal negative for eggs/no complication
H3902981	45	Male	Positive	2	D. nihonkaiensis	Intermittent stomach ache or stomach pain, gas.	Intermittent stomach ache or Eating cooked bear meat, and raw fish Praziquantel 10mg/kg Fecal negative for stomach pain, gas. (Cherry salmon, Oncorhynchus masou) single dose eggs/no complication six months ago	Praziquantel 10mg/kg single dose	Fecal negative for eggs/no complication
H3902982	54	Male	Postive	2	D. nihonkaiensis	Intermittent stomach ache or stomach pain, gas.	Intermittent stomach ache or Eating raw fish(Cherry salmon, Praziquantel 10mg/kg Fecal negative for stomach pain, gas. Oncorhynchus masou) regularly single dose eggs/no complication	Praziquantel 10mg/kg single dose	Fecal negative for eggs/no complication
H3902983	53	Female			D. nihonkaiensis	Loose stools	Eating raw fish (Cherry salmon, Praziquantel 10mg/kg Fecal negative for Oncorhynchus masou) regularly single dose eggs/no complication	Praziquantel 10mg/kg single dose	Fecal negative for eggs/no complication

for *D. nihonkaiensis* (Figure 1b). The phylogenetic analysis of *D. nihonkaiensis* samples from human, bear feces, and fish revealed close genetic relationships, indicating a shared transmission cycle among these hosts (Figure 1c). Samples from bears, fish, and humans clustered into distinct but closely related groups, suggesting minimal genetic divergence within the local tapeworm population.

The observed increase in D. nihonkaiensis cases between winter 2022 and spring 2023, coupled with the environmental samples (Cherry salmon, O. masou) testing positive during this period, suggests a potential rise in the risk of human infection. This temporal correlation highlights a significant aspect of epidemiology, where environmental conditions and biological activity may influence infection rates (1,2). The heightened environmental presence of D. nihonkaiensis in bear and wild Cherry salmon (O. masou) samples during these months could indicate a seasonal factor, which would mean climate change will contribute to increased human exposure. Given the seasonal migration patterns of cherry salmon in spring and the availability of immature chum salmon during summer months in northern Japan, these periods may represent peak risk windows for D. nihonkaiensis transmission.

The genetic analysis revealing close relationships between D. nihonkaiensis strains from human, wild fish (Cherry salmon, O. masou), and bear sources supports the hypothesis of a shared environmental source of infection (7). This genetic proximity indicates that contamination in the food chain, particularly through raw or undercooked wild fish, is a critical pathway for transmission to humans (1,2,7). The linkage between bear and wild fish Cherry salmon (O. masou) reservoirs with human cases underscores the need for targeted public health interventions focusing on these key reservoirs (8). Based on our findings, we also hypothesize that the natural host of D. nihonkaiensis maybe bear (and potentially other terrestrial animals), with wild fish Cherry salmon (O. masou) becoming contaminated through exposure to feces from infected hosts. In forested freshwater ecosystems, bears frequently defecate near riverbanks, shedding eggs or proglottids of zoonotic parasites such as Dibothriocephalus spp., the causative agents of diphyllobothriasis (fish tapeworm infection). These feces contaminate the surrounding environment and can attract coprophagous and saprophagous flies. Flies, acting as mechanical vectors, may carry parasite eggs to aquatic habitats or directly contaminate the insect populations residing in or near the river, including chironomids, mayflies, and stoneflies. Juvenile cherry salmon (O. masou), which remain in upstream freshwater zones for one to three years before their seaward migration, feed heavily on these aquatic and airborne insects (9,10). This feeding behavior creates a route for the salmon to become intermediate or paratenic hosts of

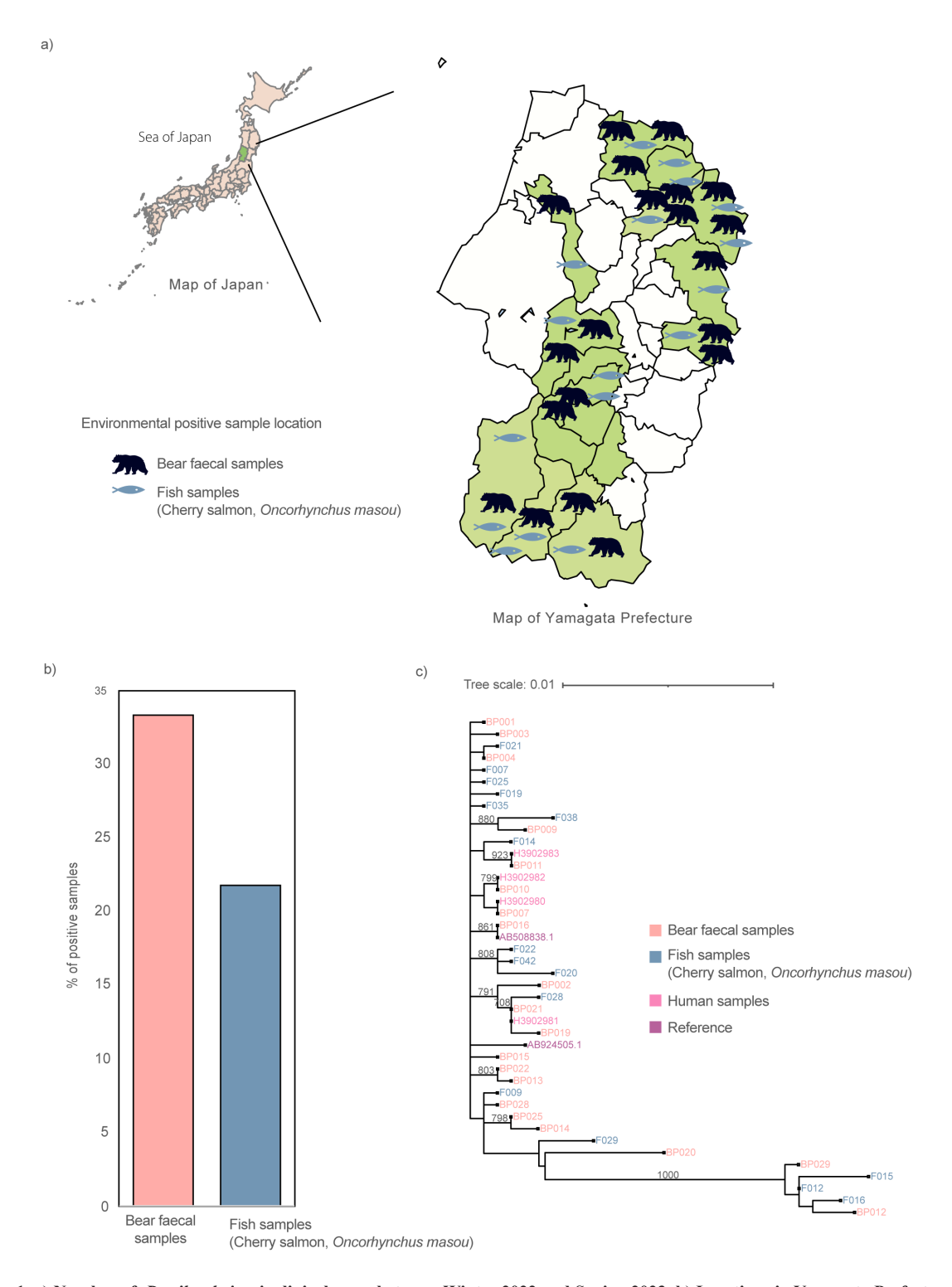


Figure 1. a) Number of *D. nihonkaiensis* clinical cases between Winter 2022 and Spring 2023, b) Locations in Yamagata Prefecture, with bear faecal and fish samples testing positive for *D. nihonkaiensis*, c) Percentage of bear faecal and wild fish meat samples tested positive for *D. nihonkaiensis*, d) The phylogenetic analysis of *D. nihonkaiensis* samples from human, bear feces, and fish (Cherry salmon, *O. masou*).

zoonotic tapeworm larvae, especially in areas where the parasite life cycle includes copepods or insect larvae as intermediate hosts (10). Transmission among bears may occur through their dietary habits, which include the consumption of plants and fish that have been exposed to parasitic contamination via faecal matter.

Additionally, studies and data from the Japan

Meteorological Agency confirm a consistent rise in both sea surface and river water temperatures around Japan, including in Yamagata Prefecture, over the past decade (11). Notably, the shortening of winter seasons, likely driven by rising regional temperatures, has significant implications for the behavior of black bears. Warmer and shorter winters delay the onset of hibernation and shorten

hibernation duration, resulting in increased roaming activity by bears in search of food. This behavioral shift extends the window during which bears defecate in the environment, depositing tapeworm eggs near rivers and streams and sustaining environmental contamination for longer periods.

Yamagata is historically known for its association with the Matagi, a traditional group of indigenous mountain hunters skilled in sustainable bear hunting (12). Bear meat remains a culturally valued food in the region, and it is often consumed in rural communities. Moreover, in Japan, people usually do not consume raw freshwater fish, following ancient wisdom that such fish are likely contaminated with parasites, including tapeworms. However, Cherry salmon (O. masou) are exceptions and are eaten raw. This aligns with the human infections in this study, as all three cases involved individuals who consumed raw or undercooked Cherry salmon (O. masou) which is abundant in Yamagata's rivers (13).

Given the correlation between human cases and the seasonal increase in positive environmental samples, public health efforts should prioritize education on the risks associated with consuming raw or undercooked fish (7,8). This is especially pertinent in regions where D. nihonkaiensis is known to be prevalent (1,2,14,15). Increasing awareness about safe food handling and preparation practices could help mitigate the risk of infection (1,2,14). Interestingly, in Japan, praziquantel is not recommended for tapeworm infections in medical guidelines and insurance reimbursements, but worldwide, it is a first-line drug for cestodes (14-16). However, the Parasitology Society of Japan recommended the use of praziquantel in its recommendations. Praziquantel is considered to be a clinically effective treatment for cestodoses, has a low burden on patients, and can be safely administered on an outpatient basis (15,16). This discrepancy in its use between Japan and the global medical community raises questions about local clinical practices and treatment guidelines (17). The variation could stem from differences in parasite strains, treatment preferences, or regulatory policies. Nevertheless, its broad efficacy, low side effects, and ease of administration have made it a staple in the management of parasitic infections in most countries (14-16). Further research may help clarify whether alternative treatments are more appropriate in specific regions or whether praziquantel's widespread acceptance should extend to areas where it is not currently recommended.

Importantly, our study does not imply that all bears, fish, or river water are inherently contaminated or dangerous; rather, it highlights that parasites like *D. nihonkaiensis* are naturally present in the environment. The recent increase in infections likely reflects the combined influence of changing climate conditions and human behaviors such as consuming raw wild meat or fish on the dynamics of parasite transmission. With appropriate hygiene practices, food safety awareness,

and ecological understanding, such zoonotic risks can be effectively mitigated without vilifying wildlife or natural ecosystems. We acknowledge, however, that our findings are based on a small number of confirmed cases and suspected case, all restricted to Yamagata Prefecture. This limited sample size may introduce randomness in the interpretation of clinical symptoms and infection routes, and the results should therefore be interpreted with caution when extrapolating to other regions of Japan where dietary habits and ecological contexts may differ. Additionally, while our seasonal risk hypothesis is supported by the clustering of cases between winter 2022 and spring 2023, we did not have access to long-term environmental surveillance data (e.g., parasite detection from 2017-2021 or host distribution records from earlier years). Thus, we cannot yet determine whether this increase reflects a long-term trend in transmission dynamics or an isolated event.

In summary, the results underscore the importance of integrating environmental surveillance data with human infection trends to better understand and manage the risk of parasitic diseases. Public health strategies should be adapted to address seasonal, environmental, and climate change factors, focusing on preferred treatment in Japan alongside reducing exposure to contaminated food sources and enhancing community education about the risks.

Acknowledgements

We thank all the volunteers who kindly supported the sample collection and all the patients. We, the authors of this paper, embrace inclusive, diverse, and equitable conduct of research. Our team comprises individuals who self-identify as underrepresented ethnic minorities, gender minorities, members of the LGBTQIA+community, and individuals living with disabilities. We actively promote gender balance in our reference list while maintaining scientific relevance.

Funding: Dhammika Leshan Wannigama was supported by Balvi Filantropic Fund and Japan Society for the Promotion of Science (JSPS), University of Western Australia (Overseas Research Experience Fellowship) and Yamagata Prefectural Central Hospital, Yamagata, Japan (Clinical Residency Fellowship). Anthony Kicic is a Rothwell Family Fellow. The funder(s) had no role in study design; in the collection, analysis, and interpretation of data; in the writing of the report; or in the decision to submit the article for publication.

Conflict of Interest: The authors declare that they have no known potential conflict of interest or competing financial or non-financial interest in relation to the manuscript.

Ethical approval: This study was conducted in

accordance with the principles of the Declaration of Helsinki, Good Clinical Practice guidelines, and other applicable laws and regulations, including STROBE guidelines. The study is part of the emerging infectious disease surveillance study and was reviewed and approved by the institutional review board at Yamagata Prefectural Central Hospital, Yamagata, Japan (XO-08/2022).

Informed consent: All volunteers or their legally acceptable representatives provided written informed consent.

References

- Ikuno H, Akao S, Yamasaki H. Epidemiology of Diphyllobothrium nihonkaiense Diphyllobothriasis, Japan, 2001-2016. Emerg Infect Dis. 2018; 24:1428-1434.
- 2. Abe N, Baba T, Nakamura Y, Murakami S. Global analysis of cytochrome c oxidase subunit 1 (cox1) gene variation in *Dibothriocephalus nihonkaiensis* (Cestoda: Diphyllobothriidae). Curr Res Parasitol Vector Borne Dis. 2021; 1:100042.
- Peccia J, Zulli A, Brackney DE, Grubaugh ND, Kaplan EH, Casanovas-Massana A, Ko AI, Malik AA, Wang D, Wang M, Warren JL, Weinberger DM, Arnold W, Omer SB. Measurement of SARS-CoV-2 RNA in wastewater tracks community infection dynamics. Nat Biotechnol. 2020; 38:1164-1167.
- Kumar S, Stecher G, Li M, Knyaz C, Tamura K. MEGA X: Molecular evolutionary genetics analysis across computing platforms. Mol Biol Evol. 2018; 35:1547-1549.
- 5. Tamura K, Stecher G, Kumar S. MEGA11: Molecular evolutionary genetics analysis version 11. Mol Biol Evol. 2021; 38:3022-3027.
- Team RC. R: A Language and Environment for Statistical Computing. R Foundation for Statistical Computing, Vienna, Austria. 2021.
- Scholz T, Kuchta R, Oros M. Tapeworms as pathogens of fish: A review. J Fish Dis. 2021; 44:1883-1900.
- 8. Scholz T, Kuchta R, Brabec J. Broad tapeworms (Diphyllobothriidae), parasites of wildlife and humans: Recent progress and future challenges. Int J Parasitol Parasites Wildl. 2019; 9:359-369.
- Christensen KA, Flores AM, Joshi J, Shibata K, Fujimoto T, Koop BF, Devlin RH. Masu salmon species complex relationships and sex chromosomes revealed from analyses

- of the masu salmon (*Oncorhynchus masou masou*) genome assembly. G3 (Bethesda). 2025; 15:jkae278.
- Malyutina AM, Savvaitova KA, Kuzishchin KV, Gruzdeva MA, Pavlov DS. Population structure of the masu salmon Oncorhynchus masou from the Kol River (Western Kamchatka) and geographic variation in the species area. J Ichthyol. 2009; 49:390-402.
- Mori N, Takemi T, Tachikawa Y, Tatano H, Shimura T, Tanaka T, Fujimi T, Osakada Y, Webb A, Nakakita E. Recent nationwide climate change impact assessments of natural hazards in Japan and East Asia. Weather Clim Extrem. 2021; 32:100309.
- 12. Ikeya K. Ethnoarchaeology of Introducing Agriculture and Social Continuity among Sedentarised Hunter–Gatherers: The Transition from the Jomon to the Yayoi Period. In: Quaternary (2021).
- Club TFFC. Cherry Salmon Yamame or Sakura Masu. 2023.
- 14. Ladzekpo D, Kwofie KD, Kawada H, Mikami F, Tsuji N, Iwanaga S, Dadzie SK, Hatta T, Ishino T. A possible circulation of a dominant *Dibothriocephalus* nihonkaiensis haplotype in Japan revealed by molecular analysis of clinical tapeworm samples. Parasitol Int. 2023; 96:102771.
- Tsang HF, Leung SWM, Hung TN, Law I, Lam KW, Chan L, Wong SCC. Molecular identification of *Dibothriocephalus nihonkaiense* infection using nanopore sequencing: A case report and literature review. Diagnostics (Basel). 2024; 14:2871.
- Nguyen David C, Desai Ankita P, Cherian Sree S. The brief case: the boy who cried worm. J Clin Microbiol. 2023; 61:e00553-00522.
- 17. Ohnishi K, Kato Y. Single low-dose treatment with praziquantel for *Diphyllobothrium nihonkaiense* infections. Intern Med. 2003; 42:41-43.

Received July 16, 2025; Revised September 23, 2025; Accepted October 6, 2025.

Dhammika Leshan Wannigama, Shuichi Abe, and Hiroshi Hamamoto, Department of Infectious Diseases, Faculty of Medicine, Yamagata University, Yamagata, Japan.

E-mail: leshanwannigama@med.id.yamagata-u.ac.jp (DLW), abeshu@icloud.com (SA), hamamoto@med.id.yamagata-u.ac.jp (HH)

Released online in J-STAGE as advance publication October 16, 2025.

[§]These authors contributed equally to this work.

^{*}Address correspondence to:

Correspondence

DOI: 10.5582/ddt.2025.01109

Paltusotine: The first selective nonpeptide agonist of somatostatin receptor 2 (SSTR2) for the treatment of acromegaly

Yueyi Sun, Daoran Lu, Jianjun Gao*

Department of Pharmacology, School of Pharmacy, Qingdao University, Qingdao, Shandong, China.

SUMMARY: Acromegaly is an endocrine disorder characterized by abnormal enlargement of the extremities and internal organs resulting from excessive secretion of growth hormone (GH) by the pituitary gland, which in turn leads to elevated levels of insulin-like growth factor 1 (IGF-1). Approximately 45% of patients remain biochemically uncontrolled after surgery and require long-term treatment with injectable somatostatin analogs such as octreotide or lanreotide. These polypeptide drugs generally require monthly administration to maintain disease control; however, many patients experience recurrence of symptoms towards the end of the dosing interval. Moreover, injection-site pain and local reactions are common, significantly impacting patients' quality of life. On September 25, 2025, the U.S. Food and Drug Administration (FDA) approved paltusotine, the first once-daily oral, nonpeptide somatostatin receptor 2 (SSTR2) agonist for the treatment of acromegaly. By enabling oral rather than injectable therapy, paltusotine reduces the treatment burden and enhances patient adherence. With its rapid onset and durable biochemical control, this novel agent has the potential to reshape the current paradigm of acromegaly pharmacotherapy and offer patients a more convenient and effective treatment option. Nevertheless, its long-term safety and efficacy warrant further evaluation in real-world clinical settings.

Keywords: acromegaly, GH, IGF-1, SRLs

Acromegaly is a rare, chronic endocrine disorder primarily caused by excessive secretion of growth hormone (GH) from pituitary adenomas, which in turn stimulates hepatic overproduction of insulin-like growth factor 1 (IGF-1) (*I*). Sustained exposure to elevated levels of GH and IGF-1 leads to a wide range of systemic complications — including cardiovascular, musculoskeletal, respiratory, and endocrine abnormalities, as well as an increased risk of malignancies — thereby imposing a substantial clinical burden, impairing quality of life, and reducing overall survival (2,3).

The primary treatment modalities for acromegaly include pituitary surgery, pharmacotherapy, and radiotherapy (4). Transsphenoidal resection of the GH-secreting pituitary adenoma remains the first-line approach (5); however, adequate disease control is not achieved in approximately 45% of patients following surgery (6). These patients receive medical therapies such as somatostatin receptor ligands (SRLs), dopamine agonists (DAs), and growth hormone receptor antagonists (GHRAs) (7). SRLs — including octreotide and lanreotide — are currently the first-line pharmacological options targeting somatostatin receptors (SSTRs). Nevertheless, the requirement for regular monthly injections places a considerable burden on patients (8). Consequently, developing a convenient, non-injectable formulation is

essential to enhancing treatment adherence and improving quality of life.

On September 25, 2025, the U.S. Food and Drug Administration (FDA) approved paltusotine, the first oncedaily oral nonpeptide SSTR2 agonist for the treatment of acromegaly (9,10). Its mechanism of action resembles that of the natural hormone somatostatin but the medication exhibits higher selectivity for SSTR2 with little or no affinity for other SSTR subtypes. Paltusotine activates human SSTR2 to suppress cyclic AMP accumulation, with a mean half-maximal effective concentration (EC₅₀) of 0.25 nM (11). Paltusotine's advantage lies in its ability to meet patients' expectations for a convenient, oncedaily oral therapy, thereby filling an unmet need in the current treatment landscape. It not only eliminates the inconvenience and injection-related complications associated with parenteral administration but also alleviates the negative impact on patients' quality of life. Moreover, the oral formulation allows for more flexible dose adjustments, as paltusotine reaches steady-state concentrations within 3-5 days. In contrast, long-acting somatostatin receptor ligands administered by monthly injection typically require at least three doses before dose optimization can be evaluated and steady-state levels achieved (12).

The approval was based on two randomized, double-

blind, parallel-group, placebo-controlled clinical studies: PATHFNDR-1 (NCT05192382) and PATHFNDR-2 (NCT04837040), which assessed the safety and efficacy of paltusotine in adults with acromegaly whose biochemical parameters were either uncontrolled or controlled at the baseline. Results indicated that paltusotine rapidly, durably, and effectively controlled biochemical markers of acromegaly (11).

PATHFNDR-1 enrolled 111 adults with biochemically uncontrolled acromegaly; 95% had undergone pituitary surgery before enrollment. Of those patients, 86 (78%) had macroadenomas (> 10 mm), 9 (8%) had microadenomas (≤ 10 mm), and 16 (14%) had tumors of unknown size (11). Participants were randomized to receive either paltusotine (n = 54) or a placebo (n = 57) for 24 weeks. The primary endpoint was the proportion of participants in whom biochemical control (IGF-1 $\leq 1.0 \times ULN$) was achieved compared to the placebo. At week 24, biochemical control was achieved in 56% of the paltusotine group versus achievement of control in only 5% in the placebo group (p-value < 0.0001) (11). IGF-1 normalization was achieved in most patients within 2-4 weeks of their starting treatment and control was maintained until the end of the study. Participants receiving paltusotine also reported alleviation of acromegaly-related symptoms such as headaches, joint pain, sweating, fatigue, weakness, swelling, and/or numbness/tingling compared to those receiving a placebo (11).

PATHFNDR-2 enrolled 58 adults with controlled biochemical parameters who had previously been treated with SRLs (octreotide or lanreotide); 86% had prior pituitary surgery. Of the patients, 33 (57%) had macroadenomas (> 10 mm), 11 (19%) had microadenomas (\leq 10 mm), and 14 (24%) had tumors of unknown size (*II*). Participants were randomized to receive either paltusotine (n = 30) or a placebo (n = 28) for 36 weeks. The primary endpoint was the proportion of participants in whom biochemical control (IGF-1 \leq 1.0 \times ULN) was maintaining compared to a placebo. At week 36, biochemical control was maintained in 83% of the paltusotine group versus 4% of the placebo group (p-value < 0.0001) (II). Symptom relief in the paltusotine group was also superior to that in the placebo group (II).

In terms of safety, the most common adverse events (\geq 5%) are diarrhea, abdominal pain, nausea, decreased appetite, sinus bradycardia, hyperglycemia, palpitations, and gastroenteritis (II).

As the first once-daily oral nonpeptide SSTR2 agonist approved by the FDA for acromegaly, paltusotine shifts therapy from injectable to oral administration, reducing the treatment burden and improving adherence. With its rapid onset, durable biochemical control, paltusotine has the potential to transform the current paradigm of acromegaly pharmacotherapy and provide a novel treatment option for patients. Nevertheless, its long-term safety and efficacy warrant further evaluation in real-world clinical settings.

Funding: None.

Conflict of Interest: The authors have no conflicts of interest to disclose.

References

- 1. Colao A, Grasso LFS, Giustina A, Melmed S, Chanson P, Pereira AM, Pivonello R. Acromegaly. Nat Rev Dis Primers. 2019; 5:20.
- Ershadinia N, Tritos NA. Diagnosis and treatment of acromegaly: An update. Mayo Clin Proc. 2022; 97:333-346.
- Giustina A, Barkan A, Beckers A, et al. A consensus on the diagnosis and treatment of acromegaly comorbidities: An update. J Clin Endocrinol Metab. 2020; 105:dgz096.
- Giustina A, Barkhoudarian G, Beckers A, et al. Multidisciplinary management of acromegaly: A consensus. Rev Endocr Metab Disord. 2020; 21:667-678.
- Fleseriu M, Biller BMK, Freda PU, Gadelha MR, Giustina A, Katznelson L, Molitch ME, Samson SL, Strasburger CJ, van der Lely AJ, Melmed S. A Pituitary Society update to acromegaly management guidelines. Pituitary. 2021; 24:1-13.
- Starnoni D, Daniel RT, Marino L, Pitteloud N, Levivier M, Messerer M. Surgical treatment of acromegaly according to the 2010 remission criteria: Systematic review and metaanalysis. Acta Neurochir (Wien). 2016; 158:2109-2121.
- Melmed S, Bronstein MD, Chanson P, Klibanski A, Casanueva FF, Wass JAH, Strasburger CJ, Luger A, Clemmons DR, Giustina A. A Consensus Statement on acromegaly therapeutic outcomes. Nat Rev Endocrinol. 2018; 14:552-561.
- Geer EB, Sisco J, Adelman DT, Ludlam WH, Haviv A, Liu S, Mathias SD, Gelbaum D, Shi L. Patient reported outcome data from acromegaly patients treated with injectable somatostatin receptor ligands (SRLs) in routine clinical practice. BMC Endocr Disord. 2020; 20:117.
- FDA approves new treatment for acromegaly, a rare endocrine disorder. https://www.fda.gov/drugs/news-eventshuman-drugs/fda-approves-new-treatment-acromegalyrare-endocrine-disorder (Accessed October 4, 2025).
- Crinetics Announces FDA Approval of PALSONIFYTM
 (paltusotine) for the Treatment of Acromegaly in Adults.

 https://crinetics.com/crinetics-announces-fda-approval-ofpalsonify-paltusotine-for-the-treatment-of-acromegaly-inadults (Accessed October 4, 2025).
- PALSONIFY (paltusotine) tablets, for oral use. https://www.accessdata.fda.gov/drugsatfda_docs/ label/2025/219070s000lbl.pdf (Accessed October 4, 2025).
- Melmed S, di Filippo L, Fleseriu M, et al. Consensus on acromegaly therapeutic outcomes: An update. Nat Rev Endocrinol. 2025; 21:718-737.

Received October 4, 2025; Revised October 25, 2025; Accepted October 27, 2025.

*Address correspondence to:

Jianjun Gao, Department of Pharmacology, School of Pharmacy, Qingdao University, Qingdao, Shandong, China.

E-mail: gaojj@qdu.edu.cn

Released online in J-STAGE as advance publication October 29, 2025



Guide for Authors

1. Scope of Articles

Drug Discoveries & Therapeutics (Print ISSN 1881-7831, Online ISSN 1881-784X) welcomes contributions in all fields of pharmaceutical and therapeutic research such as medicinal chemistry, pharmacology, pharmaceutical analysis, pharmaceutics, pharmaceutical administration, and experimental and clinical studies of effects, mechanisms, or uses of various treatments. Studies in drug-related fields such as biology, biochemistry, physiology, microbiology, and immunology are also within the scope of this journal.

2. Submission Types

Original Articles should be well-documented, novel, and significant to the field as a whole. An Original Article should be arranged into the following sections: Title page, Abstract, Introduction, Materials and Methods, Results, Discussion, Acknowledgments, and References. Original articles should not exceed 5,000 words in length (excluding references) and should be limited to a maximum of 50 references. Articles may contain a maximum of 10 figures and/or tables. Supplementary Data are permitted but should be limited to information that is not essential to the general understanding of the research presented in the main text, such as unaltered blots and source data as well as other file types.

Brief Reports definitively documenting either experimental results or informative clinical observations will be considered for publication in this category. Brief Reports are not intended for publication of incomplete or preliminary findings. Brief Reports should not exceed 3,000 words in length (excluding references) and should be limited to a maximum of 4 figures and/or tables and 30 references. A Brief Report contains the same sections as an Original Article, but the Results and Discussion sections should be combined.

Reviews should present a full and up-to-date account of recent developments within an area of research. Normally, reviews should not exceed 8,000 words in length (excluding references) and should be limited to a maximum of 10 figures and/or tables and 100 references. Mini reviews are also accepted, which should not exceed 4,000 words in length (excluding references) and should be limited to a maximum of 5 figures and/or tables and 50 references.

Policy Forum articles discuss research and policy issues in areas related to life science such as public health, the medical care system, and social science and may address governmental issues at district, national, and international levels of discourse. Policy Forum articles should not exceed 3,000 words in length (excluding references) and should be limited to a maximum of 5 figures and/or tables and 30 references.

Case Reports should be detailed reports of the symptoms, signs, diagnosis, treatment, and follow-up of an individual patient. Case reports may contain a demographic profile of the patient but usually describe an unusual or novel occurrence. Unreported or unusual side effects or adverse interactions involving medications will also be considered. Case Reports should not exceed 3,000 words in length (excluding references).

Communications are short, timely pieces that spotlight new research findings or policy issues of interest to the field of global health and medical practice that are of immediate importance. Depending on their content, Communications will be published as "Comments" or

"Correspondence". Communications should not exceed 1,500 words in length (excluding references) and should be limited to a maximum of 2 figures and/or tables and 20 references.

Editorials are short, invited opinion pieces that discuss an issue of immediate importance to the fields of global health, medical practice, and basic science oriented for clinical application. Editorials should not exceed 1,000 words in length (excluding references) and should be limited to a maximum of 10 references. Editorials may contain one figure or table.

News articles should report the latest events in health sciences and medical research from around the world. News should not exceed 500 words in length.

Letters should present considered opinions in response to articles published in *Drug Discoveries & Therapeutics* in the last 6 months or issues of general interest. Letters should not exceed 800 words in length and may contain a maximum of 10 references. Letters may contain one figure or table.

3. Editorial Policies

For publishing and ethical standards, *Drug Discoveries & Therapeutics* follows the Recommendations for the Conduct, Reporting, Editing, and Publication of Scholarly Work in Medical Journals issued by the International Committee of Medical Journal Editors (ICMJE, *https://icmje.org/recommendations*), and the Principles of Transparency and Best Practice in Scholarly Publishing jointly issued by the Committee on Publication Ethics (COPE, *https://publicationethics.org/resources/guidelines-new/principles-transparency-and-best-practice-scholarly-publishing*), the Directory of Open Access Journals (DOAJ, *https://doaj.org/apply/transparency)*, the Open Access Scholarly Publishers Association (OASPA, *https://oaspa.org/principles-of-transparency-and-best-practice-in-scholarly-publishing-4*), and the World Association of Medical Editors (WAME, *https://wame.org/principles-of-transparency-and-best-practice-in-scholarly-publishing-1*).

Drug Discoveries & Therapeutics will perform an especially prompt review to encourage innovative work. All original research will be subjected to a rigorous standard of peer review and will be edited by experienced copy editors to the highest standards.

Ethical Approval of Studies and Informed Consent: For all manuscripts reporting data from studies involving human participants or animals, formal review and approval, or formal review and waiver, by an appropriate institutional review board or ethics committee is required and should be described in the Methods section. When your manuscript contains any case details, personal information and/or images of patients or other individuals, authors must obtain appropriate written consent, permission and release in order to comply with all applicable laws and regulations concerning privacy and/or security of personal information. The consent form needs to comply with the relevant legal requirements of your particular jurisdiction, and please do not send signed consent form to Drug Discoveries & Therapeutics to respect your patient's and any other individual's privacy. Please instead describe the information clearly in the Methods (patient consent) section of your manuscript while retaining copies of the signed forms in the event they should be needed. Authors should also state that the study conformed to the provisions of the Declaration of Helsinki (as revised in 2013, https://wma.net/what-we-do/medical-ethics/ declaration-of-helsinki). When reporting experiments on animals, authors should indicate whether the institutional and national guide for the care and use of laboratory animals was followed.

Reporting Clinical Trials: The ICMJE (https://icmje.org/recommendations/browse/publishing-and-editorial-issues/clinical-trial-registration.html) defines a clinical trial as any research project that prospectively assigns people or a group of people to an intervention, with or without concurrent comparison or control groups, to study the relationship between a health-related intervention and a health outcome. Registration of clinical trials in a public trial registry

at or before the time of first patient enrollment is a condition of consideration for publication in *Drug Discoveries & Therapeutics*, and the trial registration number will be published at the end of the Abstract. The registry must be independent of for-profit interest and publicly accessible. Reports of trials must conform to CONSORT 2010 guidelines (https://consort-statement.org/consort-2010). Articles reporting the results of randomized trials must include the CONSORT flow diagram showing the progress of patients throughout the trial.

Conflict of Interest: All authors are required to disclose any actual or potential conflict of interest including financial interests or relationships with other people or organizations that might raise questions of bias in the work reported. If no conflict of interest exists for each author, please state "There is no conflict of interest to disclose".

Submission Declaration: When a manuscript is considered for submission to *Drug Discoveries & Therapeutics*, the authors should confirm that 1) no part of this manuscript is currently under consideration for publication elsewhere; 2) this manuscript does not contain the same information in whole or in part as manuscripts that have been published, accepted, or are under review elsewhere, except in the form of an abstract, a letter to the editor, or part of a published lecture or academic thesis; 3) authorization for publication has been obtained from the authors' employer or institution; and 4) all contributing authors have agreed to submit this manuscript.

Initial Editorial Check: Immediately after submission, the journal's managing editor will perform an initial check of the manuscript. A suitable academic editor will be notified of the submission and invited to check the manuscript and recommend reviewers. Academic editors will check for plagiarism and duplicate publication at this stage. The journal has a formal recusal process in place to help manage potential conflicts of interest of editors. In the event that an editor has a conflict of interest with a submitted manuscript or with the authors, the manuscript, review, and editorial decisions are managed by another designated editor without a conflict of interest related to the manuscript.

Peer Review: Drug Discoveries & Therapeutics operates a singleanonymized review process, which means that reviewers know the names of the authors, but the authors do not know who reviewed their manuscript. All articles are evaluated objectively based on academic content. External peer review of research articles is performed by at least two reviewers, and sometimes the opinions of more reviewers are sought. Peer reviewers are selected based on their expertise and ability to provide quality, constructive, and fair reviews. For research manuscripts, the editors may, in addition, seek the opinion of a statistical reviewer. Every reviewer is expected to evaluate the manuscript in a timely, transparent, and ethical manner, following the COPE guidelines (https://publicationethics.org/files/cope-ethicalguidelines-peer-reviewers-v2_0.pdf). We ask authors for sufficient revisions (with a second round of peer review, when necessary) before a final decision is made. Consideration for publication is based on the article's originality, novelty, and scientific soundness, and the appropriateness of its analysis.

Suggested Reviewers: A list of up to 3 reviewers who are qualified to assess the scientific merit of the study is welcomed. Reviewer information including names, affiliations, addresses, and e-mail should be provided at the same time the manuscript is submitted online. Please do not suggest reviewers with known conflicts of interest, including participants or anyone with a stake in the proposed research; anyone from the same institution; former students, advisors, or research collaborators (within the last three years); or close personal contacts. Please note that the Editor-in-Chief may accept one or more of the proposed reviewers or may request a review by other qualified persons.

Language Editing: Manuscripts prepared by authors whose native language is not English should have their work proofread by a native English speaker before submission. If not, this might delay the publication of your manuscript in *Drug Discoveries & Therapeutics*.

The Editing Support Organization can provide English

proofreading, Japanese-English translation, and Chinese-English translation services to authors who want to publish in *Drug Discoveries & Therapeutics* and need assistance before submitting a manuscript. Authors can visit this organization directly at https://www.iacmhr.com/iac-eso/support.php?lang=en.IAC-ESO was established to facilitate manuscript preparation by researchers whose native language is not English and to help edit works intended for international academic journals.

Copyright and Reuse: Before a manuscript is accepted for publication in *Drug Discoveries & Therapeutics*, authors will be asked to sign a transfer of copyright agreement, which recognizes the common interest that both the journal and author(s) have in the protection of copyright. We accept that some authors (e.g., government employees in some countries) are unable to transfer copyright. A JOURNAL PUBLISHING AGREEMENT (JPA) form will be e-mailed to the authors by the Editorial Office and must be returned by the authors by mail, fax, or as a scan. Only forms with a hand-written signature from the corresponding author are accepted. This copyright will ensure the widest possible dissemination of information. Please note that the manuscript will not proceed to the next step in publication until the JPA Form is received. In addition, if excerpts from other copyrighted works are included, the author(s) must obtain written permission from the copyright owners and credit the source(s) in the article.

4. Cover Letter

The manuscript must be accompanied by a cover letter prepared by the corresponding author on behalf of all authors. The letter should indicate the basic findings of the work and their significance. The letter should also include a statement affirming that all authors concur with the submission and that the material submitted for publication has not been published previously or is not under consideration for publication elsewhere. The cover letter should be submitted in PDF format. For an example of Cover Letter, please visit: Download Centre (https://www.ddtjournal.com/downcentre).

5. Submission Checklist

The Submission Checklist should be submitted when submitting a manuscript through the Online Submission System. Please visit Download Centre (https://www.ddtjournal.com/downcentre) and download the Submission Checklist file. We recommend that authors use this checklist when preparing your manuscript to check that all the necessary information is included in your article (if applicable), especially with regard to Ethics Statements.

6. Manuscript Preparation

Manuscripts are suggested to be prepared in accordance with the "Recommendations for the Conduct, Reporting, Editing, and Publication of Scholarly Work in Medical Journals", as presented at http://www.ICMJE.org.

Manuscripts should be written in clear, grammatically correct English and submitted as a Microsoft Word file in a single-column format. Manuscripts must be paginated and typed in 12-point Times New Roman font with 24-point line spacing. Please do not embed figures in the text. Abbreviations should be used as little as possible and should be explained at first mention unless the term is a well-known abbreviation (e.g. DNA). Single words should not be abbreviated.

Title page: The title page must include 1) the title of the paper (Please note the title should be short, informative, and contain the major key words); 2) full name(s) and affiliation(s) of the author(s), 3) abbreviated names of the author(s), 4) full name, mailing address, telephone/fax numbers, and e-mail address of the corresponding author; 5) author contribution statements to specify the individual contributions of all authors to this manuscript, and 6) conflicts of interest (if you have an actual or potential conflict of interest to disclose, it must be included as a footnote on the title page of the manuscript; if no conflict of interest

exists for each author, please state "There is no conflict of interest to disclose").

Abstract: The abstract should briefly state the purpose of the study, methods, main findings, and conclusions. For article types including Original Article, Brief Report, Review, Policy Forum, and Case Report, a one-paragraph abstract consisting of no more than 250 words must be included in the manuscript. For Communications, Editorials, News, or Letters, a brief summary of main content in 150 words or fewer should be included in the manuscript. For articles reporting clinical trials, the trial registration number should be stated at the end of the Abstract. Abbreviations must be kept to a minimum and non-standard abbreviations explained in brackets at first mention. References should be avoided in the abstract. Three to six key words or phrases that do not occur in the title should be included in the Abstract page.

Introduction: The introduction should provide sufficient background information to make the article intelligible to readers in other disciplines and sufficient context clarifying the significance of the experimental findings.

Materials/Patients and Methods: The description should be brief but with sufficient detail to enable others to reproduce the experiments. Procedures that have been published previously should not be described in detail but appropriate references should simply be cited. Only new and significant modifications of previously published procedures require complete description. Names of products and manufacturers with their locations (city and state/country) should be given and sources of animals and cell lines should always be indicated. All clinical investigations must have been conducted in accordance with the Declaration of Helsinki (as revised in 2013, https://wma.net/what-we-do/medical-ethics/declaration-of-helsinki). All human and animal studies must have been approved by the appropriate institutional review board(s) and a specific declaration of approval must be made within this section.

Results: The description of the experimental results should be succinct but in sufficient detail to allow the experiments to be analyzed and interpreted by an independent reader. If necessary, subheadings may be used for an orderly presentation. All Figures and Tables should be referred to in the text in order, including those in the Supplementary Data.

Discussion: The data should be interpreted concisely without repeating material already presented in the Results section. Speculation is permissible, but it must be well-founded, and discussion of the wider implications of the findings is encouraged. Conclusions derived from the study should be included in this section.

Acknowledgments: All funding sources (including grant identification) should be credited in the Acknowledgments section. Authors should also describe the role of the study sponsor(s), if any, in study design; in the collection, analysis, and interpretation of data; in the writing of the report; and in the decision to submit the paper for publication. If the funding source had no such involvement, the authors should so state.

In addition, people who contributed to the work but who do not meet the criteria for authors should be listed along with their contributions.

References: References should be numbered in the order in which they appear in the text. Citing of unpublished results, personal communications, conference abstracts, and theses in the reference list is not recommended but these sources may be mentioned in the text. In the reference list, cite the names of all authors when there are fifteen or fewer authors; if there are sixteen or more authors, list the first three followed by et al. Names of journals should be abbreviated in the style used in PubMed. Authors are responsible for the accuracy of the references. The EndNote Style of Drug Discoveries & Therapeutics could be downloaded at EndNote (https://www.ddtjournal.com/examples/Drug Discoveries Therapeutics.ens).

Examples are given below:

Example 1 (Sample journal reference):

Nakata M, Tang W. Japan-China Joint Medical Workshop on Drug Discoveries and Therapeutics 2008: The need of Asian pharmaceutical researchers' cooperation. Drug Discov Ther. 2008; 2:262-263.

Example 2 (Sample journal reference with more than 15 authors):

Darby S, Hill D, Auvinen A, et al. Radon in homes and risk of lung cancer: Collaborative analysis of individual data from 13 European case-control studies. BMJ. 2005; 330:223.

Example 3 (Sample book reference):

Shalev AY. Post-traumatic stress disorder: Diagnosis, history and life course. In: Post-traumatic Stress Disorder, Diagnosis, Management and Treatment (Nutt DJ, Davidson JR, Zohar J, eds.). Martin Dunitz, London, UK, 2000; pp. 1-15.

Example 4 (Sample web page reference):

World Health Organization. The World Health Report 2008 – primary health care: Now more than ever. https://apps.who.int/iris/handle/10665/43949 (accessed September 23, 2022).

Tables: All tables should be prepared in Microsoft Word or Excel and should be arranged at the end of the manuscript after the References section. Please note that tables should not in image format. All tables should have a concise title and should be numbered consecutively with Arabic numerals. If necessary, additional information should be given below the table.

Figure Legend: The figure legend should be typed on a separate page of the main manuscript and should include a short title and explanation. The legend should be concise but comprehensive and should be understood without referring to the text. Symbols used in figures must be explained. Any individually labeled figure parts or panels (A, B, *etc.*) should be specifically described by part name within the legend.

Figure Preparation: All figures should be clear and cited in numerical order in the text. Figures must fit a one- or two-column format on the journal page: 8.3 cm (3.3 in.) wide for a single column, 17.3 cm (6.8 in.) wide for a double column; maximum height: 24.0 cm (9.5 in.). Please make sure that artwork files are in an acceptable format (TIFF or JPEG) at minimum resolution (600 dpi for illustrations, graphs, and annotated artwork, and 300 dpi for micrographs and photographs). Please provide all figures as separate files. Please note that low-resolution images are one of the leading causes of article resubmission and schedule delays.

Units and Symbols: Units and symbols conforming to the International System of Units (SI) should be used for physicochemical quantities. Solidus notation (*e.g.* mg/kg, mg/mL, mol/mm²/min) should be used. Please refer to the SI Guide *www.bipm.org/en/si/* for standard units.

Supplemental data: Supplemental data might be useful for supporting and enhancing your scientific research and *Drug Discoveries & Therapeutics* accepts the submission of these materials which will be only published online alongside the electronic version of your article. Supplemental files (figures, tables, and other text materials) should be prepared according to the above guidelines, numbered in Arabic numerals (*e.g.*, Figure S1, Figure S2, and Table S1, Table S2) and referred to in the text. All figures and tables should have titles and legends. All figure legends, tables and supplemental text materials should be placed at the end of the paper. Please note all of these supplemental data should be provided at the time of initial submission and note that the editors reserve the right to limit the size

and length of Supplemental Data.

7. Online Submission

Manuscripts should be submitted to *Drug Discoveries & Therapeutics* online at *https://www.ddtjournal.com/login*. Receipt of your manuscripts submitted online will be acknowledged by an e-mail from Editorial Office containing a reference number, which should be used in all future communications. If for any reason you are unable to submit a file online, please contact the Editorial Office by e-mail at *office@ddtjournal.com*

8. Accepted Manuscripts

Page Charge: Page charges will be levied on all manuscripts accepted for publication in *Drug Discoveries & Therapeutics* (Original Articles / Brief Reports / Reviews / Policy Forum / Communications: \$140 per page for black white pages, \$340 per page for color pages; News / Letters: a total cost of \$600). Under exceptional circumstances, the author(s) may apply to the editorial office for a waiver of the publication charges by stating the reason in the Cover Letter when the

manuscript online.

Misconduct: Drug Discoveries & Therapeutics takes seriously all allegations of potential misconduct and adhere to the ICMJE Guideline (https://icmje.org/recommendations) and COPE Guideline (https://publicationethics.org/files/Code_of_conduct_for_journal_editors.pdf). In cases of suspected research or publication misconduct, it may be necessary for the Editor or Publisher to contact and share submission details with third parties including authors' institutions and ethics committees. The corrections, retractions, or editorial expressions of concern will be performed in line with above guidelines.

(As of December 2022)

Drug Discoveries & Therapeutics
Editorial and Head Office
Pearl City Koishikawa 603,
2-4-5 Kasuga, Bunkyo-ku,
Tokyo 112-0003, Japan.
E-mail: office@ddtjournal.com

